Forschungszentrum Karlsruhe
in der Helmholtz-Gemeinschaft

Wissenschaftliche Berichte
FZKA 6980

Degradation and Oxidation of B_4C Control Rod Segments at High Temperatures

M. Steinbrück, A. Meier, E. Nold, U. Stegmaier

Institut für Materialforschung
Programm Nukleare Sicherheitsforschung

Mai 2004

Forschungszentrum Karlsruhe

in der Helmholtz-Gemeinschaft

Wissenschaftliche Berichte

FZKA 6980

Degradation and Oxidation of B_4C Control Rod Segments at High Temperatures

M. Steinbrück, A. Meier, E. Nold, U. Stegmaier

Institut für Materialforschung

Programm Nukleare Sicherheitsforschung

Forschungszentrum Karlsruhe GmbH, Karlsruhe

2004

Impressum der Print-Ausgabe:

Als Manuskript gedruckt

Forschungszentrum Karlsruhe GmbH
Postfach 3640, 76021 Karlsruhe

Mitglied der Hermann von Helmholtz-Gemeinschaft
Deutscher Forschungszentren (HGF)

ISSN 0947-8620

urn:nbn:de:0005-069808

DEGRADATION UND OXIDATION VON B_4C STEUERSTABSEGMENTEN BEI HOHEN TEMPERATUREN

ZUSAMMENFASSUNG

Borkarbid wird weltweit in verschiedenen Kernreaktoren als Absorbermaterial in Steuerstäben eingesetzt. Während eines hypothetischen schweren Störfalls führen eutektische Wechselwirkungen zwischen B_4C und den umgebenden Hüllrohren aus rostfreiem Stahl schon bei Temperaturen um 1200 °C, und somit weit unterhalb der Schmelztemperaturen der einzelnen Komponenten, zur Bildung von Schmelzphasen. Das so freigelegte Absorbermaterial sowie gebildete B_4C/Metall-Schmelzen sind dem Dampf im Reaktor ausgesetzt. Die Oxidation von Borkarbid und B_4C-haltigen Schmelzen ist stark exotherm und führt zur Bildung von gasförmigen Reaktionsprodukten, wie H_2, CO, CO_2 and CH_4, die u. a. die Spaltproduktchemie beeinflussen.

Es wurden umfangreiche Testserien zur Degradation von B_4C Absorberstäben und zur Oxidation der dabei gebildeten Absorberschmelzen durchgeführt. Dabei wurden unterschiedliche, mit einem bzw. sechs B_4C Pellets gefüllte Proben aus kommerziellen in französischen Druckwasserreaktoren verwendeten Materialien im Temperaturbereich zwischen 800 und 1700 °C in dampfhaltiger Atmosphäre untersucht. Die gasförmigen Reaktionsprodukte wurden mittels quantitativer Massenspektrometrie analysiert und somit Oxidationsraten bestimmt. Ausführliche Nachuntersuchungen der Proben mittels Lichtmikroskopie, REM/EDX und Auger-Spektroskopie wurden vorgenommen.

Eutektische Wechselwirkungen zwischen dem rostfreien Stahl und B_4C sowie zwischen Stahl und dem Zircaloy-4 Führungsrohr führen bei Temperaturen oberhalb ca. 1250 °C zur Bildung komplexer Multikomponenten- und Multiphasenschmelzen. Eine äußere ZrO_2-Schicht hält die Schmelze im Führungsrohr und verzögert somit die Verlagerung und Oxidation der Absorberschmelzen. Nach Versagen dieser schützenden Oxidschicht oberhalb ca. 1450 °C oxidieren die Schmelze und das verbleibende B_4C sehr schnell unter Bildung großer Mengen Wasserstoff, CO und CO_2. Lokale Oxidation von B_4C sowie die Verlagerung von Absorberschmelze im Spalt zwischen B_4C Pellets und äußerer Oxidschicht konnten bei den längeren Steuerstabproben beobachtet werden.

In speziellen Einzeleffektuntersuchungen wurden extrem hohe Oxidationsraten von Absorberschmelzen unterschiedlicher Zusammensetzung schon bei niedrigen Temperaturen um 1200 °C nachgewiesen. Darüber hinaus konnte gezeigt werden, dass große Mengen Stahl schon 200 K unterhalb dessen Schmelztemperatur in Anwesenheit geringer Mengen Borkarbid verflüssigt werden können.

Bei den gewählten Versuchsbedingungen wurden nur sehr geringe Mengen Methan gebildet. Dieses Gas ist von besonderem Interesse, weil es wegen der Bildung von flüchtigen organischen Verbindungen einen großen Einfluss auf die Chemie des Spaltprodukts Jod hat.

Dieser Bericht aktualisiert und ersetzt den im Rahmen des EU-Programms COLOSS (5. Rahmenprogramm 2000-2003) erstellten internen Bericht SAM-COLOSS-P028.

ABSTRACT

Boron carbide is widely used as neutron absorbing control rod material in Western Boiling Water Reactors (BWR) and Russian RBMKs and VVERs and some Pressurised Water Reactors (PWR). During a hypothetical severe accident the B_4C reacts with the surrounding stainless steel cladding forming eutectic melts at temperatures above 1200 °C which is far below the melting temperatures of all components. The remaining uncovered absorber material as well as the B_4C/metal mixtures may be exposed to the steam in the reactor core. The oxidation of boron carbide is highly exothermic and produces various gaseous reaction products like H_2, CO, CO_2 and CH_4 which may affect the fission product chemistry.

Extensive test series on the degradation of boron carbide absorber rods and the oxidation of the resulting absorber melts were performed. Two types of 1-pellet-size as well as 10-cm long control rod segments manufactured from commercial materials used in French 1300 MW PWRs were investigated in the temperature range between 800 and 1700 °C in steam atmosphere. The gaseous reaction products were quantitatively analysed by mass spectroscopy allowing the evaluation of oxidation rates. Extensive post-test examinations by light microscopy, scanning electron microscopy as well as EDX and Auger spectroscopy were performed.

Rapid melt formation due to eutectic interactions between stainless steel (cladding tube) and B_4C on the one hand and between the steel and Zircaloy-4 (guide tube) on the other hand was observed at temperatures above 1250 °C. Complex multi-component and multi-phase melts were formed. An outer ZrO_2 oxide scale kept the melt inside the guide tube and prevented early relocation and oxidation of the melt. Rapid oxidation of the absorber melts and the remaining boron carbide pellets took place after failure of the protecting oxide shell above 1450 °C. Local oxidation of the B_4C pellets and internal melt relocation was seen at the longer CR specimens.

Separate-effects tests on the oxidation of SS/B_4C/Zry-4 absorber melts of various compositions confirmed the fast oxidation seen in the tests with control rod segments. The oxidation rates of such mixtures increased by a factor of up to 30 after reaching their melting points at temperatures of about 1200 °C. Furthermore, it was shown that B_4C can liquefy huge amounts of stainless steel 200 K below its melting temperature.

Only very low amounts of methane - which is of interest for the fission gas chemistry due to the formation of organic iodine - were produced in these tests.

This report updates and replaces the internal report SAM-COLOSS-P028 published as one deliverable of the EC COLOSS program (5^{th} Framework Program 2000-2003).

CONTENTS

LIST OF TABLES

LIST OF FIGURES

1 Introduction

Boron carbide (B_4C) is widely used as neutron absorbing control rod material in Western Boiling Water Reactors (BWR) and Russian RBMKs and VVERs. Additionally, in French Pressurised Water Reactors (PWR) it is used in hybrid rods together with silver/indium/cadmium alloy (SIC) [1]. During a hypothetical severe accident the B_4C reacts with the surrounding stainless steel (SS) cladding forming eutectic melts at temperatures above 1200 °C [2-4] which is far below the melting temperatures of all components. After failure of the control rod the remaining uncovered absorber material as well as the B_4C/metal mixtures are exposed to the steam in the reactor core.

The oxidation of B_4C by steam is highly exothermic and produces 6-7 times the amount of hydrogen as the oxidation of the same mass of Zircaloy. Furthermore, gaseous carbon- and boron-containing species are formed which may affect the fission product chemistry in the containment, e.g. for the release of organic iodine compounds. The oxidation kinetics of pure B_4C materials has been extensively studied within the COLOSS program [5, 6]. So far, no data were available for the oxidation of absorber melts.

The main objective of the work presented here was to investigate the degradation and failure of B_4C containing control rod segments as well as the resulting release of carbon and boron containing gaseous species. Various types of specimens were investigated in the temperature range between 1000 and 1700 °C, namely 1-pellet- size control rod segment of two different designs, 10-cm long control rod segments and SS/B_4C/Zry-4 absorber melts of various compositions. Additionally, the capability of boron carbide to liquefy stainless steel far below the melting temperature was investigated in special tests.

The experimental program was run at Forschungszentrum Karlsruhe (FZK) within the COLOSS project of the Euratom 5th Framework Programme. It is closely related to the FZK bundle tests QUENCH-07 [7] and QUENCH-09 [8] with a B_4C control rod and the French Phebus FPT-3 test [9].

2 Experimental set-up

Three experimental set-ups have been used for the experiments described in this report: the BOX Rig, the single rod QUENCH Rig and the LAVA furnace which are briefly described in the following.

All tests with small, 1-pellet-size specimens as well as the oxidation tests with absorber melts were performed in the BOX Rig which was put into operation in the first year of the project and first used for the test program on B_4C oxidation [5]. The BOX Rig (Fig. 1) consists of

- A gas supply system for Ar, H_2 and steam (0-4 mol/h each) with two gas flow controllers, one liquid flow controller and a so-called controlled evaporator mixer unit (CEM), where

the liquid water is evaporated and mixed with the non-condensable gas. The whole system was delivered by Bronkhorst High-Tech B.V.

- A tube furnace with maximum working temperatures of 1700 °C, with an alumina reaction tube (inner diameter: 32 mm, length: 600 mm) and molybdenum heaters, delivered by HTM Reetz GmbH Berlin.

- A quadrupole mass spectrometer (MS) Balzers GAM 300.

The off-gas tube from the furnace to the MS (SS, inner diameter: 6 mm, length: 2.7 m) is heated to about 150 °C to prevent steam condensation. The mass spectrometer allows the quantitative analysis of all gaseous reaction products. In particular, the hydrogen release rate was used in most of the tests as a continuous measure for the reaction kinetics. All parts of the system are computer controlled by a LabView program especially written for the BOX Rig.

The mass spectrometer is calibrated for H_2, CO, CO_2 and CH_4 using certificated Ar-5%gas mixtures and for steam using the Bronkhorst CEM system.

The furnace temperature is measured and controlled by two Pt/Rh thermocouples surrounded by a one-side-closed alumina tube and located near the specimen in the reaction tube.

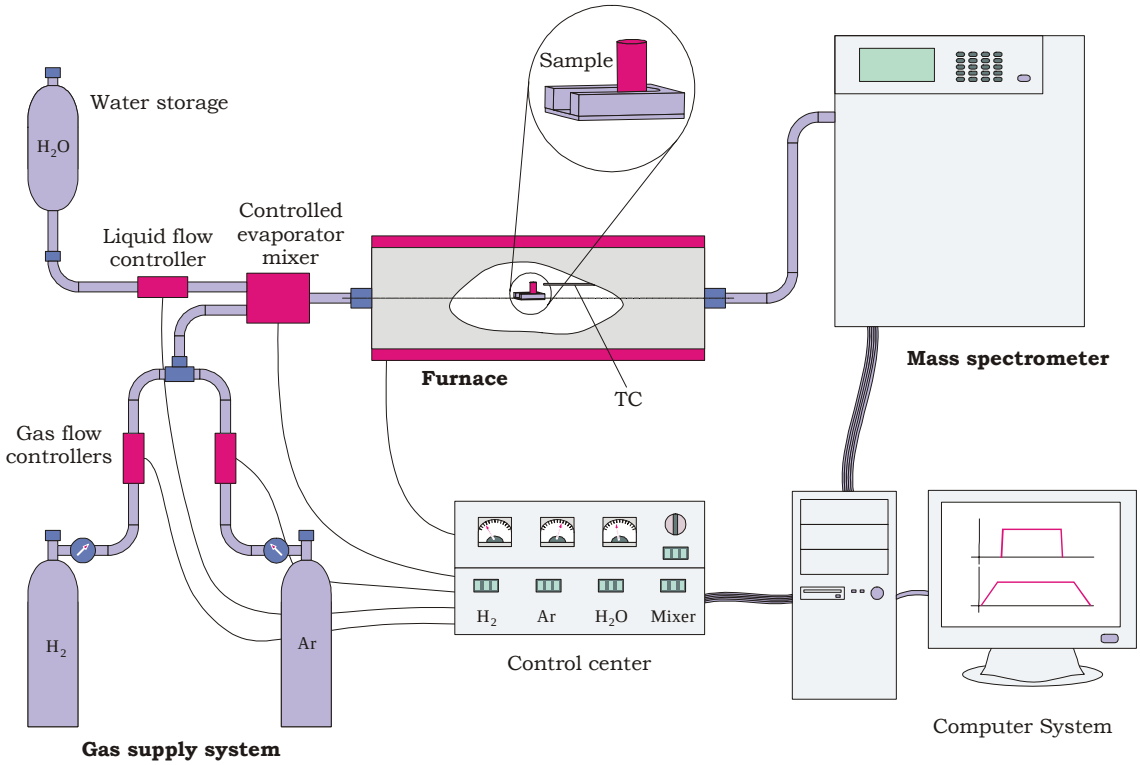

Figure 1: BOX Rig for the investigation of the degradation and oxidation of small B_4C control rod segments and absorber melts

The QUENCH-SR rig (Figs. 2, 3) was used for tests with longer, about 10 cm control rod segments. Here, heating of the specimen is provided by an induction coil around the section of a quartz tube enclosing the specimen. Power is supplied to the coil from a 20 kW oscillator at a frequency of 700 kHz, which induces surface currents in the metal with consequent

Joule heating. For this kind of tests a new sample support was designed which allows further heating of the specimen even after its failure (Fig. 3). Temperature was controlled by a pyrometer and additionally measured by a thermocouple fixed to the surface of the control rod segment at the axially mid position. Sometimes the difference between pyrometer and thermocouple measurements were quite large (>100 K), which could be addressed to a change of the contact of the TC at the specimen surface as well as to changes in the emissivity of the surface or the bending of the specimen.

The SS/B_4C/Zry-4 melts were prepared in the LAVA Furnace (Fig. 4) in inert atmosphere. This inductive furnace with tungsten susceptor is powered by the same HF oscillator as the QUENCH-SR rig. Maximum temperatures of 2300 °C can be obtained with this furnace. The LAVA furnace was also used for the B_4C-stainless steel dissolution tests.

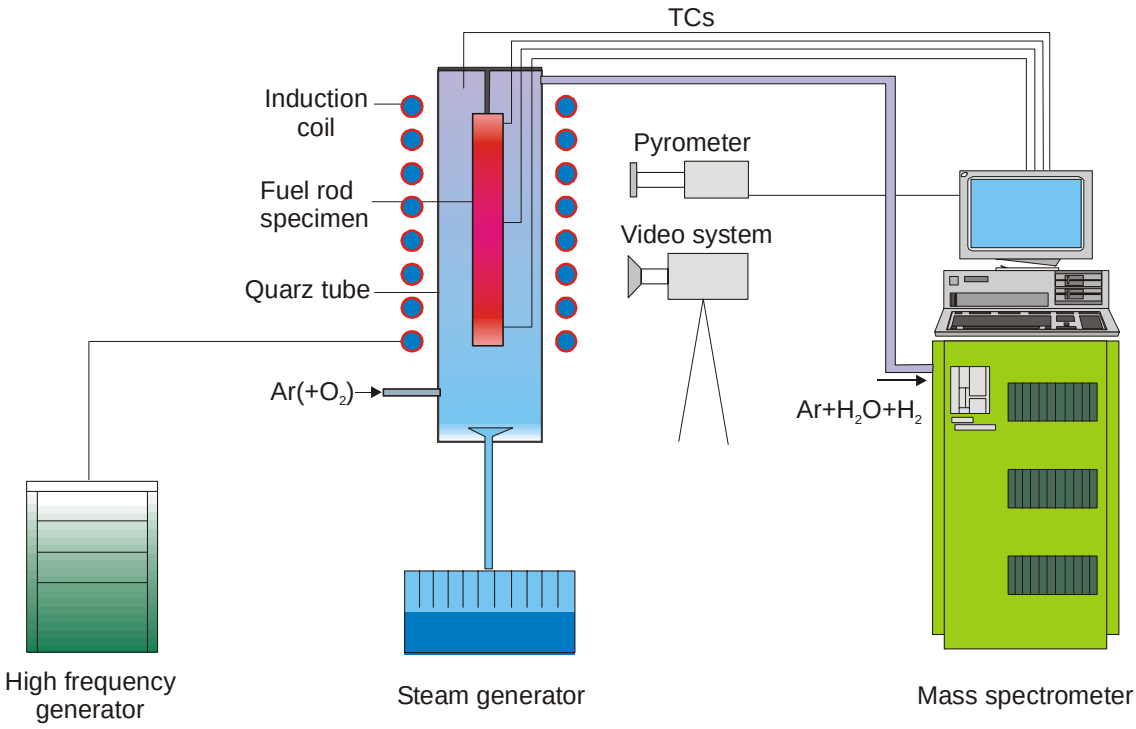

Figure 2: QUENCH-SR rig for the investigation of 10 cm control rod segments

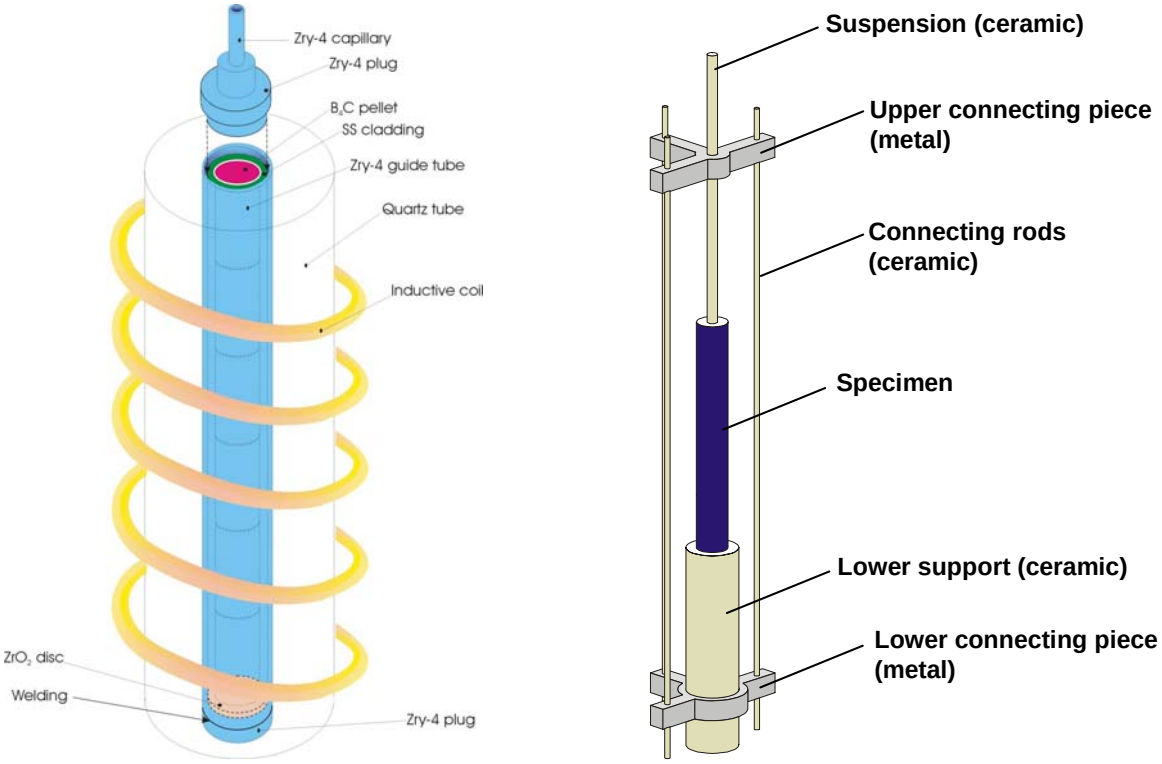

Figure 3: B_4C control rod specimen in the QUENCH-SR rig: specimen design (left) and sample support (right)

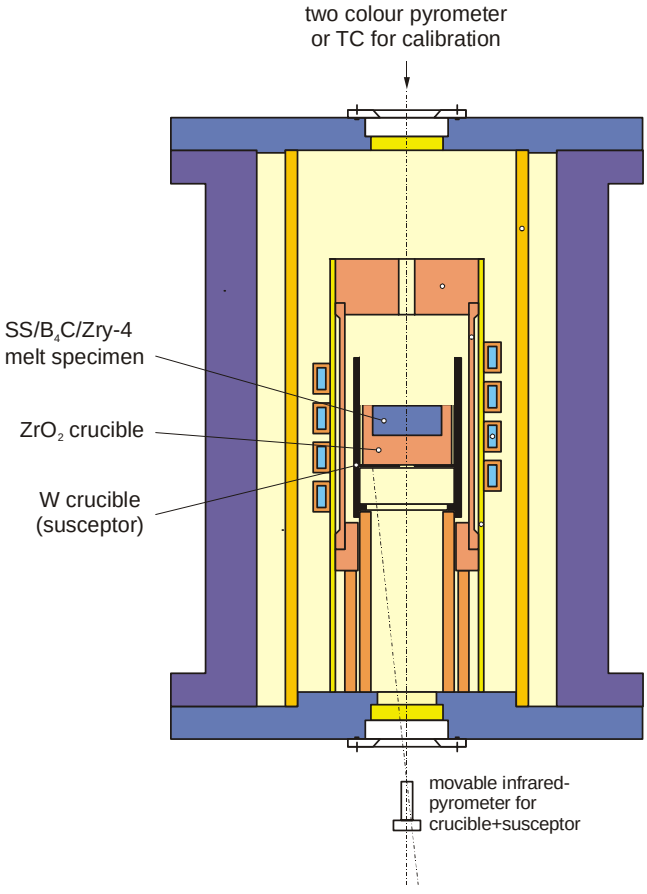

Figure 4: LAVA apparatus for the preparation of absorber melts

3 Specimens

Various types of specimens were investigated as can be seen in Fig. 5. The materials are commercial control rod materials used in French 1300 MW PWRs and were delivered by Framatome. The boron carbide pellets (Framatome, diameter 14 mm, height 7.47 mm, 70 % density) are surrounded by a stainless steel cladding tube (Framatome, AISI 308 modified, outer diameter 9.68 mm, inner diameter 7.72 mm) and the Zircaloy-4 guide tube (outer diameter 10.92 mm, inner diameter 10.12 mm).

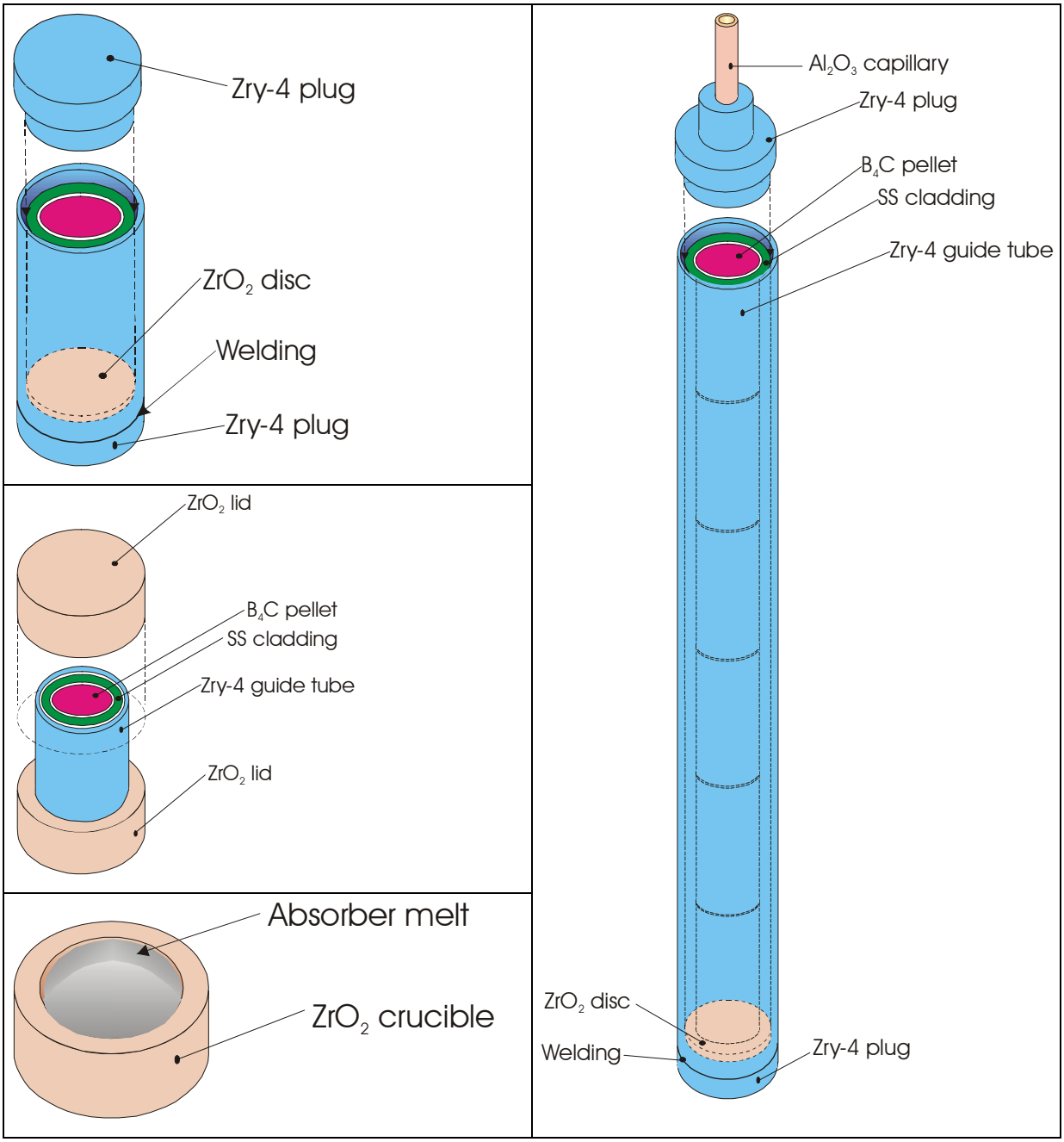

Figure 5: Specimens for control rod degradation and oxidation tests

The small specimens with metal plugs and the long specimen were designed in the same way. They were electron beam welded under vacuum. A zirconia disc was used to separate

the B_4C pellet and SS cladding from the Zircaloy plugs. Some of the long specimens were subsequently filled with helium to see the influence of inner pressure build-up. In addition, 1-pellet-size CR segments with ceramic caps were studied characterised by exactly the same mass ratio B_4C:SS:Zry-4 as for the commercial absorber rod.

The SS/B_4C/Zry-4 absorber melts were prepared in the LAVA furnace. Thin discs of the single materials were stacked in a shallow zirconia crucible and melted at temperatures between 1900 and 2100 °C. Tests with pressed powder mixtures were not successful. The specimens did not melt completely or they were characterised by a large void volume probably due to the high surface areas and the formation of protective oxide scales at the grain surfaces.

Finally, specimens for experiments on the eutectic interaction between boron carbide and stainless steel were performed with Framatome B_4C pellets and SS (AISI 304) hollow cylinders as illustrated in Fig. 31.

4 Test conduct

For oxidation tests the specimens were usually heated in an inert atmosphere (50 l/h at normal conditions, i.e. 0 °C and 1 bar, in the BOX, and 100 l/h in the QUENCH Rig) up to 800 °C. Then, the steam injection was switched on, usually with a flow rate of 30 g/h in the BOX and 100 g/h in the QUENCH tests and the specimens were heated to the desired temperature. Oxidising conditions were chosen relatively early during the heat-up phase to prevent degradation of the specimens as seen in tests under inert atmosphere (see chapter 5). Figure 6 shows as an example a typical test conduct of an isothermal oxidation experiment in the BOX rig. The injected steam mass flow rates were in a large surplus in comparison to the amount of steam consumed by the oxidation reaction, as can be seen from the both steam curves (injected, off-gas) in the diagrams. Thus, no steam starvation was expected to occur during these tests. The heating rate during the heat-up phase and in the transient tests was 20 K/min. The test conduct and results of the MS gas measurements of all tests are compiled in the appendix (A1-4, A13).

Experiments on the eutectic interaction between SS and B_4C were performed under inert conditions in the LAVA furnace. The specimens were heated at 1 K/s to the desired plateau temperature of 1250 °C and the heating was switched off at the end of the isothermal phase.

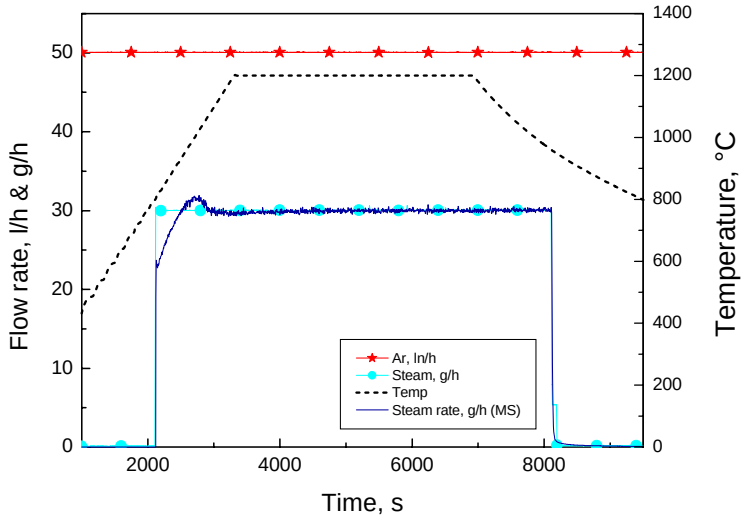

Figure 6: Typical test conduct of an isothermal test, here: at 1200 °C

5 Experimental results

In the following section the main experimental results of the various test series will be presented and discussed. The test parameters and the results of the MS gas analyses of all tests are compiled in the appendices A1-A4 (tables) and A13 (diagrams).

5.1 Transient tests with 1-pellet-size specimens under different atmospheres

To get a feeling for the behaviour of the control rod segments at high temperatures first tests were performed transiently between 800 and 1500 °C under oxidising and inert atmosphere. The degradation of the control rods is strongly dependent on the atmosphere (Fig. 7). The specimen completely degraded in inert gas due to the eutectic interactions between the stainless steel cladding and the Zircaloy guide tube as well as between stainless steel and B_4C. The specimen heated under oxidising Ar/steam flow did not fail due to the formation of an outer ZrO_2 oxide scale which kept the melt inside and prevented its relocation.

before test | after steam test | after inert test

Figure 7: B_4C control rod segments after transient tests between 800 and 1500 °C in oxidising and inert atmosphere

5.2 Isothermal test series with 1-pellet-size specimens with metal plugs

In an isothermal test series, specimens with metal plugs were kept at temperatures from 800 to 1700 °C for one hour in steam/argon atmosphere. Figure 8 gives an overview on the post-test appearance of the specimens and Fig. 9 shows axial cross sections of the samples.

1000 °C **1200 °C** **1400 °C** **1600 °C** **1700 °C**

Figure 8: Post-test appearance of the specimens after 1 h isothermal tests at the specified temperature

Up to 1000 °C no interactions at all took place between the components. At 1200 °C small interactions between SS and B_4C as well as between SS and Zircaloy-4 with local melt formation were observed. Significant melt formation was seen at 1400 °C and higher temperatures. The steel cladding was completely dissolved during these tests and the consumption of the boron carbide pellet due to the interaction with the metal melts increased with temperature. The formation of an outer ZrO_2 scale prevented the specimens from early failure. Only in the 1700 °C test, the scale failed after approx. 40 minutes leading to the access of steam to B_4C and absorber melt accompanied by a strong formation of CO and CO_2 and additional hydrogen, as can be seen in Fig. 10. As already seen in the experiments on the oxidation of pure B_4C [5], almost no methane is released during the high temperature oxidation of absorber melt.

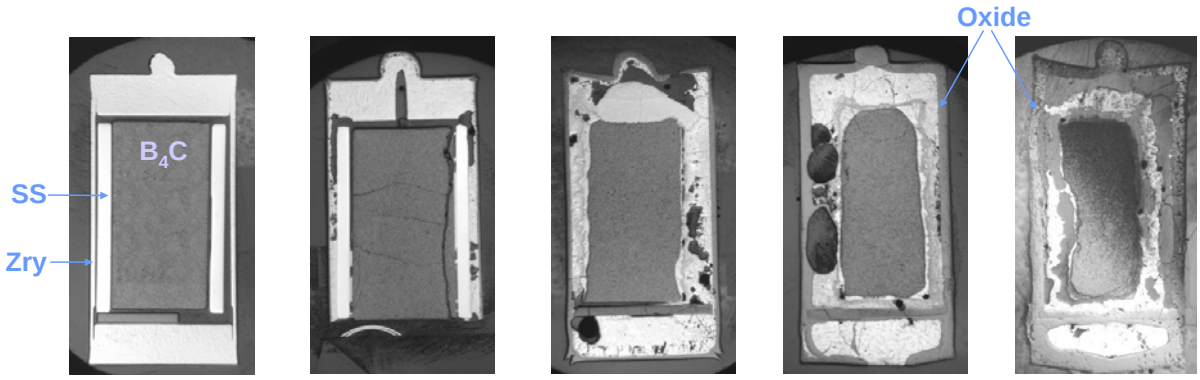

Figure 9: Cross sections of short B_4C control rod segments after isothermal tests for one hour at the specified temperature

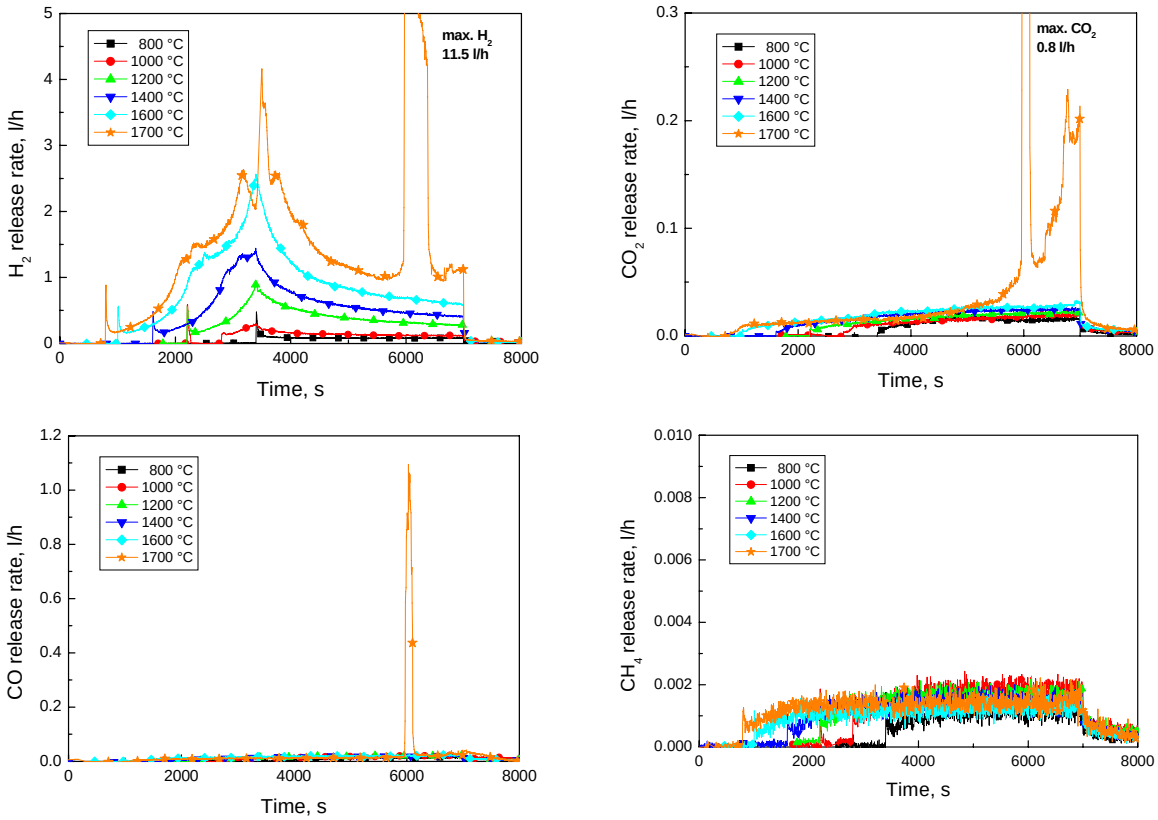

Figure 10: Gas release during isothermal oxidation of short B_4C control rod segments with metal plugs in steam

Extensive post-test examinations by light microscopy, scanning electron microscopy (SEM/EDX) and Auger analysis have been performed. The compilation of all these results is obtained in the appendix (A6, A7). Here some significant results of this work are discussed. So, Fig. 11 shows the beginning interaction between the single components of the control rod with local melt formation for the 1200 °C specimen. Liquid interaction layers are formed between Zircaloy and the still solid steel guide tube as well as between B_4C and steel. After the test at 1400 °C a complex multi-component, multi-phase mixture is enclosed in the gap between B_4C pellet and outer oxide scale (see also Fig. 13).

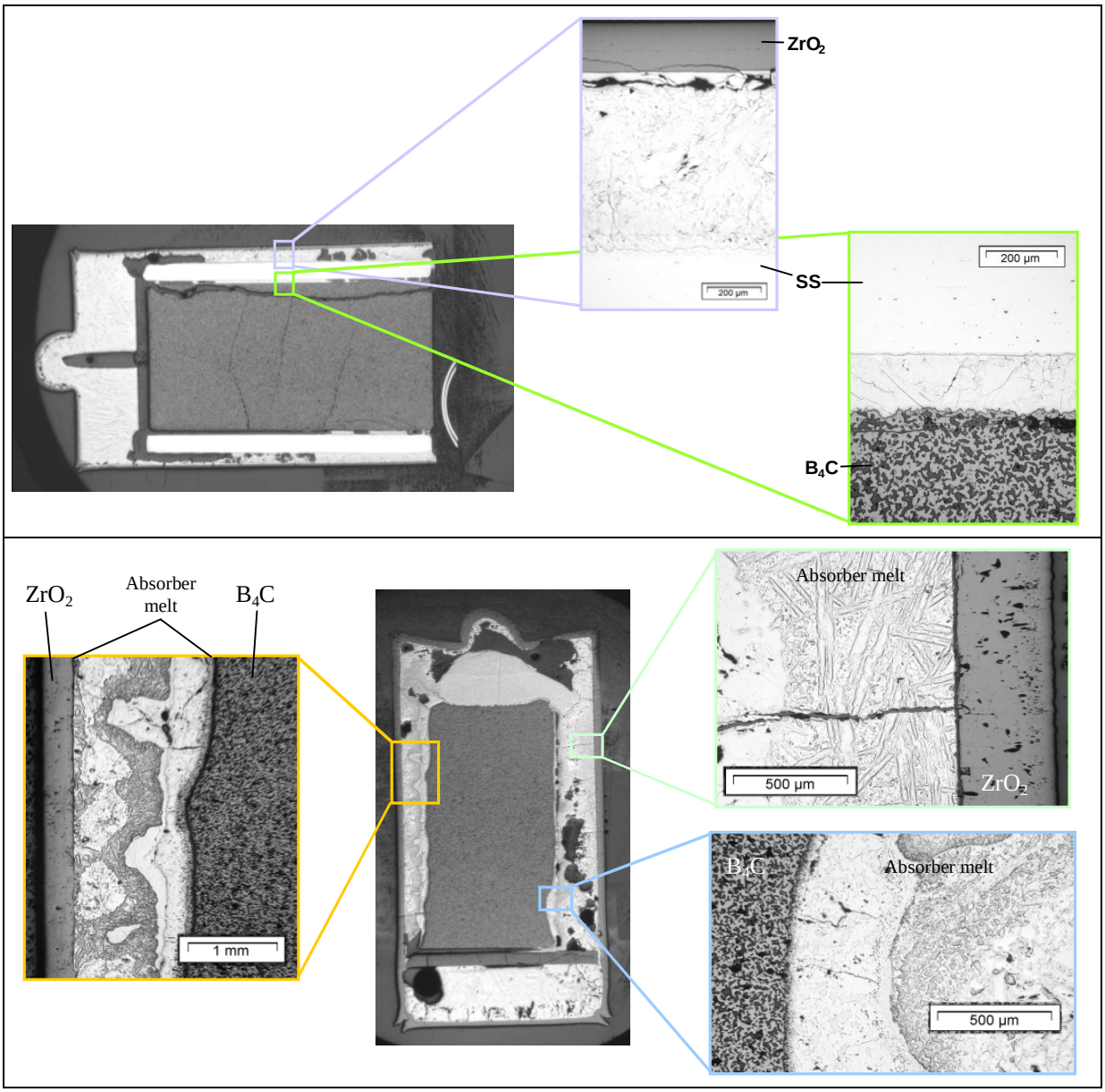

Figure 11: Metallographic post-test examination of the CR specimens after isothermal oxidation at 1200 (top) and 1400 °C (bottom)

Figure 12 shows EDX line-scans through the originally Zry/SS/B_4C arrangement after the tests at 1200 and 1400 °C. Both samples have two maxima of zirconium concentration, one at the outer surface of the specimens where an oxide scale was formed and one in the gap between stainless steel cladding and B_4C pellet. Obviously, Zircaloy (containing eutectic) melts filled the gap due to capillary forces from the top of the specimen where Zircaloy from the plugs was available.

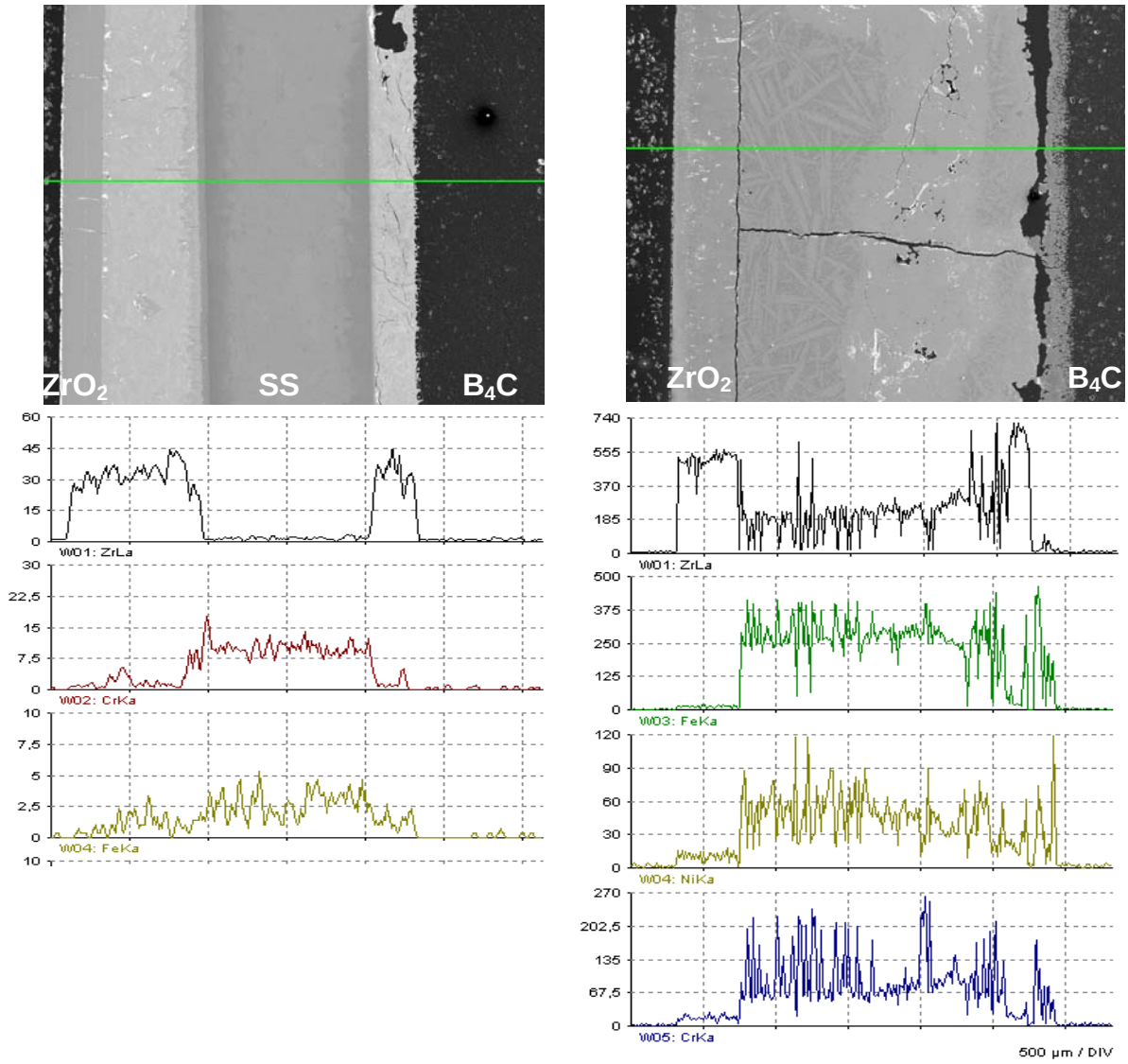

Figure 12: EDX line-scans through the sequence of layers in a control rod after isothermal tests at 1200 °C (left) and 1400 °C (right)

The most detailed results on the phase distribution were obtained by Auger analysis. The results are compiled in appendix A7. Here only a typical example of these analyses will be discussed. Figure 14 shows a detail of the solidified melt after the test at 1400 °C. At the left hand side of the magnified image boride phases of the steel components Fe, Cr, Ni are seen. Ni- and Cr- rich phases are separated from each other; this was also observed for the other specimens. The phase diagrams compiled in Annex A12 show a miscibility gap in the solid state in the Cr-Ni system whereas Fe-Cr and Fe-Ni are completely miscible. The boride phases of the steel components (especially of Ni) have relatively low melting points. The melting points of the zirconium boride and carbide are well above 3000 °C. So, it can be assumed that the round Zr carbide phases and the longish, sometimes needle-like Zr boride phases were formed during the test at temperature. These kinds of phases were found in all specimens with melt formation as can be recognised in the many images in the appendix as well as in Fig. 13.

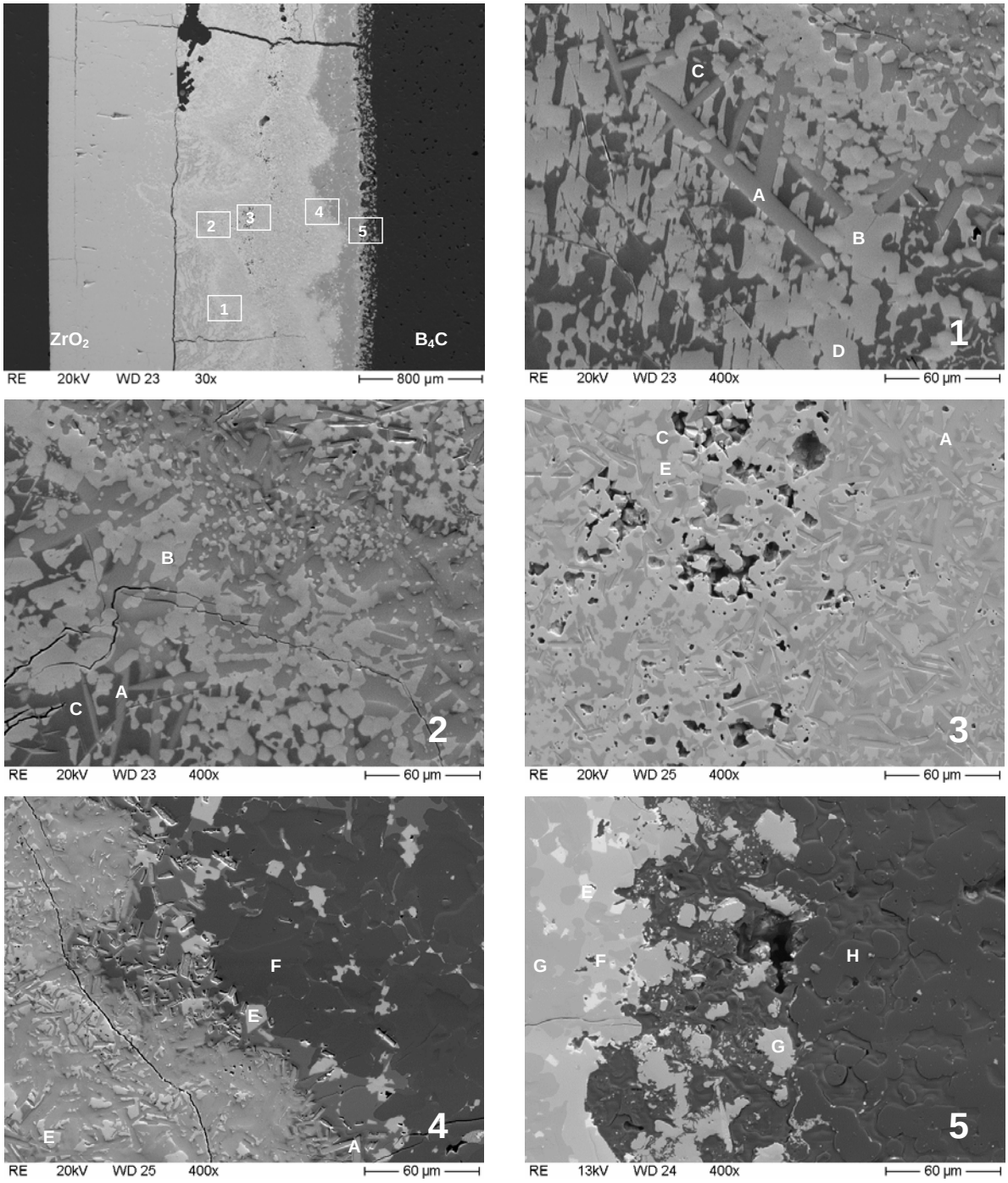

Figure 13: SEM images of the CR specimen after 1 h isothermal oxidation at 1600 °C illustrating the multitude and complexity of phases in the solidified melt

Analysed phases: A) ZrB_2, B) M-Zr-C, C) Fe-Cr, D) M_3C+B, E) $Zr(B, C)_2$, F) M_2B, G) MB(+ dissolved C), H) B_4C
with M=(Fe, Cr, Ni)

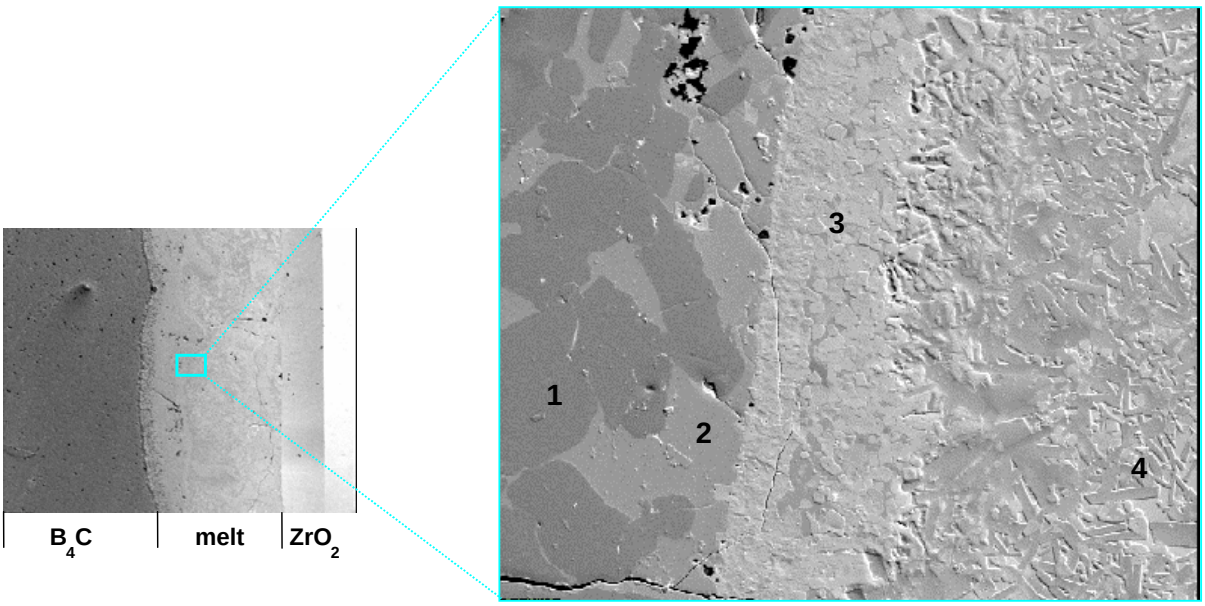

Figure 14: Phase composition of the solidified melt in the gap between B_4C pellet and outer oxide scale after 1 h isothermal test at 1400 °C under steam:
1: (Fe, Cr) boride, 2: (Fe, Ni, Cr)$_2$ boride, 3: Zr (oxo-)carbides, 4: Zr boride in metal matrix

5.3 Isothermal test series with 1-pellet-size specimens with ceramic caps

A second isothermal test series was conducted with specimens of a different design, namely with ceramic caps instead of metal plugs. These more simple specimens have the same mass ratio of the three components B_4C, stainless steel and Zircaloy as the whole rod, which is one advantage in comparison with the first type of samples.

In contrast to the first isothermal series the failure of the outer oxide shell occurred already at 1500 °C (Fig. 15) and was accompanied by a very rapid, almost explosive reaction of the absorber melt and/or the remaining boron carbide pellet with steam. After the test at 1600 °C, only the oxide shell and a small globular piece of metal was left. Huge amounts of hydrogen, CO and CO_2 as well as boric acids were produced during that period as can be seen from the Figures 16 and 17. No methane CH_4 was produced during all tests. The melt was sprayed to the top of the reaction tube of the BOX Rig during the second test at 1500 °C (20610). The specimen shifted within the alumina boat and a lot of condensed boric acids was found at the outlet flange of the reaction tube. The off-gas pipes were blocked by the boric acids, therefore, mass spectrometric measurements were not possible anymore after that phase in the test at 1600 °C. The second test at 1500 °C was prematurely finished after failure of the oxide shell to prevent further strong formation of boric acids leading to problems with the test rig.

The hydrogen release rates increased by a factor of 30 after failure due to the rapid reaction of B_4C containing melt as it is shown in Fig. 17. Figure 18 compiles the masses of boron carbide oxidised during all tests with 1-pellet-size specimens (metal plugs, ceramic caps) based on the total release of carbon monoxide and dioxide (neglecting possible oxidation of

the carbon coming from the steel). According to this, between 30 and 50 % of the B_4C pellet were consumed by the oxidation reaction. The real values may be even higher, having in mind that the MS measurement was affected in the late phase in some of these tests due to the (partial) blockade of the off-gas system.

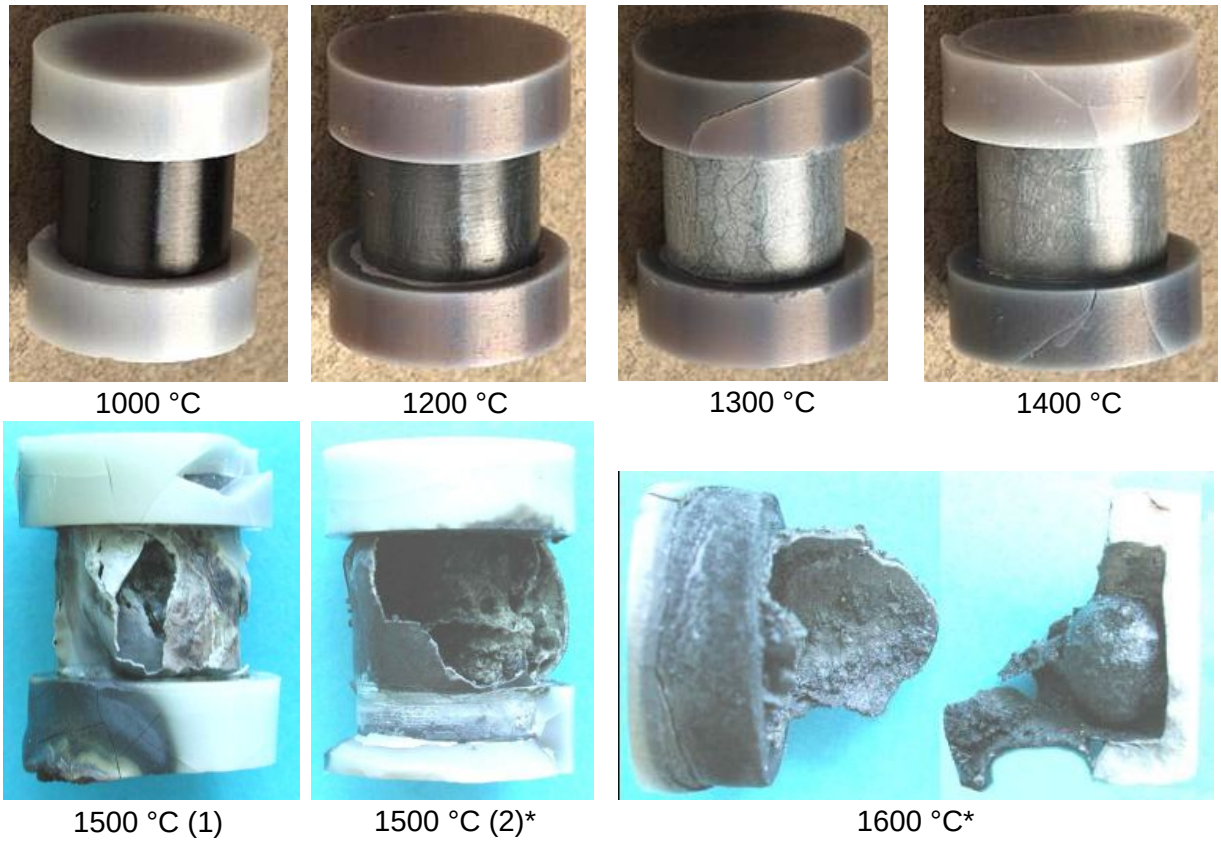

Figure 15: Post-test appearance of the specimens with ceramic caps after 1 h isothermal tests at the specified temperatures under flowing Ar/steam atmosphere.
* *The second test at 1500 °C and the test at 1600 °C were prematurely finished*

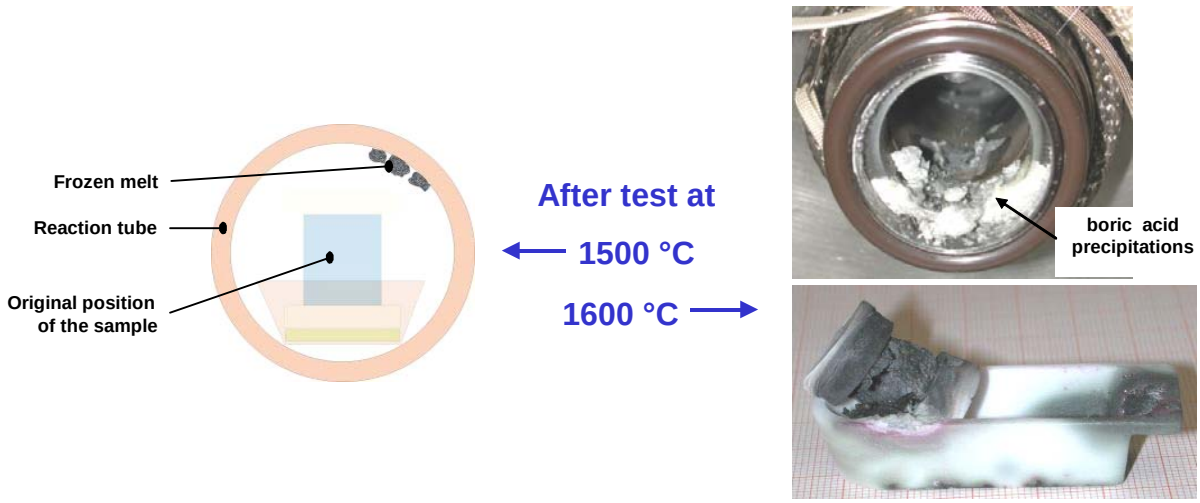

Figure 16: Post-test appearance of furnace and specimens after failure of the control rod segments during tests at high temperatures, showing results of rapid reactions with melt splashing in the reaction tube, relocation of the specimen during the test, and huge precipitations of boric acids at the outlet of the reaction tube flange.

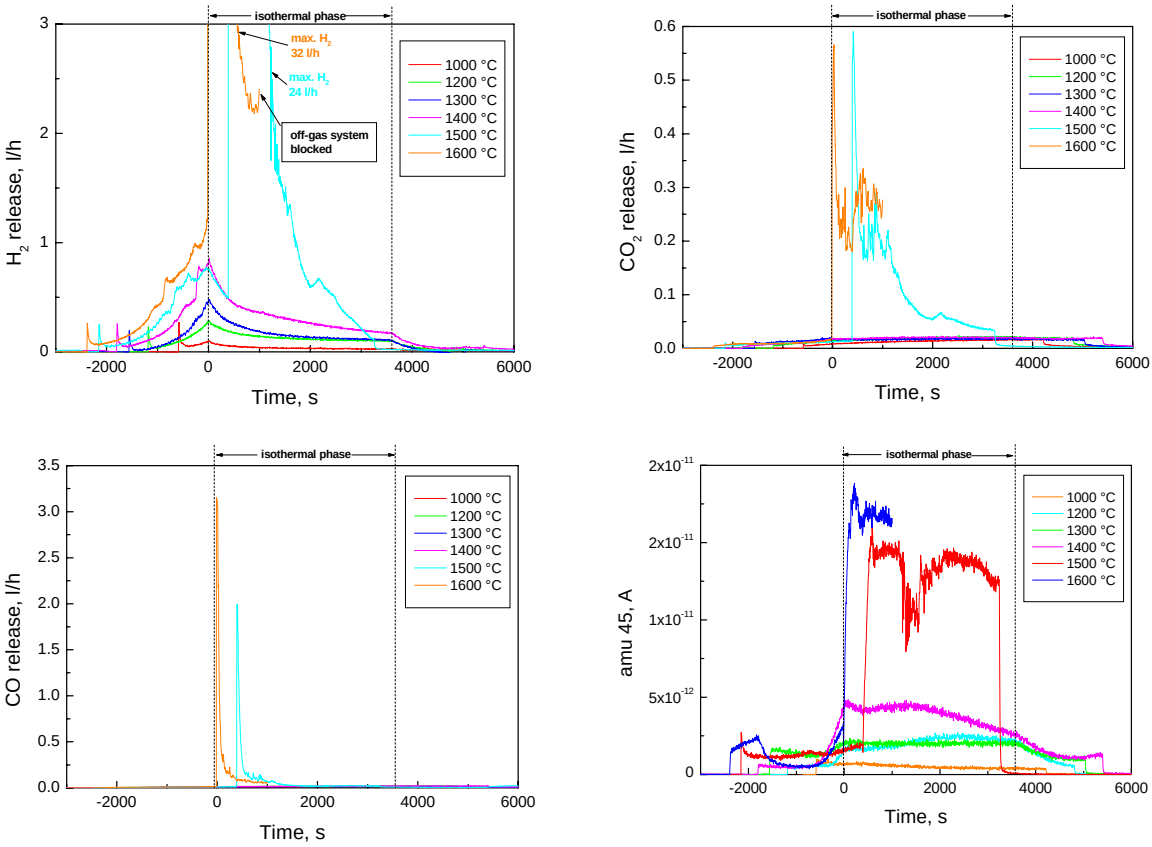

Figure 17: Gas and boric acid release during isothermal tests at the specified temperatures in Ar/steam atmosphere.

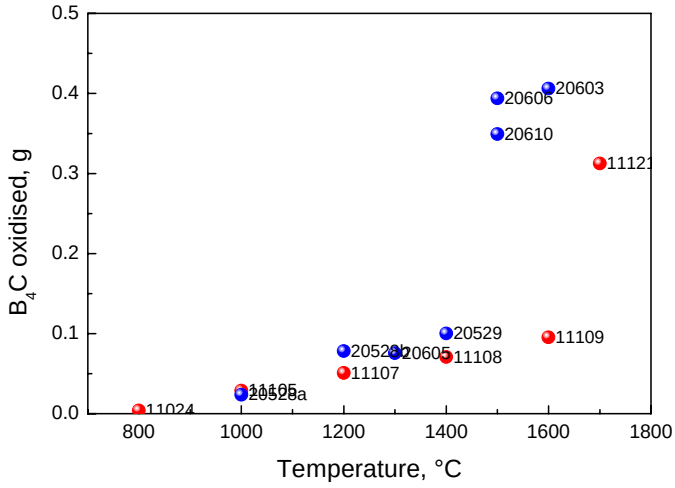

Figure 18: Mass of boron carbide oxidised during the isothermal tests of 1-pellet-size specimens with metal plugs (red symbols) and ceramic caps (blue symbols). The mass of a fresh B_4C pellet is around 1 g.

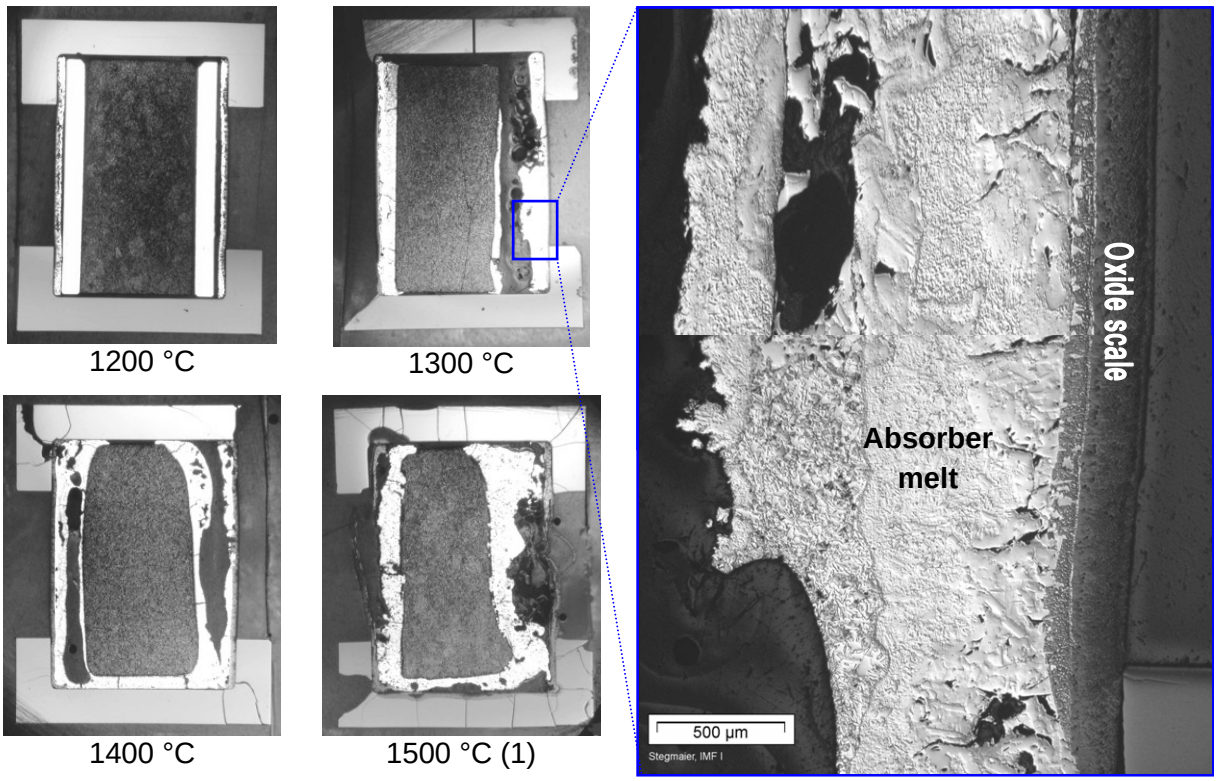

Figure 19: Cross sections through specimens with ceramic caps after 1 h isothermal oxidation at the specified temperature in Ar/steam flow.

The magnified image of the 1300 °C specimen illustrates the formation of an oxide scale acting as a crucible for the absorber melt

The polished cross sections of the specimens with ceramic caps (Fig. 19) look similar to the specimens with metal plugs. After 1 hour at 1200 °C the single components of the control rod segments interacted only slightly. No melt formation was observed after this test. At 1300 °C and higher temperatures the stainless steel cladding was completely liquefied due to the eutectic reactions with B_4C and Zircaloy. The microscope images (see appendix A8) show many different phases which were identified by Auger analysis (see appendix A9).

Near the B_4C pellet a (Fe, Cr)B / $(Fe, Cr, Ni)_2B$ (matrix) mixture is predominant in all specimens. ZrC and Zr(C, O) was also found in this region. These phases were preferably observed in a SS matrix near the external ZrO_2 oxide scale. A clear separation between Cr and Ni (containing phases) was seen at all specimens. Sn enrichment was found in Ni phases. Further phases identified were NiB, CrC_2, ZrB_2 as well as $Zr(B, C)_x$ and $Zr(B, C, O)_x$. The diffusion of the elements and/or convection of the melt increased with increasing temperature. So, on the one hand the oxygen content near the B_4C pellet and on the other hand the boron and carbon concentrations near the ZrO_2 scale increased with temperature. There, B was predominantly found in the metal phase (SS borides) and C in the oxide phase

(Zr(O ,C)). The overall amount of boron in the melt increased with temperature indicating a higher dissolution. Chromium enriched near the B_4C pellet, especially at higher temperatures.

5.4 Tests with 10-cm specimens in the QUENCH Rig

Fourteen tests were conducted with 10-cm long specimens which were inductively heated in the single rod QUENCH Rig. The first three tests were performed with specimens kept in position by a Zircaloy capillary tube from the top. After break of the specimens they fell down and could not be heated anymore. That's why a new sample support was constructed (Fig. 3) which keeps the specimen in position also after failure and allows further heating. The first two tests were conducted in inert atmosphere, all other tests in Ar/steam. All test parameters are summarised in table A2 and annex A13.

The specimens were electron beam welded under vacuum. Thus, they were originally "filled" with vacuum which supported a close contact between the components of the control rod segment during annealing. Some of the specimens were subsequently filled with helium at normal pressure to investigate the influence of pressure build-up during heat-up on degradation and failure of the specimens.

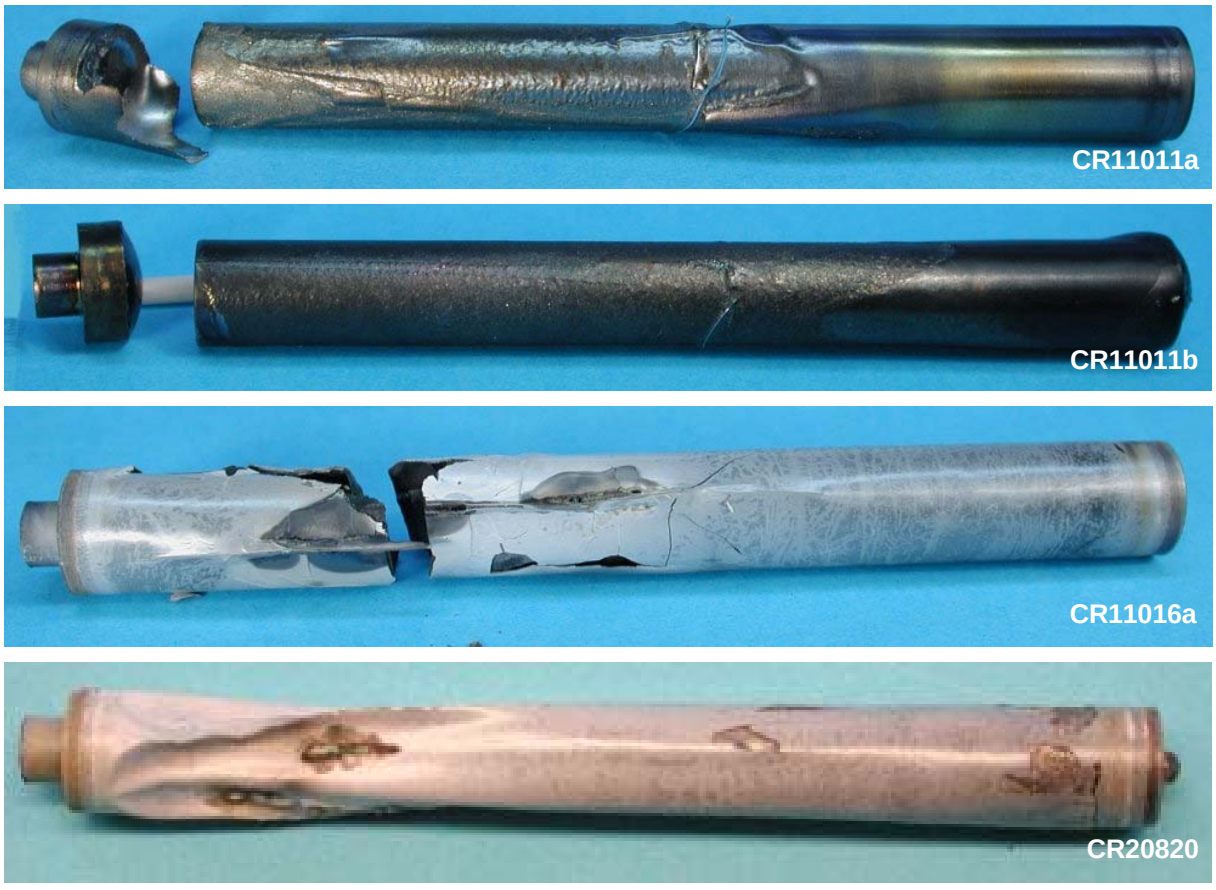


CR20822


CR20826a


CR20826b

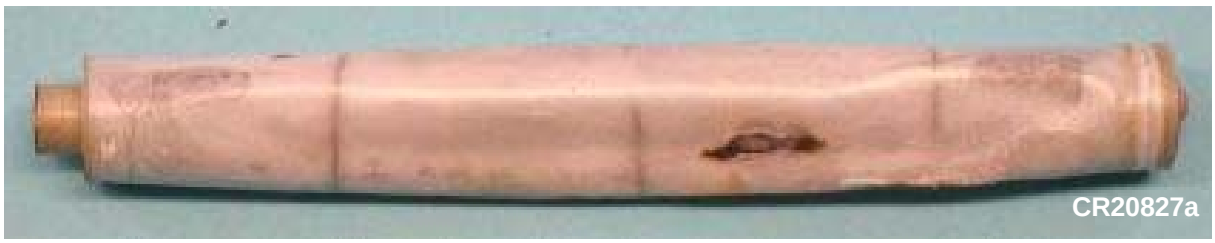
CR20827a


CR20827b


CR20828a

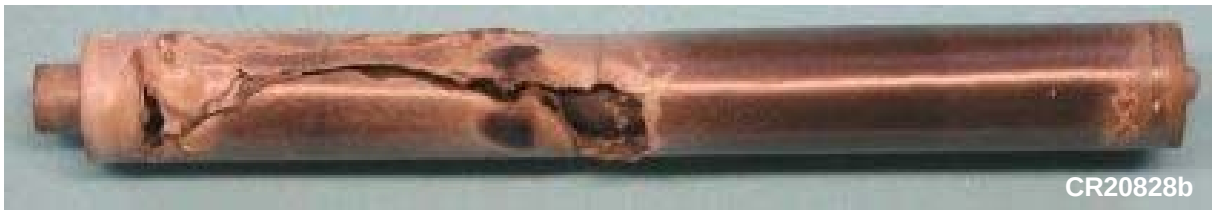
CR20828b


CR20829a

Figure 20: Post-test appearance of the 10-cm control rod specimens after transient and isothermal tests

Figure 20 gives an overview on the post-test appearance of all specimens. The two specimens heated under inert atmosphere, especially the first one (CR11011a), reveal melt formation and relocation at relatively low temperatures even from the outside. The ZrO_2 oxide scale formed during the tests under steam flow protects the B_4C pellets and absorber melt formed inside from steam access as long as it is intact. Only after failure of the oxide shell (break, dissolution by absorber melt from the inside) oxidation of boron carbide takes place locally near the position of the oxide failure as can be seen from the axial cross sections of the specimens (Fig. 21) This is also confirmed by the MS gas analyses (Table A5, Fig. 22). The eutectic melt relocated downwards inside the annulus between pellet and oxide shell. It partially also filled the gaps between the boron carbide pellets which is an indication for the low viscosity of the melt.

The image of the specimen after test CR11011a which was finished at relatively low temperatures (pyrometer 1040 °C, TC 1270 °C) clearly shows the initially local character of the interaction between the stainless steel cladding and the B_4C pellet. The stainless steel cladding completely melted/reacted in almost all other specimens. Only after the isothermal tests CR20827b and CR2029b at lower temperatures (1270 °C) some residuals of the cladding were observed in the lower half of the samples.

Like for the tests with the 1-pellet-size specimens, the solidified melt is a complex mixture of many phases which were here not further examined. Fig. 23 shows one example of solidified melt with carbide and boride phases.

The temperature of the failure (i.e. the temperature when significant release of CO and CO_2 was observed) is between 1470 and 1580 °C which is in accordance with the results obtained with the small specimens. No significant difference between vacuum and helium filled specimens was observed except for the post-test macroscopic appearance of them.

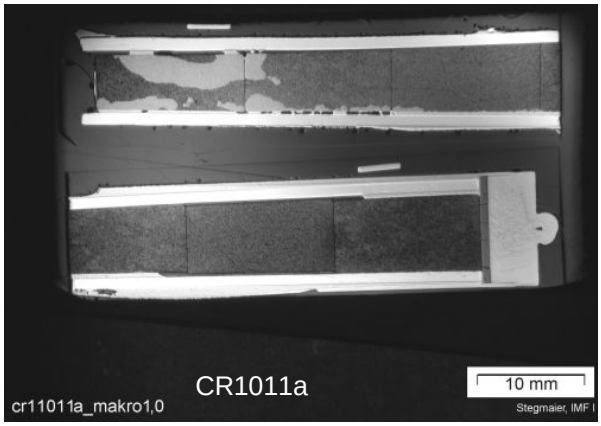
CR1011a
10 mm
cr11011a_makro1,0
Stegmaier, IMF I

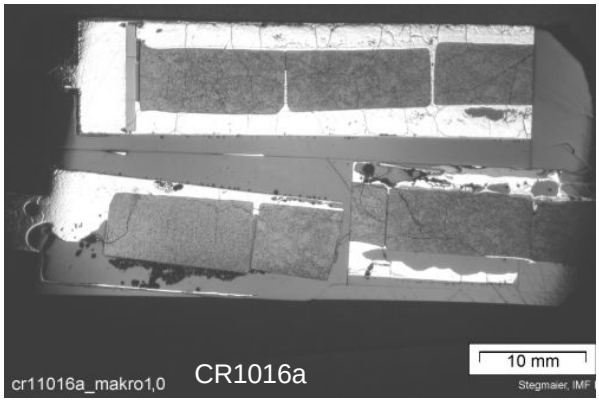
cr11016a_makro1,0
CR1016a
10 mm
Stegmaier, IMF I

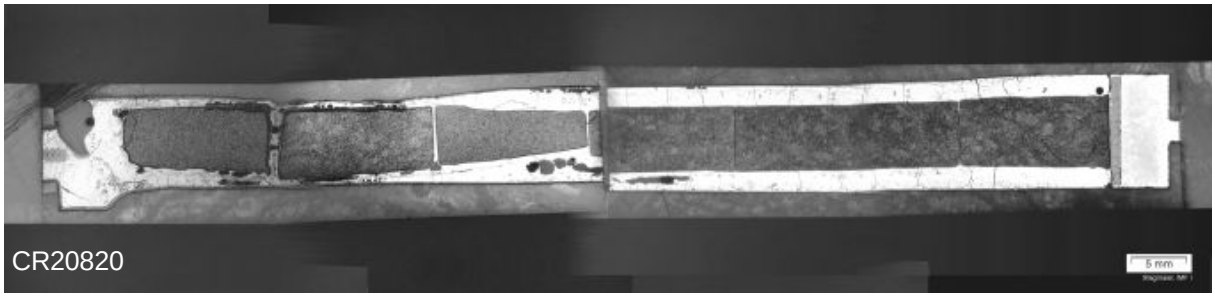
CR20820
5 mm

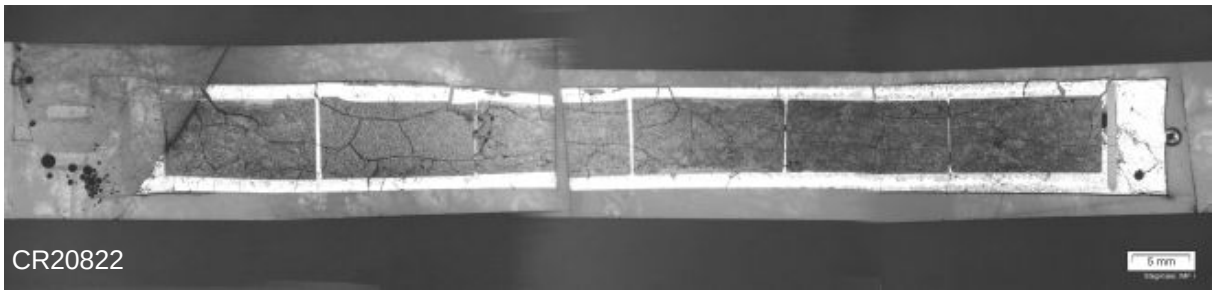
CR20822
5 mm

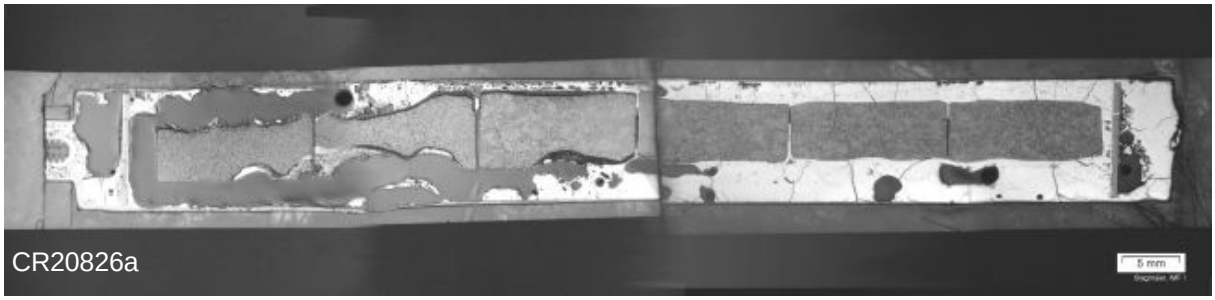
CR20826a
5 mm

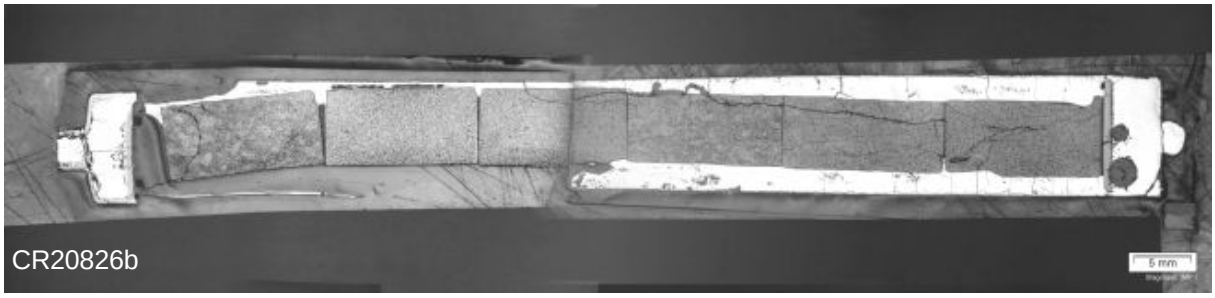
CR20826b
5 mm

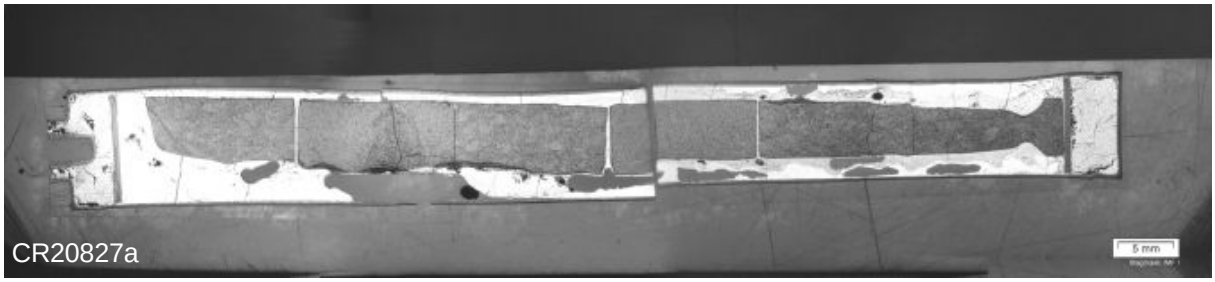
CR20827a
5 mm

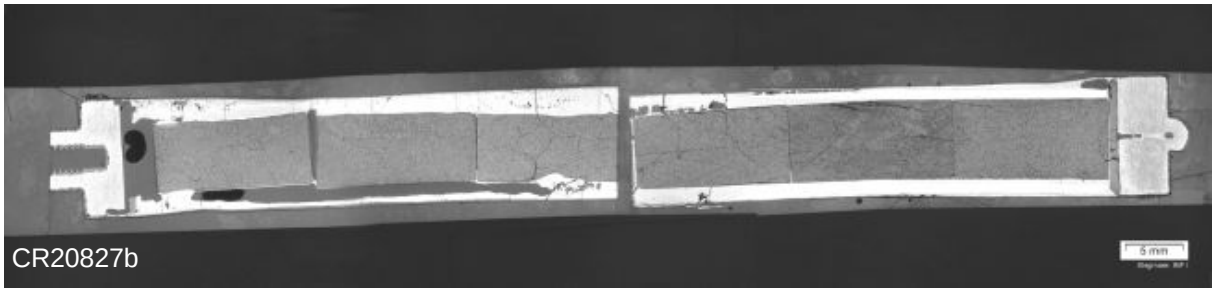
CR20827b
5 mm

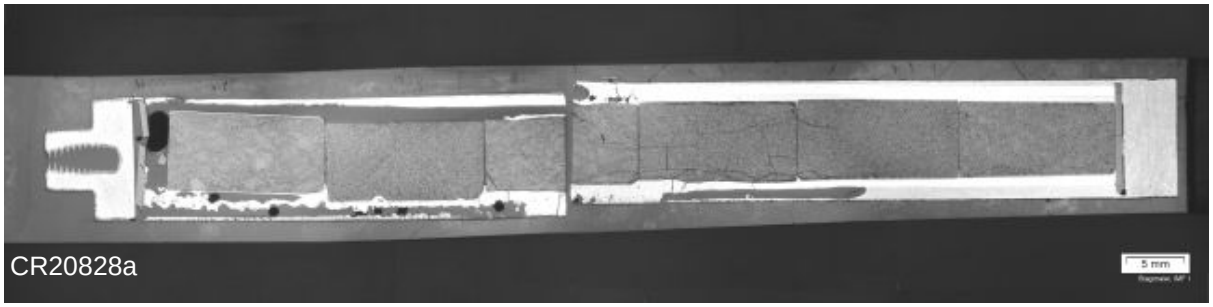
CR20828a
5 mm

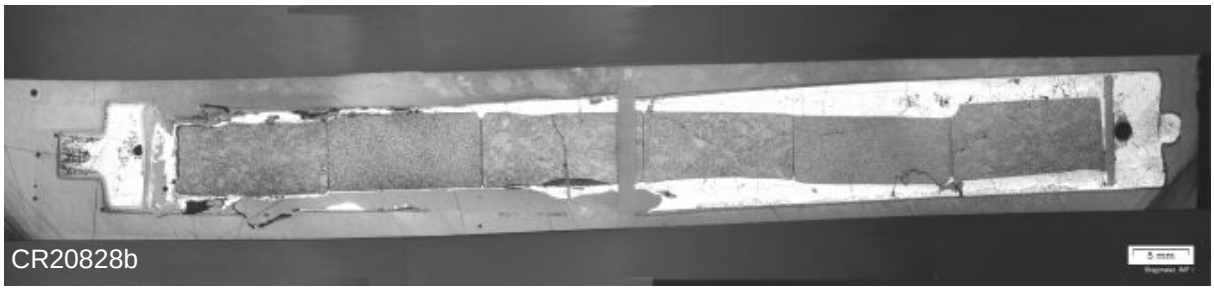
CR20828b
5 mm

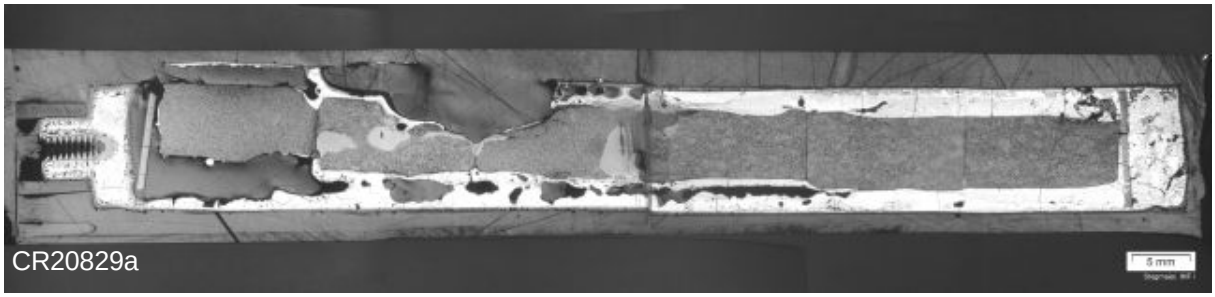
CR20829a
5 mm

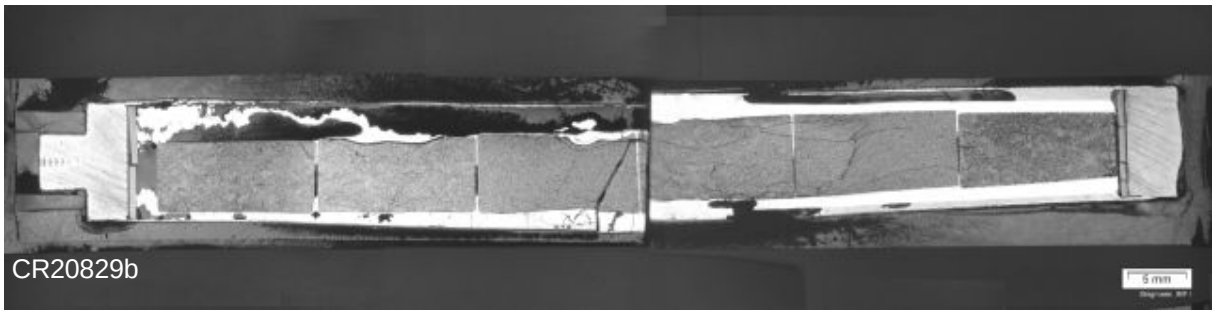
CR20829b
5 mm

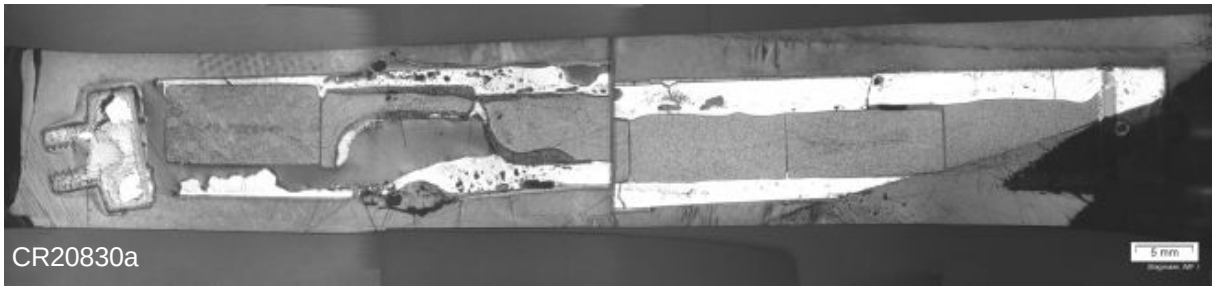

Figure 21: Axial cross sections of the 10-cm control rod segments

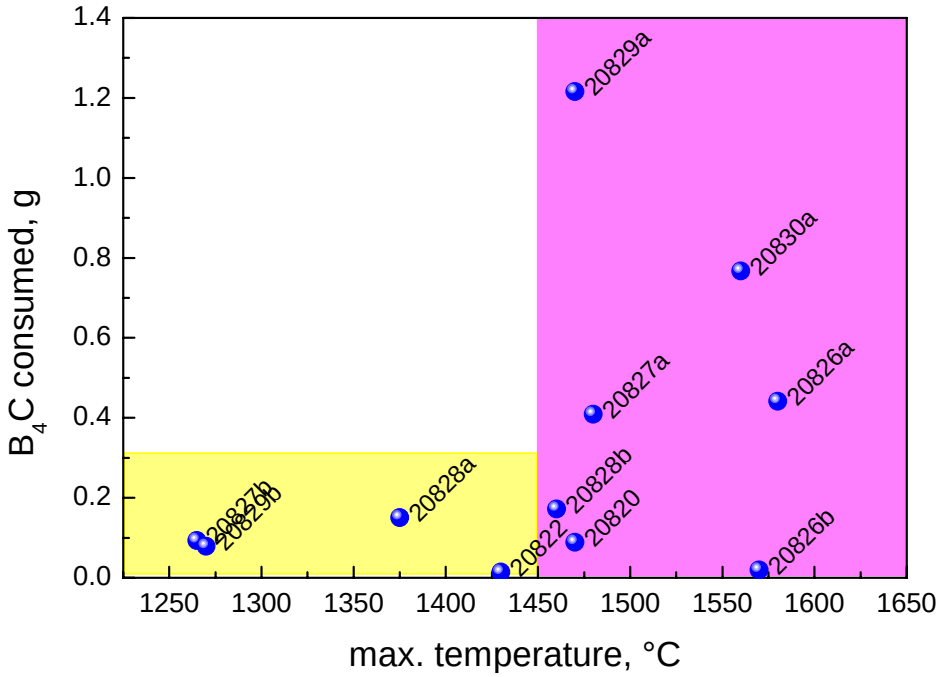

Figure 22: Boron carbide oxidised vs. maximum temperature (measured by pyrometer) during tests with 10-cm control rod segments based on the release of CO and CO_2. Failure of specimens occurred only above 1450 °C

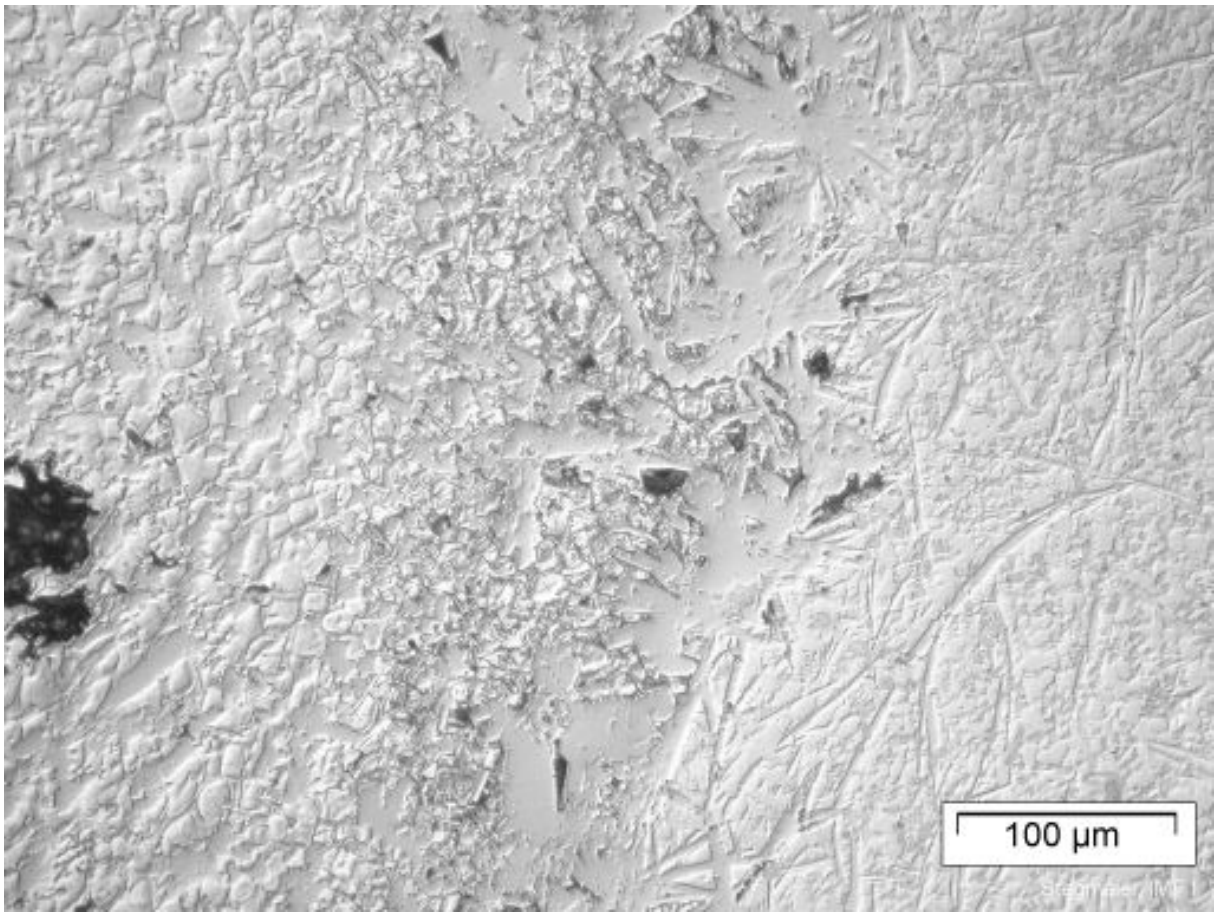

Figure 23: Solidified absorber melt with carbide (left) and boride (right) phases in metal matrix; specimen CR20830a

5.5 Oxidation of SS/B_4C/Zry-4 absorber melts

After investigations on the oxidation kinetics of pure boron carbide [5] and on the degradation of various B_4C control rod segments discussed in this report the oxidation behaviour of the resulting absorber melts was of interest. So far, no data were available on the oxidation of such kind of melts. The composition of these melts was derived from the analyses of eutectic melts formed in the control rod tests. Table 1 gives an overview on the composition of investigated specimens. Tests with the pure materials stainless steel and Zircaloy-4 were additionally conducted for comparison reasons. For the same reason, test Box00823 with pure B_4C which was performed under very similar conditions was taken into account.

The melts were prepared in the inductive LAVA furnace under inert atmosphere. Thin slices of the base materials were stacked in a shallow zirconia crucible and annealed at temperatures between 1900 and 2200 °C for about 10 minutes. Pre-tests had shown that this method gives better results than the annealing of pressed powder mixtures (Figs. 24-26).

Two specimens were prepared for each composition to allow a comparison between micro-structures before and after oxidation tests. The annealing temperatures were slightly different for the various compositions; they are compiled in the appendix A10.

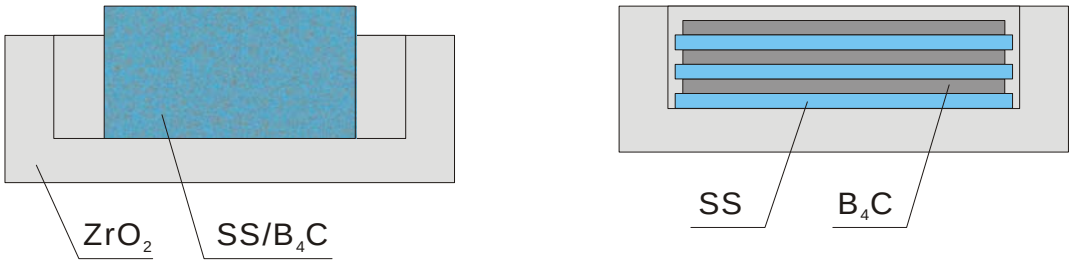

Figure 24: Preparation of absorber melts in the LAVA furnace using pressed powder mixtures (left) and stacks of thin slices (right).

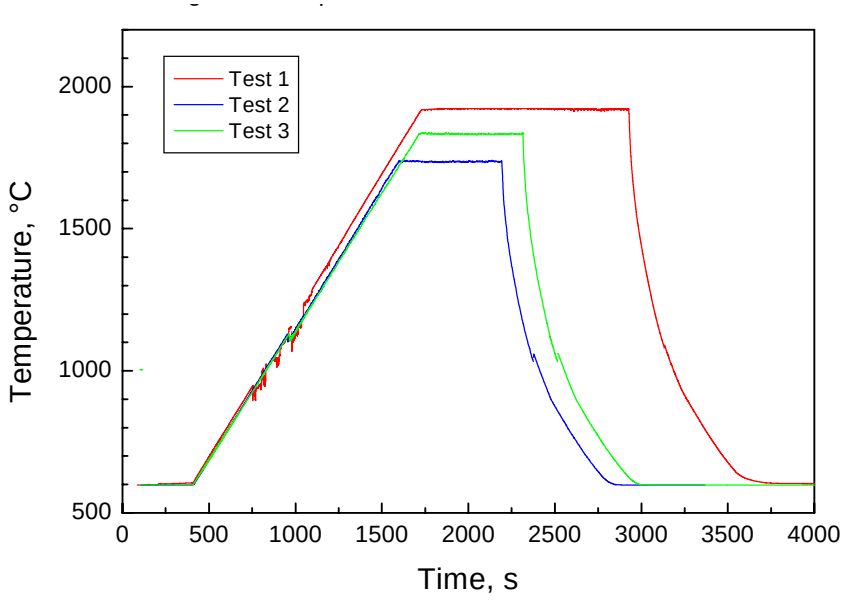

(Test1)
strong interaction
between absorber
melt and crucible

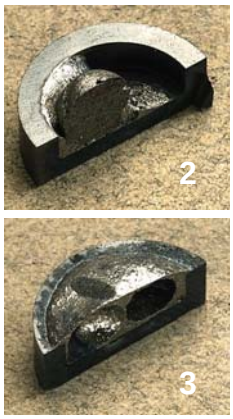

Figure 25: Pre-tests for preparation of absorber melts using powder mixtures. The specimens were either incompletely molten or had large voids.

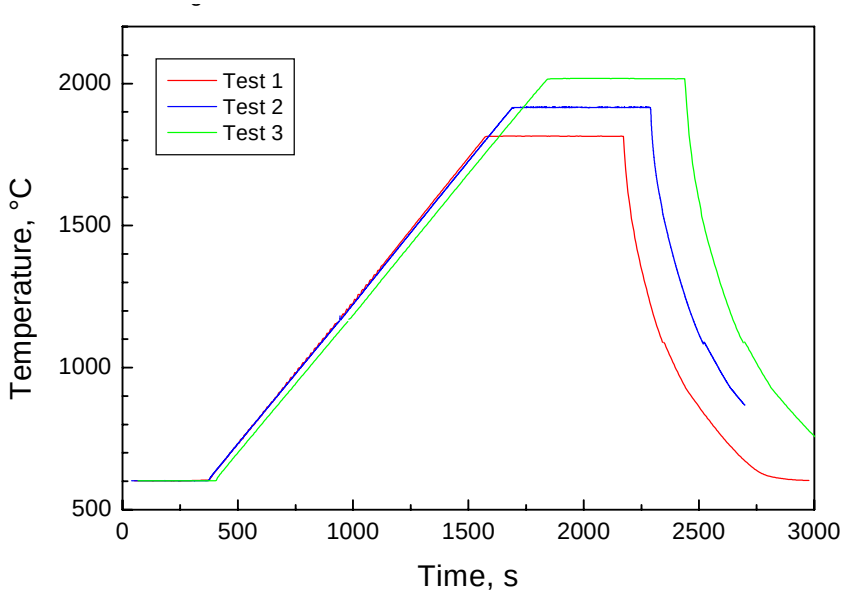

Figure 26: Pre-tests for preparation of absorber melts using stacks of thin slices of the starting materials. Good results were obtained at 1800 and 1900 °C.

Table 1: Composition of absorber melts for oxidation tests

No.	B_4C wt-%	SS wt-%	Zry wt-%	Oxidation test
1	0	100	0	21108
2	5	95	0	21111
3	10	90	0	21119a
4	20	80	0	21113
5	30	70	0	21119
6	9	81	10	21114
7	7	63	30	21120
8	0	70	30	21121
9	0	0	100	21125
10	100	0	0	00823*

** release rates of H_2, CO, CO_2 divided by 3 to take into account the larger surface of the B_4C pellet in comparison with the melt specimens*

The oxidation tests were performed in the BOX Rig. The specimens were heated in inert atmosphere (50 l/h Ar) up to 800 °C, then steam at a rate of 30 g/h was switched on and the specimens were heated to 1550 °C with 20 K/s. The cool-down again took place in inert atmosphere. The test diagrams of all experiments performed are compiled in the appendix A13; the parameters are compiled in table A3.

The composition of the melt sample, especially its melting point has a strong influence on the oxidation kinetics and thus on gas release as it is shown in Fig. 27. Pure boron carbide and pure Zircaloy which are in the solid state during the whole test have relatively low and smooth oxidation rates. The same is true for steel up to its melting at about 1410 °C. After melting the oxidation rate steeply increases and becomes more unstable. Due to eutectic interaction the melting of the mixed absorber melts occurs at lower temperatures which leads to significantly higher oxidation rates at lower temperatures. So, the first peak gas production in test CR21111 (5% B_4C, 95% SS) was measured at 1170 °C. The maximum oxidation rates of the melts are by more than one order of magnitude higher than the oxidation rates of solid materials at the same temperatures.

The rates are strongly scattering due to the formation of inhomogeneous and unstable oxide scales. Additionally, this unstable behaviour can be caused by the rapid local oxidation connected with spraying and fragmentation of melt, as can be seen in Fig. 29 from the post-test appearance of the crucibles. Small fragmented melt particles offer a large surface to the steam and are consumed very rapidly.

Furthermore, there is the tendency of lower oxidation rates with increasing amount of B_4C and Zircaloy in the steel (Fig. 28). It is assumed that the content of solid phases in the melt

increases which causes a rise of the viscosity of the mixture and impedes convection in the melt.

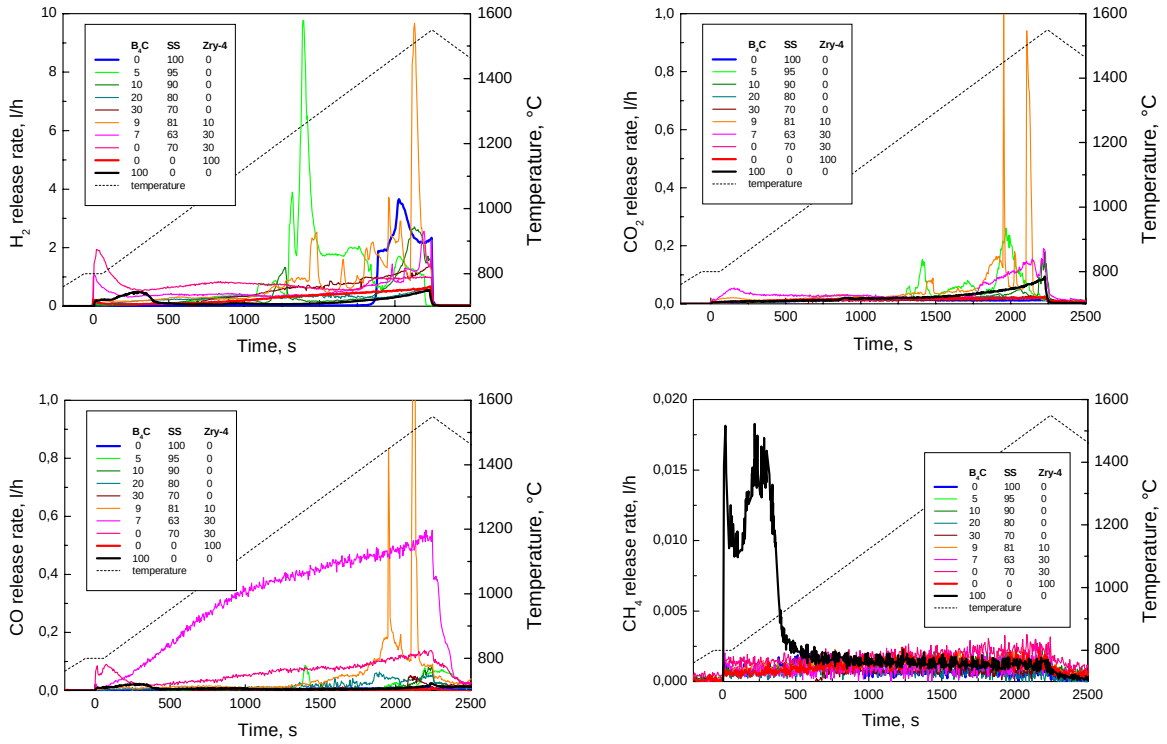

Figure 27: Release of H_2, CO_2, CO and CH_4 during transient oxidation of absorber melts in Ar/steam. The pure compounds are plotted with bold lines for comparison

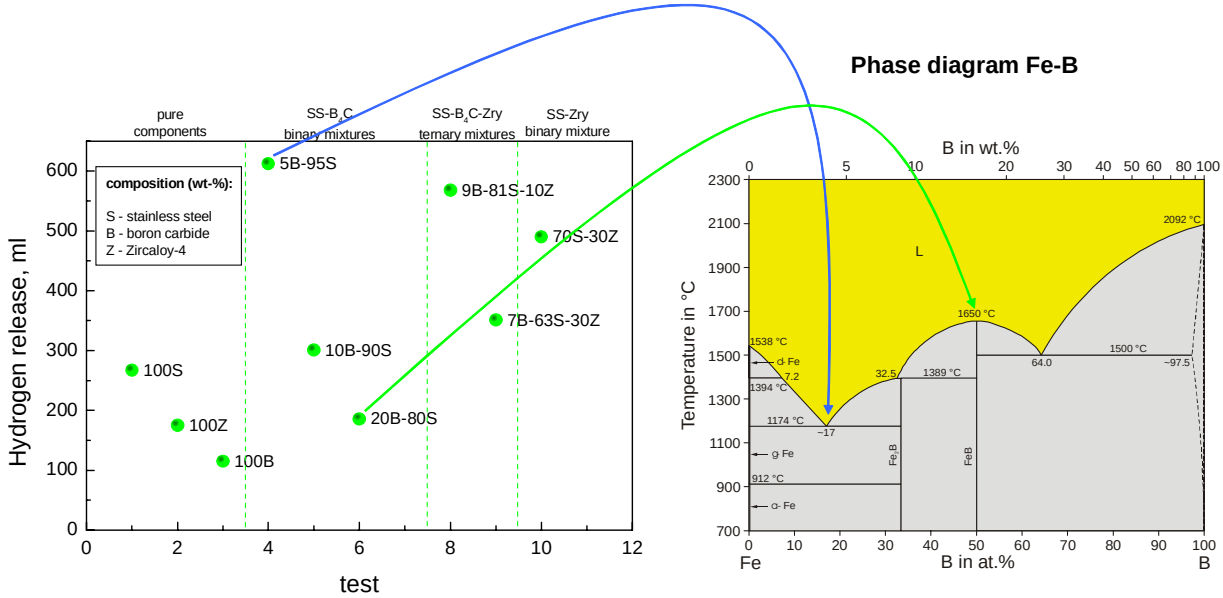

Figure 28: Integral hydrogen release during oxidation of pseudo-binary and pseudo-ternary absorber melts as well as of the pure components during transient oxidation in steam (left) and phase diagram Fe-B (right)
Note: For better understanding, test number is not equivalent with melt number

The CO/CO_2 ratio increases with increasing content of Zircaloy in the mixture due to the strongly reducing properties of the zirconium alloy. (The very high amount of CO measured during oxidation of melt #7 is obviously the result of an erroneous measurement.) The production of methane is negligible for all tests; only at the initiation of the oxidation of pure B_4C a small but measurable CH_4 release was observed.

Figure 29: Alumina boat with absorber melt specimens after oxidation tests showing splashing of melt and strong interactions between melt and crucible. Left: melt 2, right: melt 6.

Figure 30 shows the cross sections of all melt specimens after preparation and after oxidation. Although the wetting of the melts changes with composition there is almost no interaction between melt and zirconia crucible under inert conditions even at temperatures above 2000 °C. Metallographic post-test examinations by SEM/EDX of these melts before and after oxidation tests are compiled in the appendix A11. Under oxidising conditions the interaction between melt and crucible is even strong at the lower temperatures (800 to 1550 °C, 20 K/min) and becomes more intense with increasing complexity of the melt. The degradation of the crucible seems to be driven by the formation of zirconium oxo-carbides and eutectic interactions between ZrO_2 and Fe_2O_3 (see appendix A11).

The oxidation of the melts is obviously not controlled by the formation of a protecting oxide scale which is one reason for the high oxidation rates discussed above. In the pseudo-binary system SS-B_4C the highest oxidation was obtained for the sample with the lowest boron carbide content. This composition is near to the eutectic one (e.g. the phase diagram Fe-B shows the lowest eutectic temperature for 17 at-% B or approx. 4 wt-% B, see Fig. 28). With increasing content of B_4C in the mixture its composition goes away from the eutectic one and the melting temperature increases causing a lower oxidation. So, the melt with 20 wt-% B_4C corresponds to the composition of iron boride FeB in the binary phase diagram Fe-B with a melting point of 1650 °C. The shift of melting temperatures with increasing B_4C content is confirmed by their estimation on the basis of the time of rapid transition from low to higher gas release rates given in table A6.

All Zr containing melts are completely oxidised. They attacked the (Y_2O_3 stabilised) ZrO_2 crucibles most aggressively.

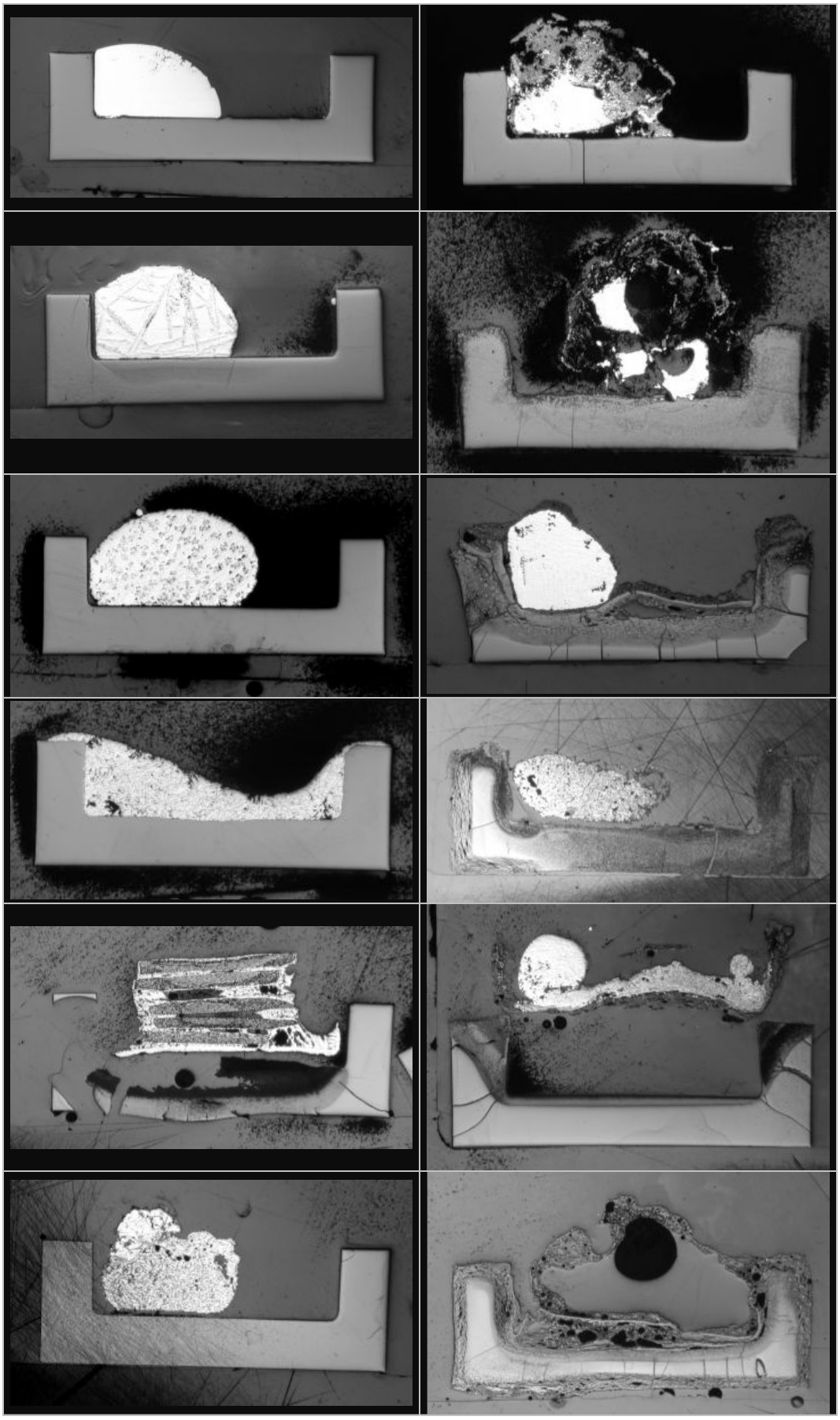
0 B_4C
100 SS
0 Zry
#1
5 B_4C
95 SS
0 Zry
#2
10 B_4C
90 SS
0 Zry
#3
20 B_4C
80 SS
0 Zry
#4
30 B_4C
70 SS
0 Zry
#5
9 B_4C
81 SS
10 Zry
#6

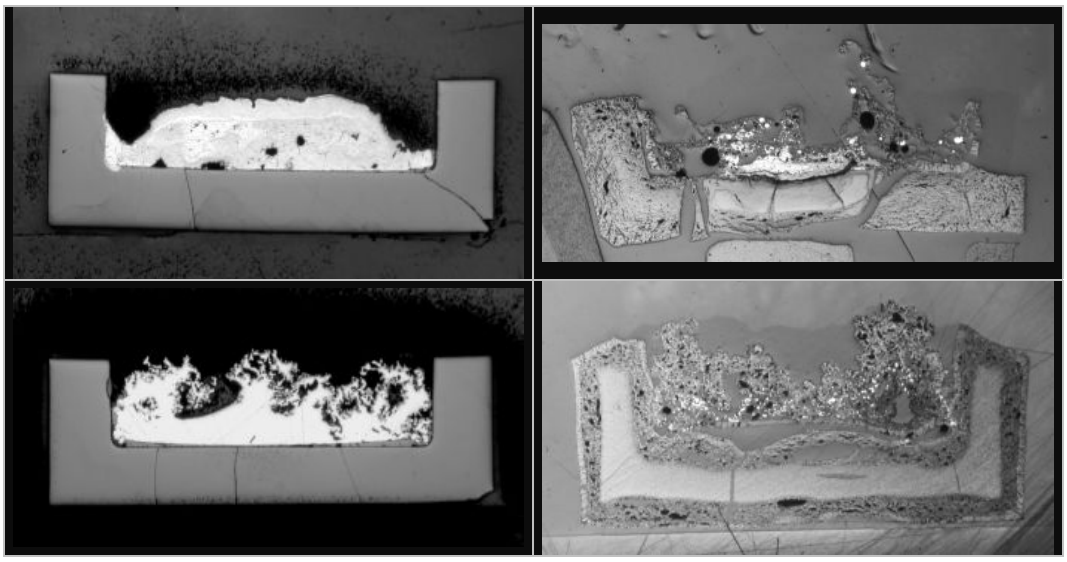

Figure 30: Cross sections of absorber melt specimens before (left) and after (right) transient oxidation between 800 and 1550 °C in steam

Note: The parameters for the preparation of melts #5;6;7 were not identical for the both specimens, the oxidised sample was prepared at higher temperatures to ensure complete melting (see appendix A10)

5.6 Tests on liquefaction of stainless steel by boron carbide

In the previous chapters it was demonstrated that above around 1250 °C fast and complete liquefaction of the stainless steel absorber rod cladding takes place without complete or even considerable consumption of the boron carbide pellets. Therefore, the question arose, how much steel can be liquefied by the eutectic interaction with B_4C about 200 K below its melting temperature.

Various tests have been performed with hollow cylindrical stainless steel (AISI 304) specimens with central boron carbide pellet under inert atmosphere in the LAVA furnace. The specimens with different B_4C masses (approx. 5, 1, and 0.3 wt-%) were kept at about 1250 °C for one hour to allow equilibrium conditions. Additionally, tests with shorter times at plateau temperature (300, 0 s) with the medium sized B_4C pellets and one reference test with pure stainless steel hollow cylinder were performed for comparison reasons. The experimental parameters of these tests are compiled in Table A7 as well as in the appendix A14.

Figure 31 shows the specimens with three different boron carbide cylinders which were kept in a zirconia crucible and covered with an yttria disc.

The boron carbide was completely consumed during the 1-h-tests, as can be seen from Fig. 32. 5 and 1 wt-% boron carbide completely liquefied the stainless steel, whereas the specimen with 0.3 wt-% was only liquefied by about one third. (The black zones in the two left overview images are pores.) The magnified metallographic images in Fig. 32 show a homogeneous melt formation for the specimens with the higher B_4C content and the transition between eutectic melt and still solid stainless steel for the specimen with the

smallest B_4C pellet. Block shaped and needle-like precipitates of iron/chromium borides with some carbon dissolved $(Fe, Cr)_n(B, C)$ with n between 1.8 and 2.7 are found in the specimens with the highest B_4C content. The complex eutectic matrix mainly consists of boron free (Fe, Cr, Ni) and (Fe, Cr) carbides as well as borocarbides with similar composition (but higher carbon content) like the large block crystals. The phase composition of the solidified eutectic melt of the 1-wt-% specimen also consists of boron free (Fe, Cr, Ni) carbides and (Fe, Cr) boro-carbides. As expected, the reference specimen of pure stainless steel did not show any evidence of molten phases.

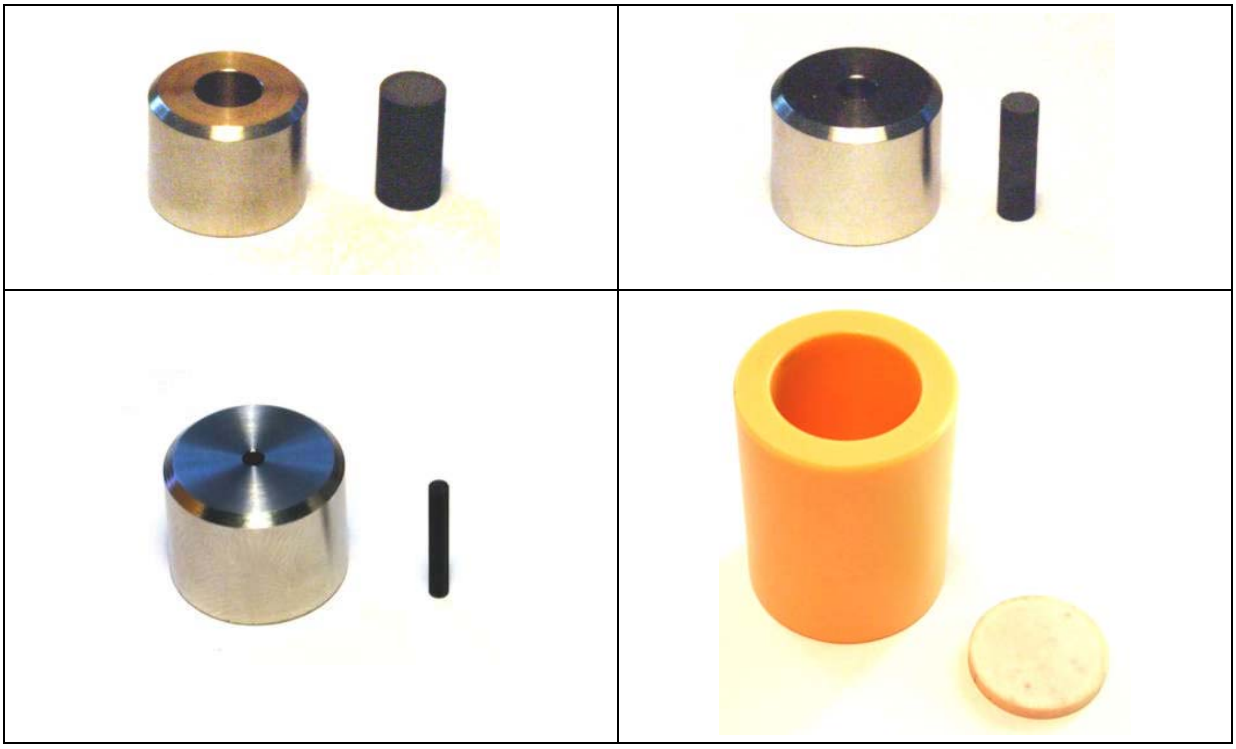

Figure 31: Stainless steel / boron carbide specimens with large (5 wt-%), medium (1 wt-%) and small (0.3 wt-%) B_4C pellet. The lower right picture shows ZrO_2 crucible and Y_2O_3 cover plate.

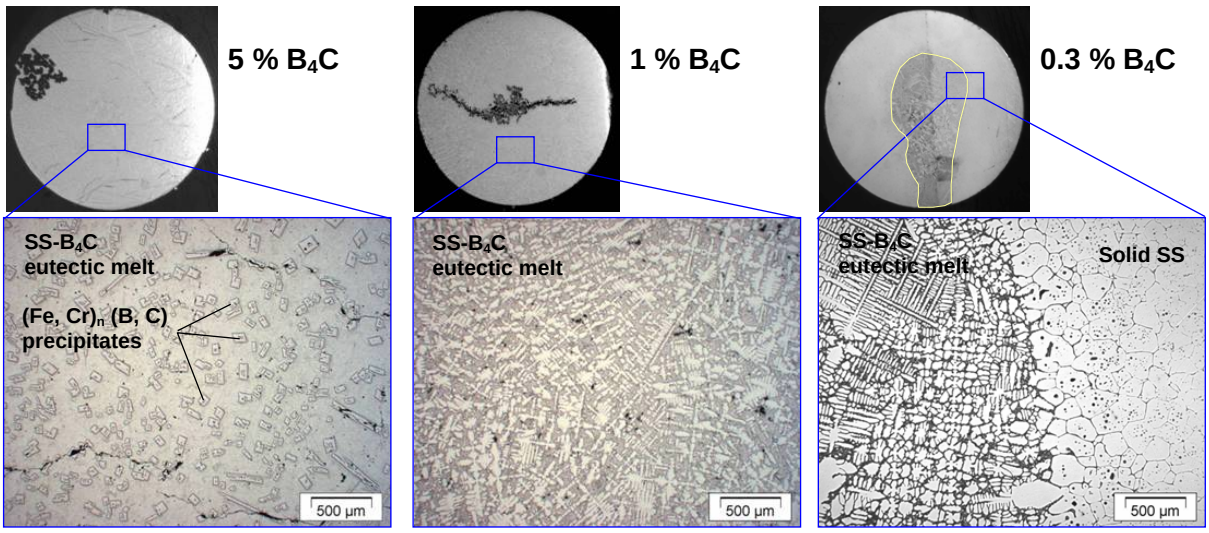

Figure 32: SS/B_4C specimens with 5, 1, and 0.3 wt-% boron carbide after one hour at 1250 °C under inert atmosphere.

Two further tests were performed with much shorter times at temperature. Figure 33 shows that the liquefaction takes place very rapidly. After five minutes, the boron carbide pellet is almost consumed and about half of the steel sample is liquefied. Even after less than one minute at temperature above 1200 °C a significant amount of steel is liquefied due to the eutectic interaction with B_4C as can be seen from the right image in Fig. 33.

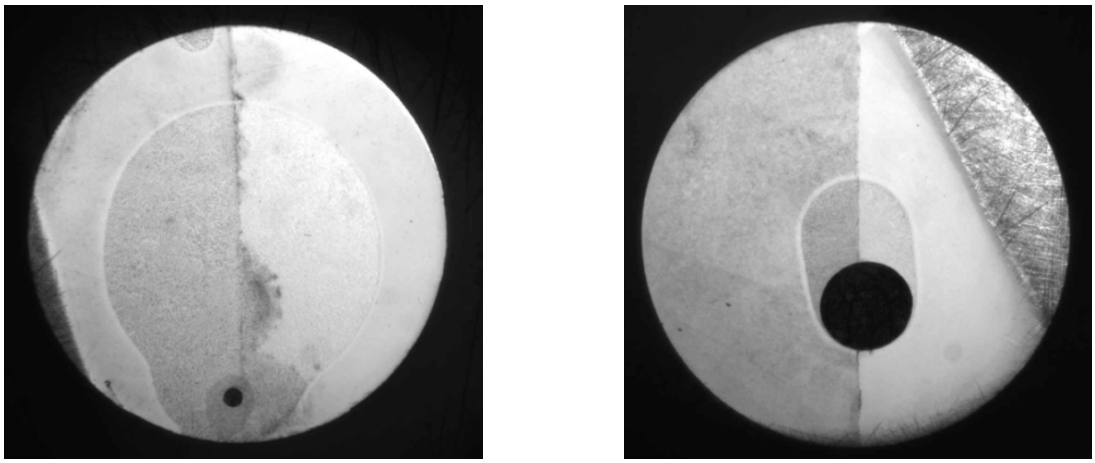

Figure 33: SS/B_4C specimens with 1 wt-% boron carbide after 5 min (left) and without plateau phase (right) at 1250 °C.

More detailed results of metallographic post-test examinations by light microscopy, SEM and EDX are compiled in appendix A15.

6 Summary and conclusions

Extensive tests on the degradation of boron carbide control rods and on the oxidation of the resulting absorber melts were performed.

Eutectic interactions between stainless steel and Zircaloy and boron carbide, respectively, cause rapid formation of complex melts at temperatures of about 1250 °C. These low viscosity melts relocate downwards inside the gap between the B_4C pellets and the external oxide scale formed at the guide tube surface, which prevents early oxidation and radial distribution of the melt. After failure of the oxide shell, the oxidation of the absorber melt takes place very rapidly. Furthermore, the pseudo-ternary SS/B_4C/Zry melt attacks the cladding (oxide scale) of the surrounding fuel rods and may initiate early release of fuel and fission products.

The following behaviour of a control rod of French PWR design in dependence on temperature can be summarised:

1000 °C: no significant interactions between stainless steel, boron carbide, and Zircaloy

1200 °C: local interactions between stainless steel, boron carbide, and Zircaloy

≥ 1250 °C: complete liquefaction of metals (steel, Zircaloy) in the gap between B_4C pellet and external ZrO_2 oxide scale

≥ 1450 °C: failure of the oxide scale and rapid oxidation of absorber melt and remaining B_4C pellets

The oxidation of the B_4C containing melts leads to the formation of CO, CO_2 and boric acids as well as to a significant additional hydrogen release. As for the oxidation of pure B_4C, no methane was released during these high temperature oxidation tests. The melts oxidise much faster than the solid materials at the same temperatures because of the formation of non-protective oxide scales.

Finally, it was shown that boron carbide is able to liquefy large amounts of steel 200 K below its melting temperature; so a specimen with 99 wt% steel and 1 wt-% B_4C was completely and homogeneously molten after one hour at about 1250 °C and significant amounts of steel were already liquefied after a few minutes at temperature.

Even the number of control rods in a nuclear reactor is small in comparison with the number of fuel rods, its degradation and oxidisation may influence the integral bundle degradation during severe accident sequences. The formation of melts at low temperature locally initiates fuel rod failure connected with early release of fission products. Additionally, the oxidation of B_4C and boron carbide containing melts is rapid and strongly exothermic, causing local chemical energy release in the bundle possibly triggering more global temperature escalations. The influence of a boron carbide absorber rod on the bundle degradation and

behaviour during reflood was also demonstrated in the QUENCH bundle experiments QU-07 and QU-09 [7, 8].

Acknowledgements

The experimental work described in this report was co-financed by the European Commission under the Euratom Fifth Framework Programme on Nuclear Fission Safety 1998-2002.

Some of the tests were prepared and conducted by guest students, namely by Marion Merl and Christina Reinhard which is acknowledged here.

References

[1] Y. Kawada
Reactors and materials of nuclear elements containing Boron
Note Technique SEMAR 98/67, IPSN Cadarache, May 1998

[2] P. Hofmann, M. Markiewicz, J. Spino
Reaction behaviour of B_4C absorber material with stainless steel and Zircaloy in severe LWR accidents
Report KfK 4598, Kernforschungszentrum Karlsruhe, July 1989

[3] L. Belovsky et al.
Chemical interaction in B_4C-filled control rod segments above 1000 °C under transient conditions
5th International Conference on Nuclear Engineering ICONE5, paper 2148, Nice, France, May 26-29, 1997

[4] F. Nagase, H. Uetsuka, T. Otomo
Chemical interactions between B_4C and stainless steel at high temperatures
J. Nucl. Mat. 52, 245 (1997)

[5] M. Steinbrück, A. Meier, U. Stegmaier, L. Steinbock
Experiments on the oxidation of boron carbide at high temperatures
Report FZKA 6979, 2004

[6] W. Krauss, G. Schanz, H. Steiner
TG-Rig tests (thermal balance) on the oxidation of B_4C. Basic experiments, modelling and evaluation approach
Report FZKA 6883, 2003

[7] M. Steinbrück et al.
Results of the B_4C control rod test QUENCH-07
Report FZKA 6746, 2004

[8] M. Steinbrück et al.
Results of the QUENCH-09 experiment with B_4C control rod
Report FZKA 6829, 2004

[9] B. Clement, G. Repetto
Test Protocol for the Phebus FP Test FPT-3 (as for January 2001)
Note Technique SEMAR 01/01, IPSN Cadarache, January 2001

[10] **TAPP2.2:** A Database of Thermochemical and Physical Properties, ES Microware, Hamilton, Ohio 1994 (and references herein)

APPENDIX

Table A1: Test parameters of experiments on B_4C control rod degradation and oxidation in the BOX rig (chronological order)

Test	Specimen	Crucible	Ar, l/h	H_2O, g/h	time, min	T, °C	Remarks
10621	CR seg. O	Al_2O_3	50	30		800-1500	1st test with CR segment with ZrO_2 caps
10625	CR seg. O	Al_2O_3	50	0		800-1500	
10627	CR seg. O	Al_2O_3	50	30		800-1500	repetition of test 10621
11024	CR seg. M	Al_2O_3+Y_2O_3	50	30	60	800	1st test with CR segment with Zry plugs
11105	CR seg. M	Al_2O_3+Y_2O_3	50	30	60	1000	
11107	CR seg. M	Al_2O_3+Y_2O_3	50	30	60	1200	
11108	CR seg. M	Al_2O_3+Y_2O_3	50	30	60	1400	
11109	CR seg. M	Al_2O_3+Y_2O_3	50	30	60	1600	
11121	CR seg. M	Al_2O_3+Y_2O_3	50	30	60	1700	
20528a	CR seg. O	Al_2O_3	50	30	60	1000	1st test with CR segments with oxide caps, 1 h
20528b	CR seg. O	Al_2O_3	50	30	60	1200	
20529	CR seg. O	Al_2O_3+ZrO_2	50	30	60	1400	
20603	CR seg. O	Al_2O_3+ZrO_2	50	30	60	1600	T&gas escalation, MS blocked during test
20605	CR seg. O	Al_2O_3+Y_2O_3	50	30	60	1300	
20606	CR seg. O	Al_2O_3+Y_2O_3	50	30	60	1500	steam injection too late
20610	CR seg. O	Al_2O_3+Y_2O_3	50	30	20	1500	repetition of test 20606, T&gas escalation, 20 min!

Table A2: Test parameters of experiments on B_4C control rod degradation and oxidation in the QUENCH rig (chronological order)

Test	Specimen filled with	Test conduct	Heating rate or isothermal time	Max. temperature °C	Ar rate, l/h	Steam rate, g/h	remarks
11011a	vacuum	transient	0.1 K/s	1040	100	0	transient test up to failure of specimen (support)
11011b	vacuum	transient	0.1 K/s	1080	100	0	transient test up to failure of specimen (support)
11016a	vacuum	transient	1 K/s	1600	100	100	transient test up to failure of specimen (support)
20820	vacuum	transient	1 K/s	1470	100	100	first test with new sample support
20822	vacuum	transient	1 K/s	1430	100	100	slightly modified temperature program (see appendix)
20826a	helium	transient	1 K/s	1580	100	100	CR failure
20826b	vacuum	transient	3 K/s	1570	100	100	
20827a	vacuum	transient	0.1 K/s	1480	100	100	
20827b	vacuum	isothermal	30 min	1265	100	100	
20828a	vacuum	isothermal	30 min	1375	100	100	CR failure
20828b	vacuum	isothermal	30 min	1460	100	100	CR failure
20829a	helium	isothermal	30 min	1470	100	100	failure, melt jet release
20829b	helium	isothermal	30 min	1270	100	100	
20830a	vacuum	isothermal	30 min	1560	100	100	CR failure, failure of the data recording system

Table A3: Composition of investigated absorber melts, test parameters for preparation and transient oxidation (800 → 1550 °C)

Nr.	B_4C wt-%	SS wt-%	Zry wt-%	Mass g	Preparation t (min)/T(°C)	Oxidation test	Ar rate l/h	H_2O rate g/h	Remarks
1	0	100	0	1.101	10/1900	21108	50	30	
2	5	95	0	0.997	10/1900	21111	50	30	splashed melt particles in crucible and reaction tube
3	10	90	0	0.914	10/1900	21119a	50	30	
4	20	80	0	~ 0.8	10/2100	21113	50	30	crucible broken
5	30	70	0	1.143	10/2100	21119	50	30	steam injection only from 1000 °C
6	9	81	10	1.036	10/2100	21114	50	30	splashed melt particles in crucible and reaction tube
7	7	63	30	~ 1	10/2100	21120	50	30	strong degradation of ZrO_2 crucible
8	0	70	30	~ 1	10/1900	21121	50	30	
9	0	0	100	0.933	-	21125	50	30	

Table A 4: Gas release during oxidation of 1-pellet-size specimens

Test	Specimen	Ar, l/h	H_2O, g/h	time, min	T, °C	H_2, ml	CO_2, ml	CO, ml
10621	CR seg. O	50	30		800-1500	246	28	22
10625	CR seg. O	50	0		800-1500	0	0	0
10627	CR seg. O	50	30		800-1500	266	28	22
11024	CR seg. M	50	30	60	800	88	16	10
11105	CR seg. M	50	30	60	1000	177	17	19
11107	CR seg. M	50	30	60	1200	539	22	23
11108	CR seg. M	50	30	60	1400	930	29	24
11109	CR seg. M	50	30	60	1600	1565	35	28
11121	CR seg. M	50	30	60	1700	2845	87	64
20528a	CR seg. O	50	30	60	1000	54	17	17
20528b	CR seg. O	50	30	60	1200	186	29	27
20529	CR seg. O	50	30	60	1400	487	34	31
20603	CR seg. O	50	30	60	1600	2275	103	86
20605	CR seg. O	50	30	60	1300	242	30	25
20606	CR seg. O	50	30	60	1500	1135	151	33
20610	CR seg. O	50	30	20	1500	2185	96	70

Table A 5: Gas release during oxidation of 10-cm specimens

Test	Specimen filled with	Test conduct	Heating rate or isothermal time	Max. temperature °C	Steam rate, g/h	Ar rate, l/h	H_2, ml	CO_2, ml	CO, ml
11011a	vacuum	transient	0.1 K/s	1040	0	100	0	0	0
11011b	vacuum	transient	0.1 K/s	1080	0	100	0	0	0
11016a	vacuum	transient	1 K/s	1600	100	100	1111	7	7
20820	vacuum	transient	1 K/s	1470	100	100	1438	27	9
20822	vacuum	transient	1 K/s	1430	100	100	998	6	0
20826a	helium	transient	1 K/s	1580	100	100	2660	77	102
20826b	vacuum	transient	3 K/s	1570	100	100	1128	8	0
20827a	vacuum	transient	0.1 K/s	1480	100	100	2892	82	84
20827b	vacuum	isothermal	30 min	1265	100	100	1481	19	19
20828a	vacuum	isothermal	30 min	1375	100	100	1288	34	27
20828b	vacuum	isothermal	30 min	1460	100	100	2543	37	33
20829a	helium	isothermal	30 min	1470	100	100	3878	114	379
20829b	helium	isothermal	30 min	1270	100	100	902	19	13
20830a	vacuum	isothermal	30 min	1560	100	100	3242	133	178

Table A 6: Gas release during oxidation of absorber melts

Nr.	B_4C wt-%	SS wt-%	Zry wt-%	Oxidation test	Ar rate l/h	H_2O rate g/h	H_2, ml	CO_2, ml	CO, ml	T_{melt}* °C
1	0	100	0	21108	50	30	267	7	4	1410
2	5	95	0	21111	50	30	612	24	9	1170
3	10	90	0	21119a	50	30	301	17	5	1185
4	20	80	0	21113	50	30	186	11	11	(1420)**
5	30	70	0	21119	50	30	300	6	3	-***
6	9	81	10	21114	50	30	568	32	36	1138
7	7	63	30	21120	50	30	351	28	205	(1287)**
8	0	70	30	21121	50	30	490	9	44	-***
9	0	0	100	21125	50	30	175	10	3	no melting
10	100	0	0	00823	50	30	115	15	6	no melting

* *Melting temperature based on rapid increase of gas release*

** *Only slow transition from low to higher gas release rates, therefore T_{melt} only difficult to determine*

*** *No clear transition*

Table A 7: Tests on liquefaction of stainless steel by boron carbide

Test	SS, g	B_4C, g	B_4C, wt-%	$T_{Plateau}$ (pyro), °C	$T_{Plateau}$, (TC), °C	Time at $T_{Plateau}$, s	Remarks
L30904b	22.722	1.090	4.58	1276	1213	3600	complete liquefaction
L30904c	26.154	0.320	1.21	1276	1232	3600	complete liquefaction
L30905a	22.725	-	0	1275	1220	3600	no melt formation
L31016a	27.084	0.080	0.29	1276	1214	3600	partial liquefaction
L31021a	26.154	0.328	1.24	1276	1246	300	partial liquefaction
L31021b	26.172	0.318	1.20	1273	1136	0	partial liquefaction

A6 Examination by light microscopy of the 1-pellet-size CR segments with metal plugs

Box11107 (Argon/Steam 1200°C)

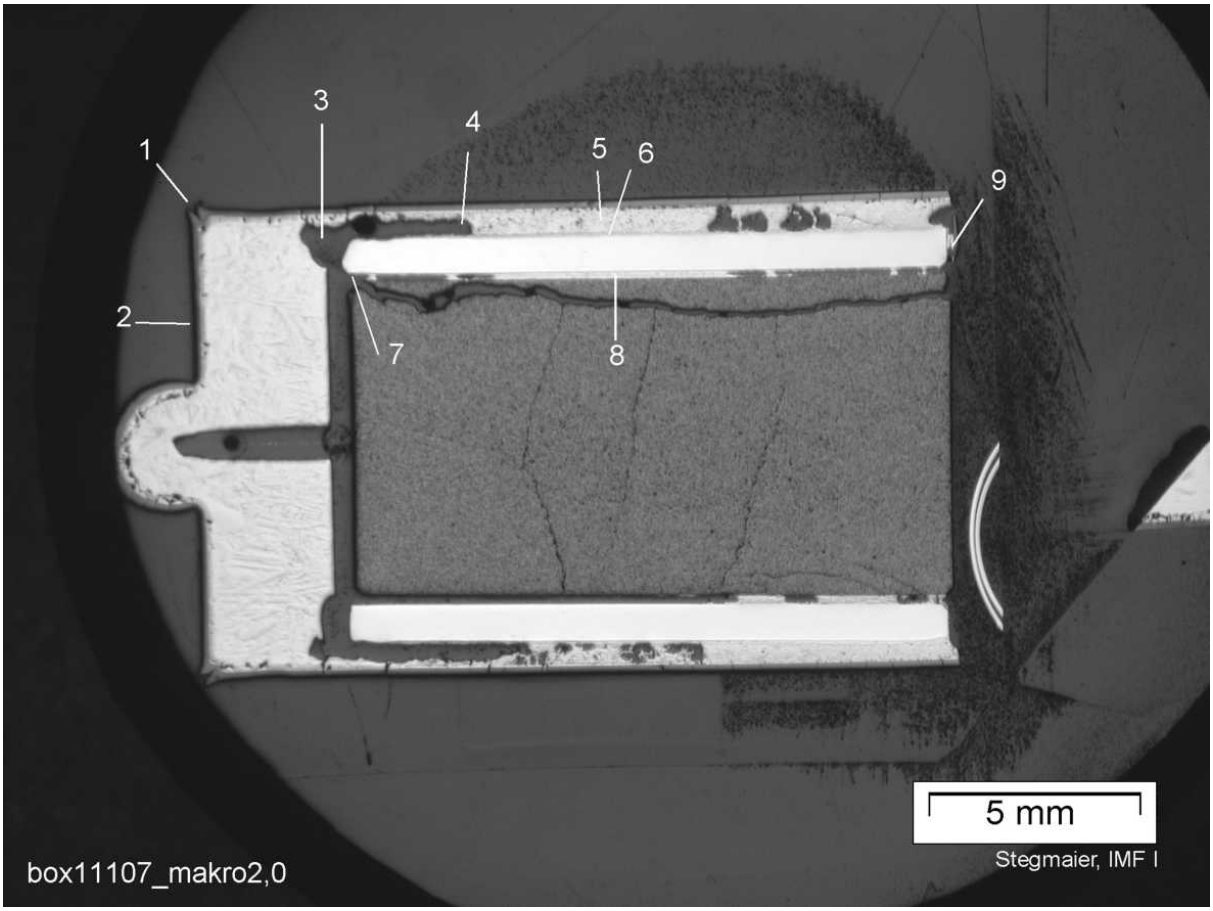

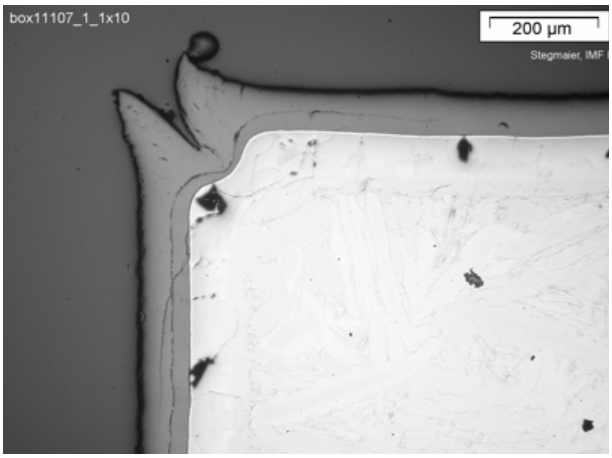

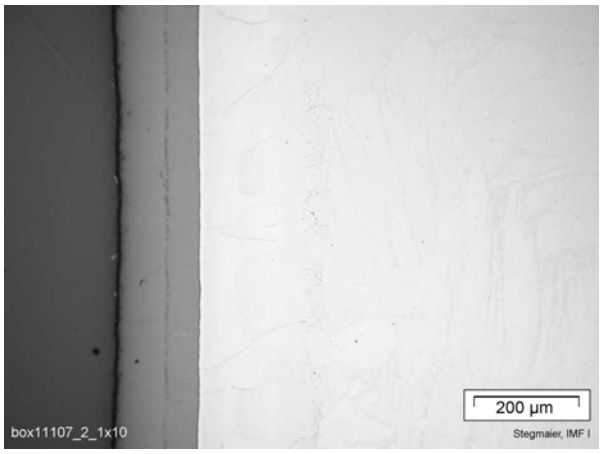

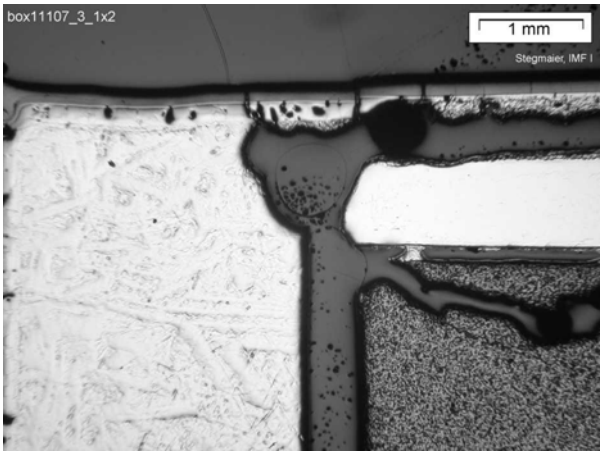
box11107_3_1x2
1 mm
Stegmaier, IMF I

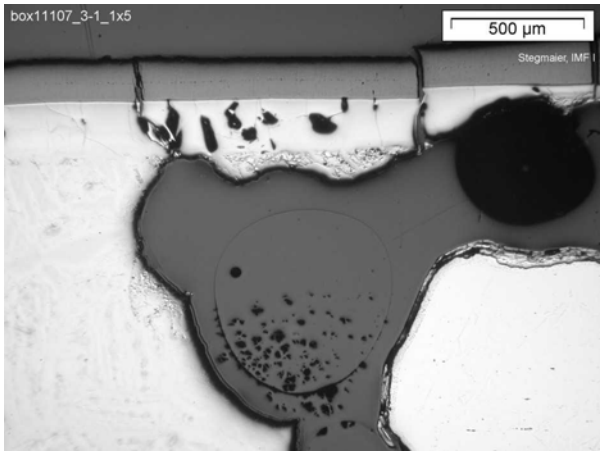
box11107_3-1_1x5
500 µm
Stegmaier, IMF I

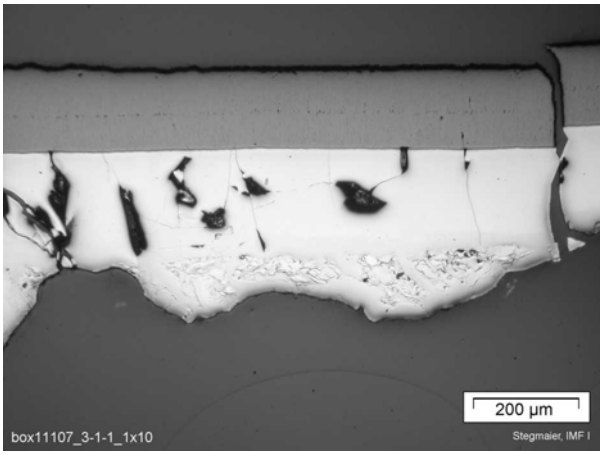
box11107_3-1-1_1x10
200 µm
Stegmaier, IMF I

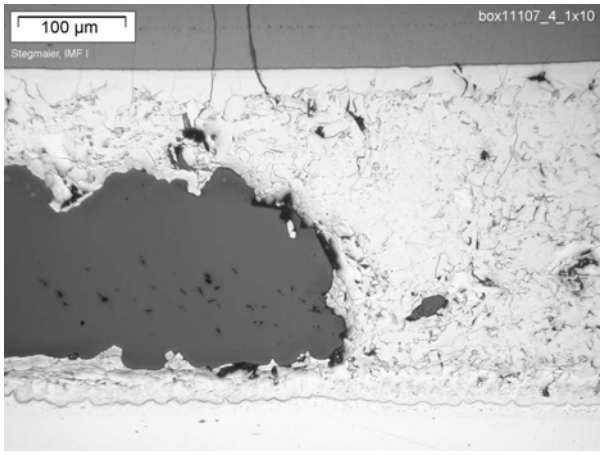
100 µm
Stegmaier, IMF I
box11107_4_1x10

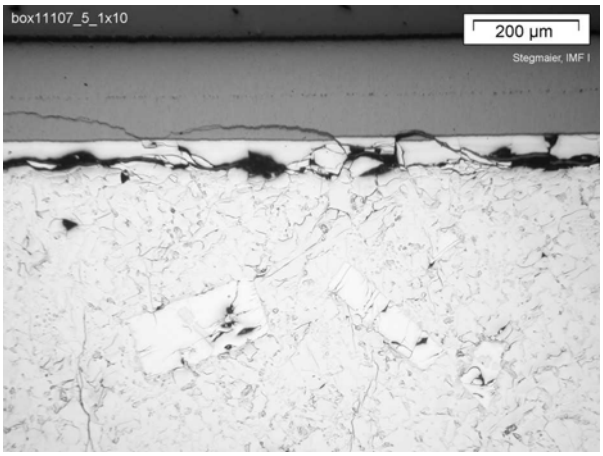
box11107_5_1x10
200 µm
Stegmaier, IMF I

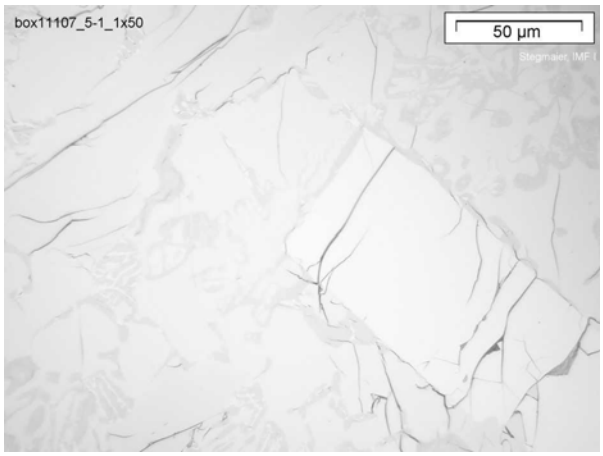
box11107_5-1_1x50
50 µm

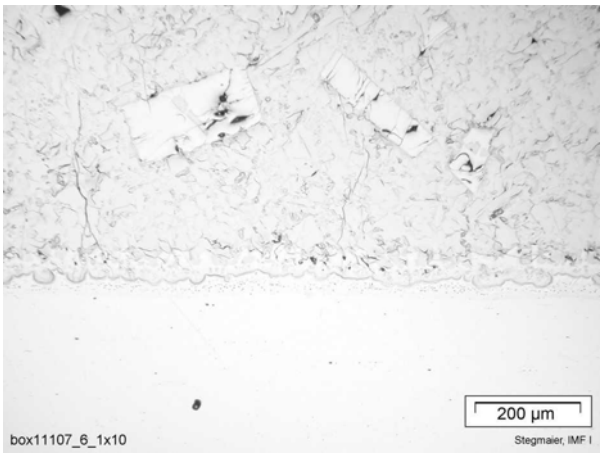
box11107_6_1x10
200 µm
Stegmaier, IMF I

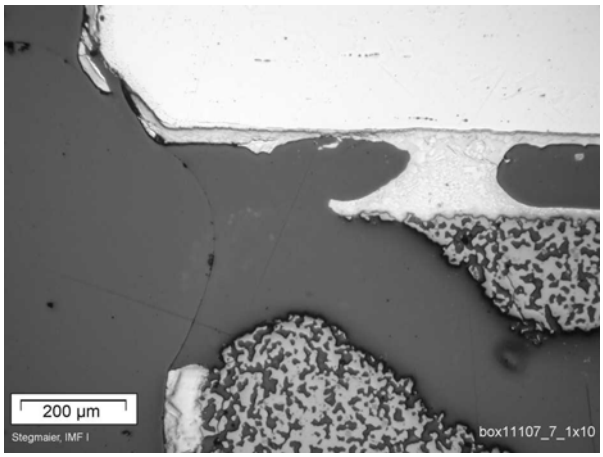
200 µm
Stegmaier, IMF I
box11107_7_1x10

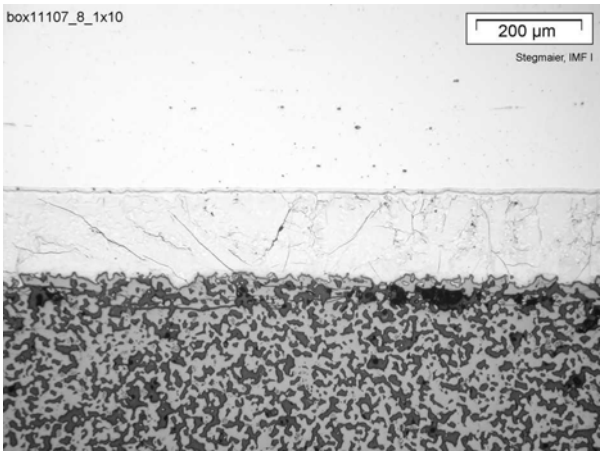
box11107_8_1x10
200 µm
Stegmaier, IMF I

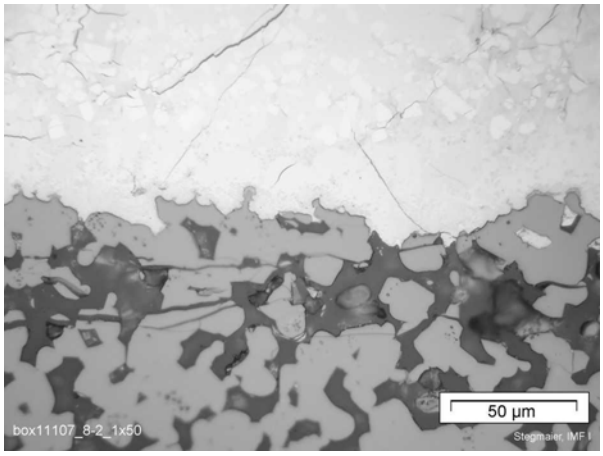
50 µm
box11107_8-2_1x50
Stegmaier, IMF I

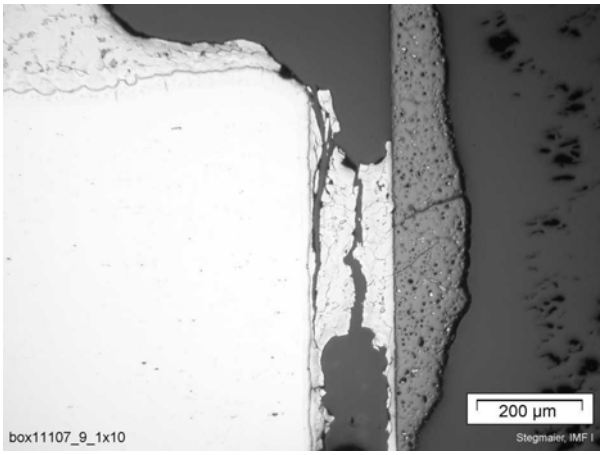
200 µm
box11107_9_1x10
Stegmaier, IMF I

Box11108 (Argon/steam 1400°C)

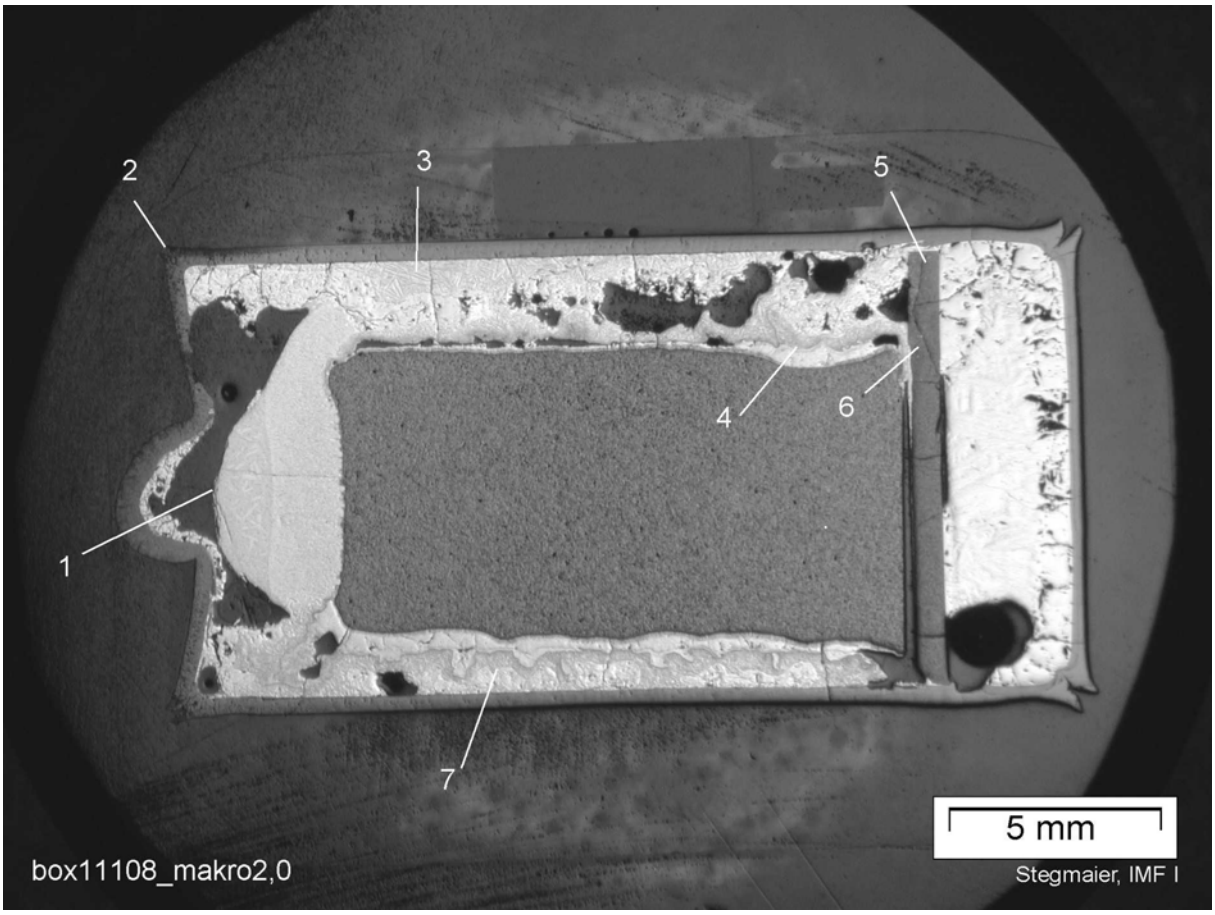

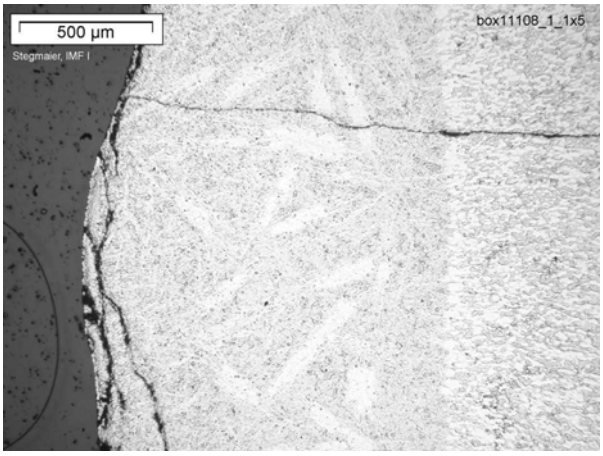

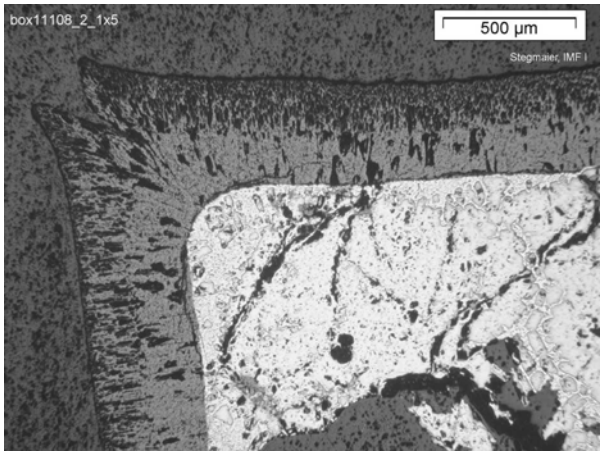

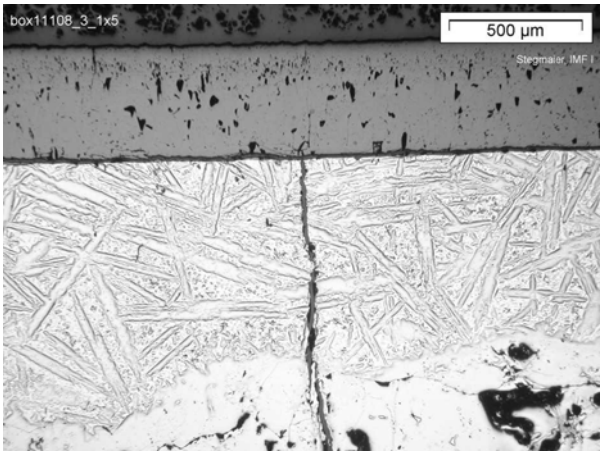
box11108_3_1x5
500 µm
Stegmaier, IMF I

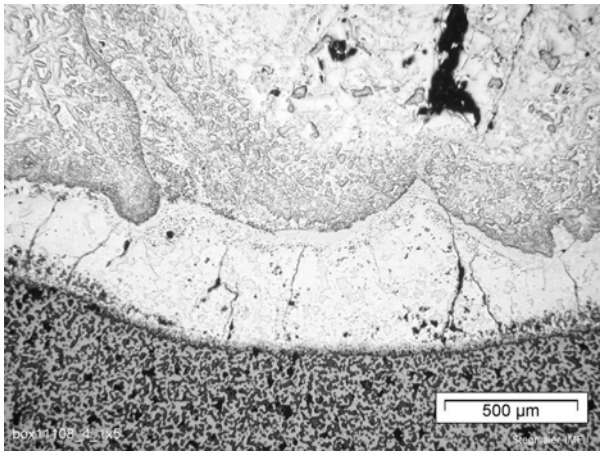
500 µm

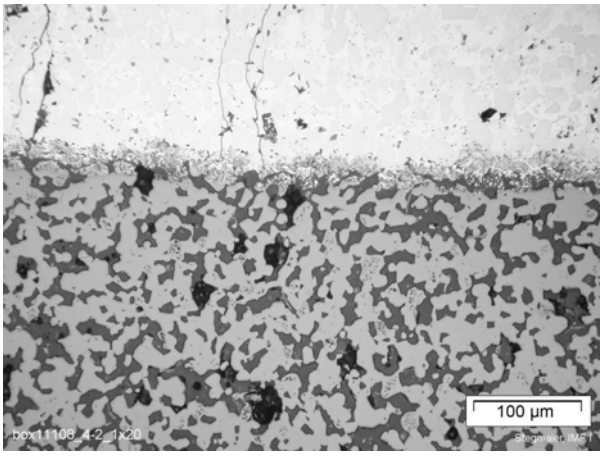
100 µm

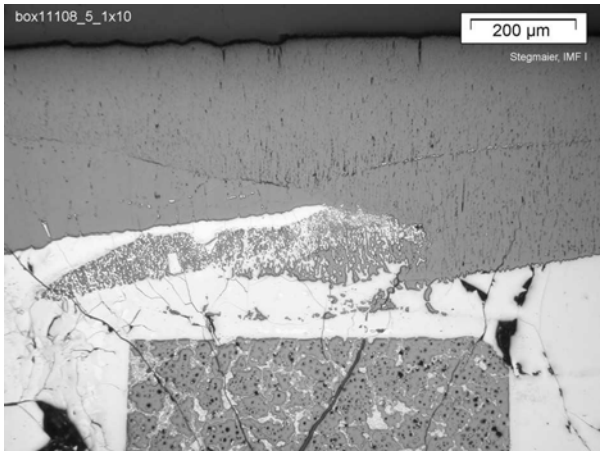
box11108_5_1x10
200 µm
Stegmaier, IMF I

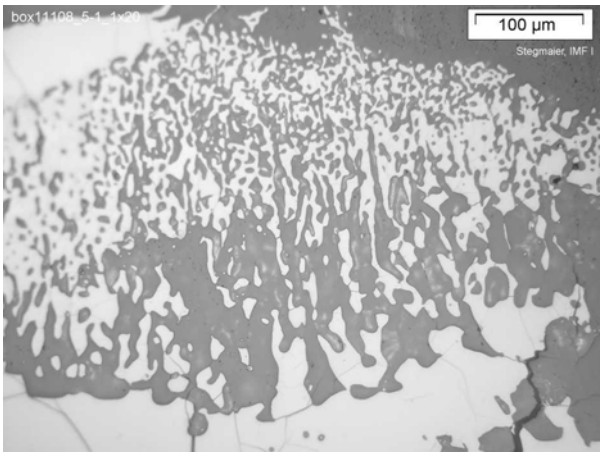
100 µm
Stegmaier, IMF I

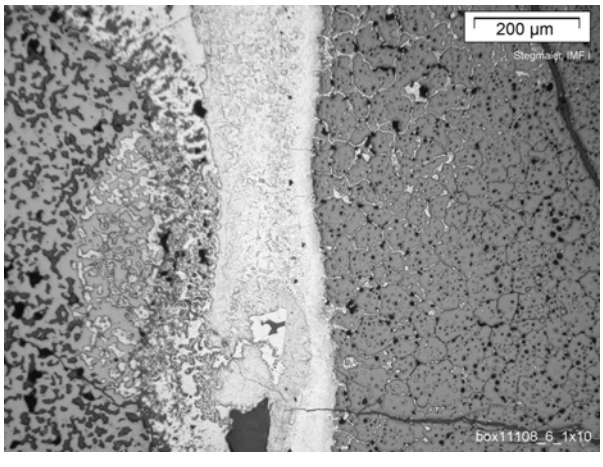
200 µm
Stegmaier, IMF I
box11108_6_1x10

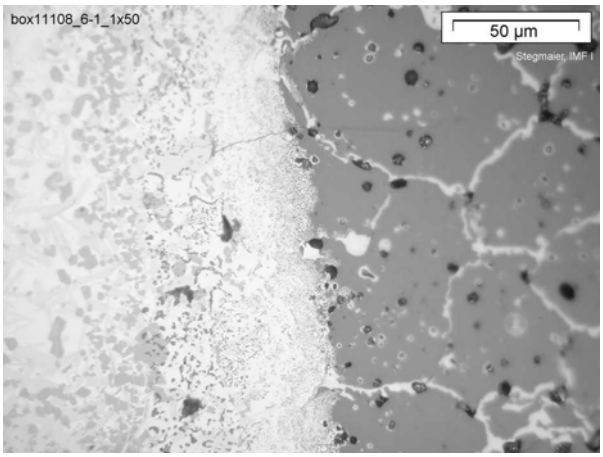
box11108_6-1_1x50
50 µm
Stegmaier, IMF I

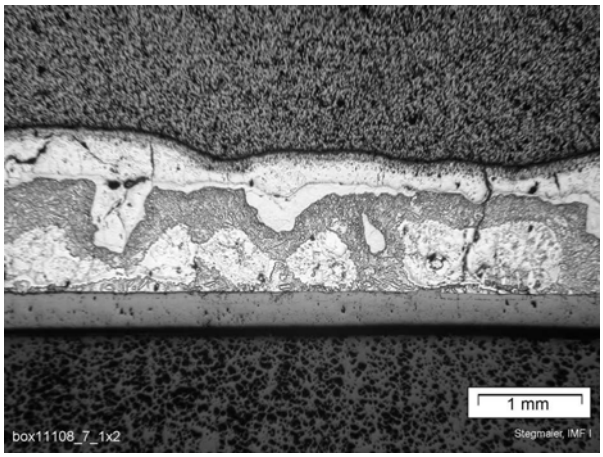
1 mm
box11108_7_1x2
Stegmaier, IMF I

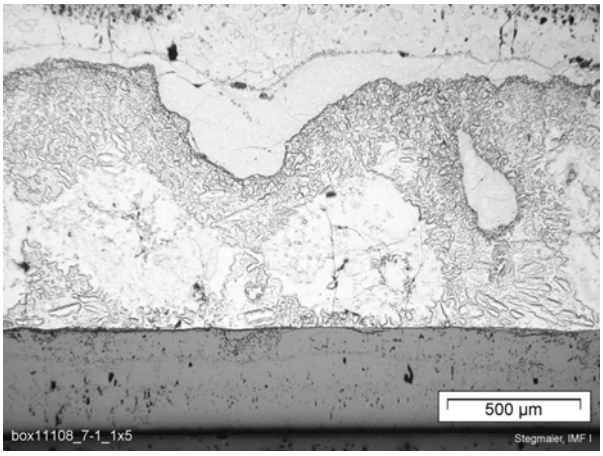
500 µm
box11108_7-1_1x5
Stegmaier, IMF I

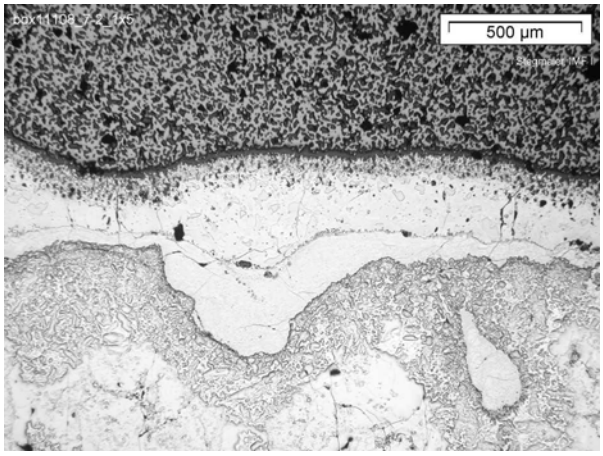
500 µm

Box11109 (Argon/steam 1600°C)

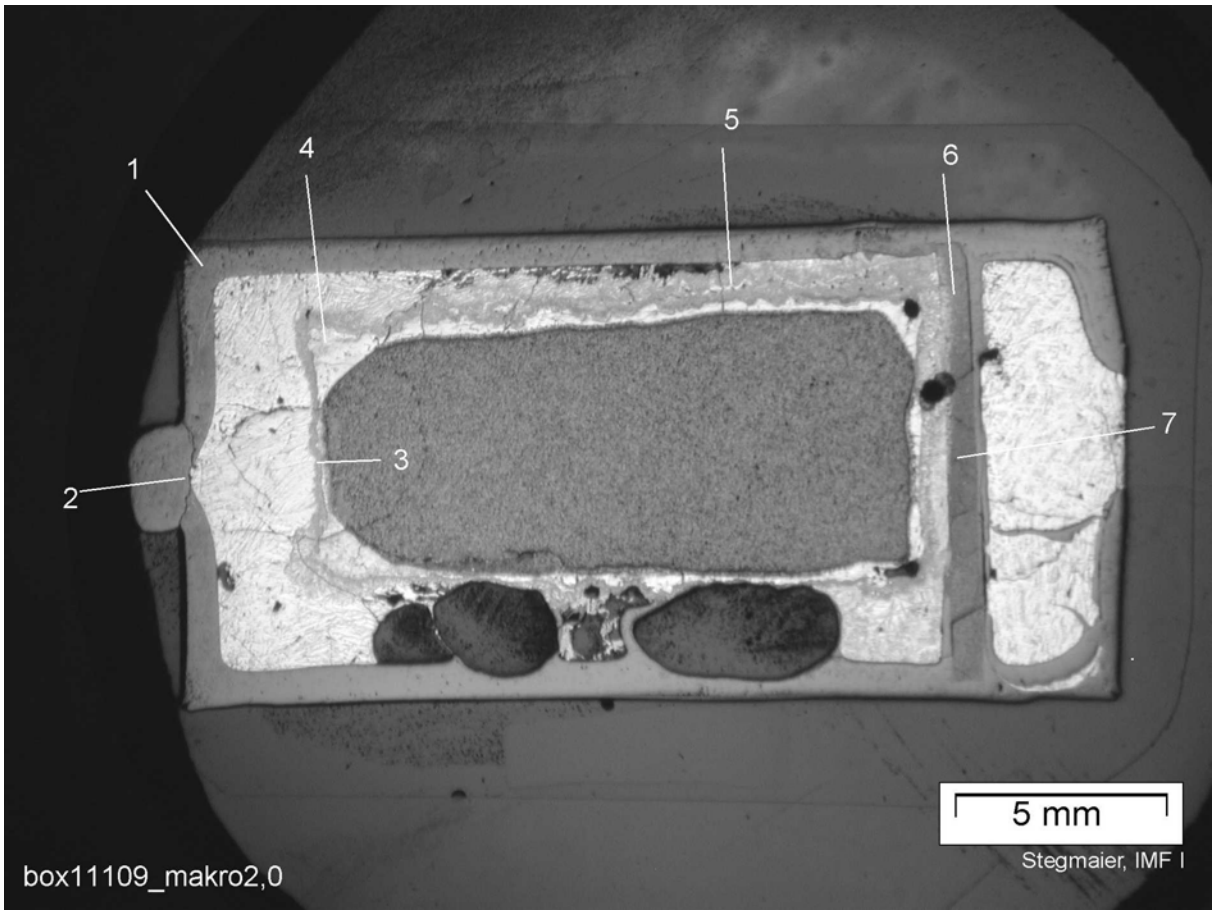

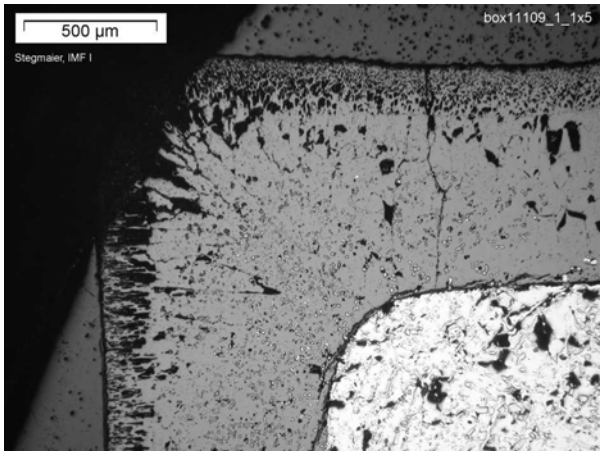

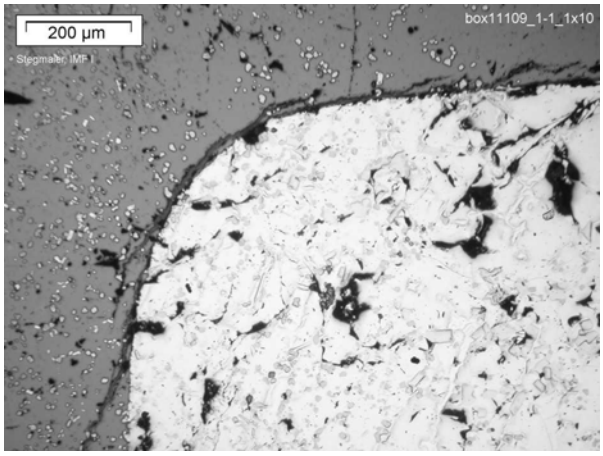

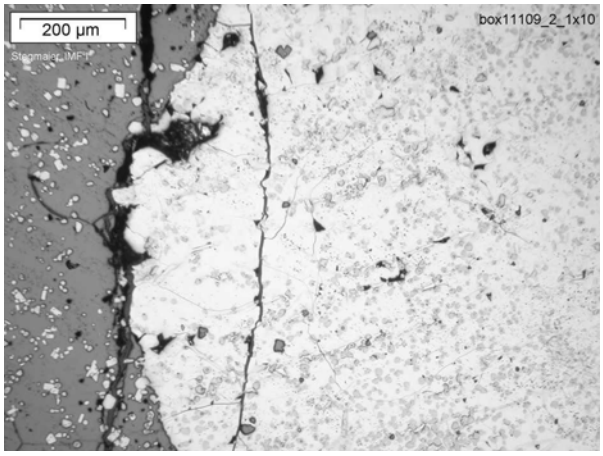
200 µm
box11109_2_1x10

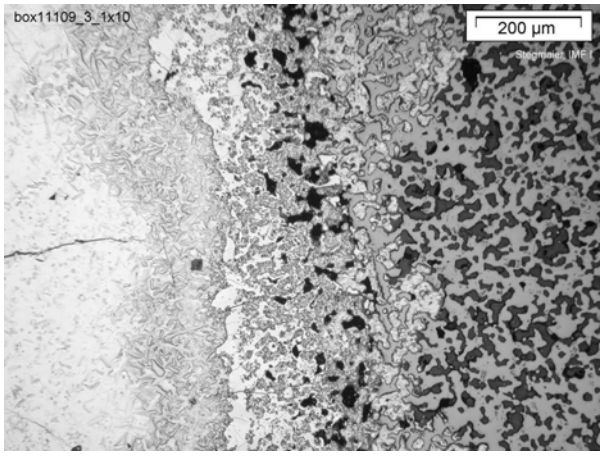
box11109_3_1x10
200 µm

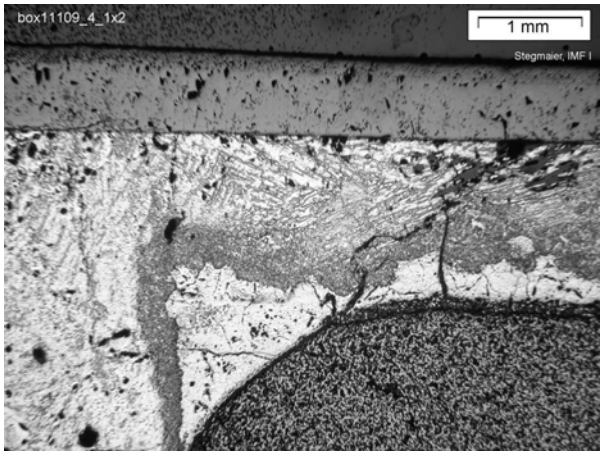
box11109_4_1x2
1 mm
Stegmaier, IMF I

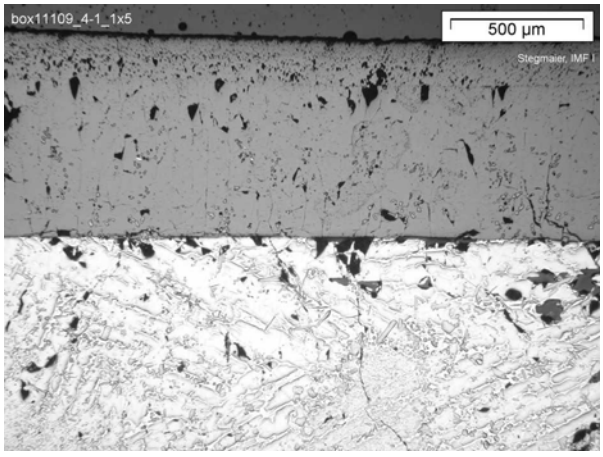
box11109_4-1_1x5
500 µm
Stegmaier, IMF I

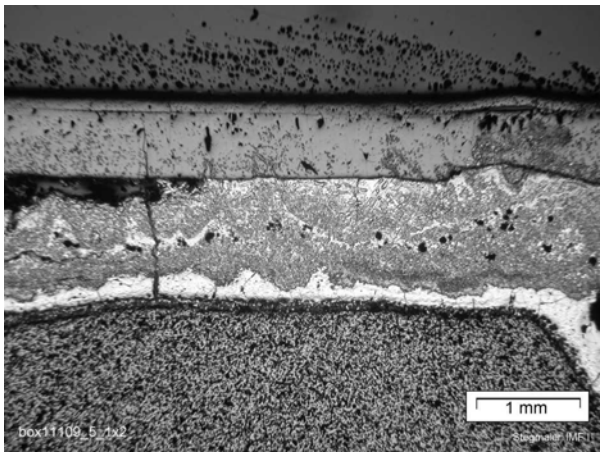
1 mm
box11109_5_1x2

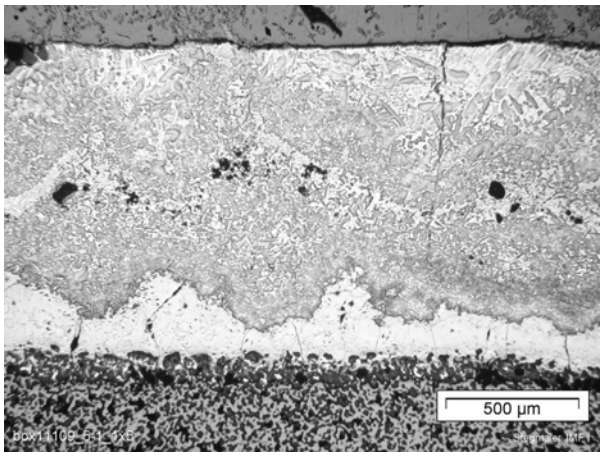
500 µm

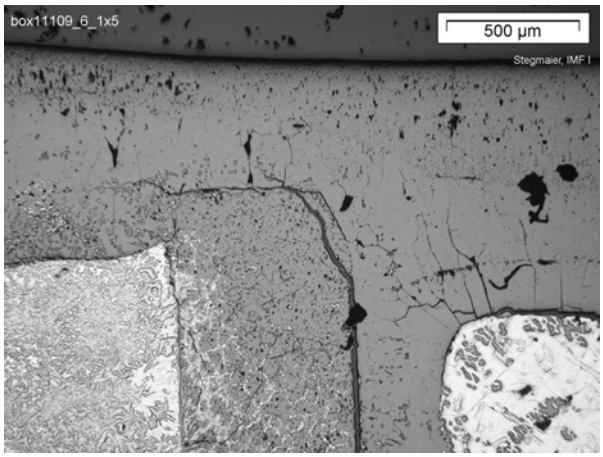
box11109_6_1x5
500 µm
Stegmaier, IMF I

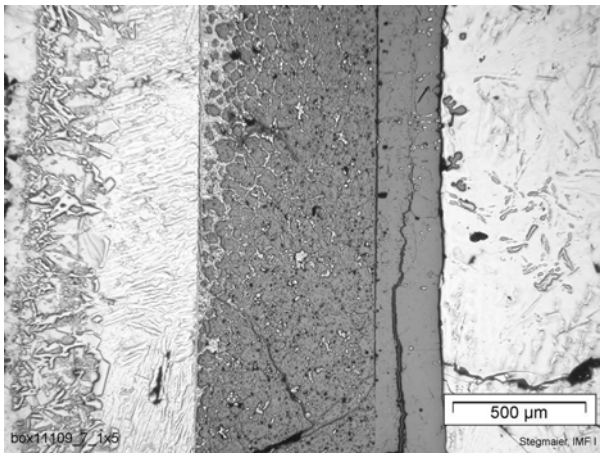
500 µm
box11109_7_1x5
Stegmaier, IMF I

Box11121 (Argon/steam 1700°C)

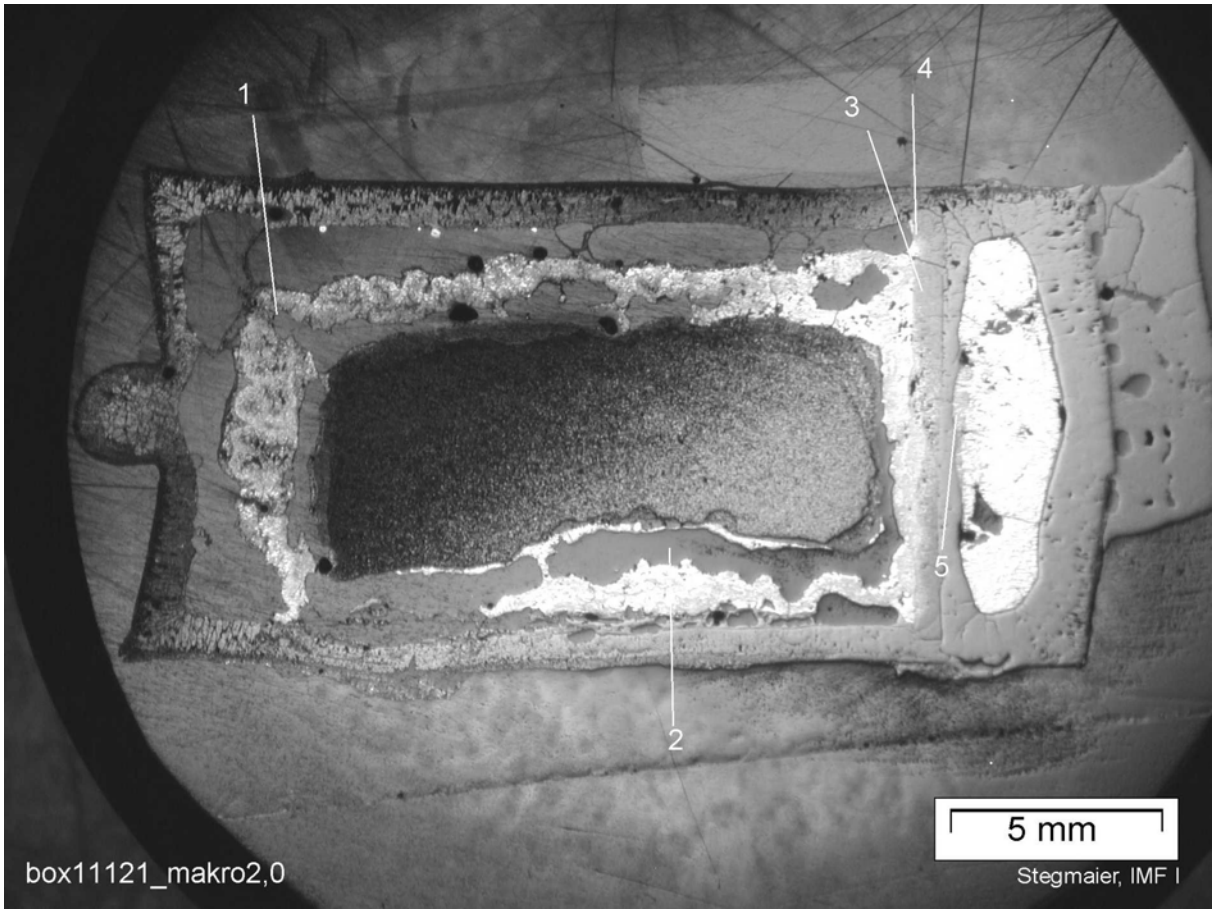

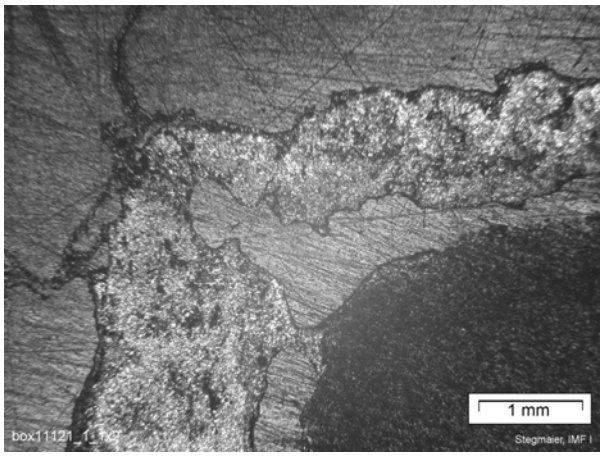

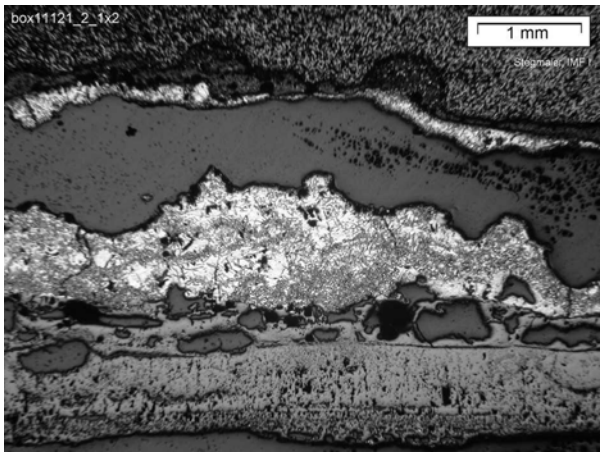

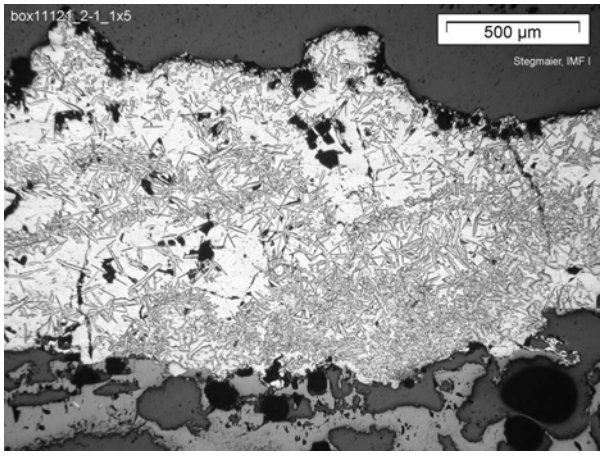
box11121_2-1_1x5
500 µm
Stegmaier, IMF I

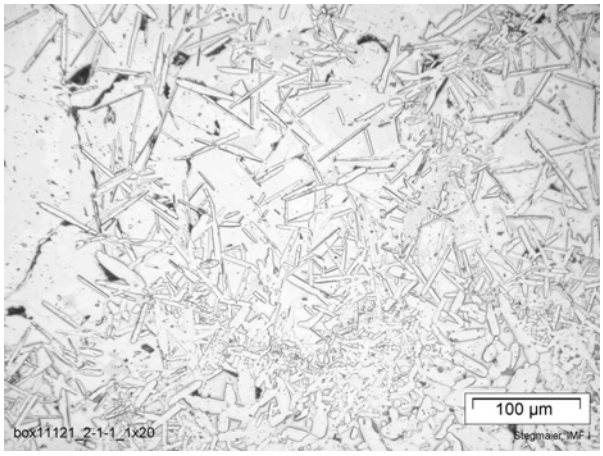
box11121_2-1-1_1x20
100 µm
Stegmaier, IMF I

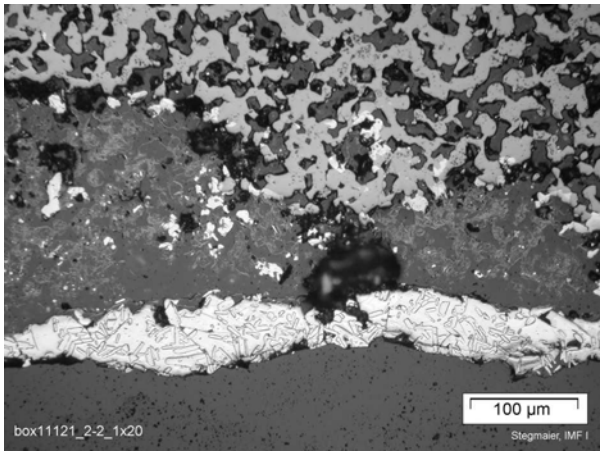
box11121_2-2_1x20
100 µm
Stegmaier, IMF I

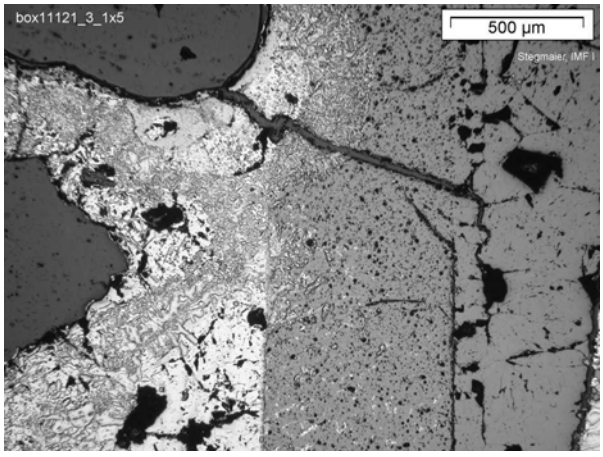
box11121_3_1x5
500 µm
Stegmaier, IMF I

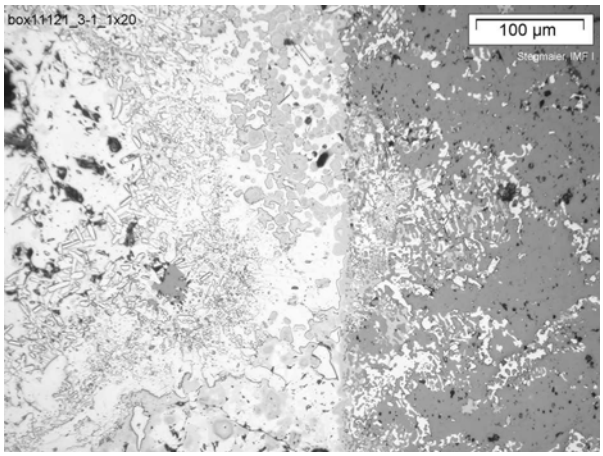
box11121_3-1_1x20
100 µm
Stegmaier, IMF I

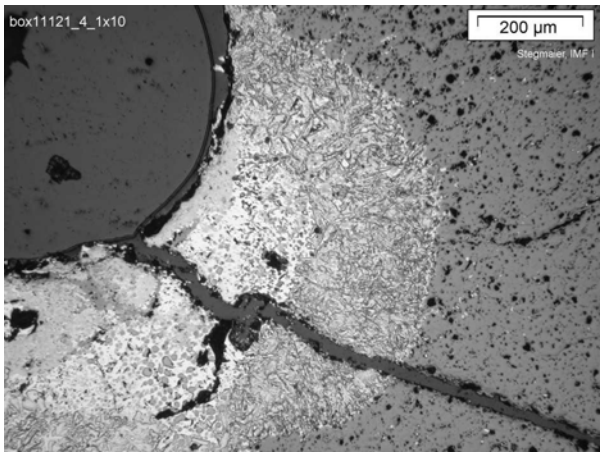
box11121_4_1x10
200 µm
Stegmaier, IMF I

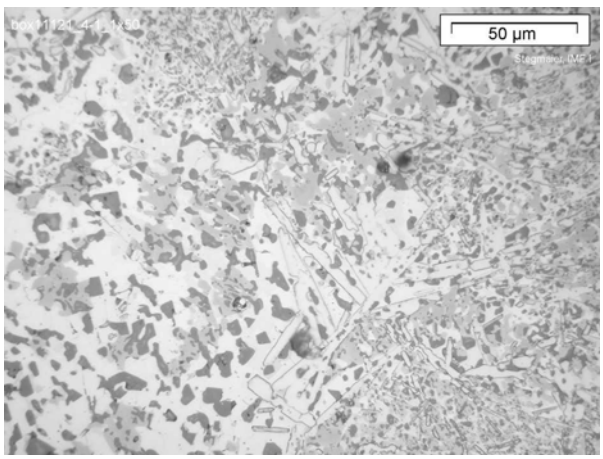
50 µm

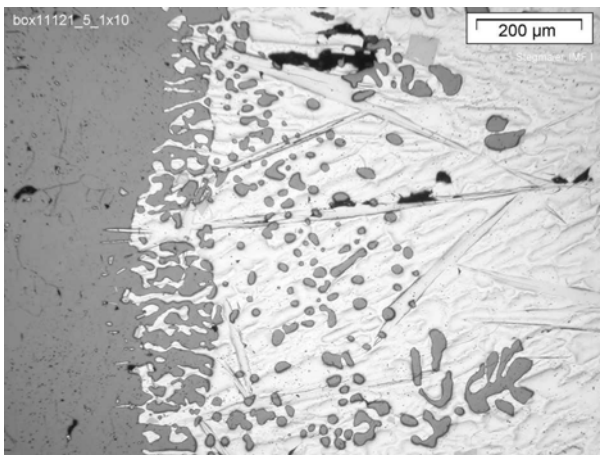
box11121_5_1x10
200 µm
Stegmaier, IMF I

A7 Auger analyses of the 1-pellet-size specimens with metal plugs

On the following pages the results of SEM/Auger investigations of the specimens after isothermal tests at 1200, 1400 and 1600 °C are summarised. Elemental compositions of the various phases as well as mappings of all available elements are given. Regarding the element mappings: The concentration of an element in a phase is the higher the brighter the colour in the image.

Test Box11107: 1h, 1200 °C

Overview

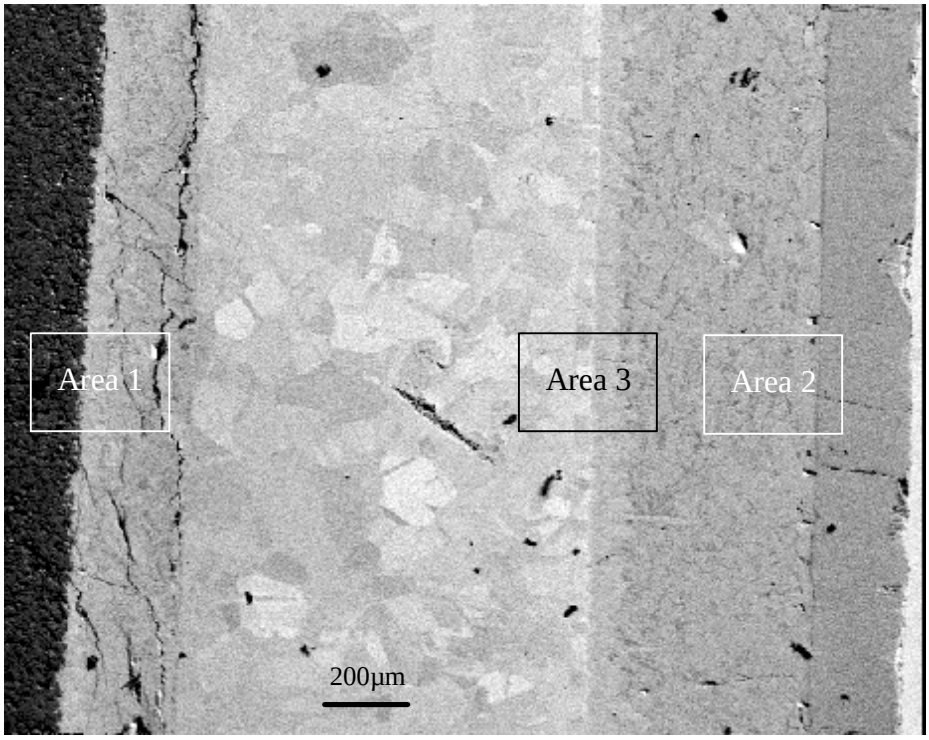

Fig. 1: Cross section through a CR segment after test at 1200 °C, left: B_4C, right: ZrO_2 with indicated areas for detailed Auger analyses

Auger elemental analysis near B_4C (Area 1)

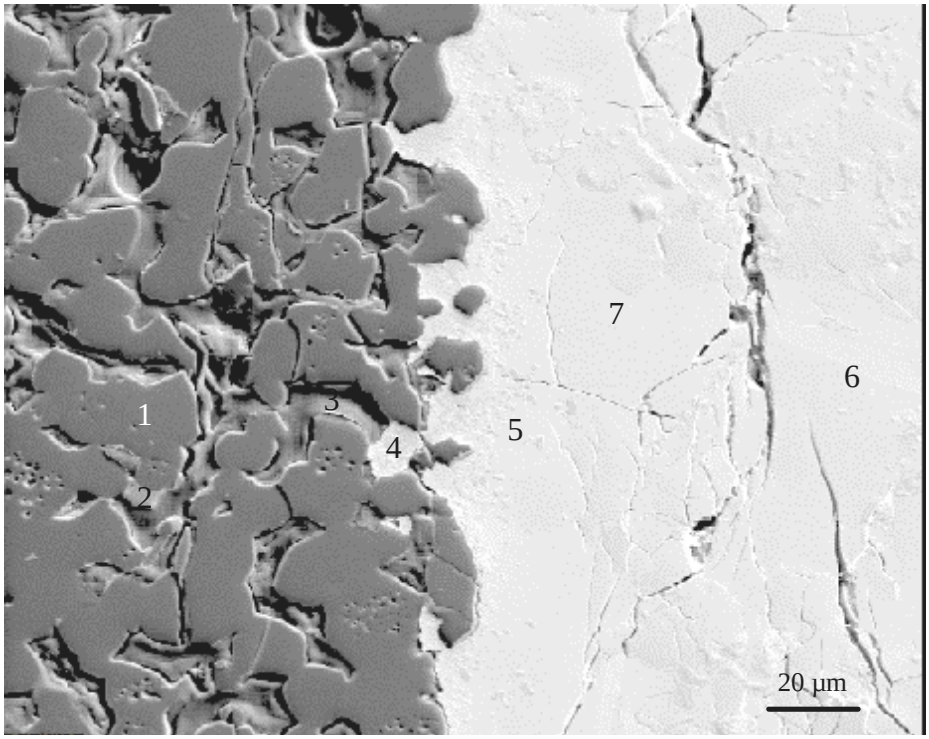

Fig. 2: SEM image of the range near B_4C with Auger measuring points

Elemental compositions (at-%) at measuring points given in Fig. 2

	B	**C**	**Fe**	**Ni**	**Zr**	**Sn**	**Si**
1	76	24					
2*		51					49
3**		100					
4	56		2		42		
5			35	11	54		
6			20	3	66	11	
7			32	11	57		

** from abrasive*

*** from embedding resin*

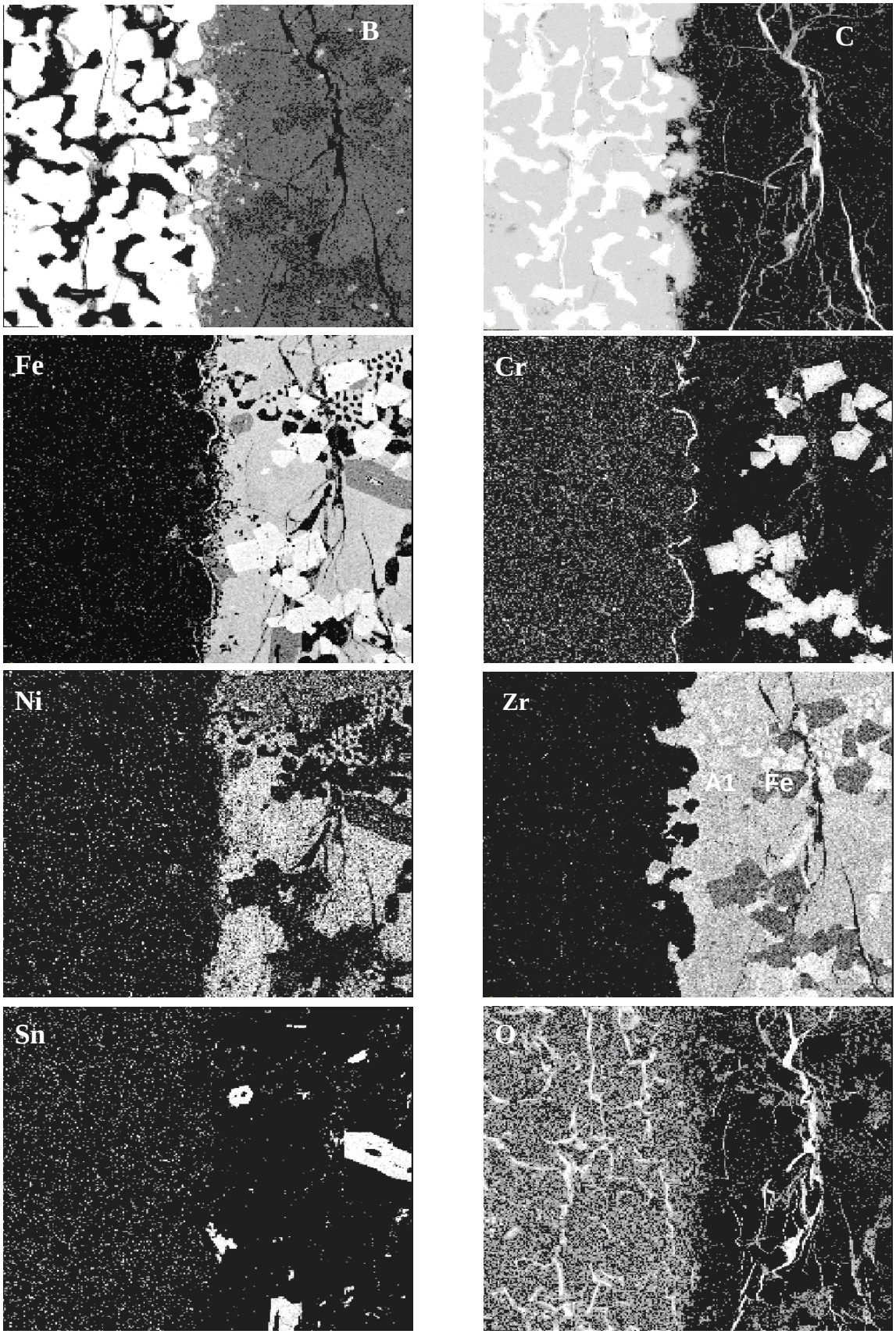

Fig. 3 a-h: Element mapping near B_4C (see Fig. 2)

Auger elemental analysis near outer ZrO_2 scale (Area 2)

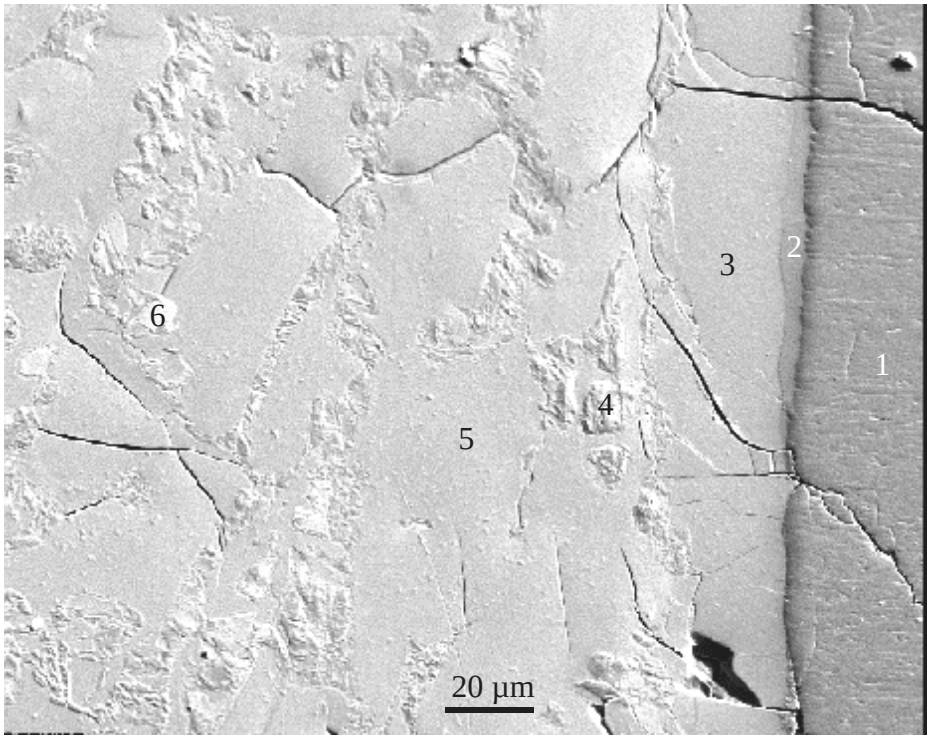

Fig. 4: SEM image of the range near ZrO_2 scale with Auger measuring points

Elemental compositions (at-%) at measuring points given in Fig. 4

	Fe	**Cr**	**Ni**	**Zr**	**O**
1				39	61
2				68	32
3	26	7	4	50	13
4				93	7
5	35		8	57	
6				90	10

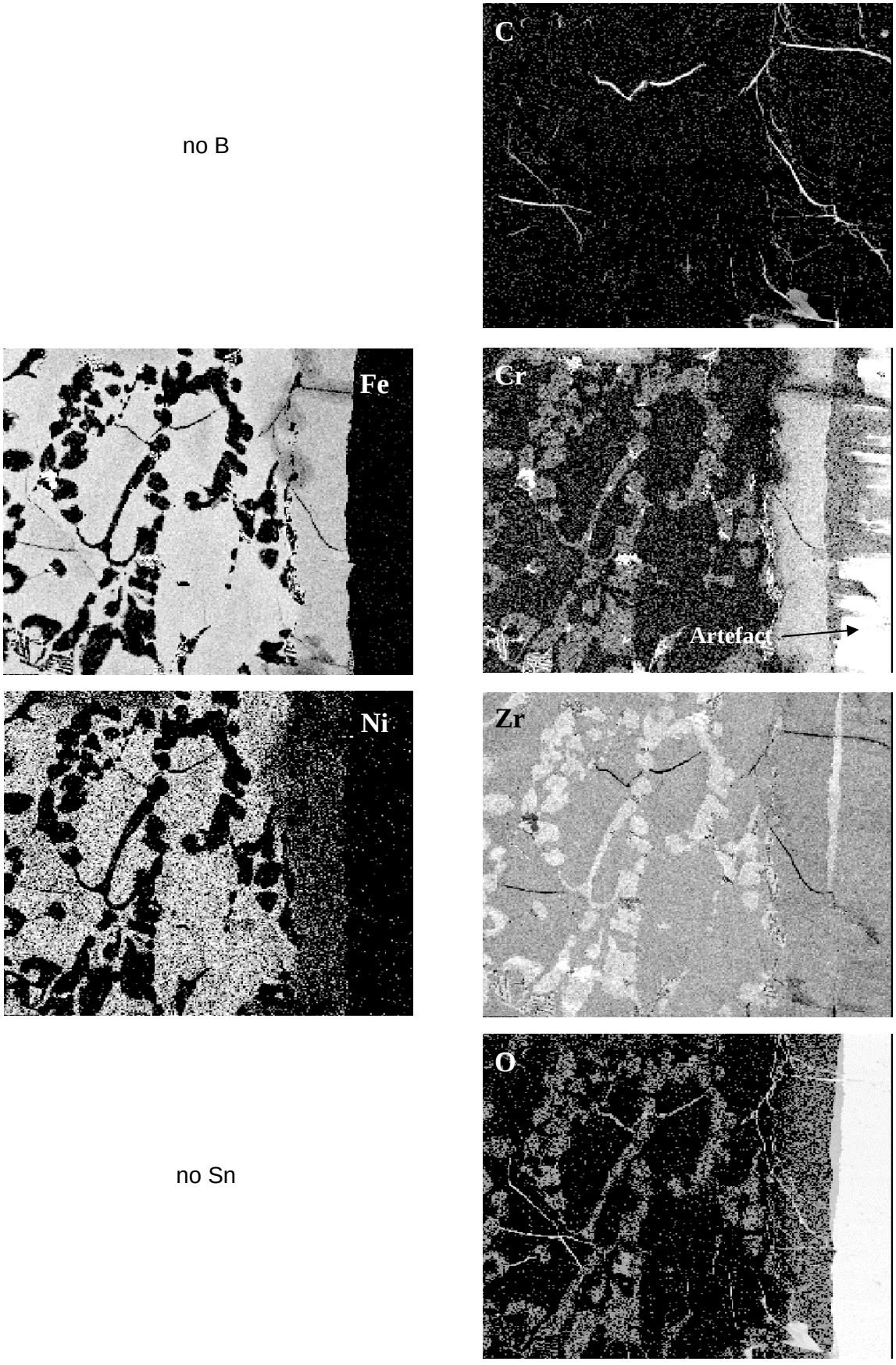

Fig. 5 a-h: Element mapping near outer ZrO_2 scale (see Fig. 4)

Auger elemental analysis near the boundary SS/Zry-4 (Area 3)

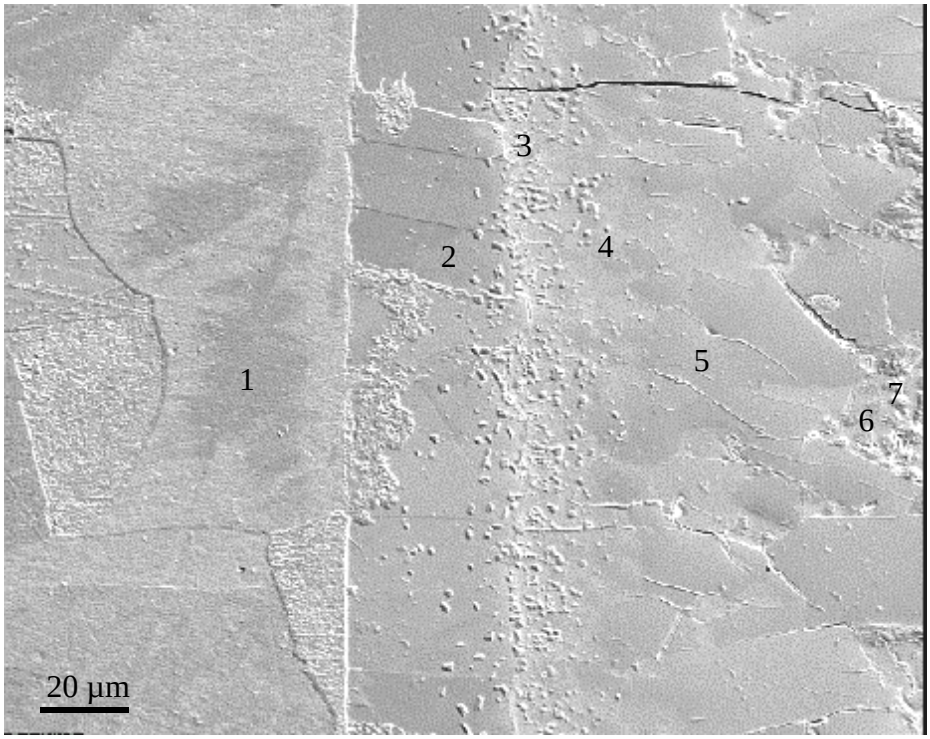

Fig. 6: SEM image of an area at the boundary SS/Zry-4 with Auger measuring points

Elemental compositions (at-%) at measuring points given in Fig. 6

	Fe	**Cr**	**Ni**	**Zr**	**Sn**	**O**	**Mo**
1	73	14	10				3
2	68	23	5				4
3	59	12	6	23			
4	32	3	6	51		7	
5	43	22		36			
6	37		8	55			
7				93	1	6	

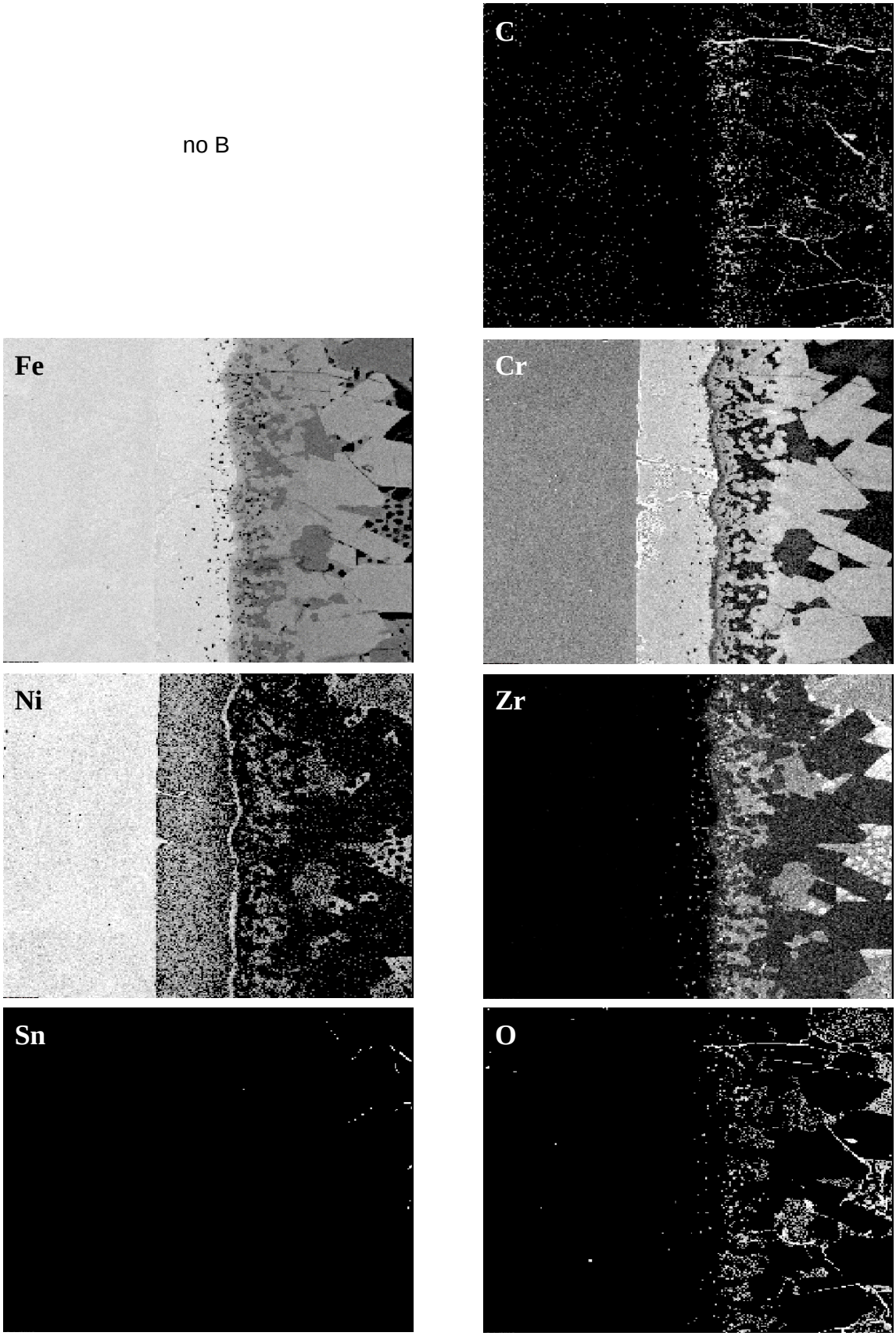

Fig. 7 a-h: Element mapping at the boundary region SS/Zry-4 (see Fig. 6)

Test Box11108: 1h, 1400 °C

Overview

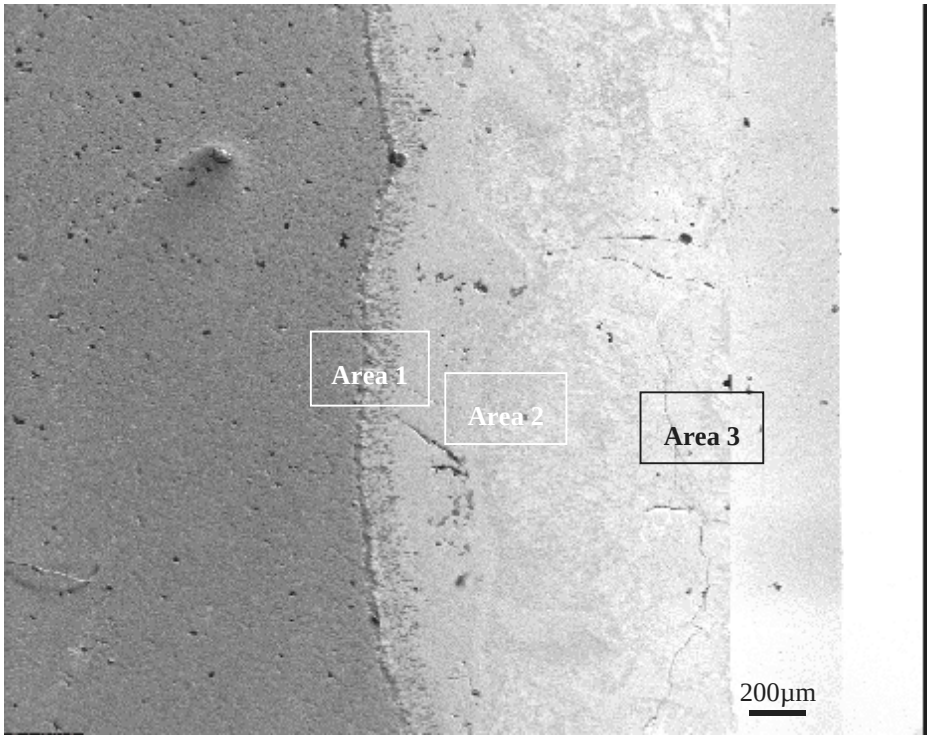

Fig1: Cross section through a CR segment after test at 1400 °C, left: B_4C, right: ZrO_2 with indicated areas for detailed Auger elemental analyses

Auger elemental analysis near B_4C (Area 1)

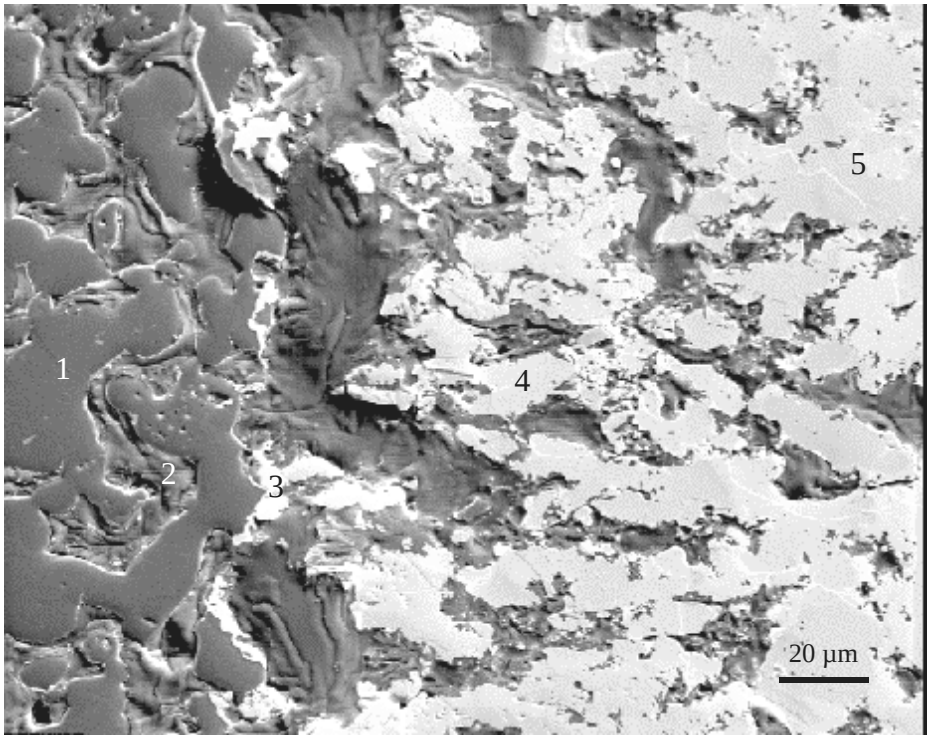

Fig. 2 : SEM image of the range near B_4C with Auger measuring points

Elemental compositions (at-%) at measuring points given in Fig. 2

	B	C	Fe	Cr	Ni	O
1	68	28				4
2*		100				
3	40		24	4	32	
4	44		41	15		
5	33		55	4	8	

** from embedding resin*

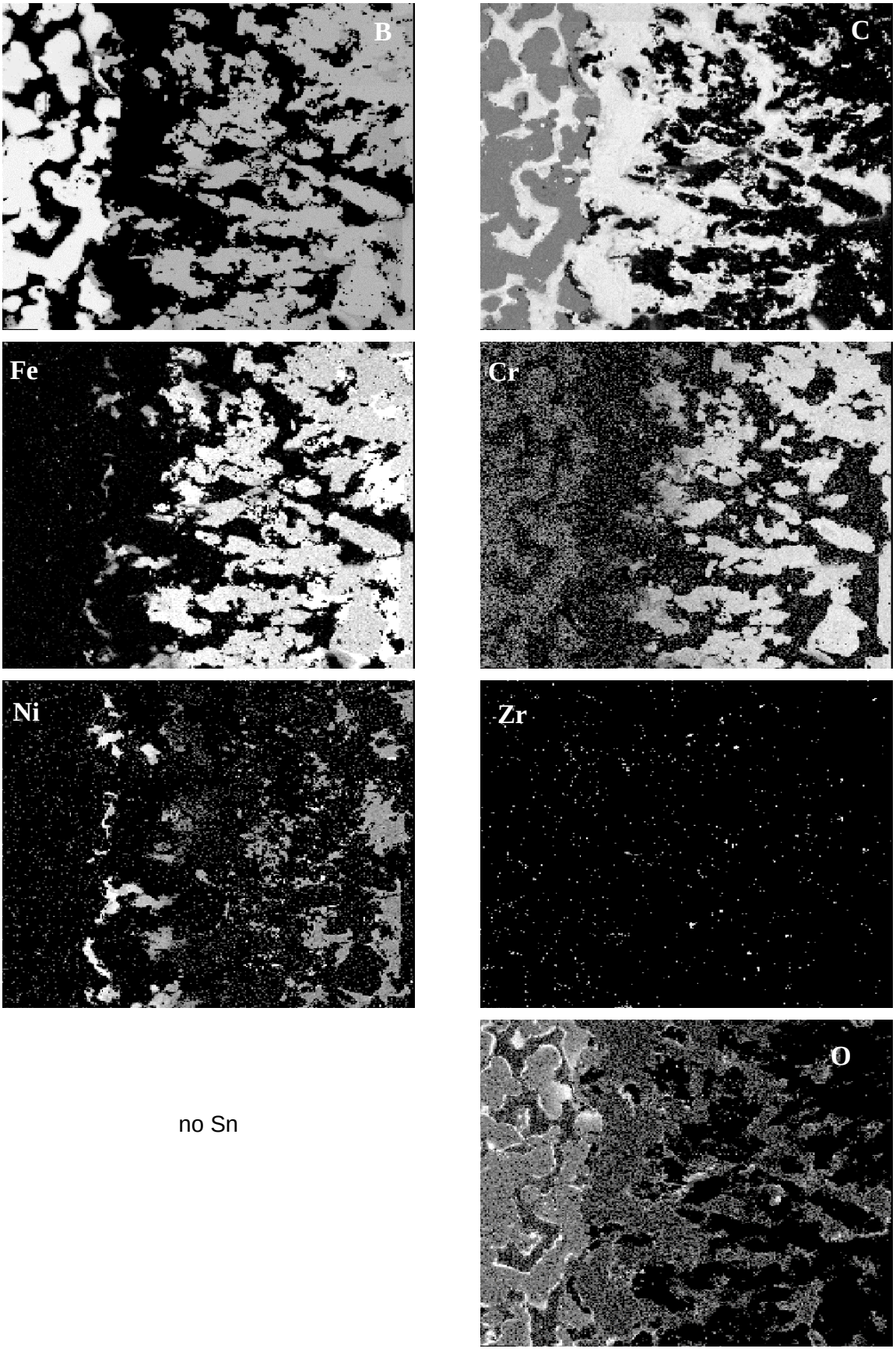

Fig. 3 a-h: Element mapping near B_4C (see Fig. 2)

Auger elemental analysis in SS/Zry melt (Area 2)

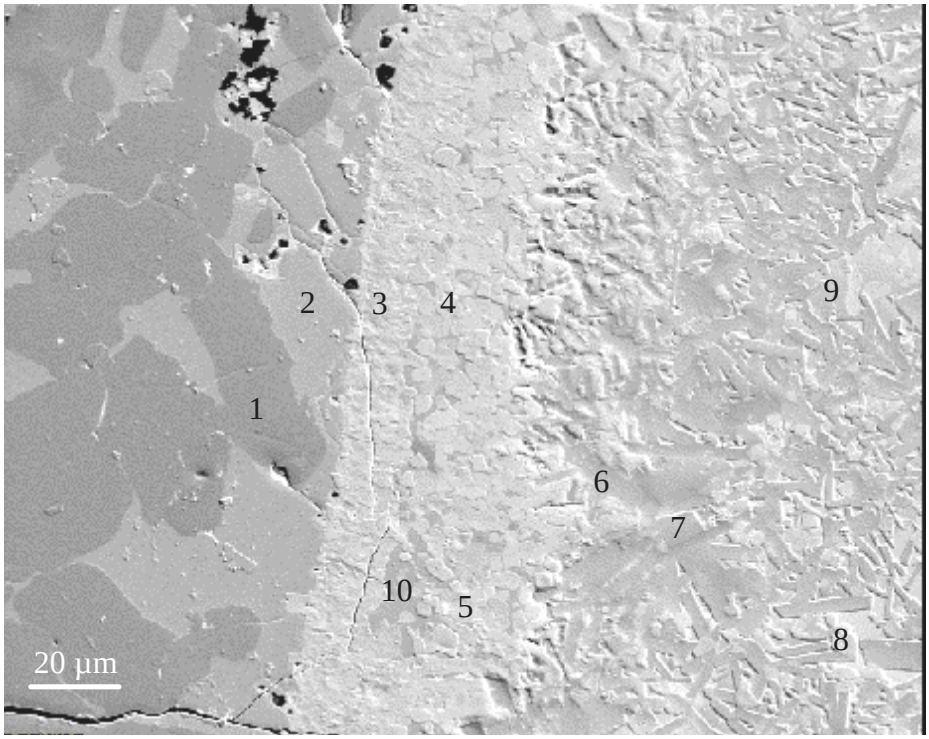

Fig. 4 : SEM image of the molten SS/Zry range with Auger measuring points

Elemental compositions (at-%) at measuring points given in Fig. 4

	B	**C**	**Fe**	**Cr**	**Ni**	**Zr**	**O**
1	47		34	19			
2	34		54	5	7		
3		52				41	7
4		59				41	
5	26	29				41	4
6	61					39	
7	60					40	
8	21	33				41	5
9			76	24			
10	35		60	5			

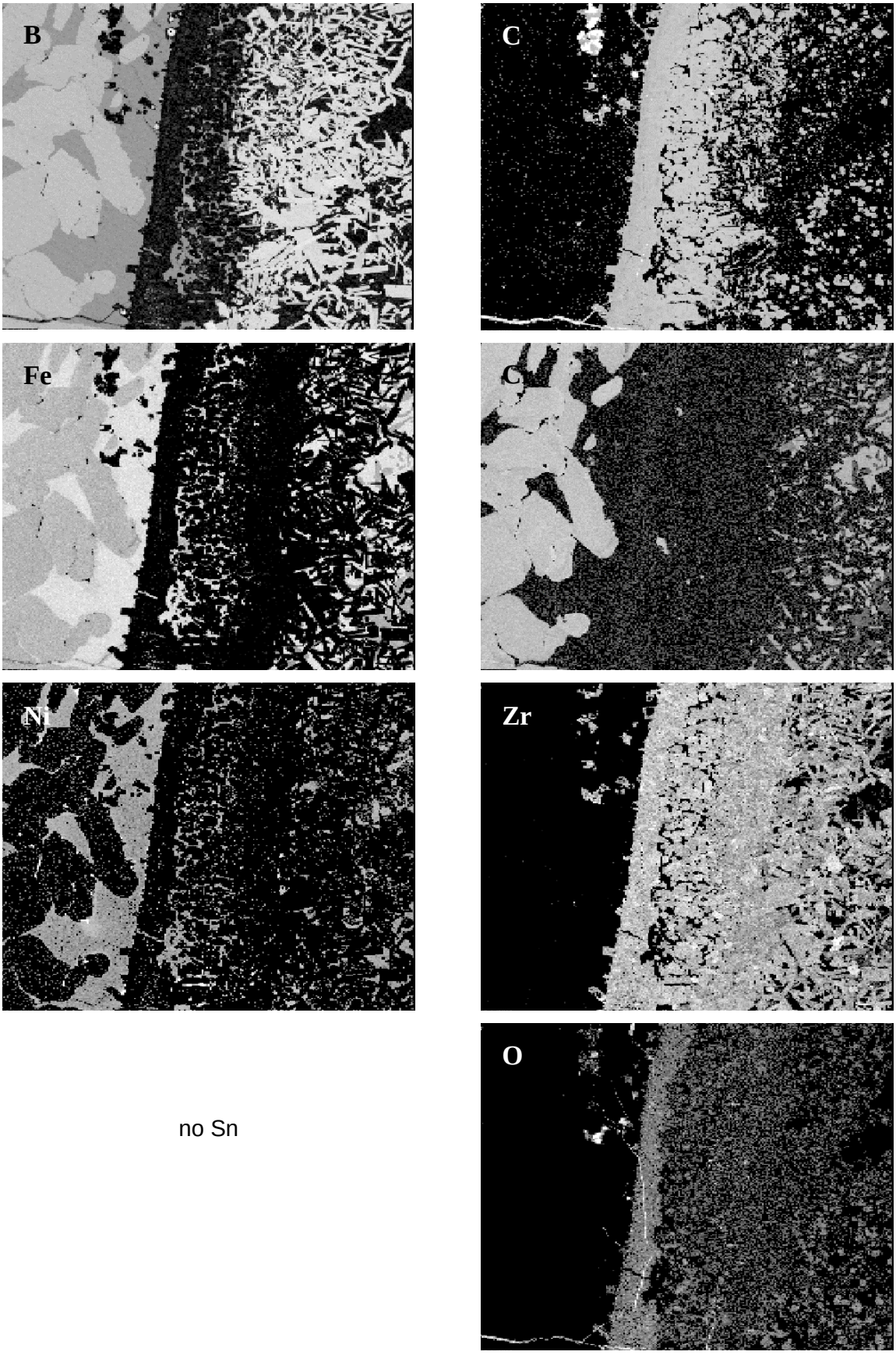

no Sn

Fig. 5 a-h: Element mapping in the molten SS/Zry range (see Fig. 4)

Auger elemental analysis near outer ZrO2 scale (Area 3)

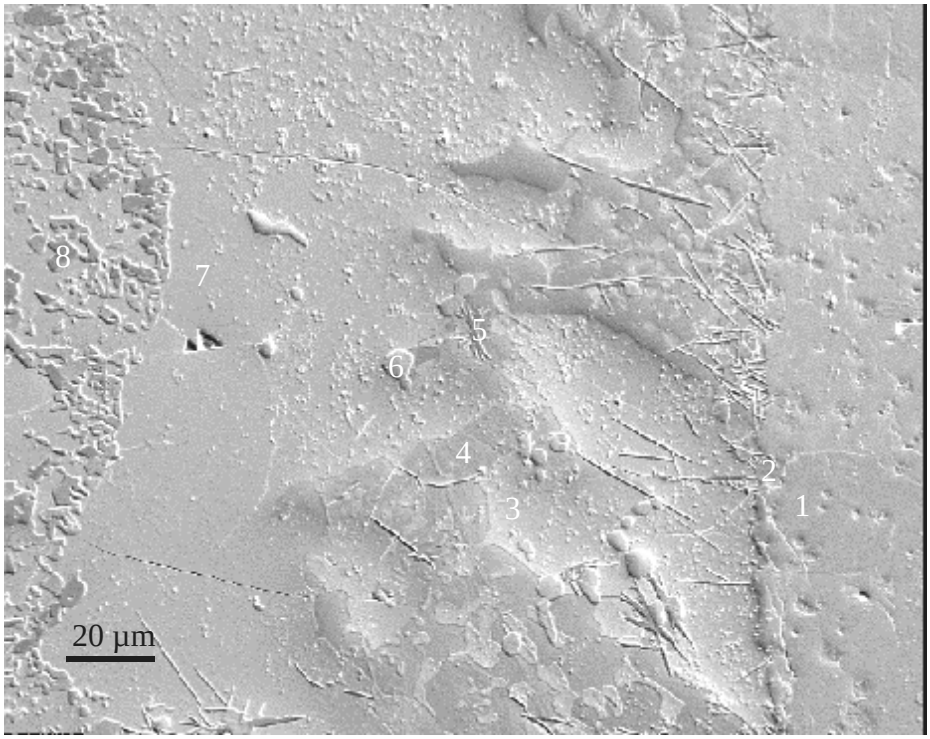

Fig. 6: SEM image of the range near outer ZrO_2 with scale measuring points

Elemental compositions (at-%) at measuring points given in Fig. 6

	B	C	Fe	Cr	Ni	Zr	O
1						37	63
2		34				43	23
3			53	8	7	32	
4			76	24			
5	61					39	
6						38	62
7			57	12		31	
8	64					36	

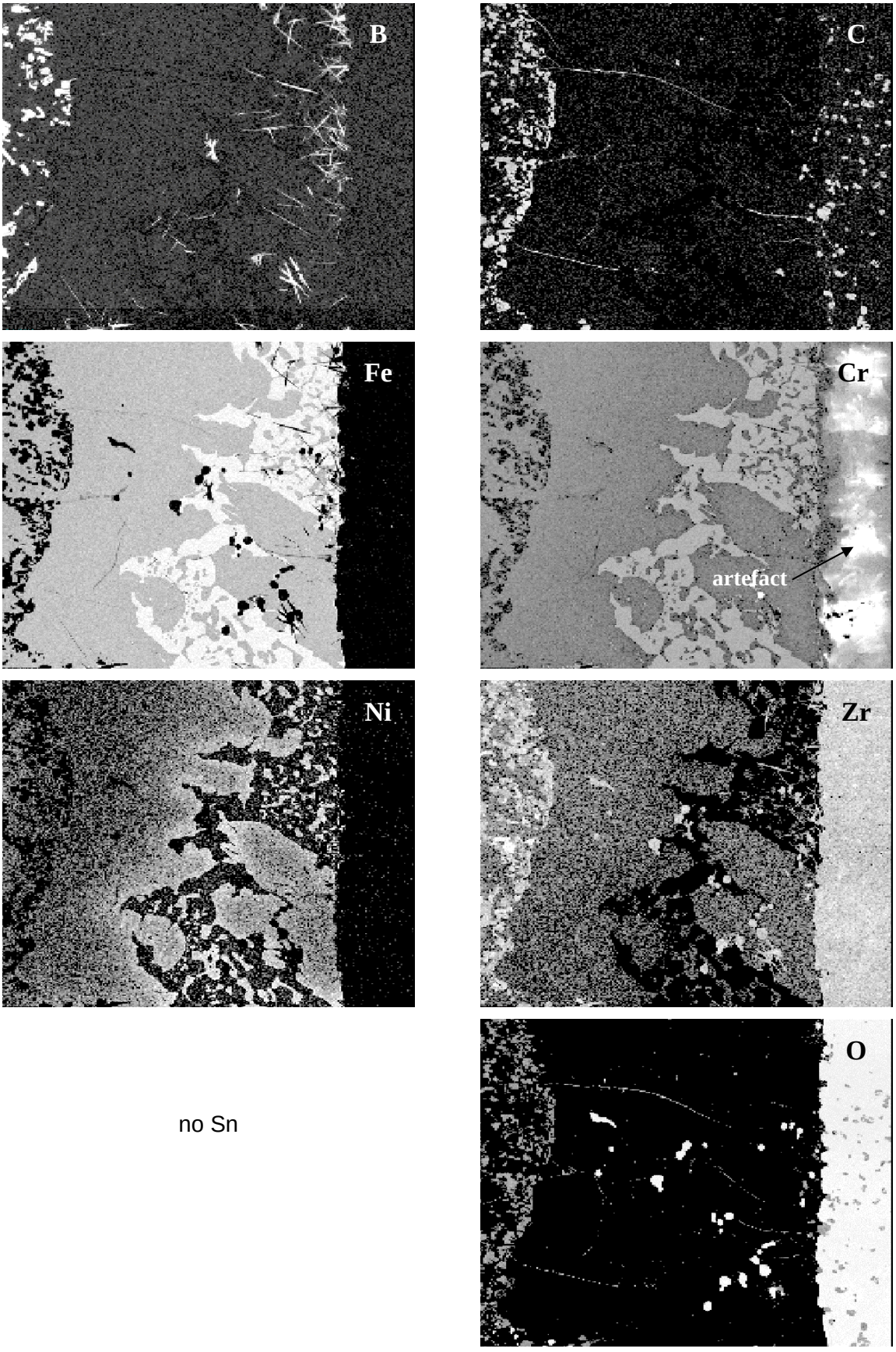

Fig. 7 a-h: Element mapping near outer ZrO_2 scale (see Fig. 6)

Test Box11109: 1h, 1600 °C

Overview

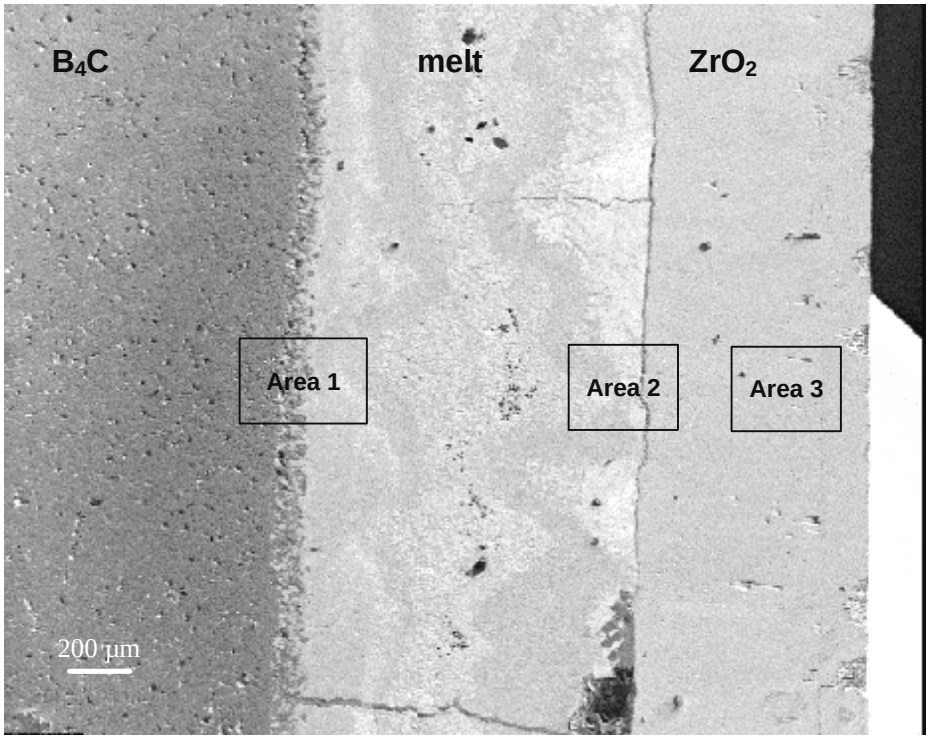

Fig. 1: Cross section through a CR segment after test at 1600 °C, left: B_4C, right: ZrO_2 with areas for detailed Auger elemental analyses

Auger elemental analysis near B_4C (Area 1)

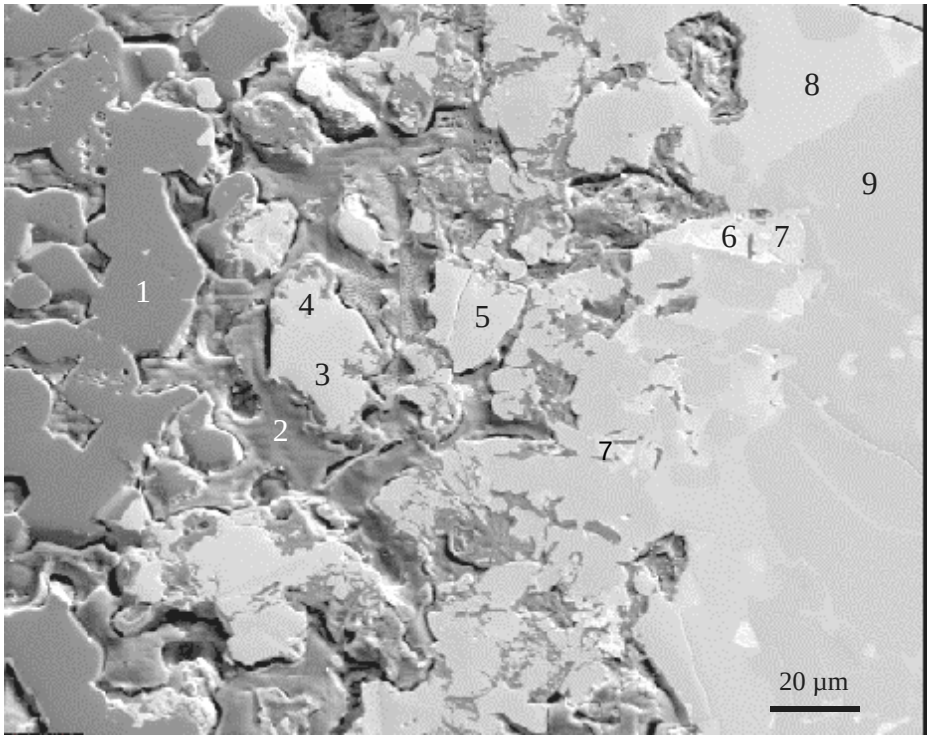

Fig. 2: SEM image of the range near B_4C with Auger measuring points

Elemental compositions (at-%) at measuring points given in Fig. 2

	B	**C**	**Fe**	**Cr**	**Ni**	**Zr**	**Sn**	**Si**
1	78	22						
2		100						
3	47		37	12	4			
4	39	8	29	6	18			
5	50		29	21				
6					83		8	9
7		12	18		42	21		7
8	35		55	5	5			
9	52		20	28				

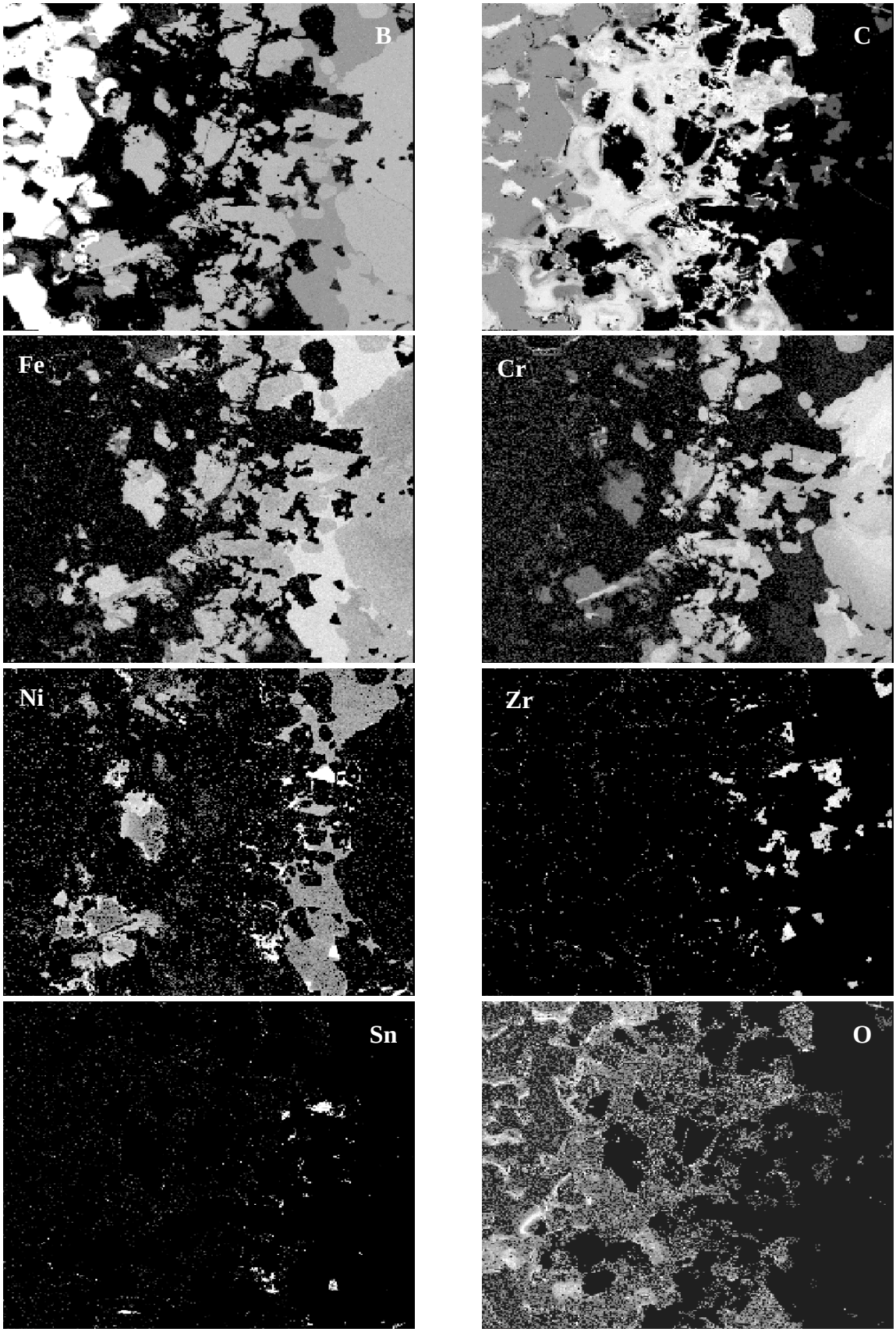

Fig. 3 a-h: Element mapping near B_4C (see Fig. 2)

Auger elemental analysis near the boundary SS/Zry-4 (Area 2)

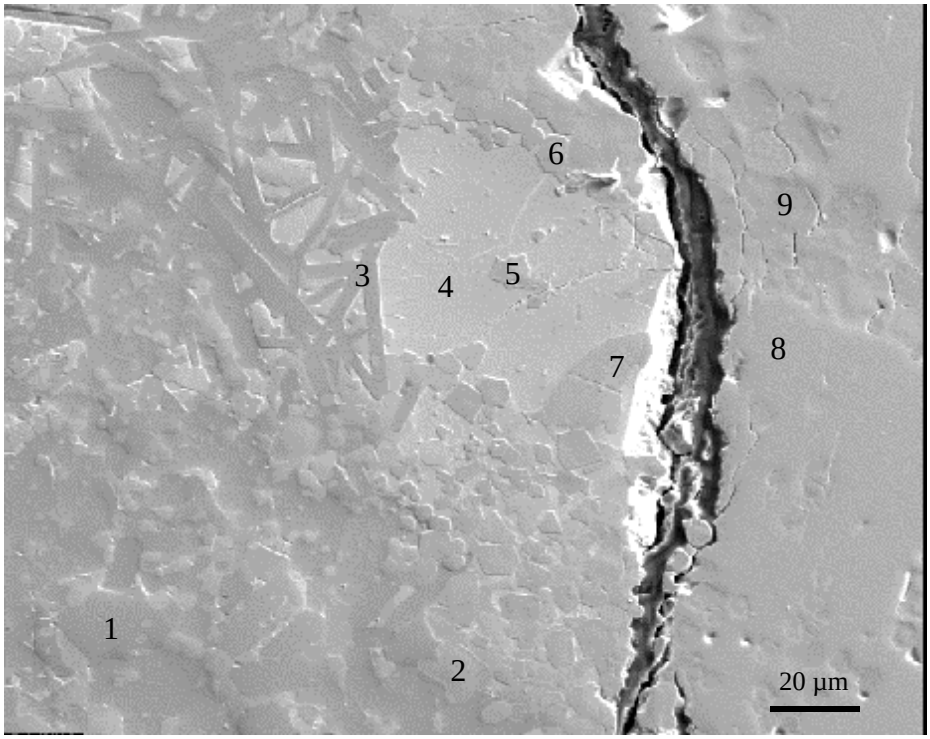

Fig. 4: SEM image of the range near the boundary SS/Zry with Auger measuring points

Elemental compositions (at-%) at measuring points given in Fig. 4

	B	**C**	**Fe**	**Cr**	**Ni**	**Zr**	**O**
1	62					38	
2		52				39	9
3	60					40	
4			53	8	10	29	
5		50				39	11
6		51				40	9
7			78	22			
8						38	62
9		48				40	12

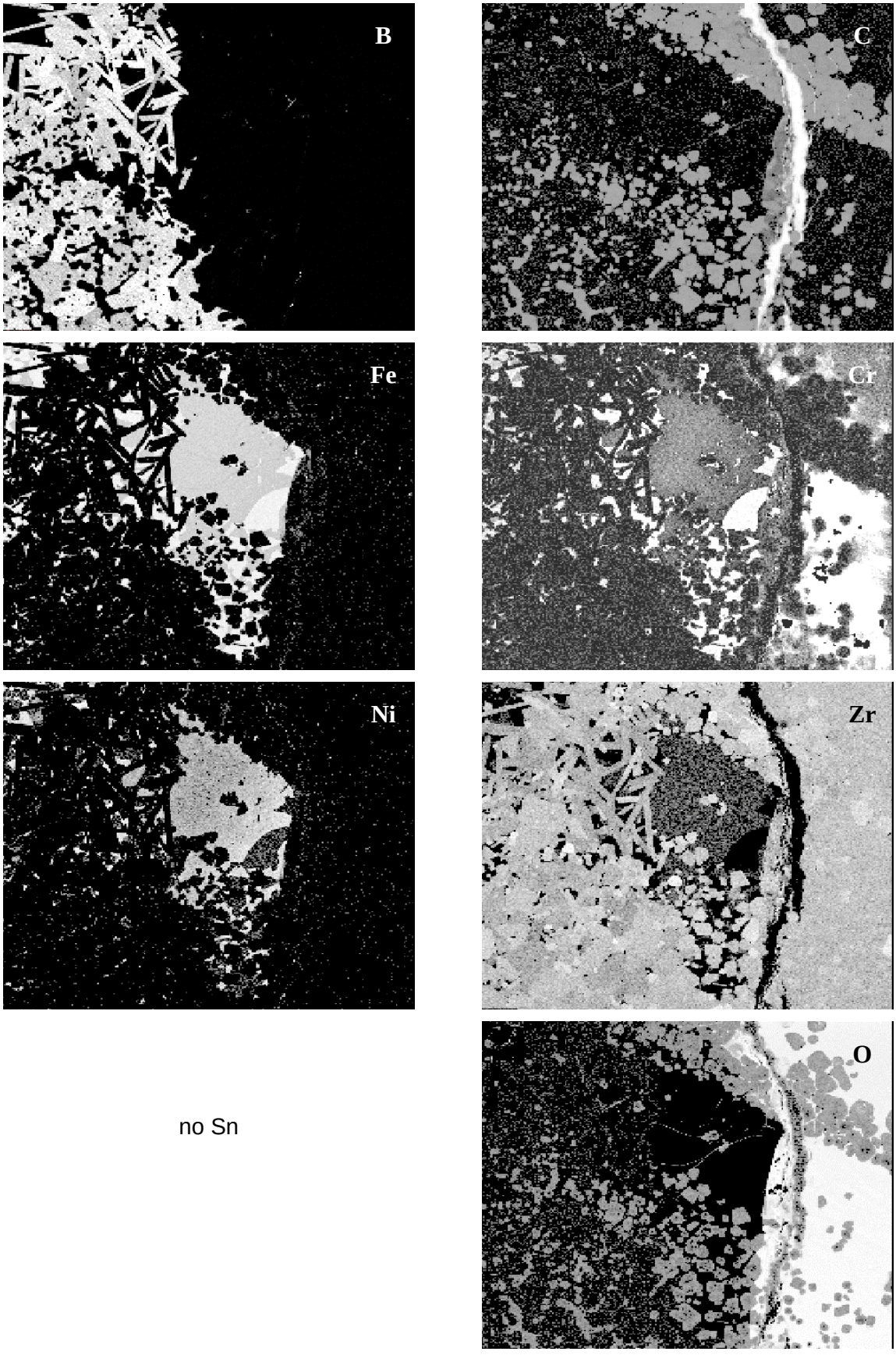

Fig. 5 a-h: Element mapping near boundary SS/Zry (see Fig. 4)

Auger elemental analysis near outer ZrO_2 scale (Area 3)

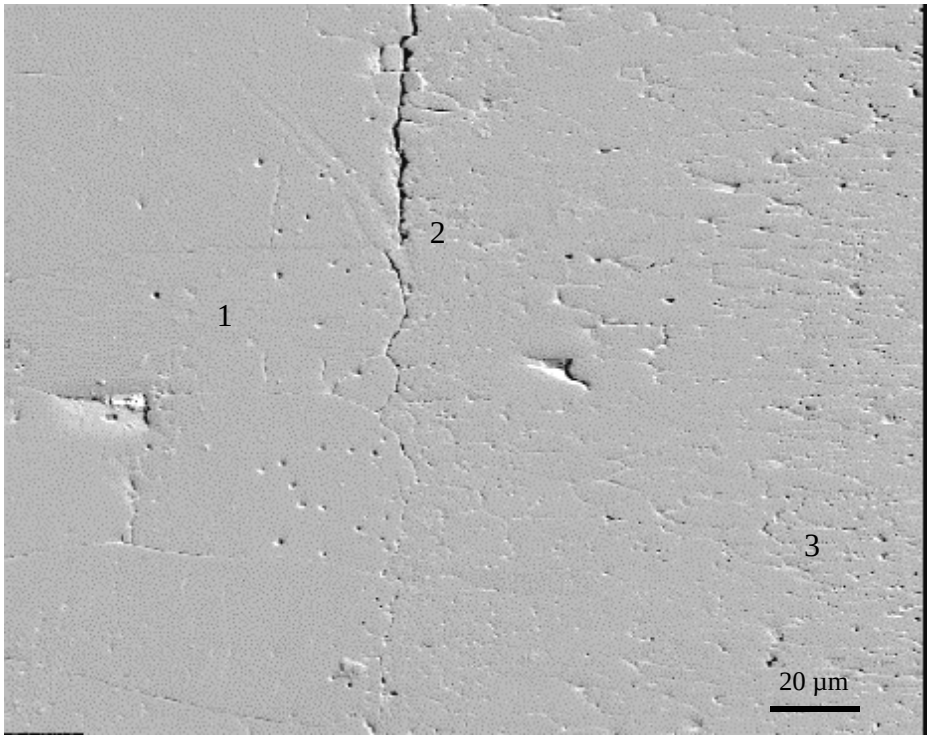

Fig. 6: SEM image of the range near the outer ZrO_2 scale with Auger measuring points

Elemental compositions (at-%) at measuring points given in Fig. 6

	Zr	**O**
1	40	60
2	43	57
3	38	62

no B

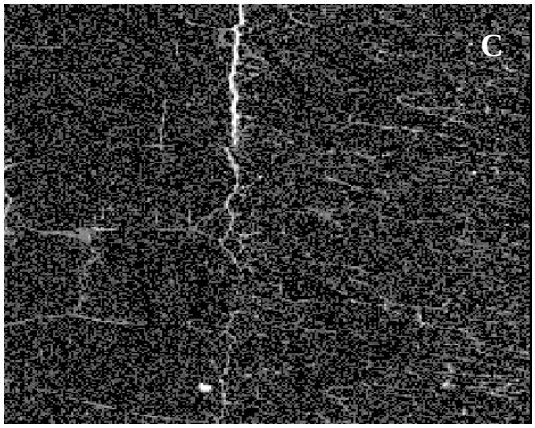

no Fe

no Cr

no Ni

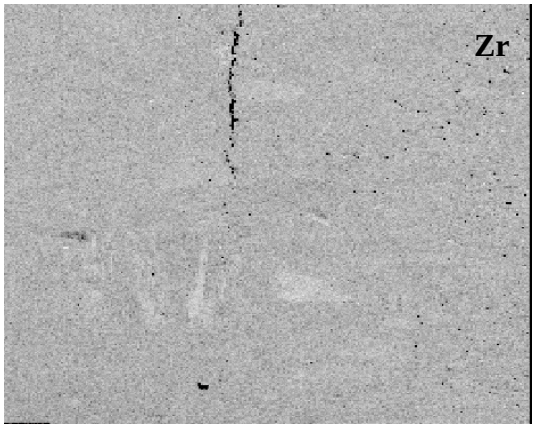

no Sn

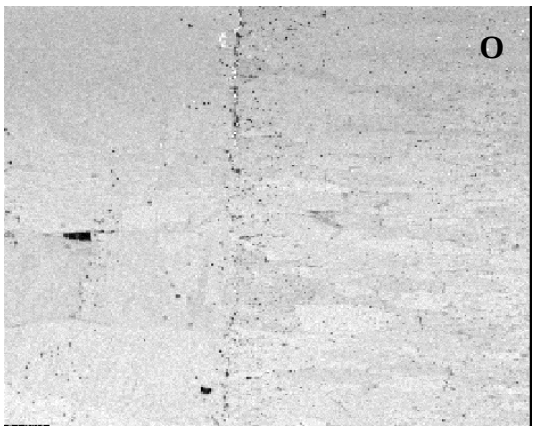

Fig. 7 a-h: Element mapping at the outer ZrO_2 scale (see Fig. 6)

A8 Light microscopic examinations of the 1-pellet-size specimens with ceramic caps

BOX20528b: 1200 °C

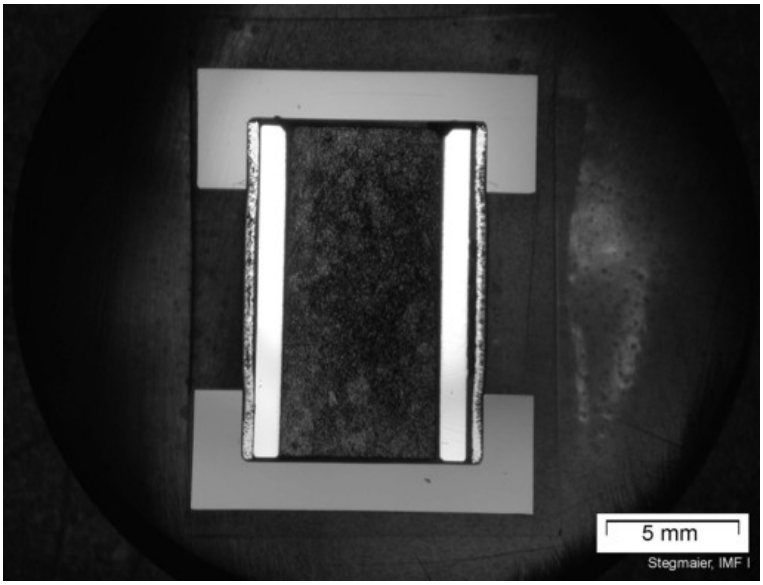

Overview
Pellet was loose in the CR segment

Box20528b.jpg

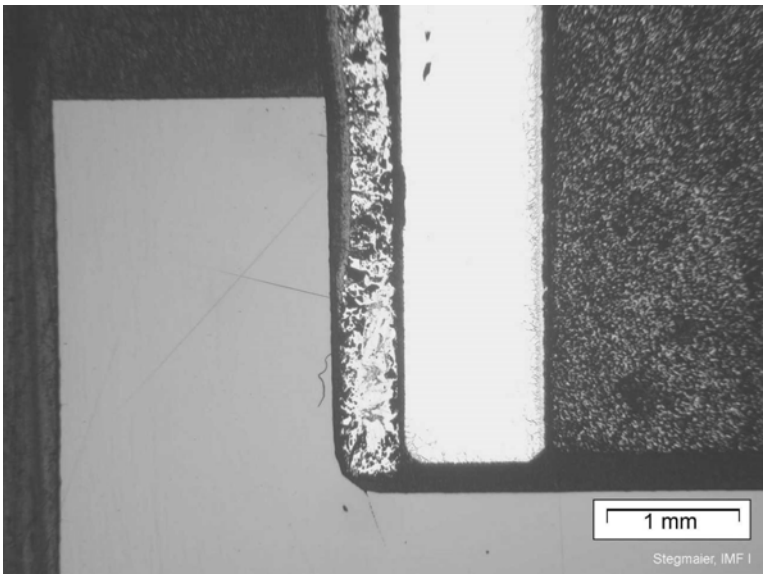

Detail of the overview image: lower left corner
Oxide up to the middle of the gap between zirconia cap and CR segment

Box205028b_1_1x2.jpg

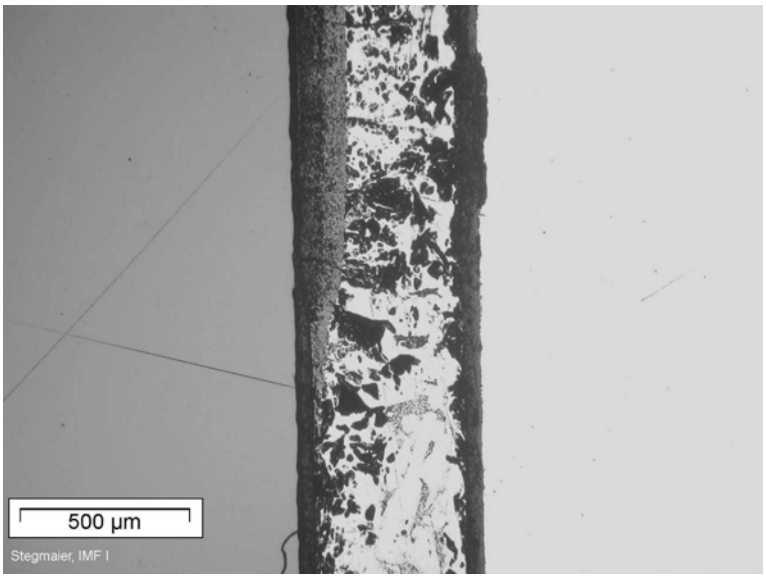

Detail of the previous image
Only slight interaction between Zircaloy and stainless steel

Box205028b_1-1_1x5.jpg

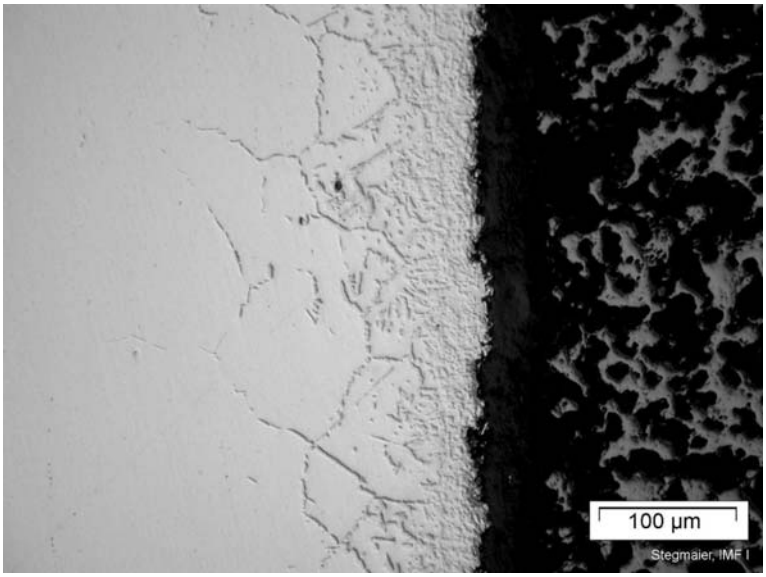

Boundary SS/B_4C
Image taken with inter-ferencial contrast
Formation of new phases in SS

Box205028b_1-2_1x20.jpg

BOX20605: 1300 °C

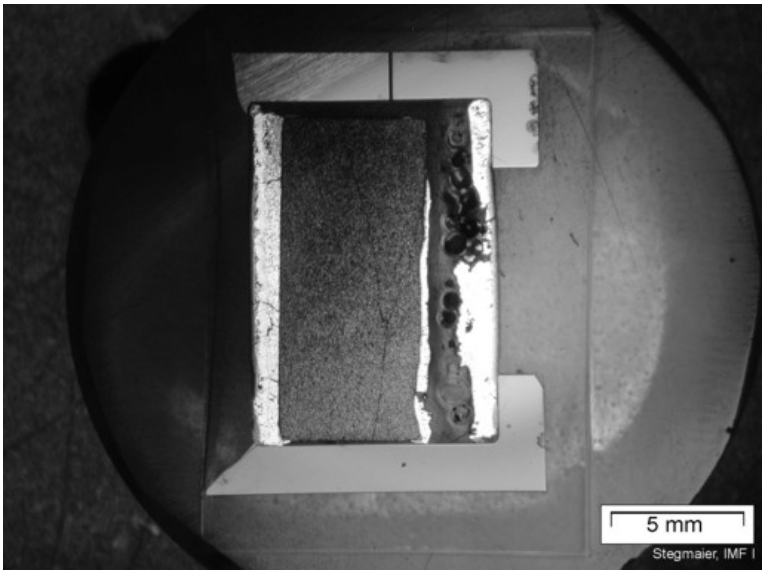

Overview
Complete reaction of the SS cladding

Box20605.jpg

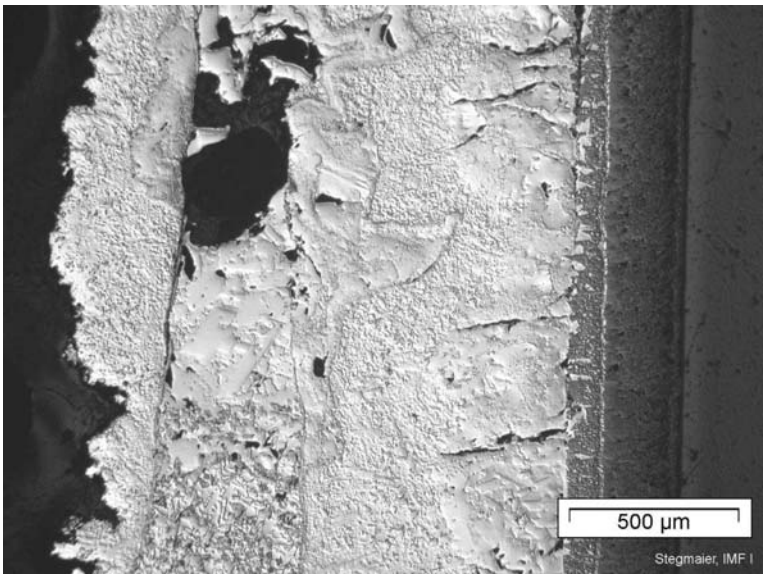

Series of images of the lower right side of the specimen (this + next three ones)
Outer oxide scale and multi-phase, multi-component solidified melt

Box20605_4_1x5.jpg

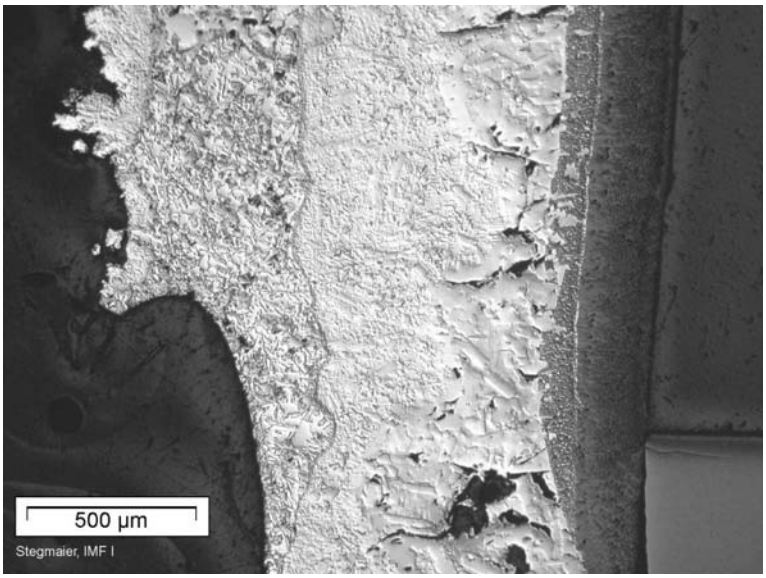

Box20605_3_1x5.jpg

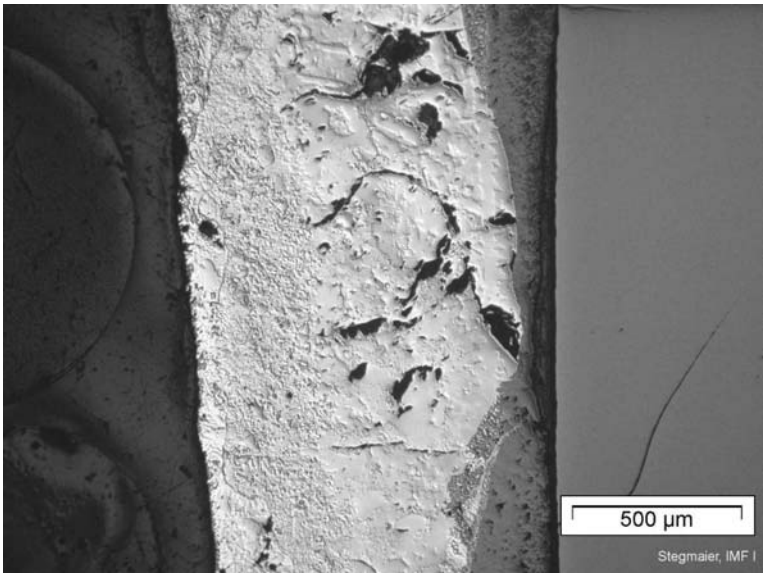

Box20605_2_1x5.jpg

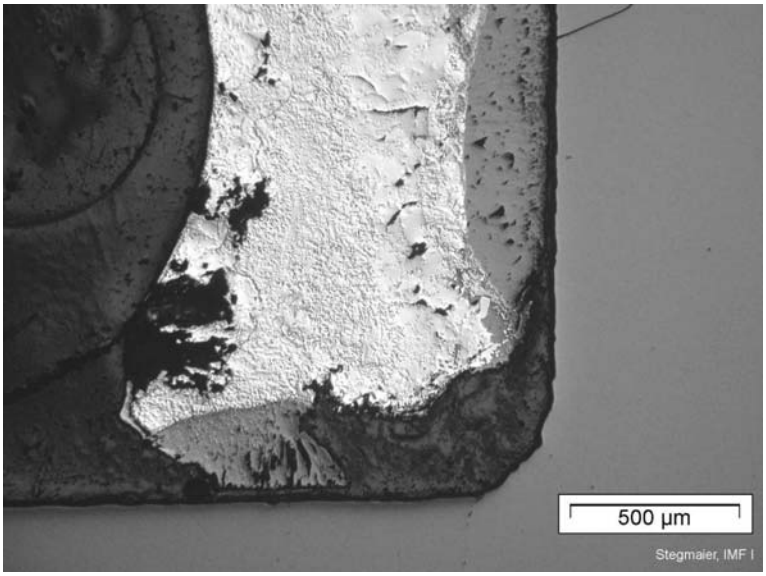

Box20605_1_1x5.jpg

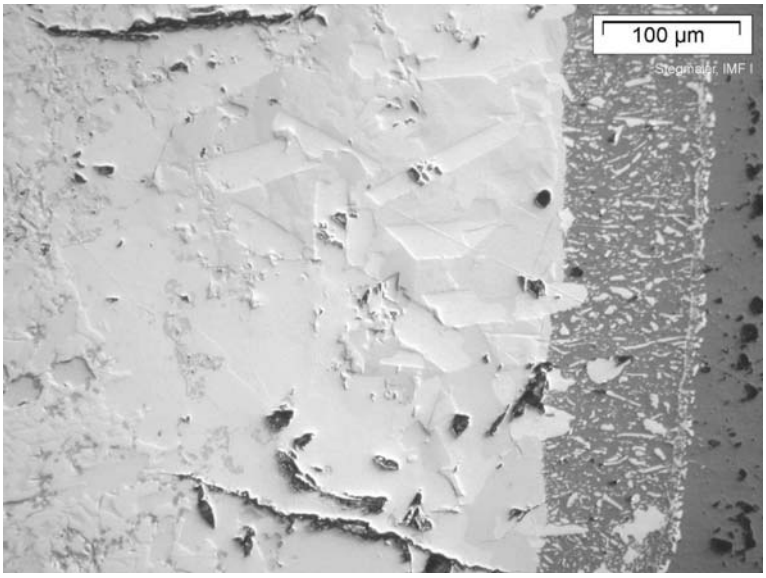

Magnification of Box20605_4

Box20605_4-7_1x20.jpg

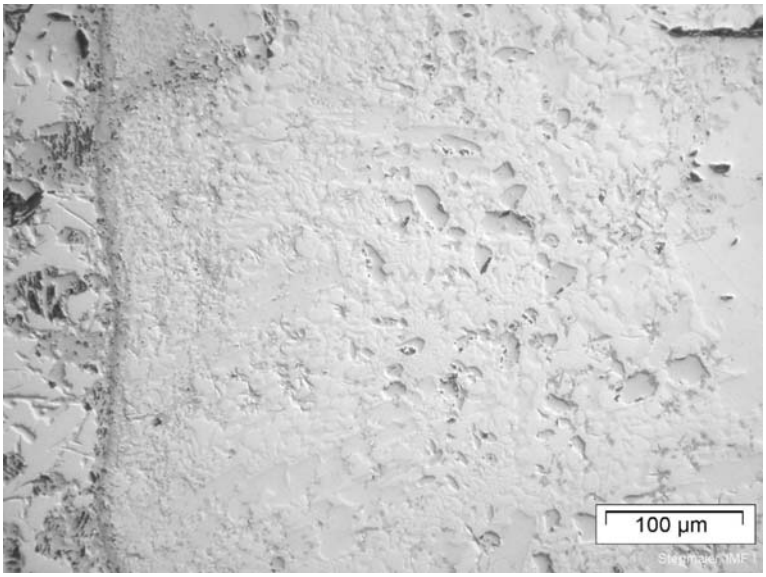

ditto

Box20605_4-6_1x20.jpg

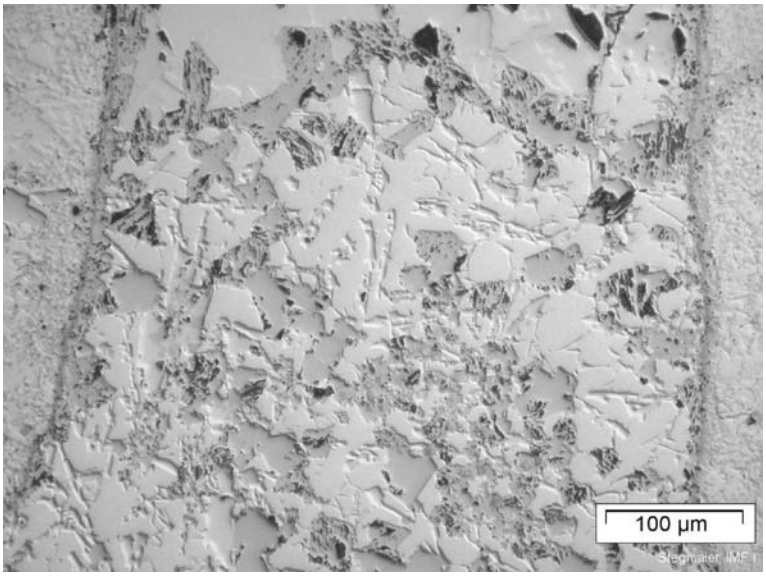

Box20605_4-5_1x20.jpg

Box20529: 1400 °C

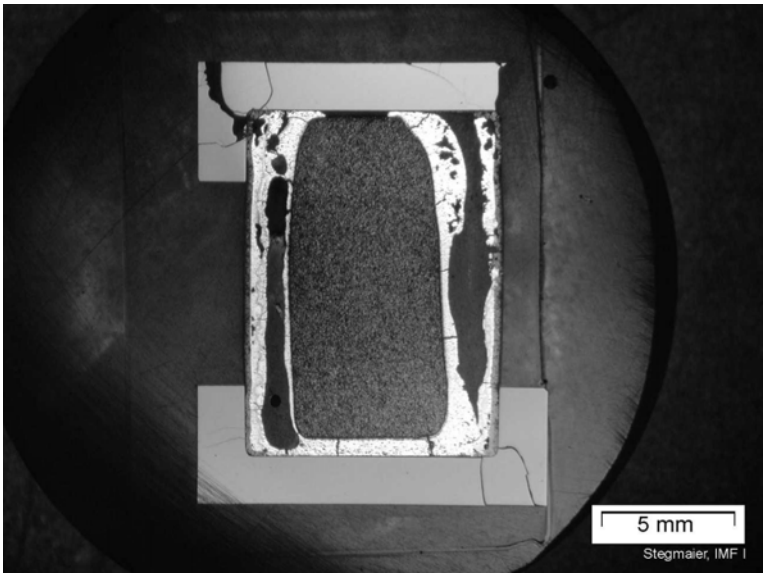

Overview

Box20529.jpg

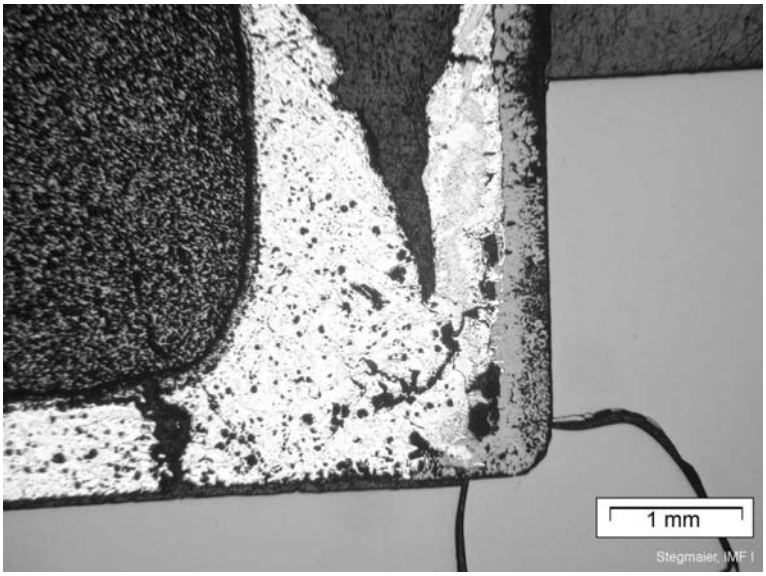

Lower right corner of the specimen

Box20529_1_1x2.jpg

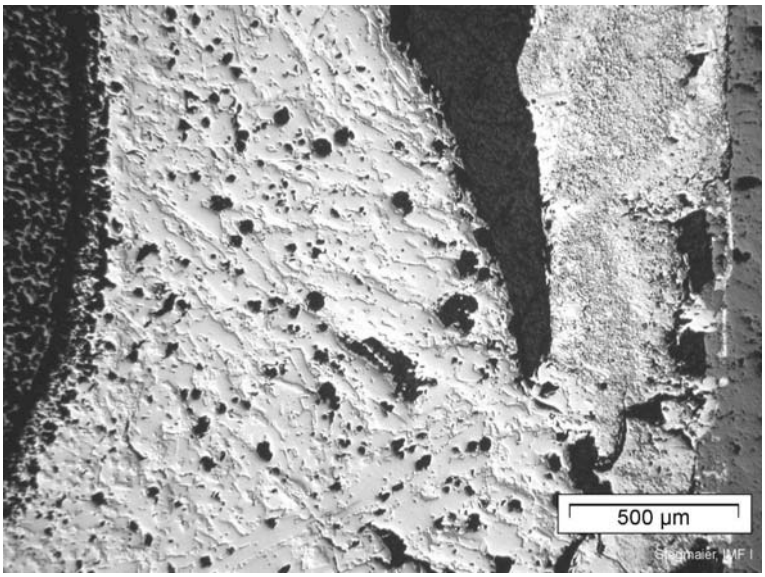

Magnification of the previous image
The following four photos are further magnified images of this one

Box20529_1-2_1x5.jpg

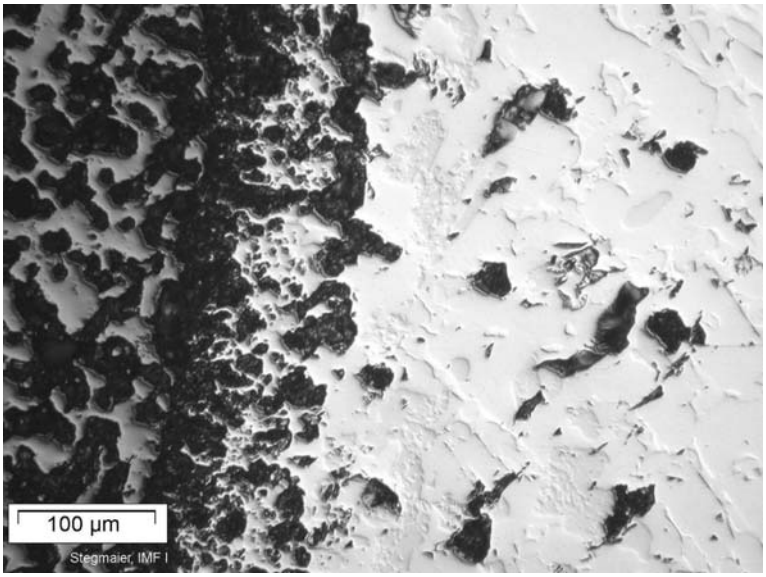

Box20529_1-2-1_1x20.jpg

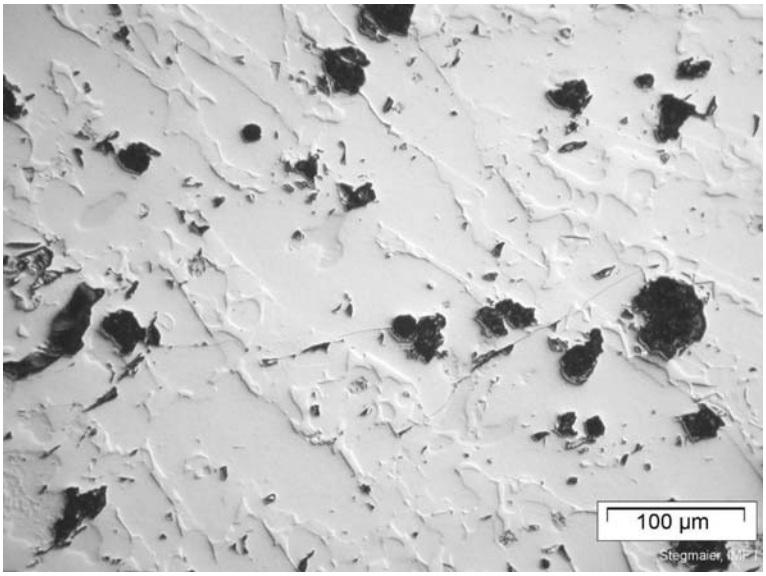

Box20529_1-2-2_1x20.jpg

Box20606: 1500 °C

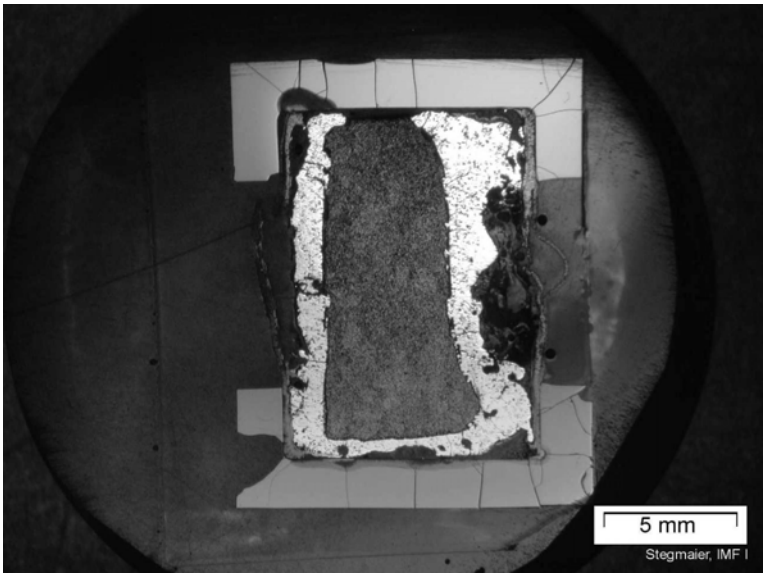

Overview

Box20606.jpg

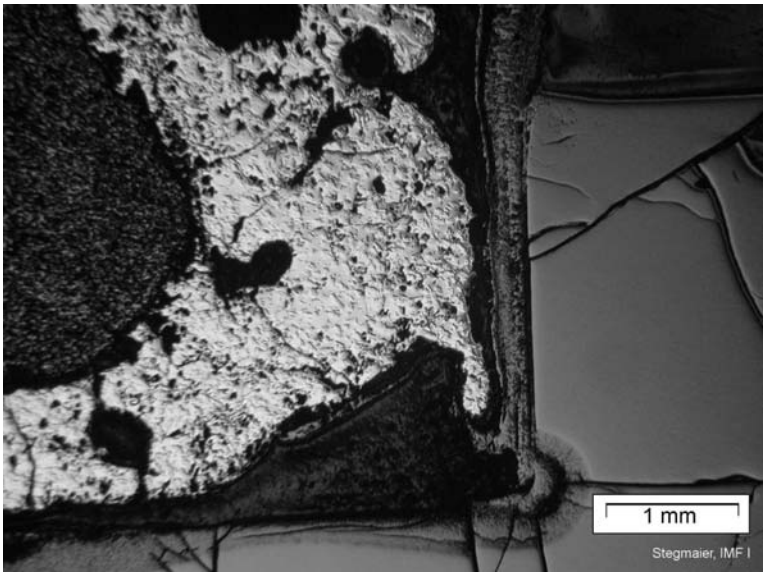

Lower right corner of the specimen

Box20606_1_1x2.jpg

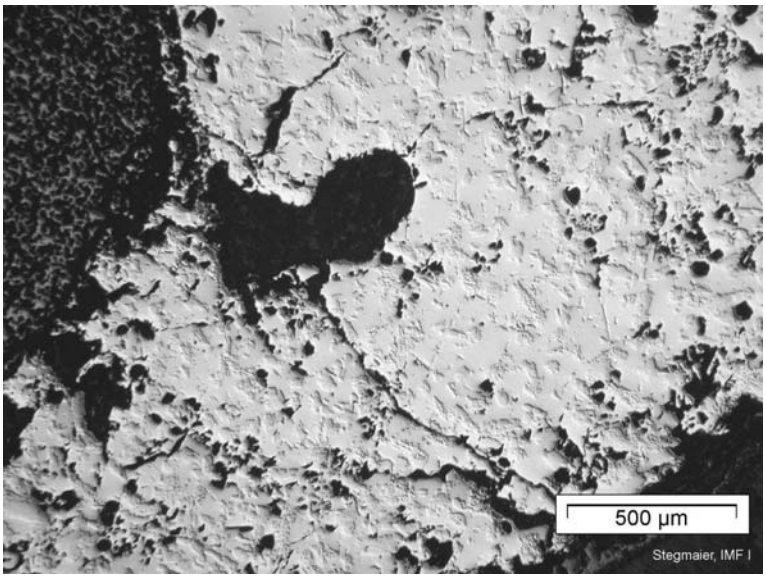

Magnification of the lower right corner
The following images show details from left to the right

Box20606_1-1_1x5.jpg

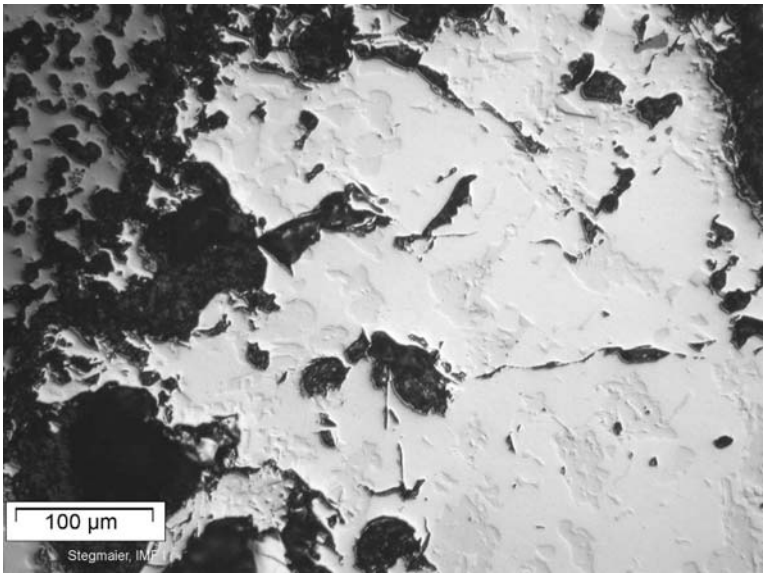

Box20606_1-1-1_1x20.jpg

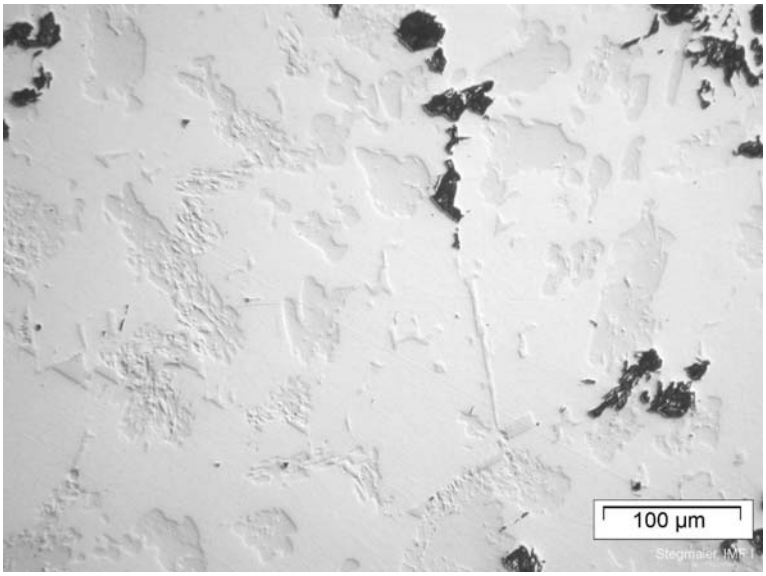

Box20606_1-1-4_1x20.jpg

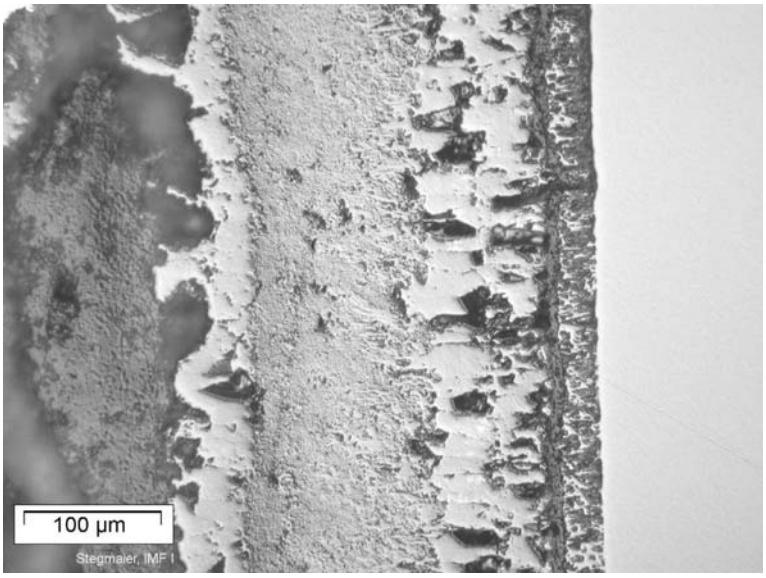

Box20606_1-1-7_1x20.jpg

Box20610: 1500 °C

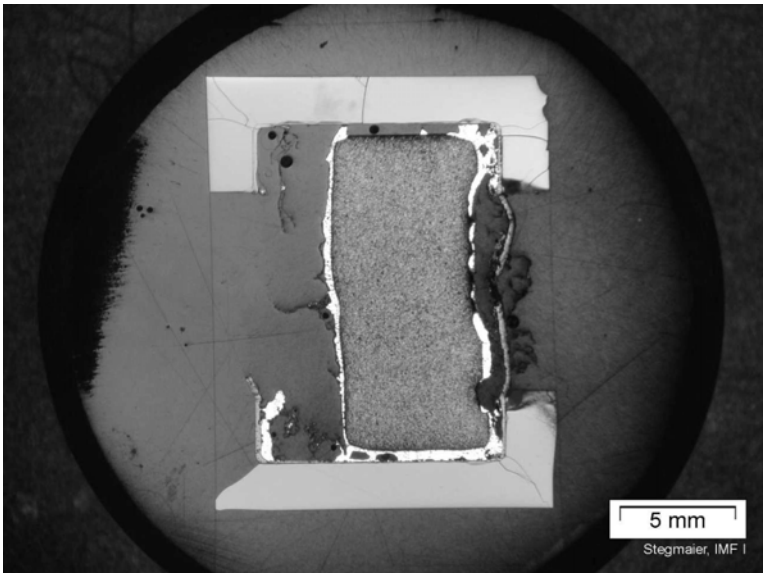

Overview
Melt was ejected into the reaction tube

Box20610.jpg

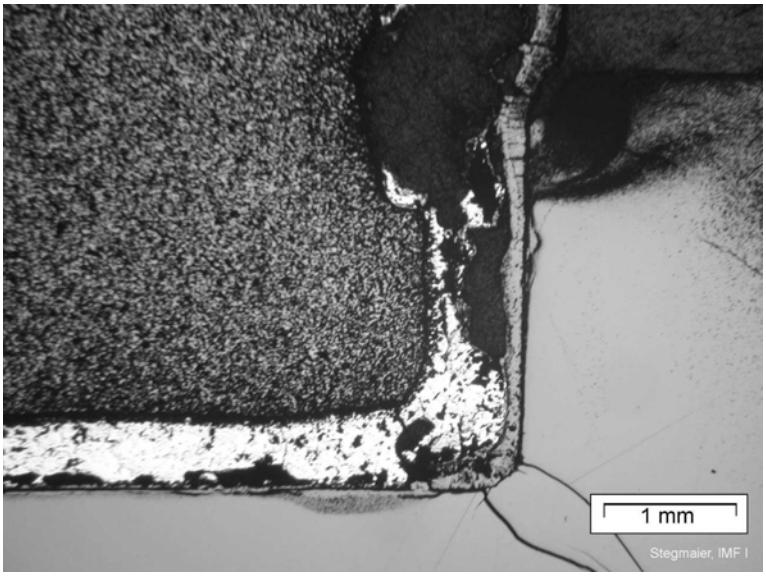

Lower right corner of the specimen
Following images with increasing magnification of that position

Box20610_1_1x2.jpg

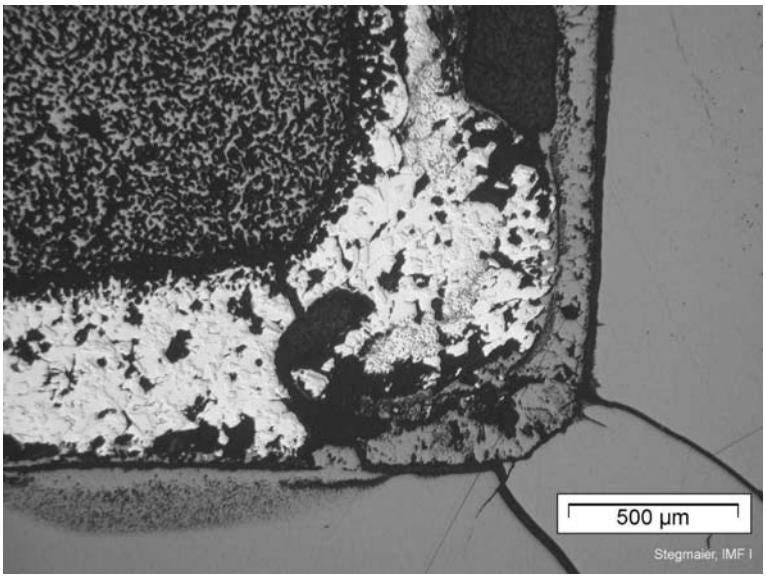

Box20610_1-1_1x5.jpg

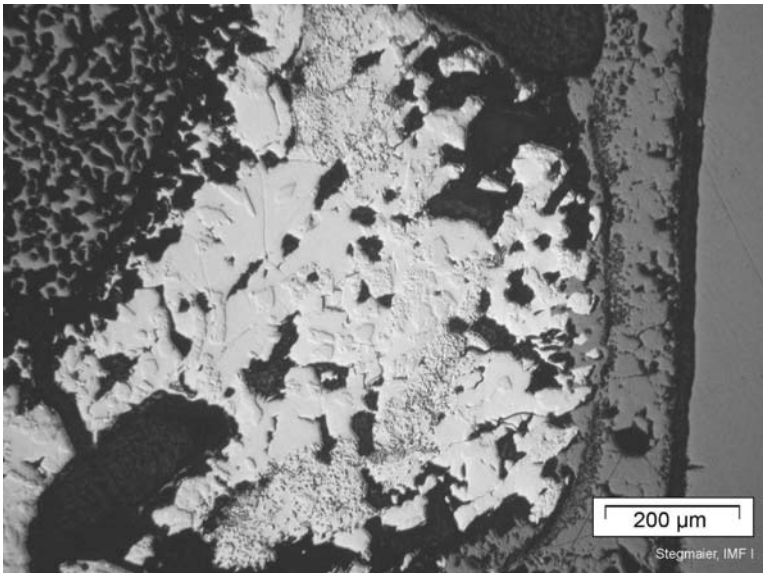

Box20610_1-1-1_1x10.jpg

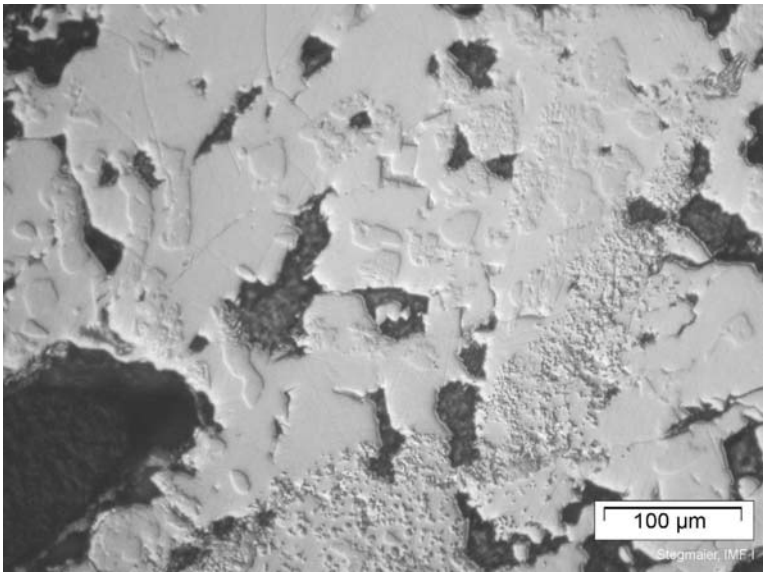

Box20610_1-1-2_1x20.jpg

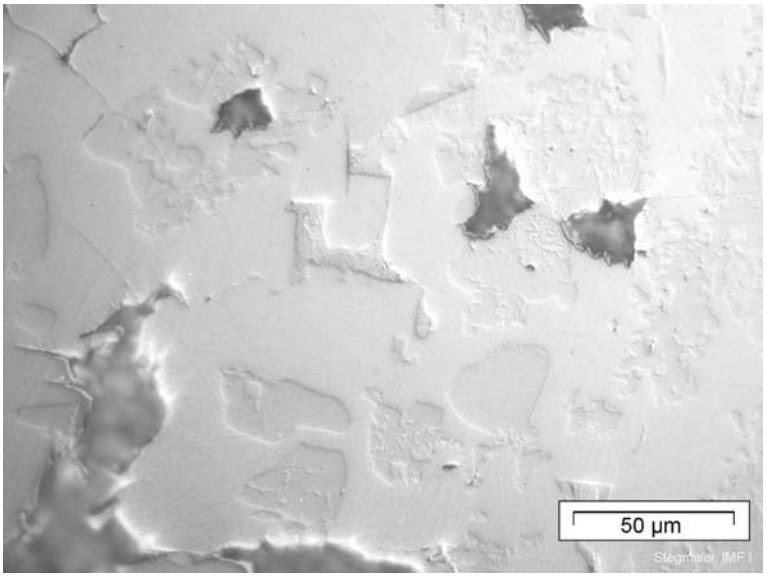

Box20610_1-1-3_1x50.jpg

A9 SEM/Auger investigations of the 1-pellet-size specimens with ceramic caps

On the following pages the results of SEM/Auger investigations of the specimens after isothermal tests at 1300, 1400 and 1500 °C are summarised. Integral compositions of the absorber melts, elemental compositions of the various phases as well as mappings of all available elements are given. Regarding the element mappings: The concentration of an element in a phase is the higher the brighter the colour in the image.

Test Box20605: 1h, 1300 °C

Overview

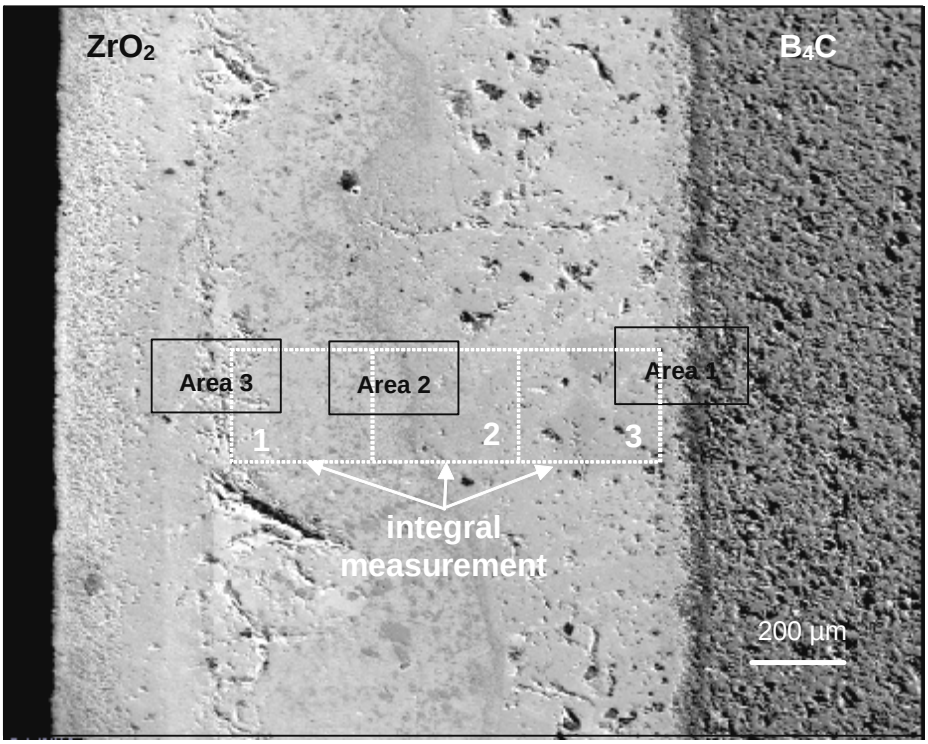

Fig. 1: Cross section through a CR segment after 1 h isothermal test at 1300 °C in argon/steam atmosphere; left: ZrO_2 scale, right: B_4C pellet; areas for detailed analyses are indicated with black rectangles; areas for integral analyses of the melt in white

Integral analyses (in at-%) of the absorber melt by Auger spectroscopy

Area	B	C	Fe	Cr	Ni	Zr	O
1	8.1	5.7	45.7	12.0	5.0	20.1	3.5
2	17.4	13.2	37.1	9.7	5.0	16.1	1.4
3	31.8	2.8	42.5	12.8	4.7	4.3	1.2
Mean	**19**	**7**	**42**	**12**	**5**	**13**	**2**

Auger elemental analyses near B_4C pellet (area 1)

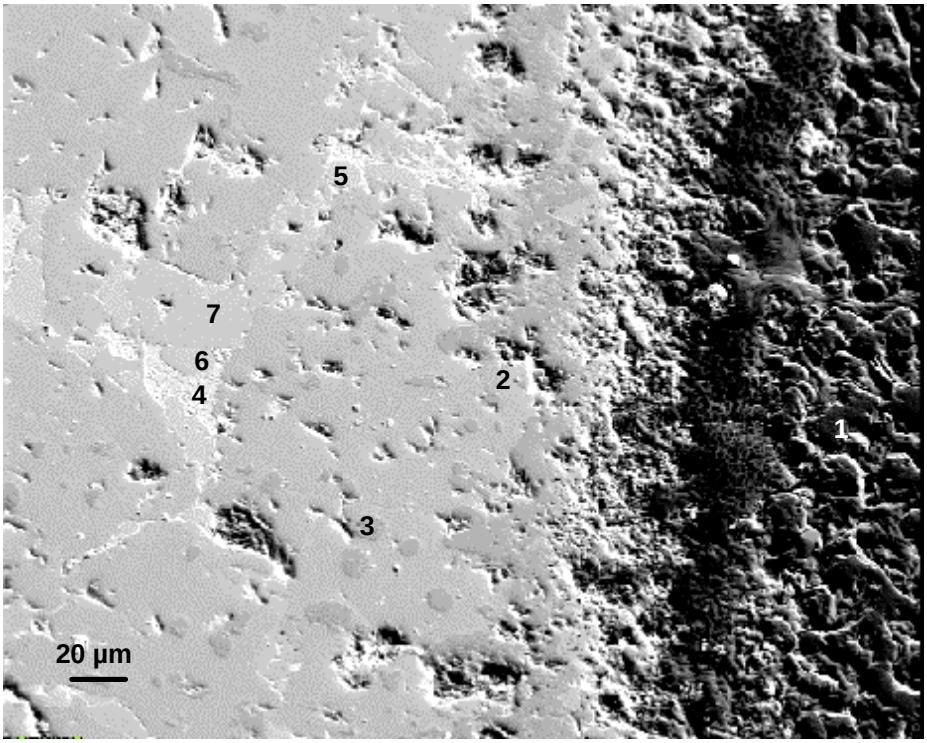

Fig. 2: SEM Image of the area near B_4C with Auger measuring points

Elemental compositions (in at-%) at measuring points given in Fig. 2

	B	**C**	**Fe**	**Cr**	**Ni**
1	79	21			
	37		47	12	4
3	51		19	30	
4			51	2	47
5	17	10	54	6	13
6	22	8	53	5	12
7	13	21	46	16	4

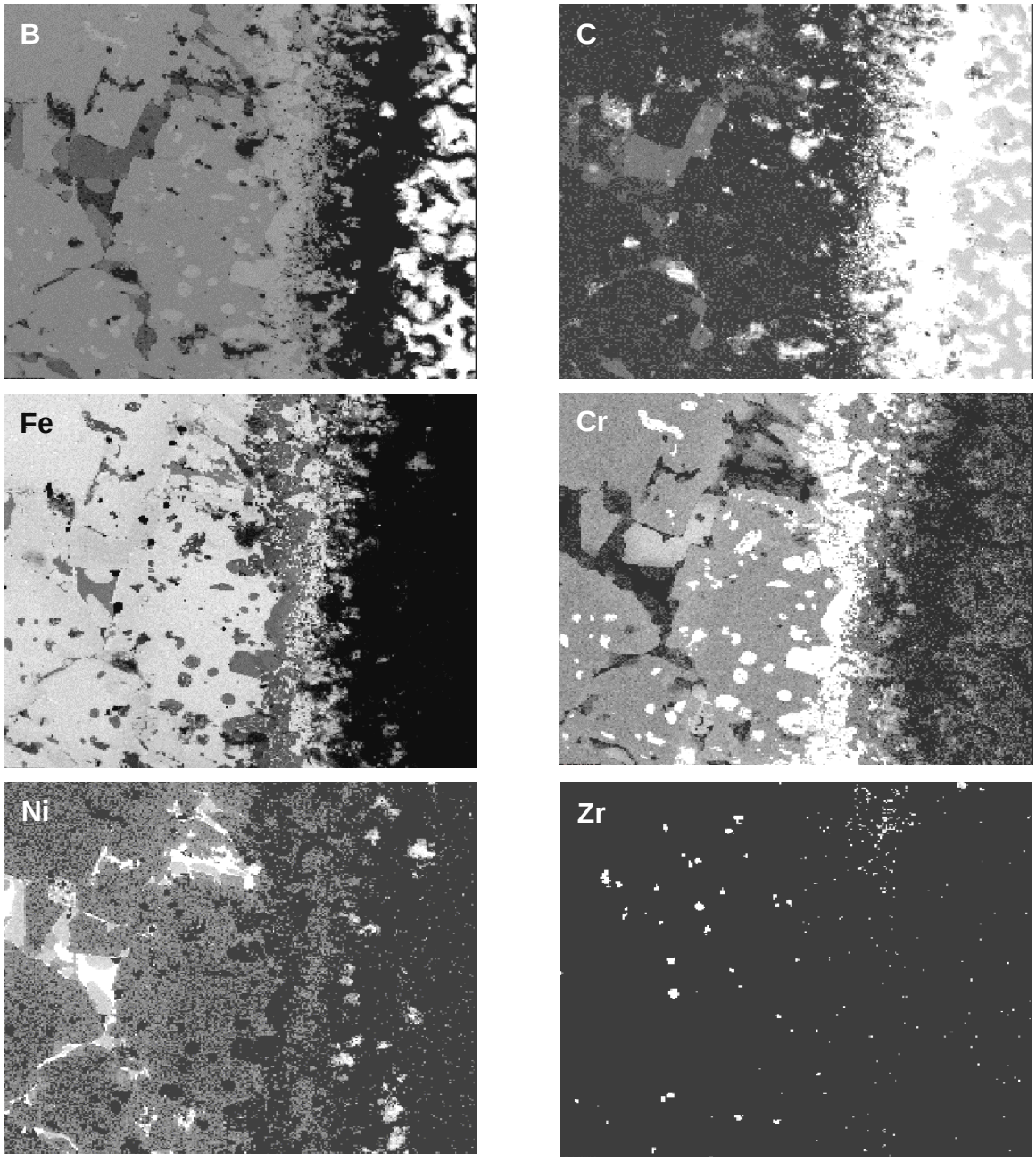

Fig. 3: Auger element mapping of the area near B_4C (Fig. 2)

Zr rich phases in the melt near B_4C pellet

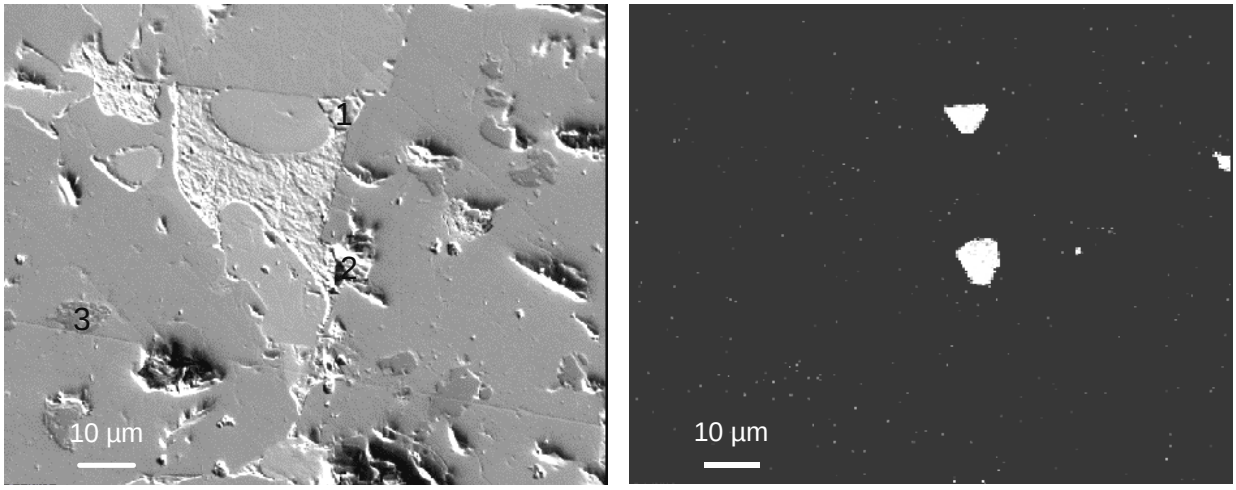

SEM image Zr map

Fig. 4: SEM image with measuring points and Zr element map showing the formation of Zr rich phases far away from the Zircaloy guide tube

Elemental compositions (in at-%) at measuring points given in Fig. 4

	B	**C**	**Fe**	**Cr**	**Zr**	**O**	**N**
1		51			45	4	
2		48			44	3	5
3	48		18	34			

Auger elemental analyses in the absorber melt between B_4C pellet and external ZrO_2 scale (area 2)

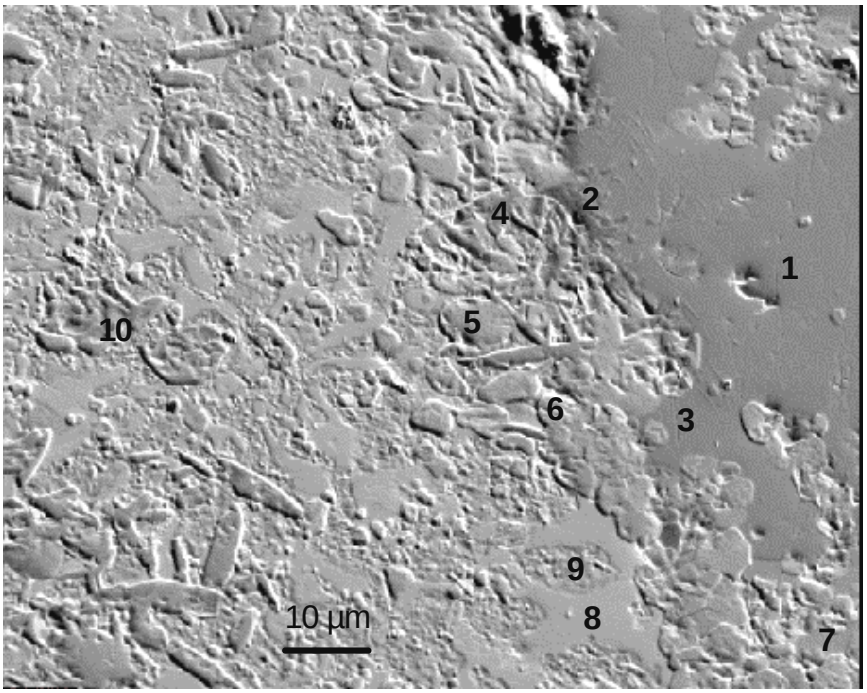

Fig. 5: SEM Image of the B_4C absorber melt with Auger measuring points

Elemental compositions (in at-%) at measuring points given in Fig. 5

	B	C	Fe	Cr	Ni	Zr	O	Mo
1	35		46	16	2			
2	47		20	33				
3	35		48	14	3			
4	61					36	3	
5	11	50				39		
6	10	50				40		
7	18	8	56	6	12			
8		6	52	12	10	20		
9			65	24	5			6
10	62					38		

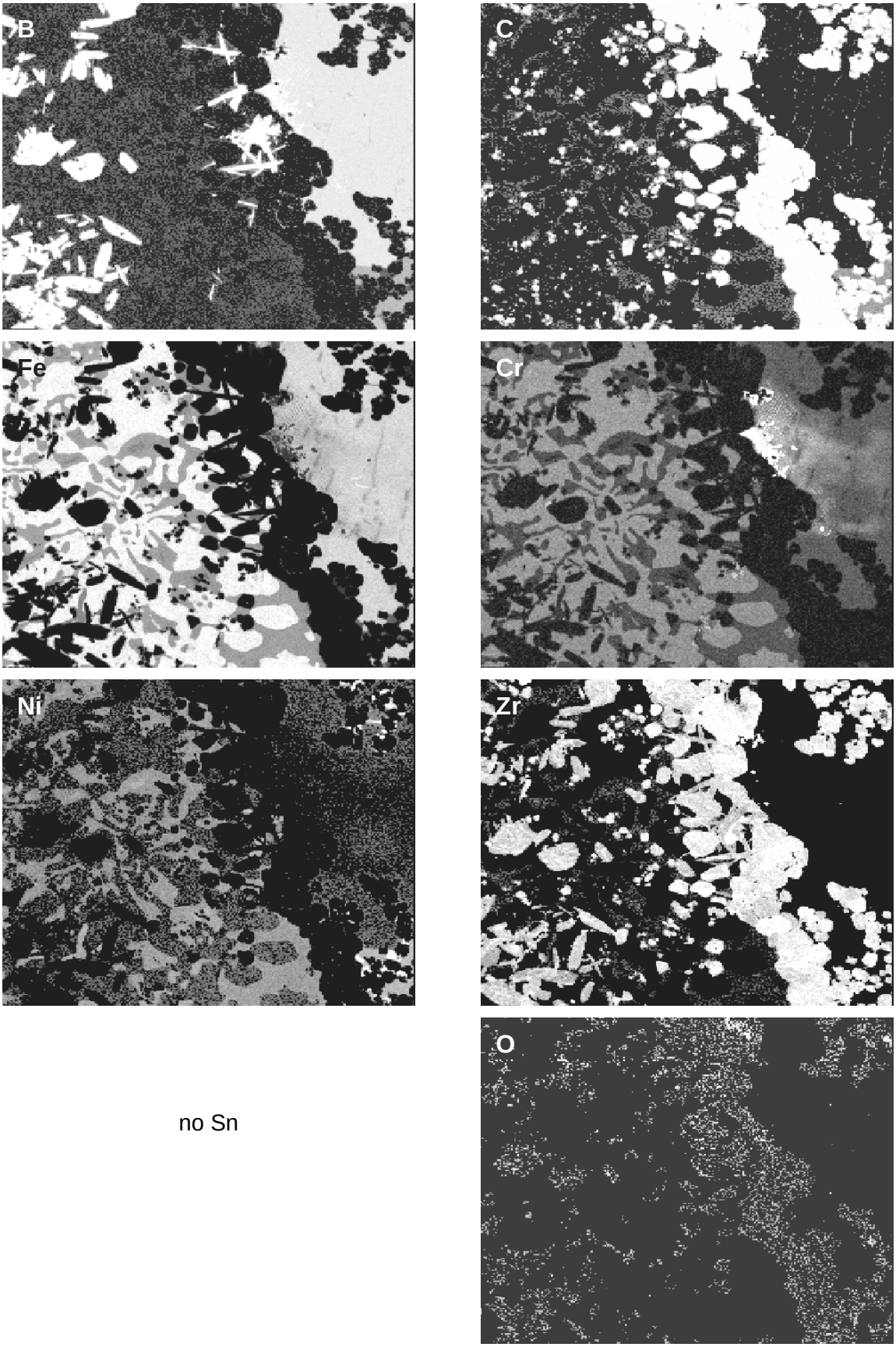

Fig. 6: Auger element mapping of an area in the absorber melt (Fig. 5)

Auger elemental analyses in the area near external ZrO_2 scale (area 3)

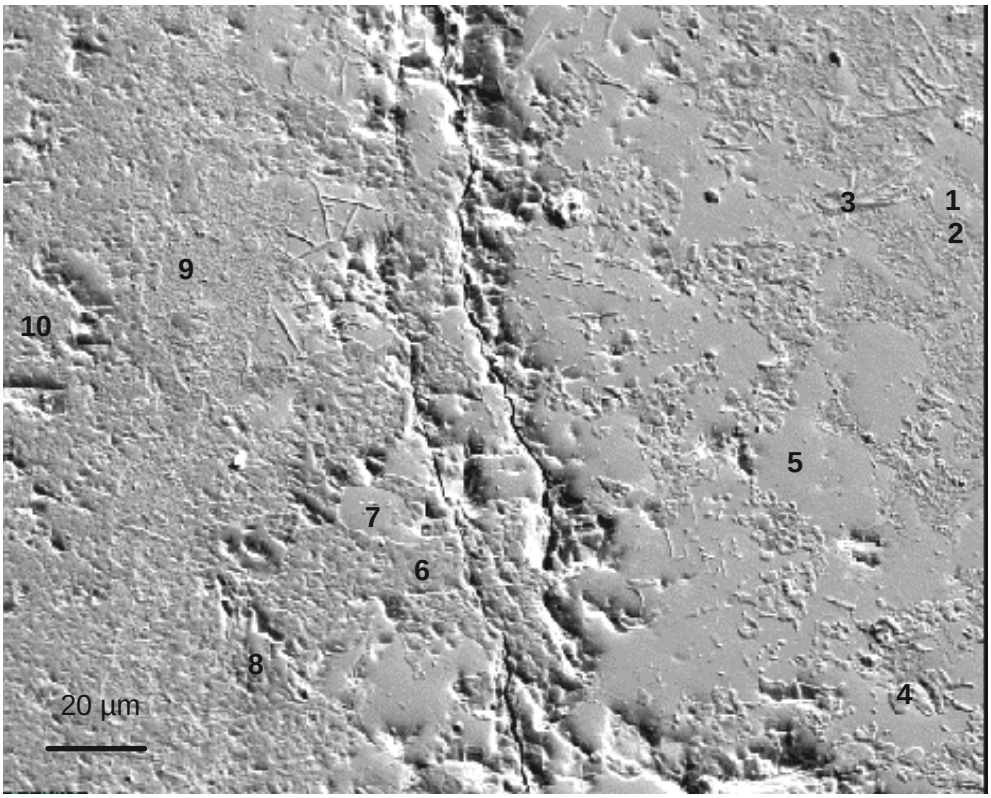

Fig. 7: SEM Image of the area near ZrO_2 scale with Auger measuring points

Elemental compositions (in at-%) at measuring points given in Fig. 7

	B	C	Fe	Cr	Ni	Zr	O
1			55	6	15	24	
2	10		63	22	5		
3	54		3	2	41		
4		38				48	14
5			50	10	8	32	
6						42	58
7			50	11	9	30	
8	63					37	
9			77	15	7		
10						38	62

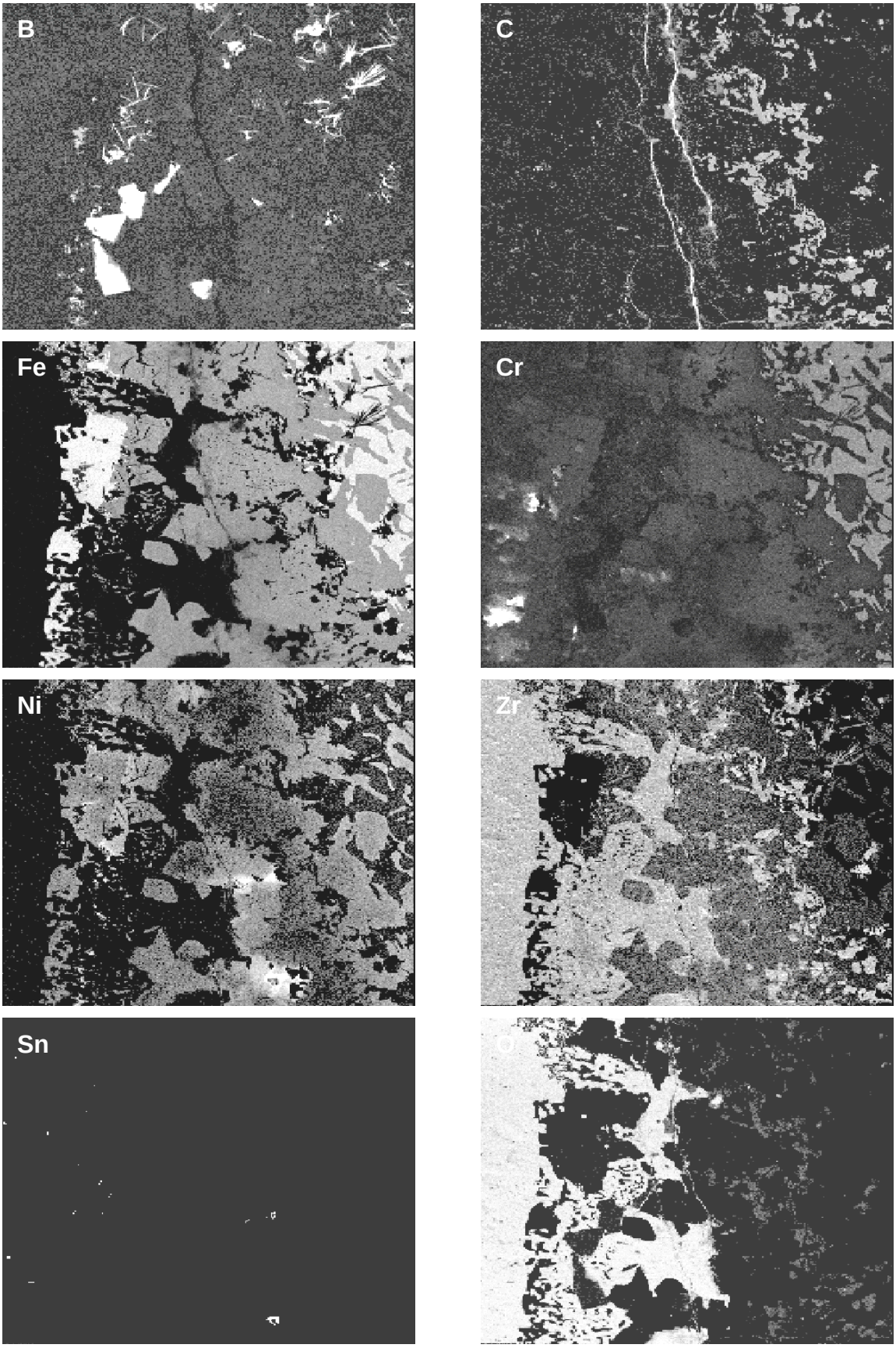

Fig. 8: Auger element mapping of the area near the external ZrO_2 scale (Fig. 7)

Test Box20529: 1h, 1400 °C

Overview

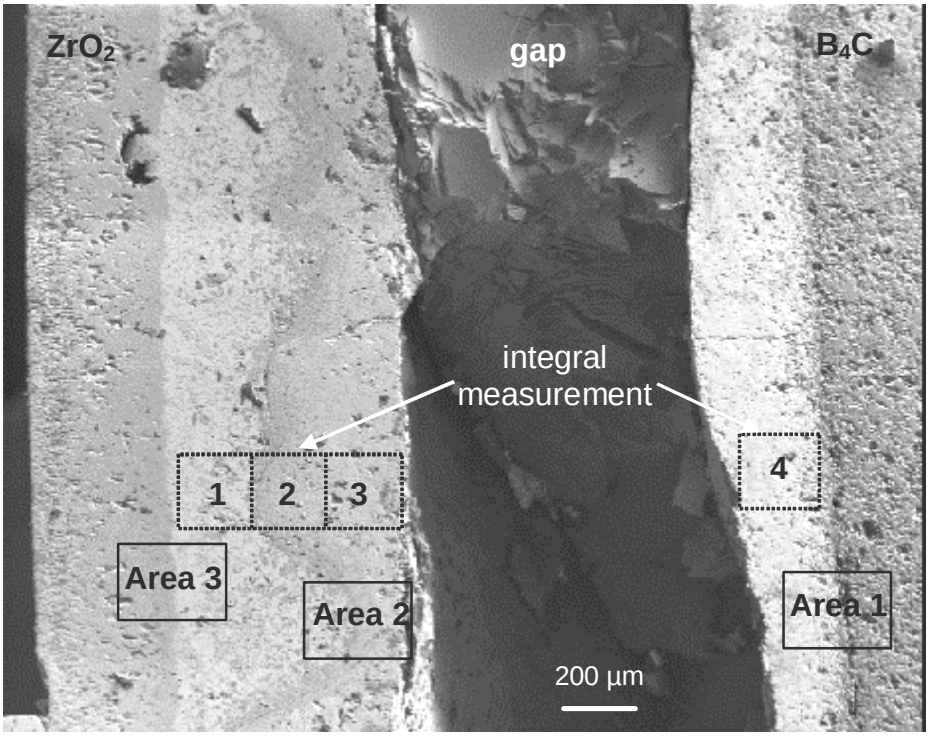

Fig. 1: Cross section through a CR segment after 1 h isothermal test at 1400 °C in argon/steam atmosphere; left: ZrO_2 scale, right: B_4C pellet; areas for detailed analyses are indicated in black; areas for integral analyses of the melt in white

Integral analyses (in at-%) of the absorber melt by Auger spectroscopy

Area	B	C	Fe	Cr	Ni	Zr	O
1	12.6	8.8	44.9	5.2	9.4	14.2	4.9
2	22.9	22.9	20.3	5.0	2.5	21.2	5.1
3	28.2	7.8	40.3	9.1	6.0	6.7	1.9
4	32.9	5.0	37.8	12.0	4.3	5.7	2.4
Mean	**24**	**11**	**36**	**8**	**6**	**12**	**4**

Auger elemental analyses near B_4C pellet (area 1)

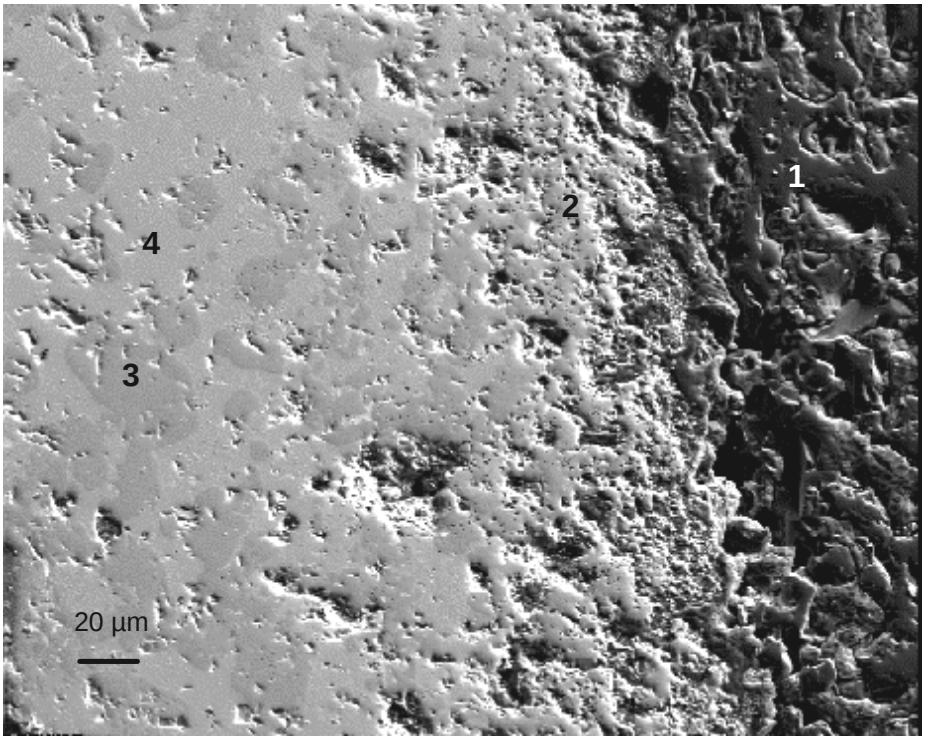

Fig. 2: SEM Image of the area near B_4C with Auger measuring points

Elemental compositions (in at-%) at measuring points given in Fig. 2

	B	C	Fe	Cr	Ni
1	78	22			
2	48		31	21	
3	50		29	21	
4	35		54	8	3

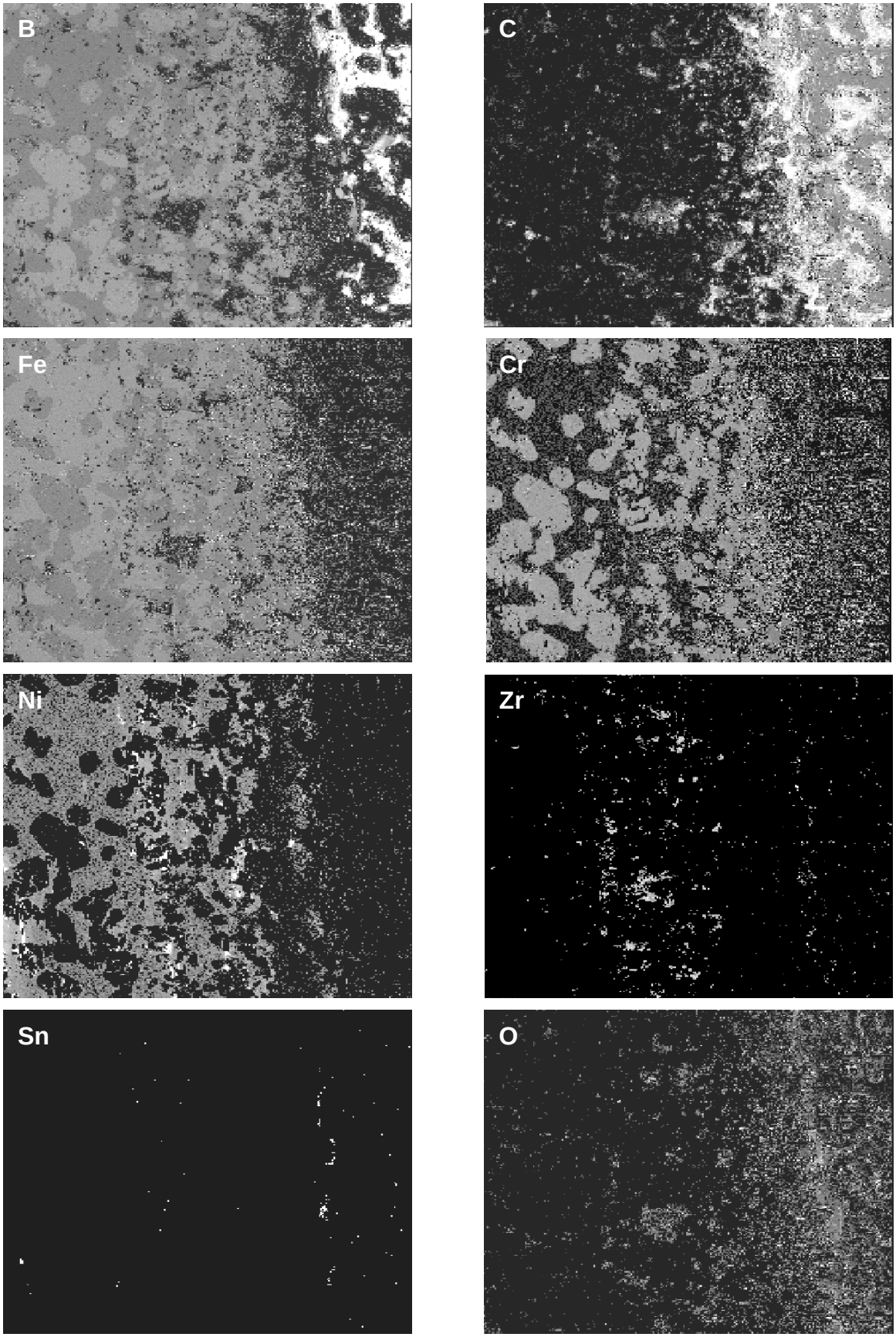

Fig. 3: Auger element mapping of the area near B_4C (see Fig. 2)

Zr-rich phases in the melt near B_4C pellet

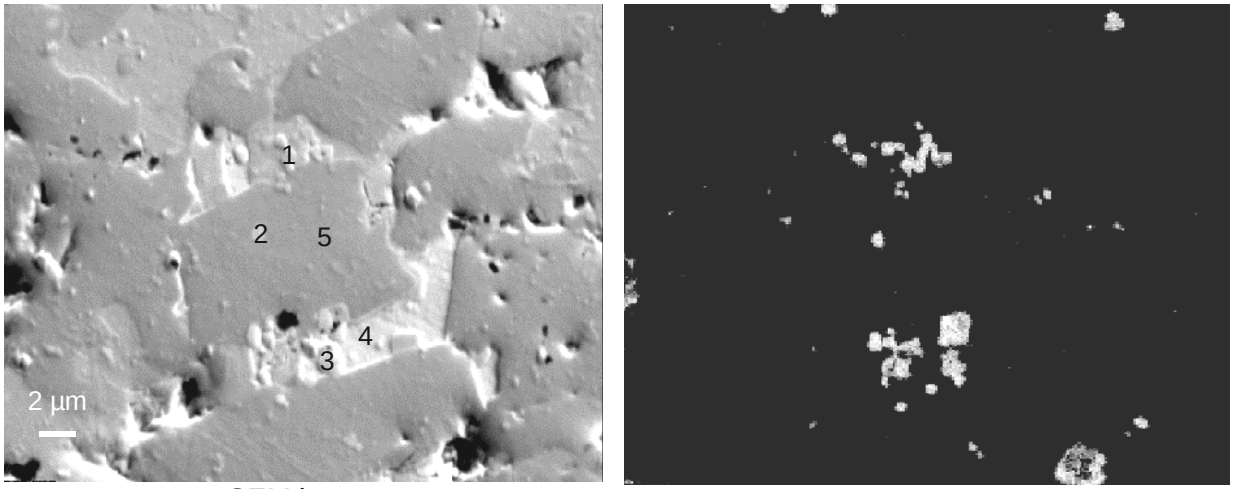

SEM image Zr map

Fig. 4: SEM image with measuring points and Zr element map showing the formation of Zr rich phases far away from the Zircaloy guide tube

Elemental compositions (in at-%) at measuring points given in Fig. 4

	B	C	Fe	Cr	Ni	Zr	O	N
1		50				37	9	5
2		52				37	7	4
3		49				39	8	4
4*		6			79			
5	49		28	23				

* +15% Si from grinding powder

Auger elemental analyses in the absorber melt between B_4C pellet and external ZrO_2 scale (area 2)

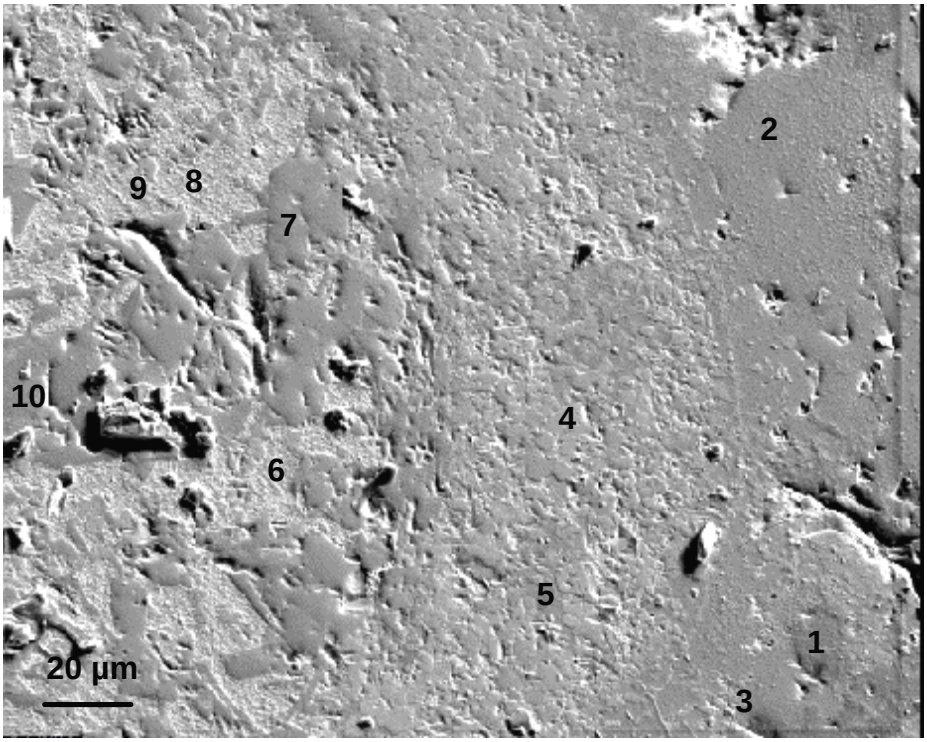

Fig. 5: SEM Image of the B_4C absorber melt with Auger measuring points

Elemental compositions (in at-%) at measuring points given in Fig. 5

	B	C	Fe	Cr	Ni	Zr	O	N
1	47	4	21	28				
2	34	4	48	10	4			
3		48				37	13	2
4		58		37			5	
5	46	4	26	24				
6		5	72	6	16			
7	55	5				37	3	
8		6	72	7	14			
9		50				37	13	
10	36	5	30	29				

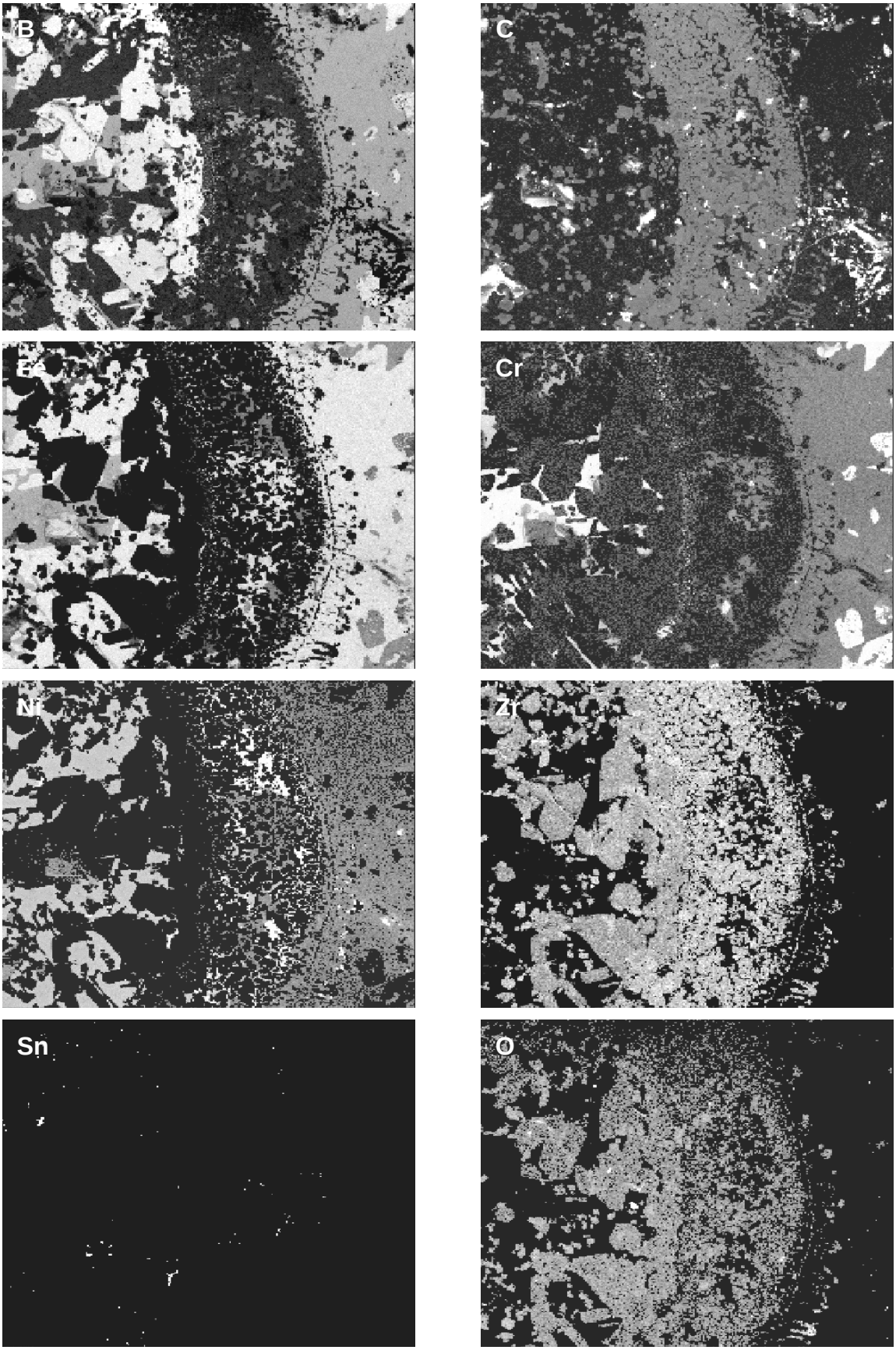

Fig. 6: Auger element mapping of an area in the absorber melt (see Fig. 5)

Auger elemental analyses in the area near external ZrO_2 scale (area 3)

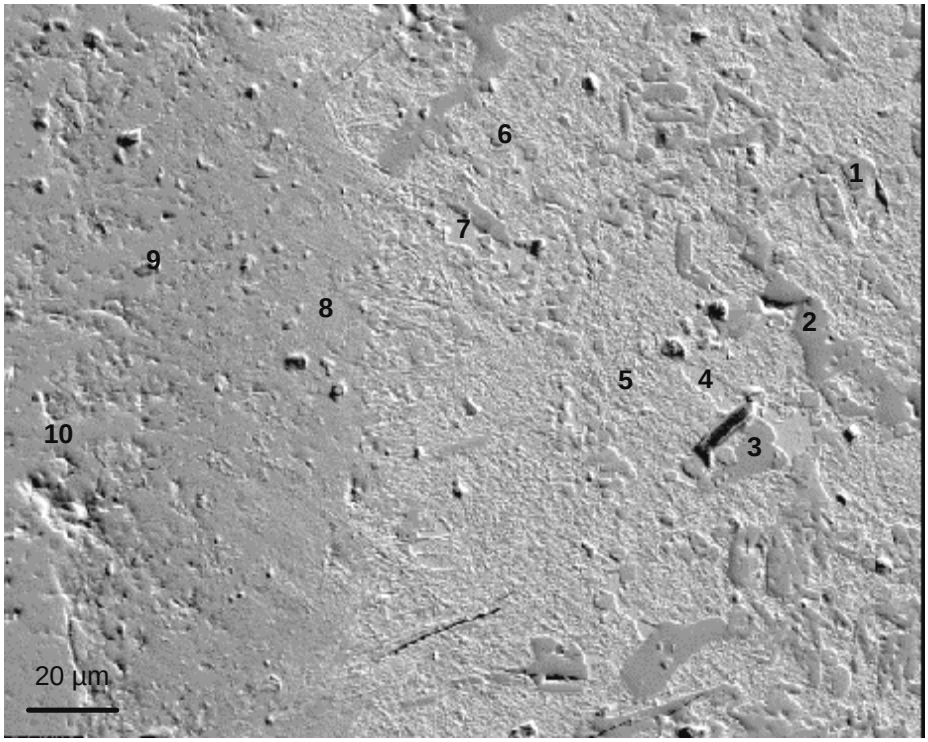

Fig. 7: SEM Image of the area near ZrO_2 scale with Auger measuring points

Elemental compositions (in at-%) at measuring points given in Fig. 7

	B	C	Fe	Cr	Ni	Zr	Sn	O	N
1	58	4				38			
2	36	3	35	26					
3	35	3	41	21					
4	16	5			41	23	13	3	
5	74	5		5	15				
6		30				39		28	3
7	16	3			41	22	14	3	
8		48				39		13	
9		55				36		9	
10		9				34		57	

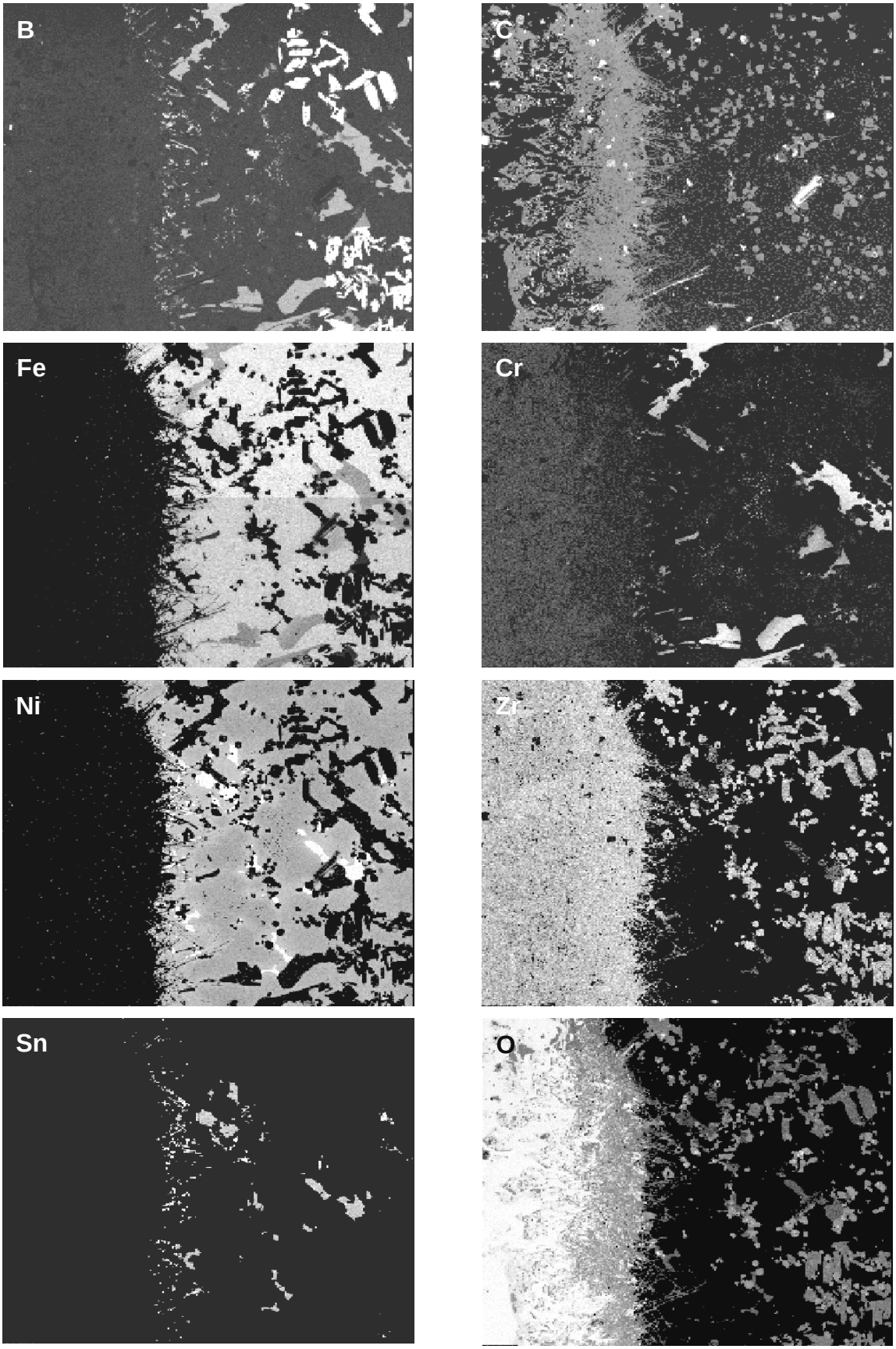

Fig. 8: Auger element mapping of the area near the external ZrO_2 scale (see Fig. 7)

Test Box20606: 1h, 1500 °C

Overview

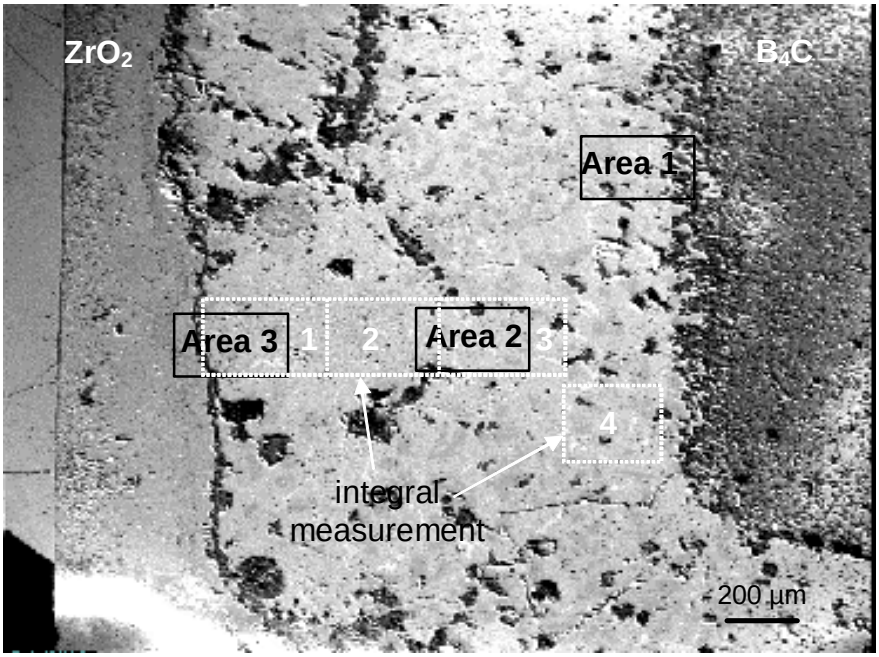

Fig. 1: Cross section through a CR segment after 1 h isothermal test at 1500 °C in argon/steam atmosphere; left: ZrO_2 scale, right: B_4C pellet; areas for detailed analyses are indicated in black; areas for integral analyses of the melt in white

Integral analyses (in at-%) of the absorber melt by Auger spectroscopy

Area	B	C	Fe	Cr	Ni	Zr	O
1	24.9	11.1	35.6	4.7	7.5	11.4	4.8
2	23.3	15.4	32.9	5.7	5.8	13.8	3.0
3	33.1	1.8	47.1	8.1	6.7	2.5	0.7
4	33.9	1.4	42.9	9.5	7.6	3.8	0.9
Mean	**29**	**7**	**40**	**7**	**7**	**8**	**2**

Auger elemental analyses near B_4C pellet (area 1)

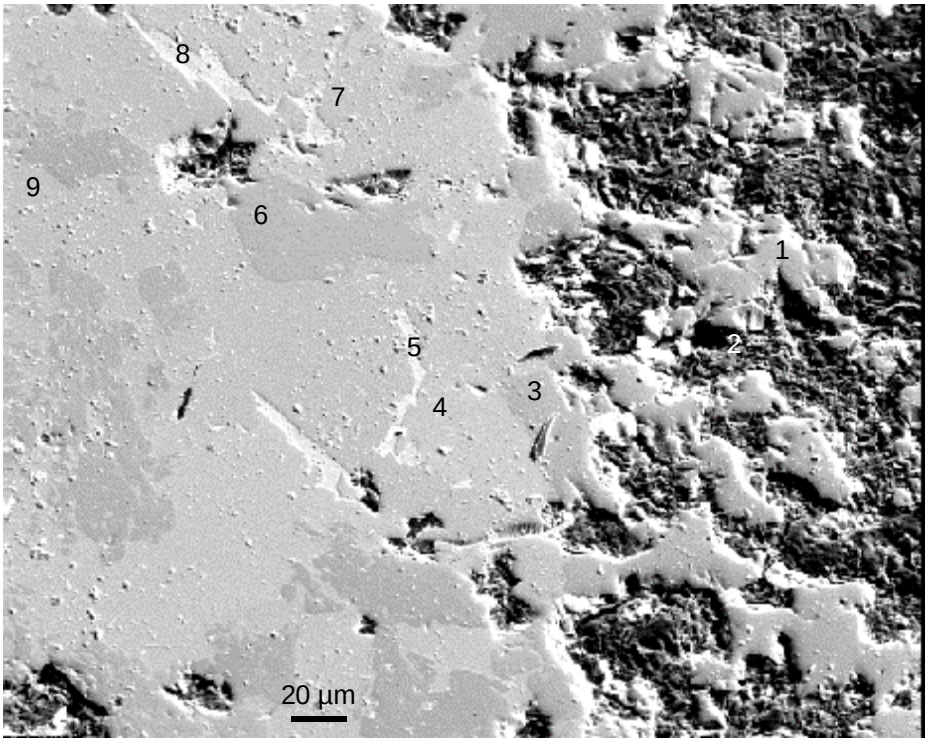

Fig. 2: SEM Image of the area near B_4C with Auger measuring points

Elemental compositions (in at-%) at measuring points given in Fig. 2

	B	**C**	**Fe**	**Cr**	**Ni**	**O**	**N**	**Sn**	**Si**
1	36	7	30	23		4			
2	5	77				15	4		
3	38		33	22		7			
4	28	3	50	5	5	7	2		
5		3	8		69	5			14
6	41	3	30	26					
7	28		48	3	11	8	2		
8		11	9		62	5		3	10
9	29		53	5	5	8			

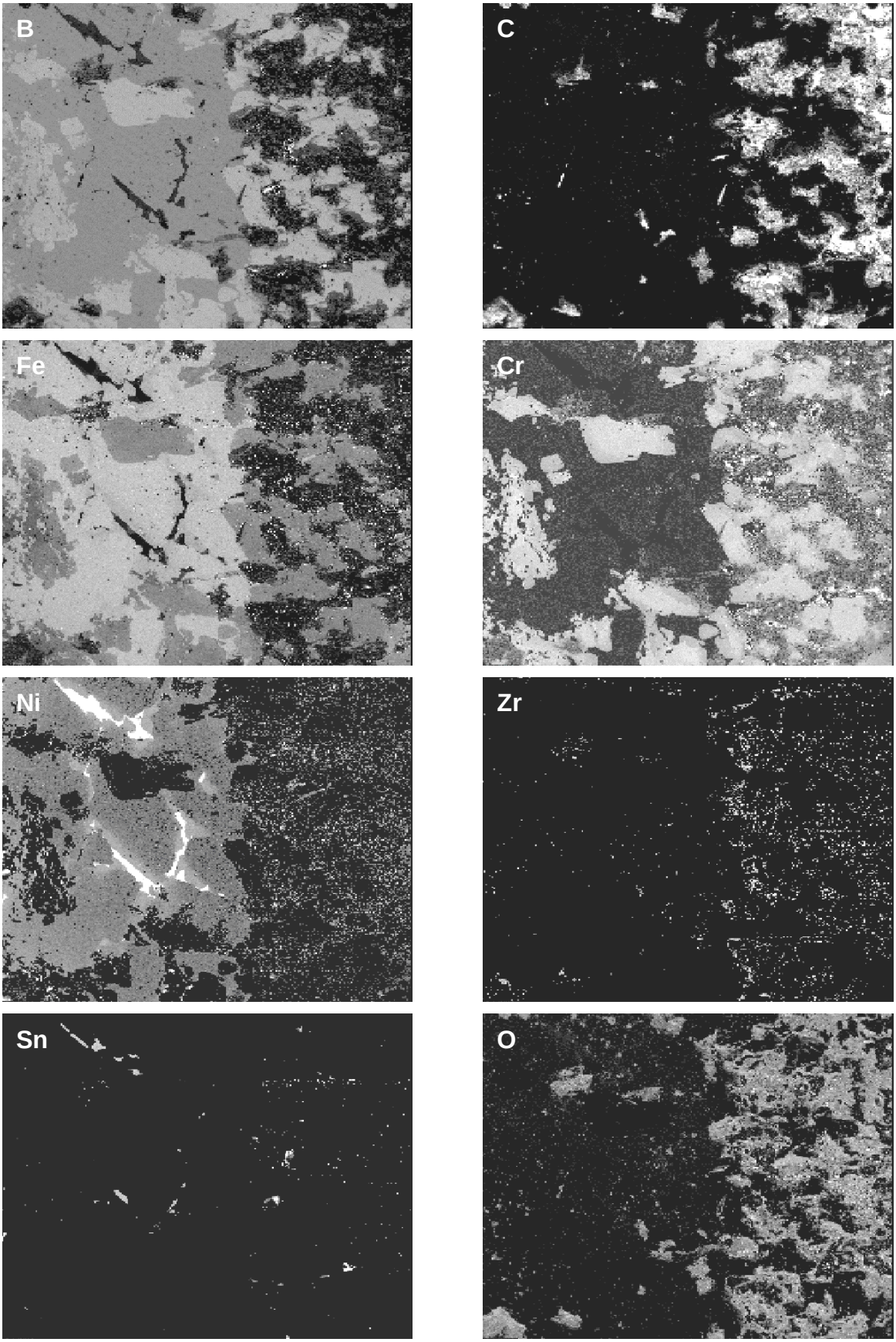

Fig. 3: Auger element mapping of the area near B_4C (see Fig. 2)

Auger elemental analyses in the absorber melt between B_4C pellet and external ZrO_2 scale (area 2)

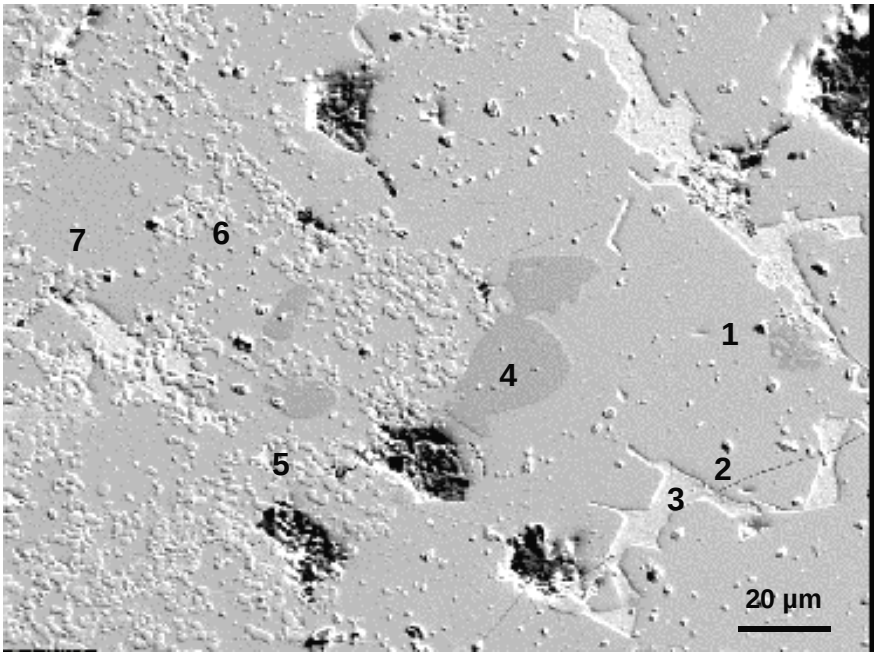

Fig. 4: SEM Image of the B_4C absorber melt with Auger measuring points

Elemental compositions (in at-%) at measuring points given in Fig. 4

	B	C	Fe	Cr	Ni	Zr	O	Si
1	32		53	7	5		3	
2	32		48	6	9		4	
3			37		51		6	6
4	48		33	19				
5		51				37	12	
6		36				36	28	
7	33		52	7	4		4	

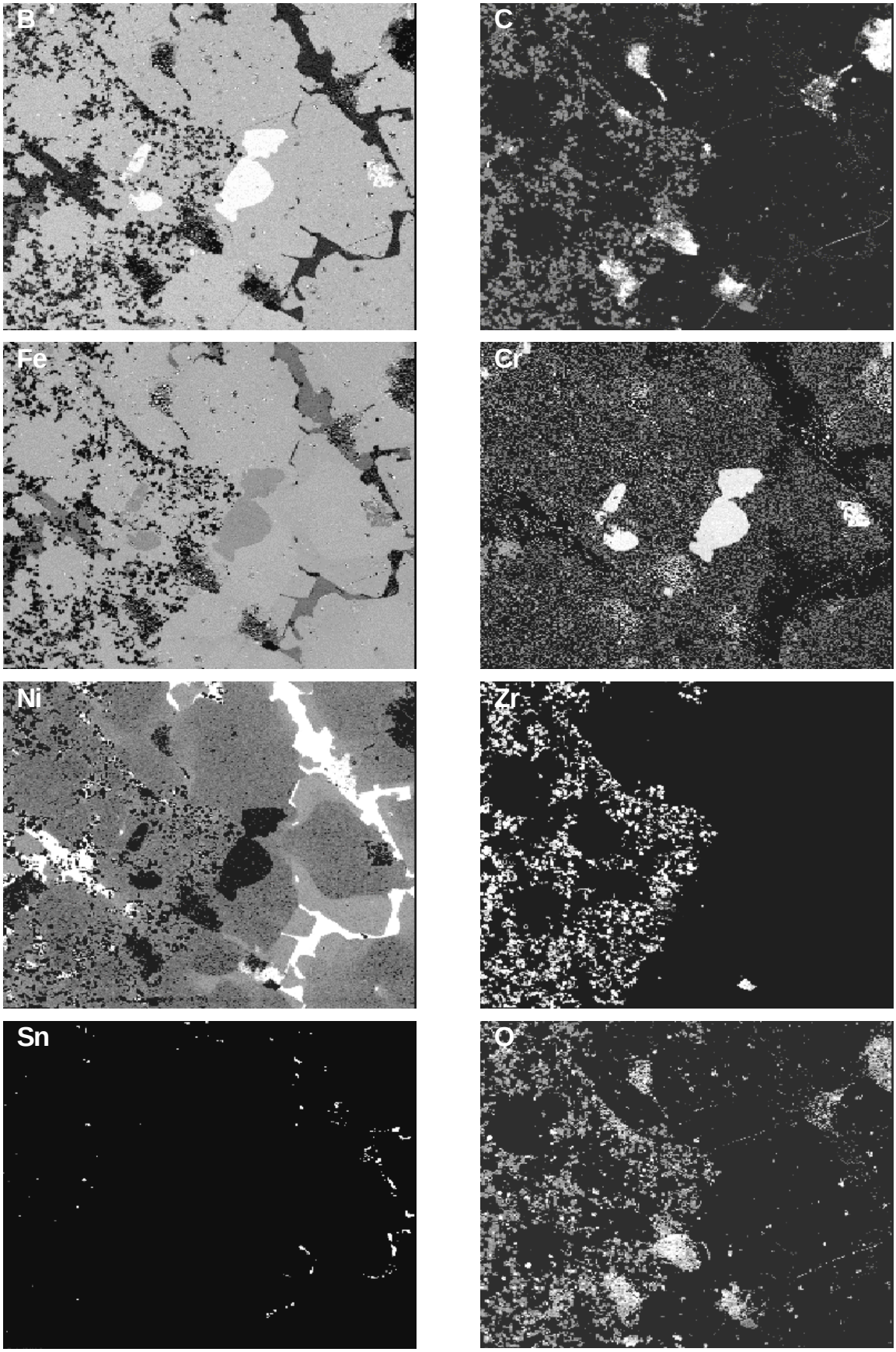

Fig. 5: Auger element mapping of an area in the absorber melt (see Fig. 4)

Auger elemental analyses in the area near external ZrO_2 scale (area 3)

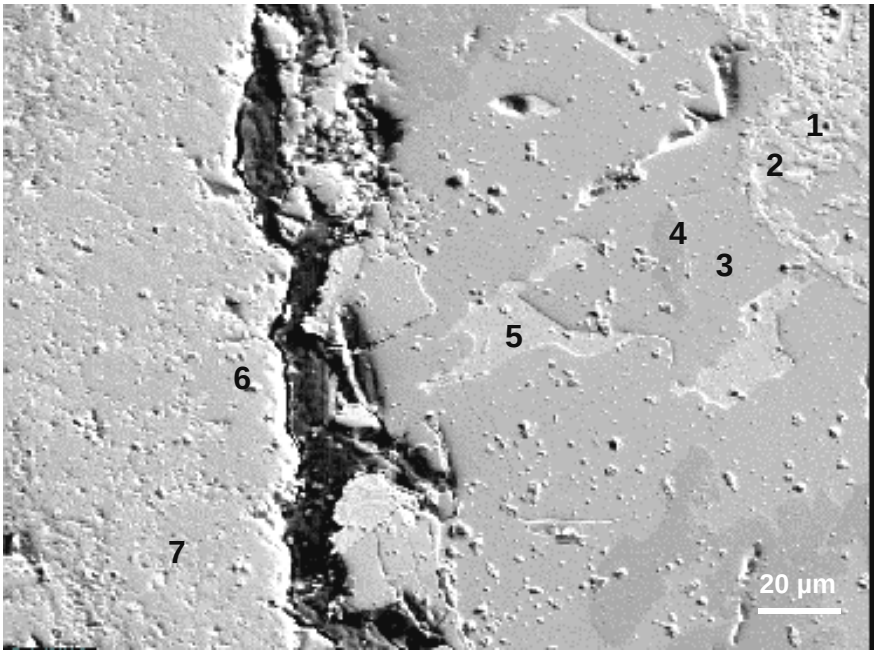

Fig. 6: SEM Image of the area near ZrO_2 scale with Auger measuring points

Elemental compositions (in at-%) at measuring points given in Fig. 6

	B	C	Fe	Cr	Ni	Zr	O	Si
1		45				41	14	
2			38		49		6	6
3	34		53	6	4		2	
4	50		31	19				
5			41		45		7	7
6						37	63	
7		39				39	22	

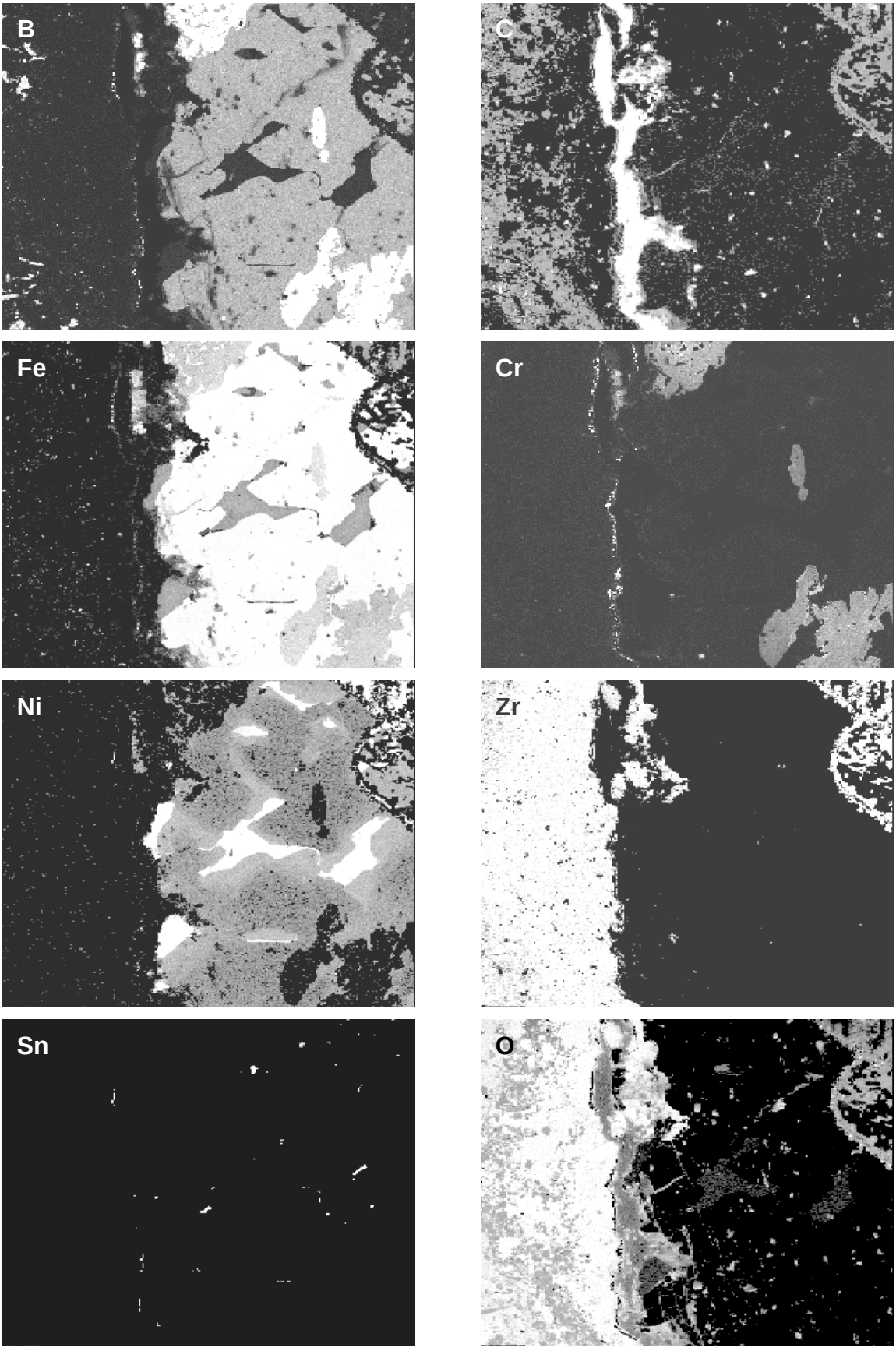

Fig. 7: Auger element mapping of the area near the external ZrO_2 scale (see Fig. 6)

A10 Preparation of absorber melts
Annealing parameters and images of the specimens before oxidation tests

Here, the appearance of the melt specimens after preparation in the LAVA furnace is compiled together with the test parameters.

Versuchsnummer	=	test number
Zusammensetzung	=	composition
Temperaturprogramm	=	temperature program

The time in min includes transient and 10 min isothermal phase.


Versuchsnummer: 1
Zusammensetzung:
B4C: 0 %
SS: 100%
Zry: 0 %
Temperaturprogramm:
In 22 min auf 1900°C


Versuchsnummer: 1.1
Zusammensetzung:
B4C: 0 %
SS: 100%
Zry: 0 %
Temperaturprogramm:
In 22 min auf 1900°C


Versuchsnummer: 2
Zusammensetzung:
B4C: 5 %
SS: 95%
Zry: 0 %
Temperaturprogramm:
In 22 min auf 1900°C


Versuchsnummer: 2.2
Zusammensetzung:
B4C: 5 %
SS: 95%
Zry: 0 %
Temperaturprogramm:
In 22 min auf 1900°C


Versuchsnummer: 3
Zusammensetzung:
B4C: 10%
SS: 90%
Zry: 0 %
Temperaturprogramm:
In 22 min auf 1900°C


Versuchsnummer: 3.3
Zusammensetzung:
B4C: 10%
SS: 90%
Zry: 0 %
Temperaturprogramm:
In 22 min auf 1900°C


Versuchsnummer: 4
Zusammensetzung:
B4C: 20%
SS: 80%
Zry: 0 %
Temperaturprogramm:
In 22 min auf 1900°C
In 24 min auf 2100°C


Versuchsnummer: 4.4
Zusammensetzung:
B4C: 20%
SS: 80%
Zry: 0 %
Temperaturprogramm:
In 22 min auf 2000°C
In 24 min auf 2100°C


Versuchsnummer: 5
Zusammensetzung:
B4C: 30%
SS: 70%
Zry: 0 %
Temperaturprogramm:
In 22 min auf 1900°C


Versuchsnummer: 5.5
Zusammensetzung:
B4C: 30%
SS: 70%
Zry: 0 %
Temperaturprogramm:
In 24 min auf 2100°C


Versuchsnummer: 6
Zusammensetzung:
B4C: 9%
SS: 81%
Zry: 10%
Temperaturprogramm:
In 22 min auf 1900°C


Versuchsnummer: 6.6
Zusammensetzung:
B4C: 9%
SS: 81%
Zry: 10%
Temperaturprogramm:
In 24 min auf 2100°C


Versuchsnummer: 7
Zusammensetzung:
B4C: 7%
SS: 63%
Zry: 30%
Temperaturprogramm:
In 22 min auf 1900°C


Versuchsnummer: 7.7
Zusammensetzung:
B4C: 7%
SS: 63%
Zry: 30%
Temperaturprogramm:
In 24 min auf 2100°C


Versuchsnummer: 8
Zusammensetzung:
B4C: 0 %
SS: 70%
Zry: 30%
Temperaturprogramm:
In 22 min auf 1900°C


Versuchsnummer: 8.8
Zusammensetzung:
B4C: 0 %
SS: 70%
Zry: 30%
Temperaturprogramm:
In 22 min auf 1900°C

A11 SEM/EDX investigations of SS/B_4C/Zry absorber melts

SEM images and results of EDX phase analyses of various absorber melts after preparation and after oxidation are shown at the next pages.

Please note, that the light elements boron and carbon can only be hardly detected by EDX and the error of these analyses is high. Only qualitative statements on the boron content could be made. Sometimes, different acceleration voltages were used to have a better resolution of the spectrum for the light elements. During analyses with low acceleration voltage oxygen and chromium peaks overlapped.

As for the Auger spectroscopy, elements appear the brighter the higher the concentration in a phase in the EDX mappings.

Melt 1: 100 % SS
after preparation

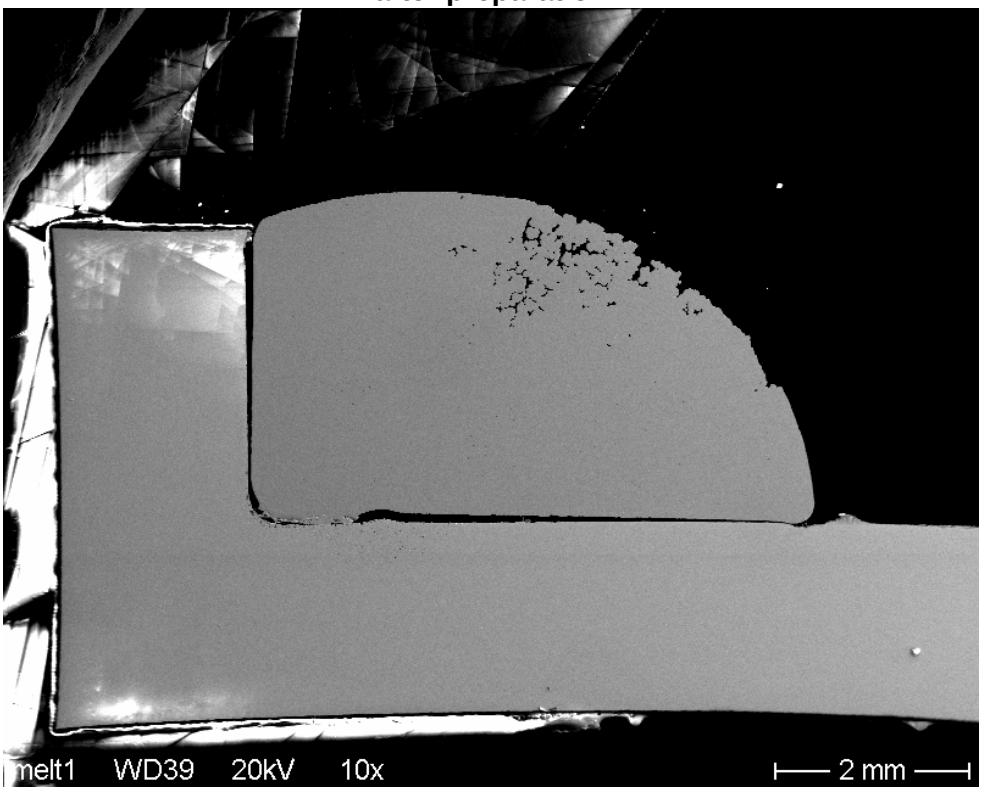

Measurement	Cr	Fe	Ni	Mn	Remark
SS melt	19.6 Ma-%	69.7 Ma-%	9.6 Ma-%	1.1 Ma-%	20 kV, standardless

Melt 2: 95 % SS, 5 % B4C
after preparation

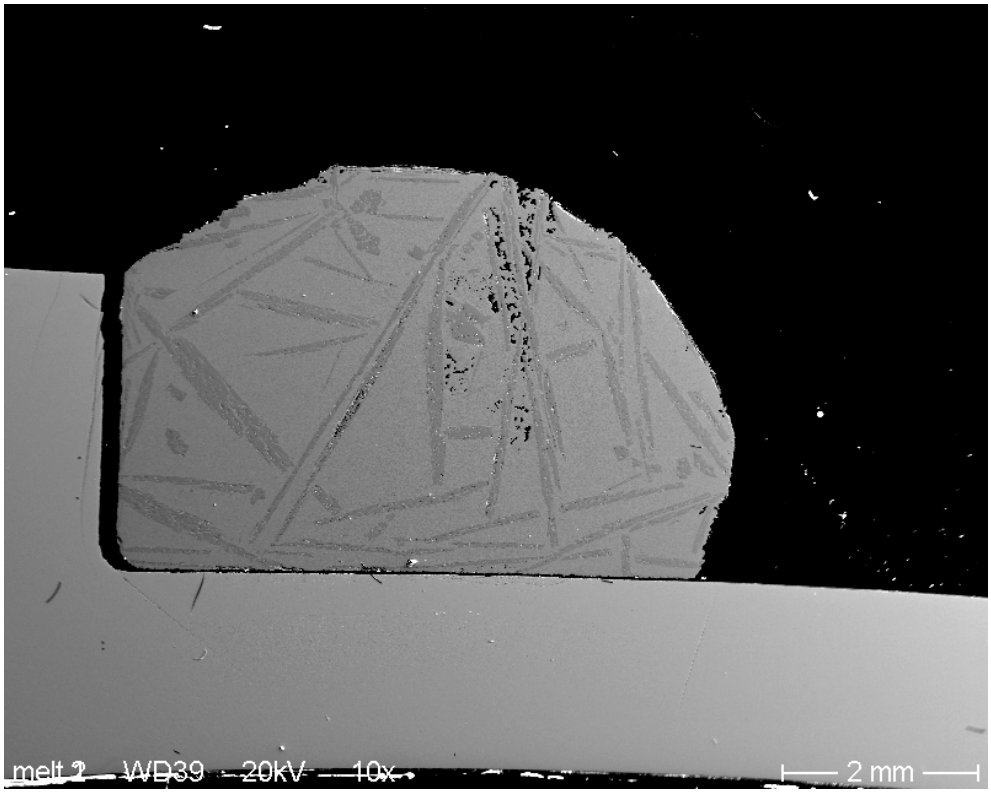

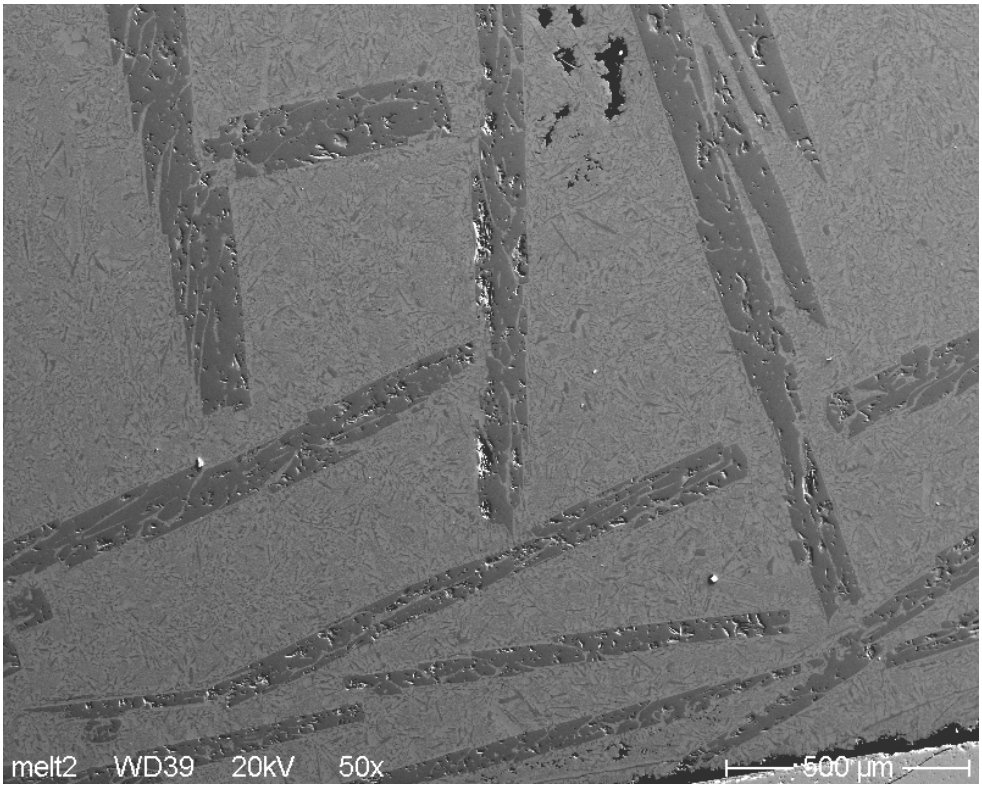

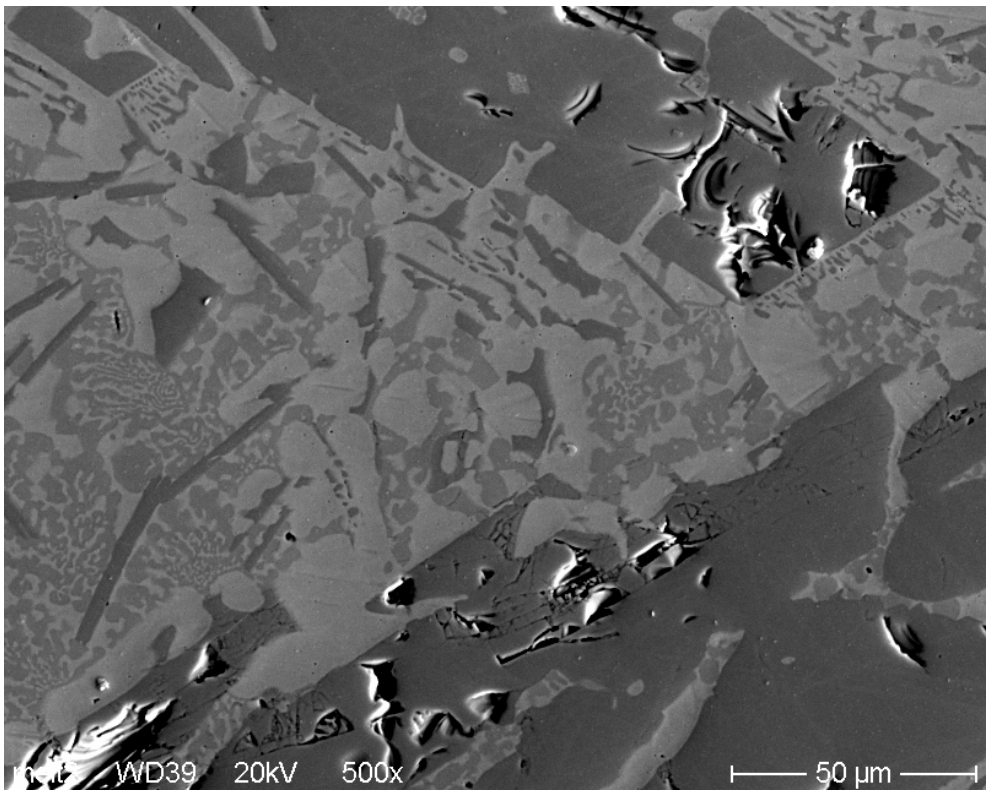
WD39 20kV 500x
50 µm

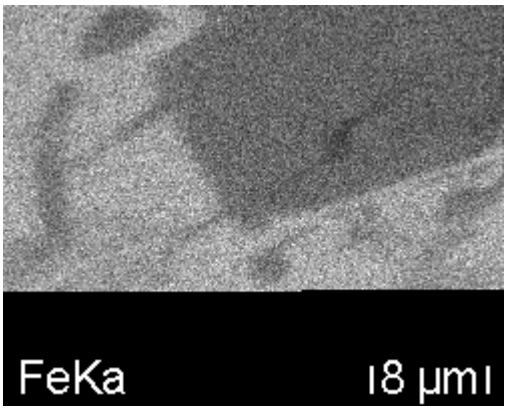
FeKa
18 µm

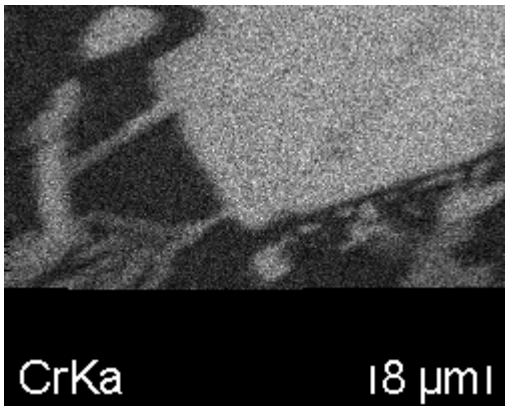
CrKa
18 µm

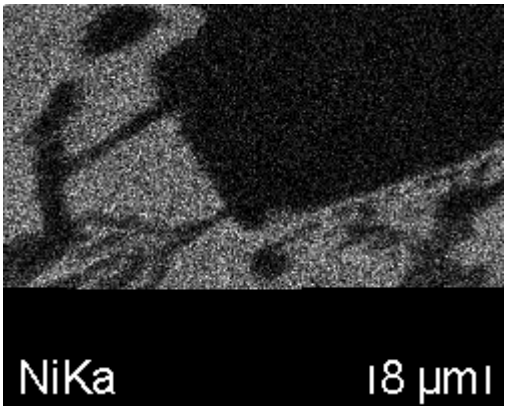
NiKa
18 µm

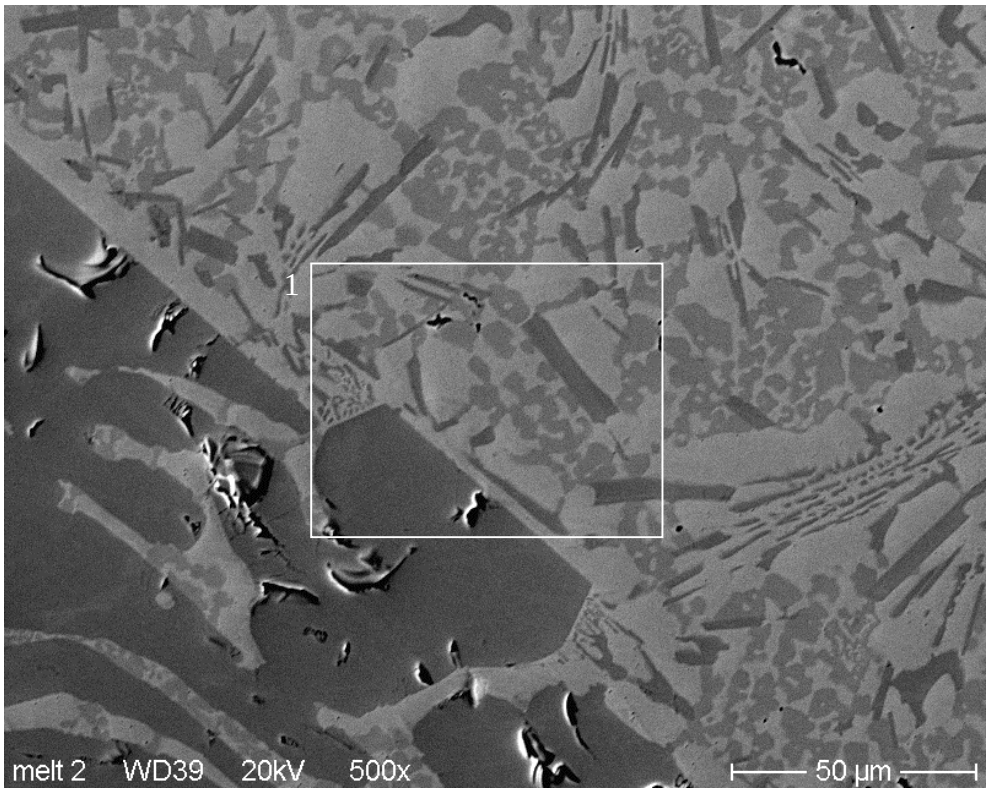
1
melt 2 WD39 20kV 500x
50 µm

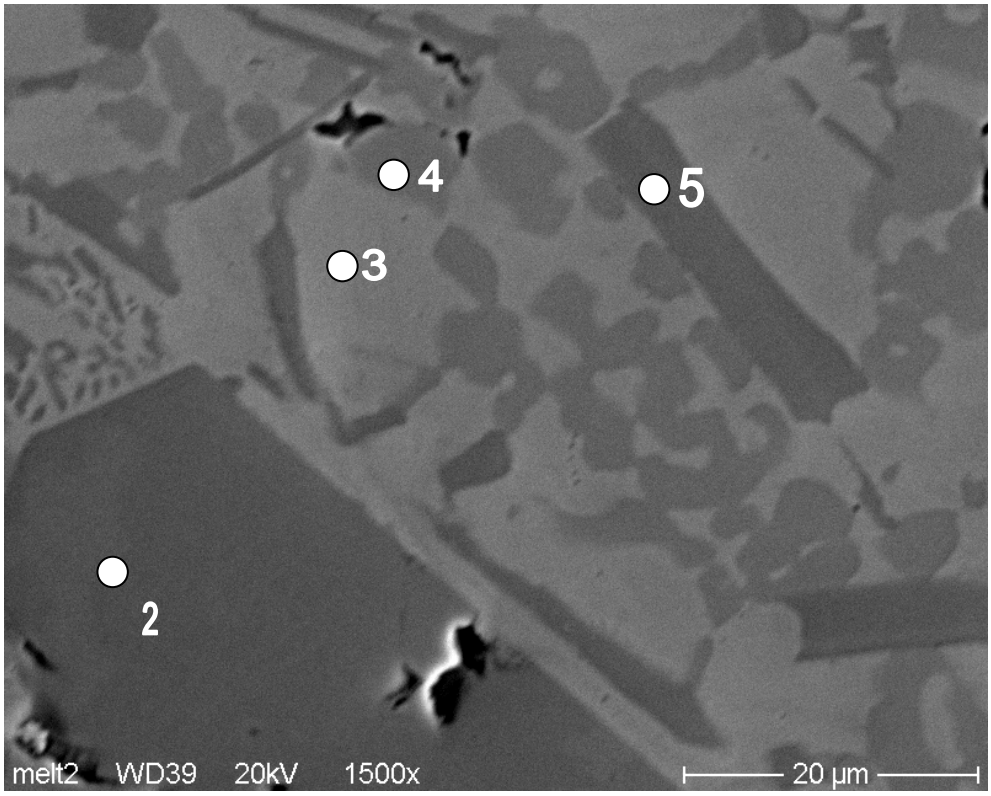
4
5
3
2
melt2 WD39 20kV 1500x
20 µm

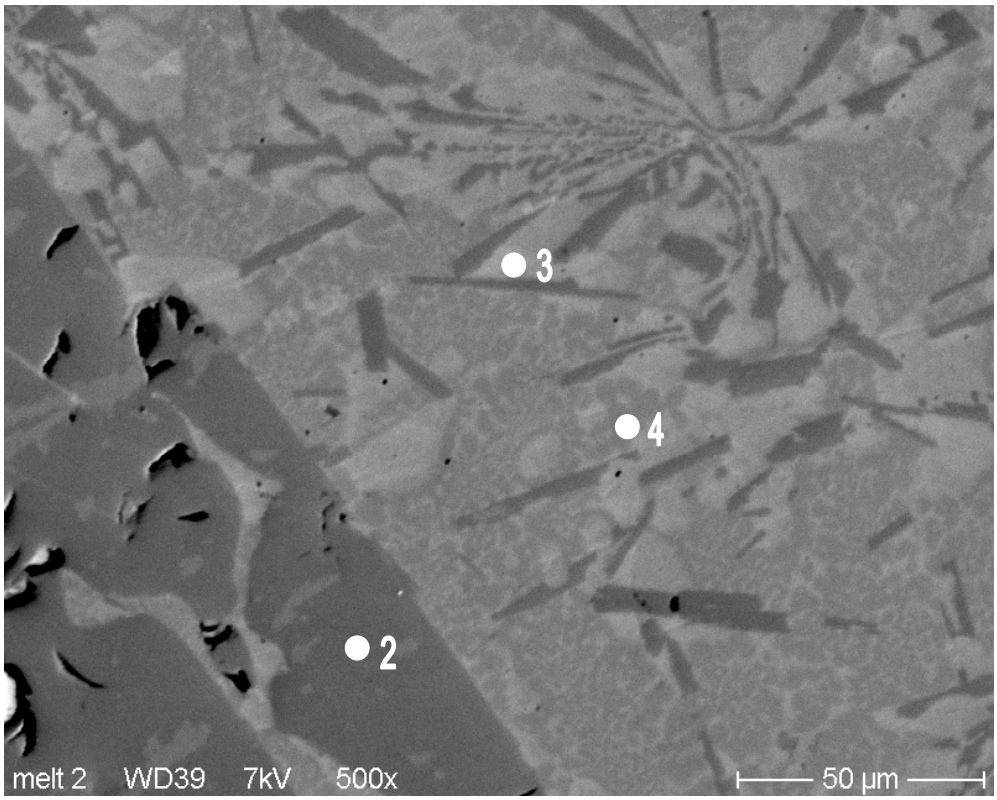

Measurement	Cr, Ma-%	Fe, Ma-%	Ni, Ma-%	Mn, Ma-%	Zr, Ma-%	Remark
point 2*	40.0	56.2	1.9	1.9		20 kV, standardless
point 3*	8.1	74.7	15.2	1.5		20 kV, standardless
point 4*	14.0	73.2	10.7	2.0		20 kV, standardless
point 5*	32.1	63.7	2.0	2.2		20 kV, standardless
point 2**	SS components and B, C					7 kV
point 3**	SS components and Si and C					7 kV
point 4**	SS components and C					7 kV

** see image preceding page*

*** see image this page*

Melt 4: 80 % SS, 20% B4C
after preparation

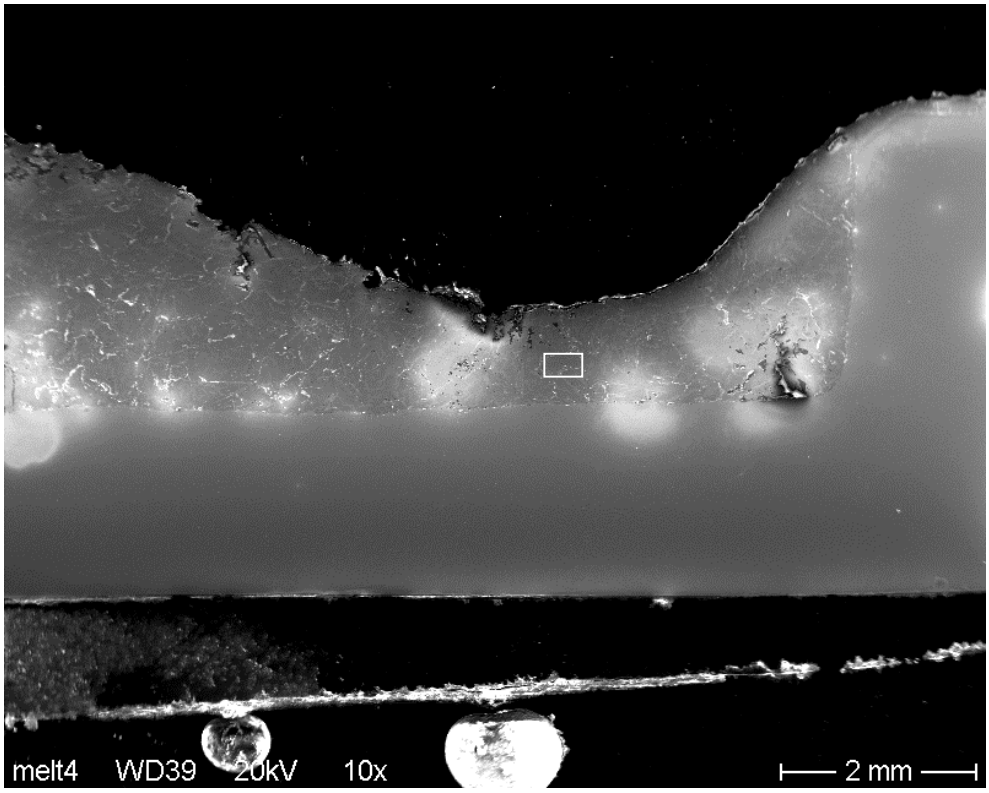

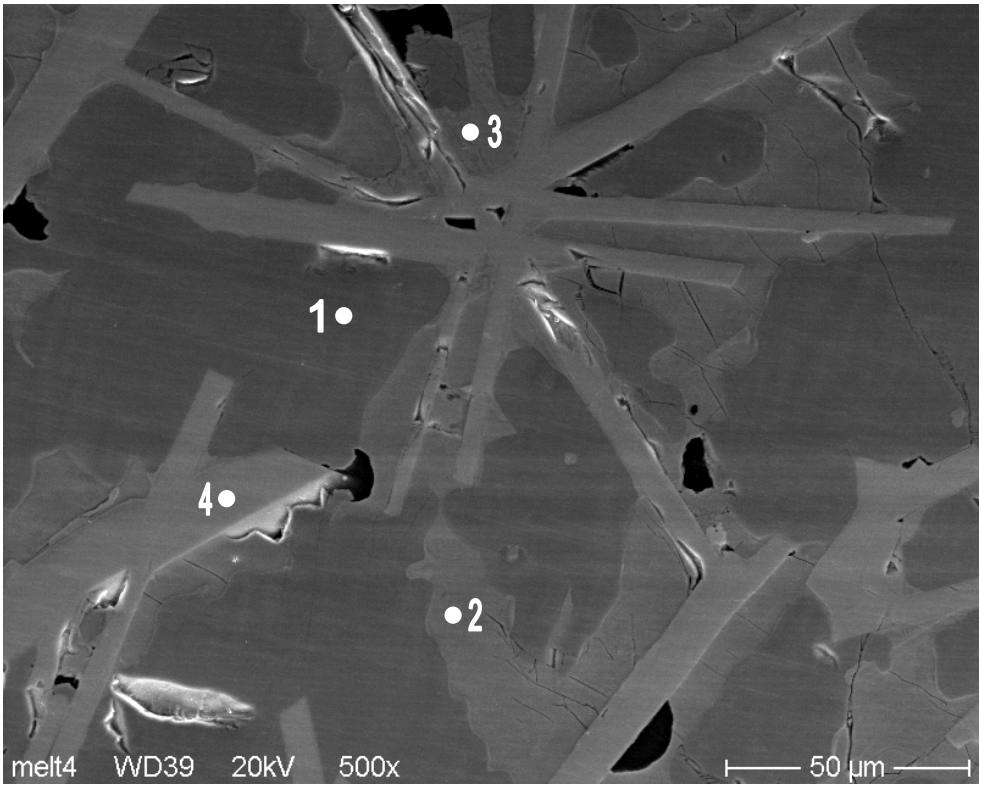

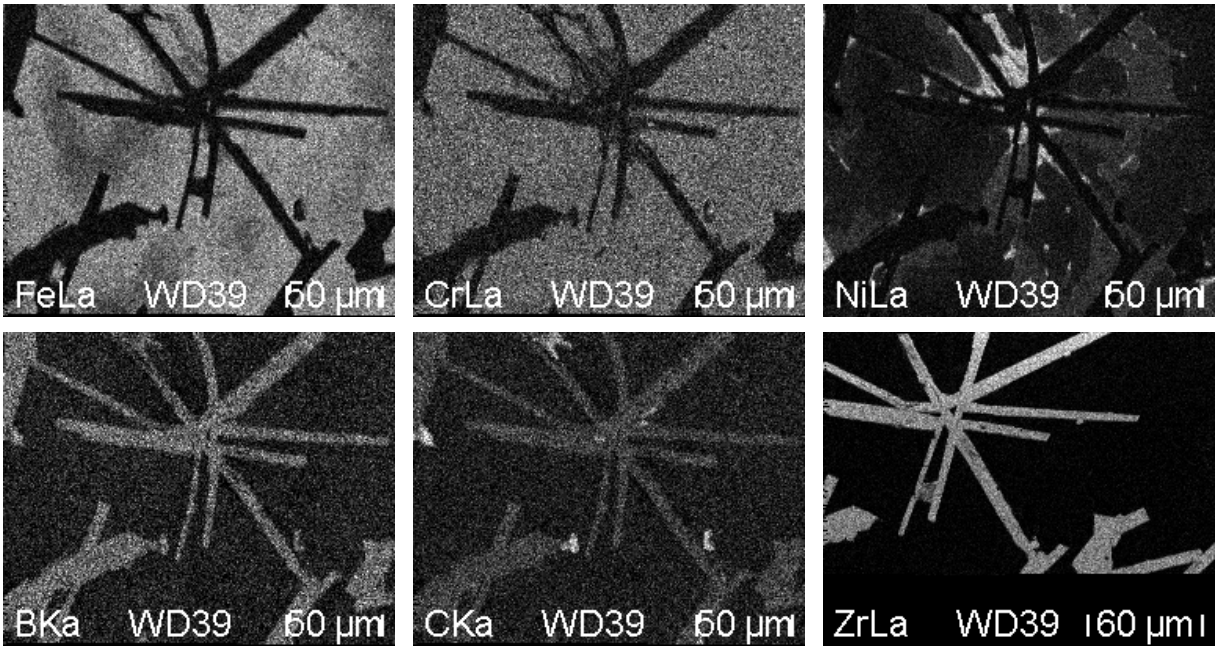

Measurement	Cr, Ma-%	Fe, Ma-%	Ni, Ma-%	Mn, Ma-%	Zr, Ma-%	Remark
point 1	SS components and B, C					7 kV
point 2	SS components and C					7 kV
point 3	Mainly Ni, Si and C					7 kV
point 4	Only Zr and B, no SS components,					7 kV

Melt 8: 70 % SS, 30 % Zry
after preparation

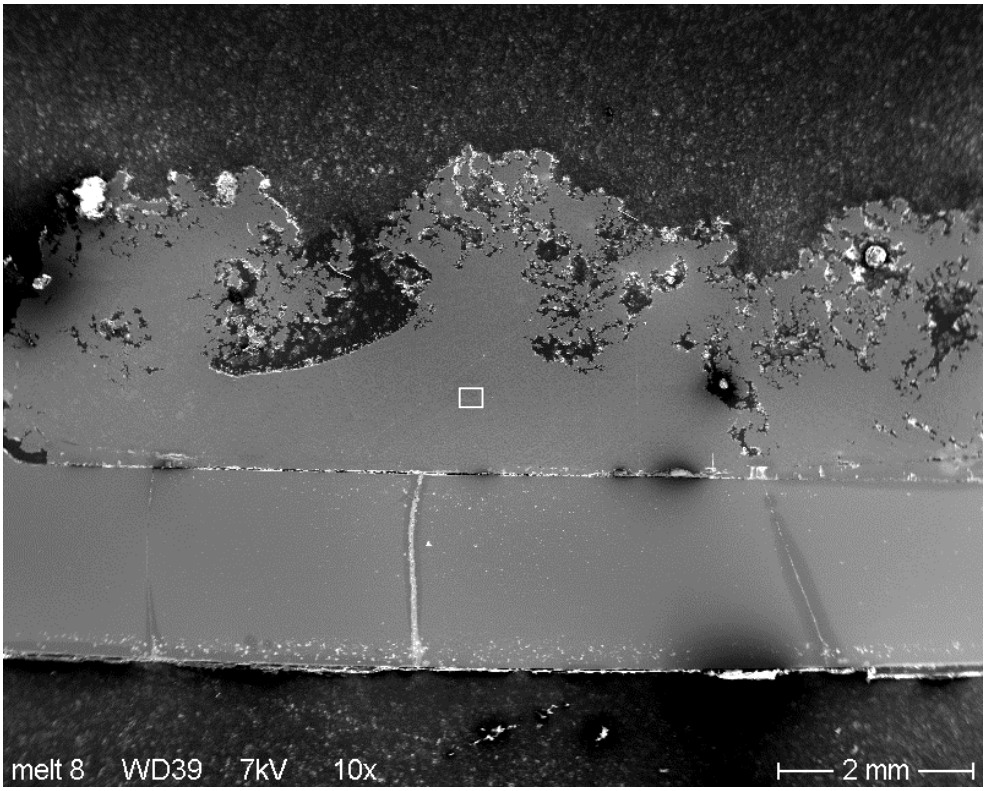

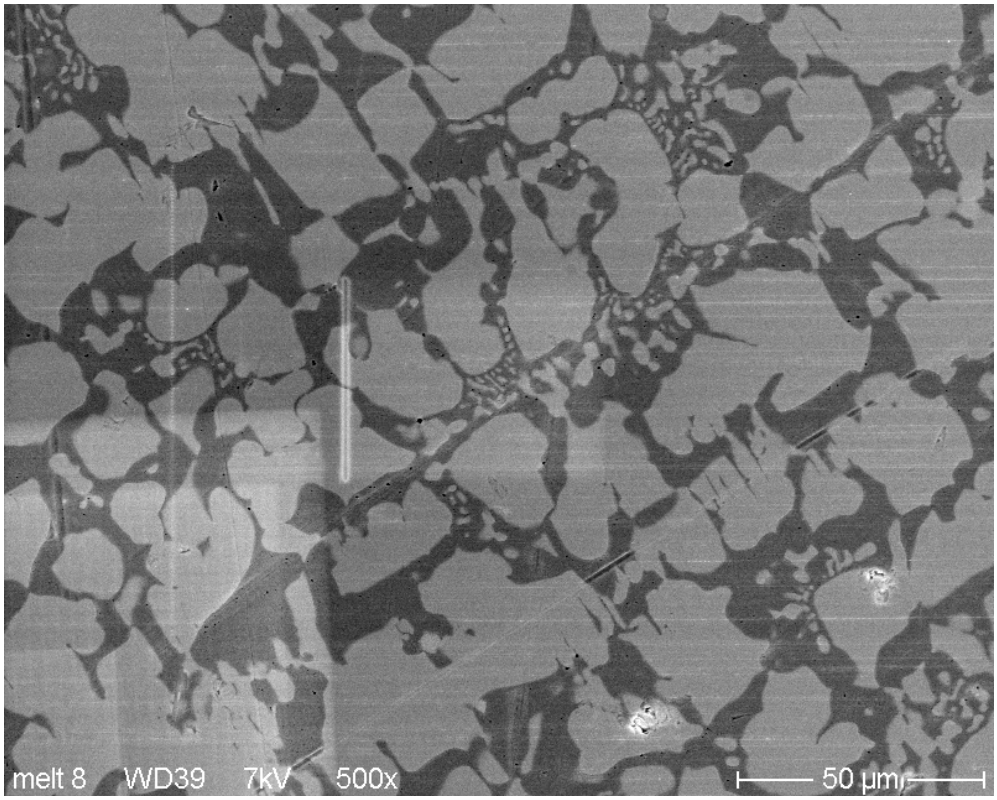

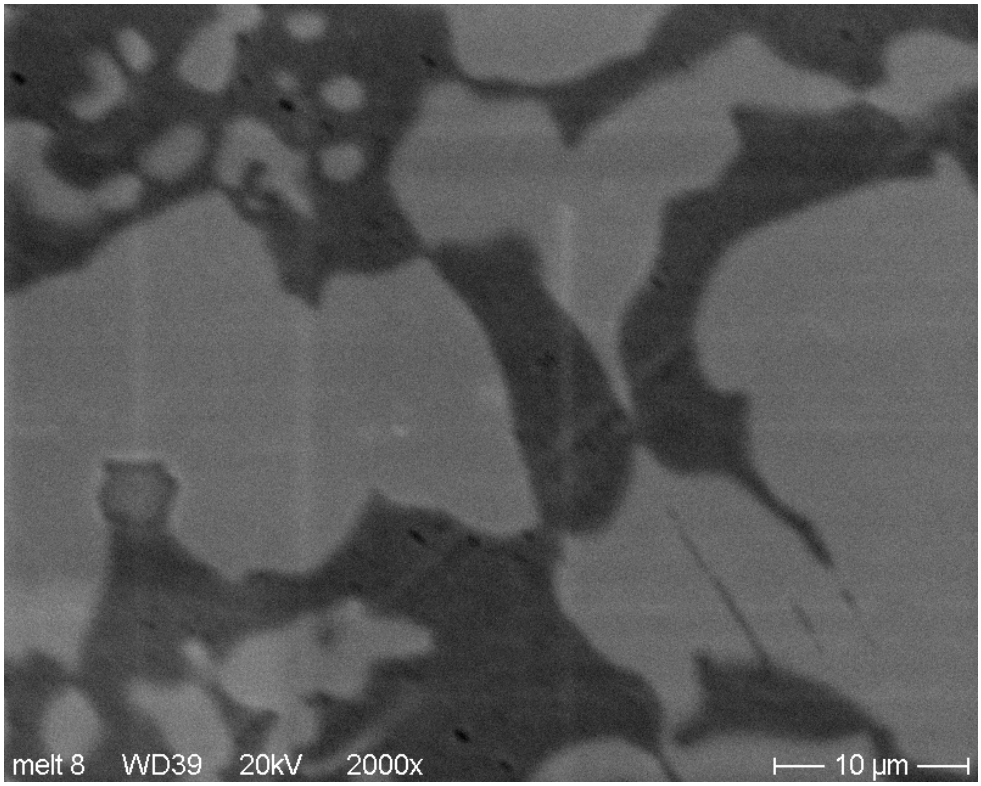

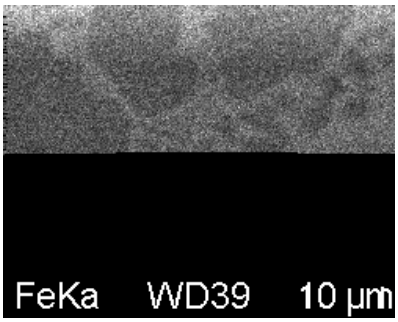

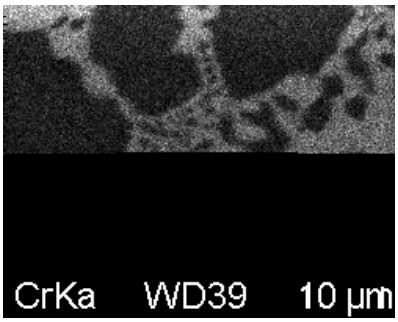

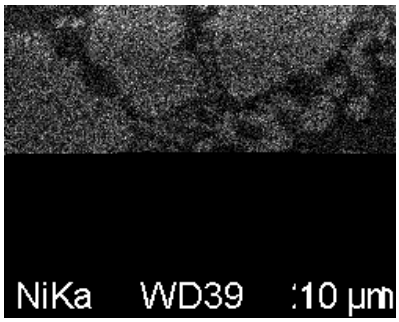

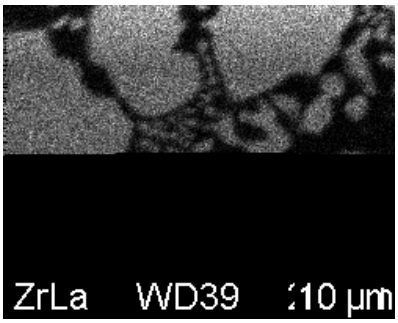

Measurement	Cr, Ma-%	Fe, Ma-%	Ni, Ma-%	Mn, Ma-%	Zr, Ma-%	Remark
dark phase	28.2	65.5	3.3	2.6	0.3	20 kV, standardless
light phase	9.2	50.2	8.5	1.8	30.0	20 kV, standardless

Melt 7: 63 % SS, 30 % Zry, 7 % B_4C
after preparation

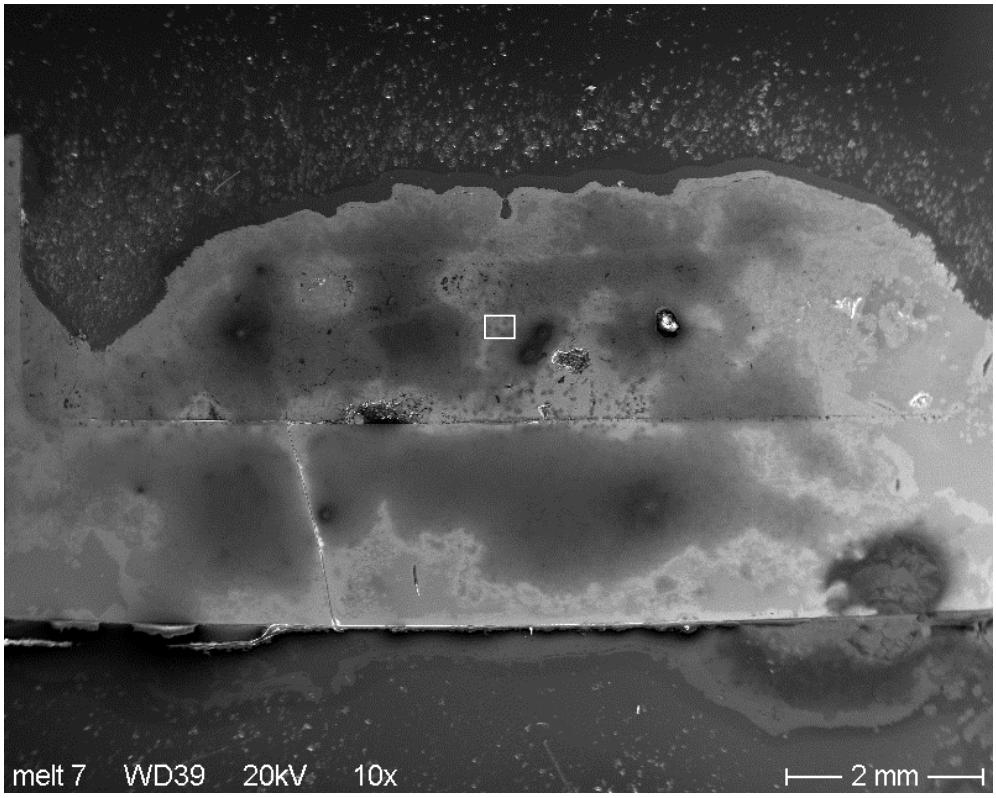

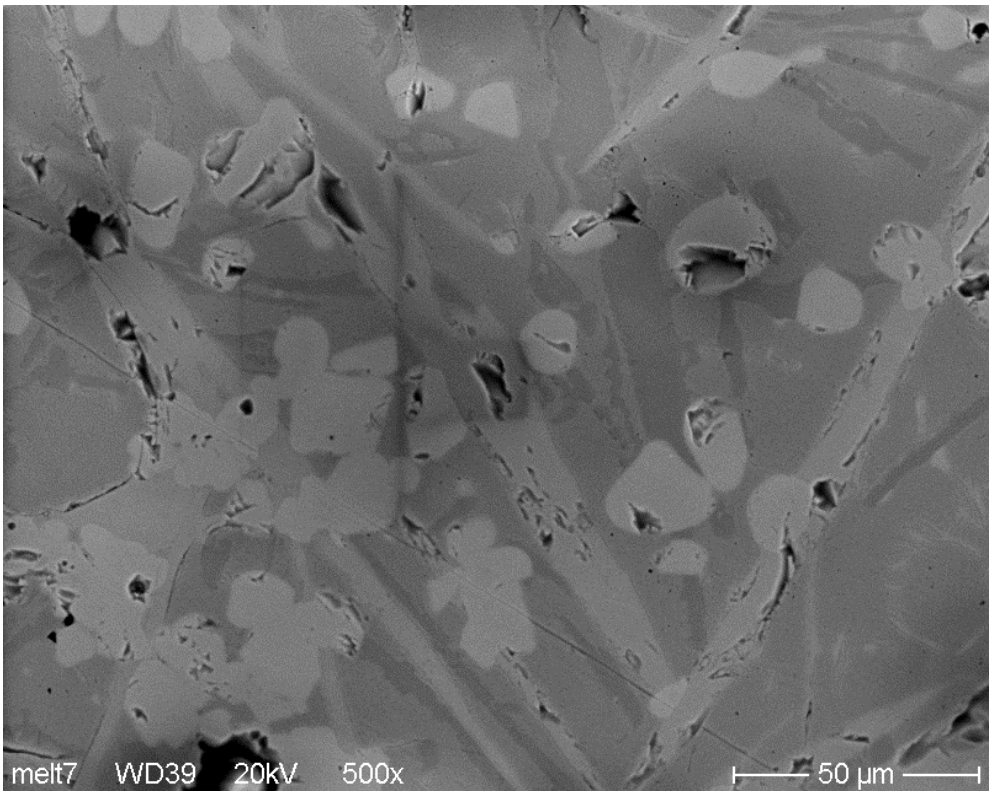

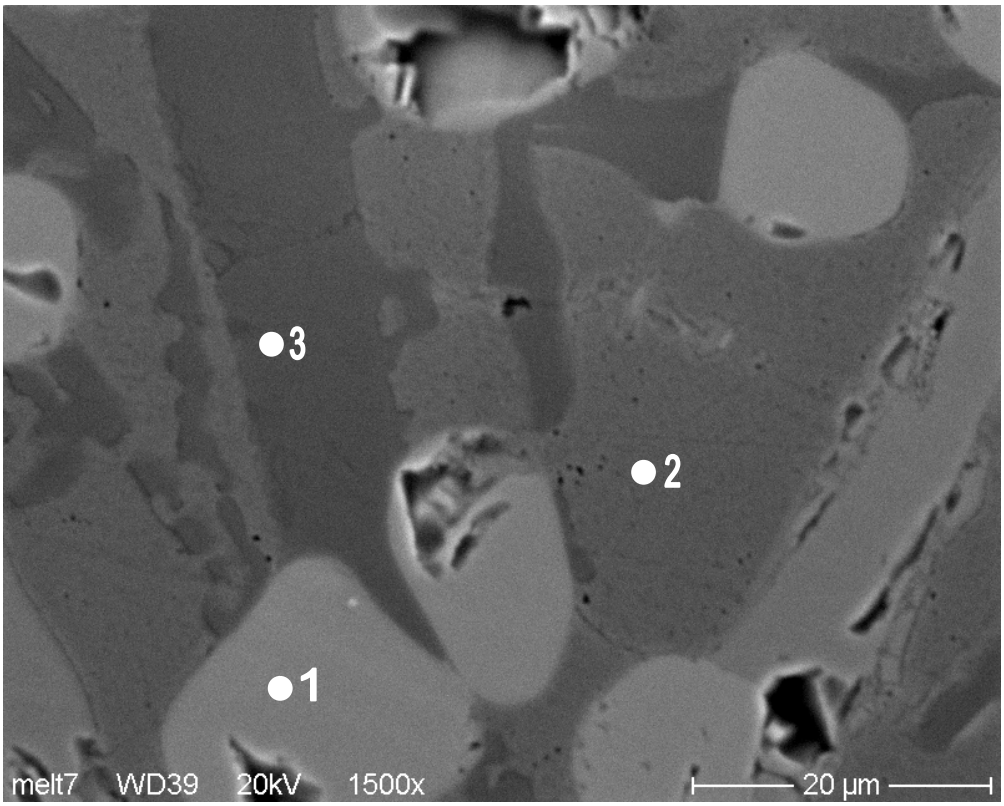

Measurement	Cr, Ma-%	Fe, Ma-%	Ni, Ma-%	Zr, Ma-%	Mn, Ma-%	Remark
point 1	0.6	1.5		97.9		20 kV, standardless
	Zr, B and C					7 kV
point 2	12.3	73.8	10.3	0.6	2.7	20 kV, standardless
	Fe, Cr, Ni, C, B, Zr					7 kV
point 3	55.4	40.1	0.3		4.1	20 kV, standardless
	Cr, Fe, C, B					7 kV

Box 21108: 100 % SS
after oxidation

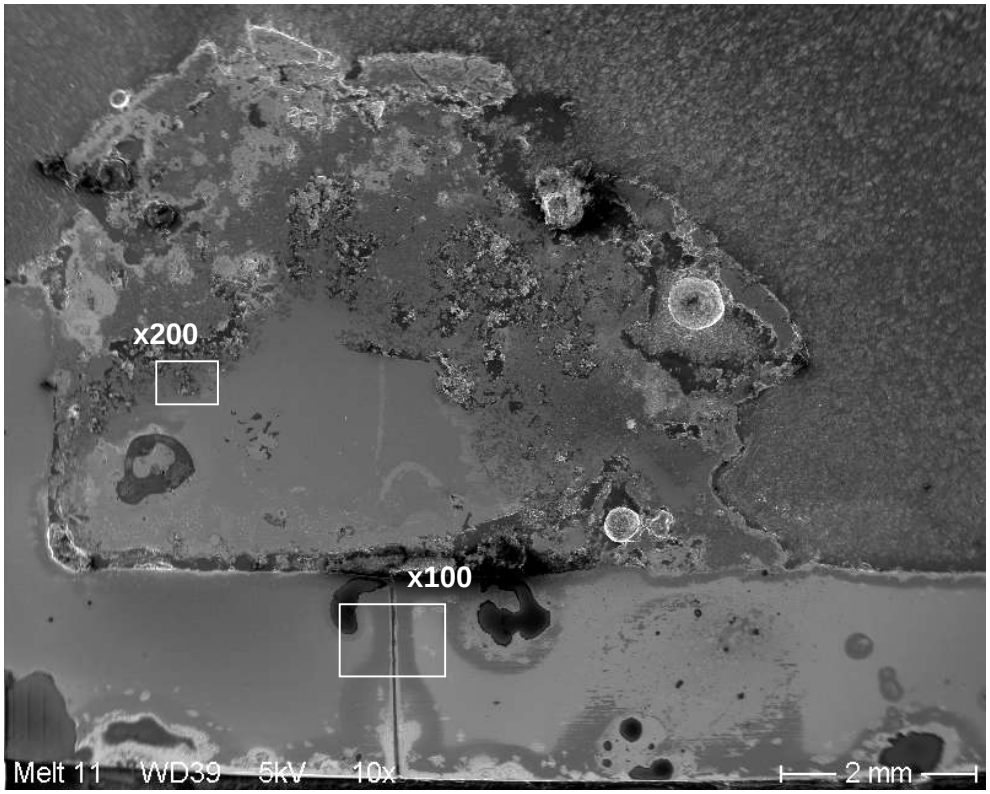

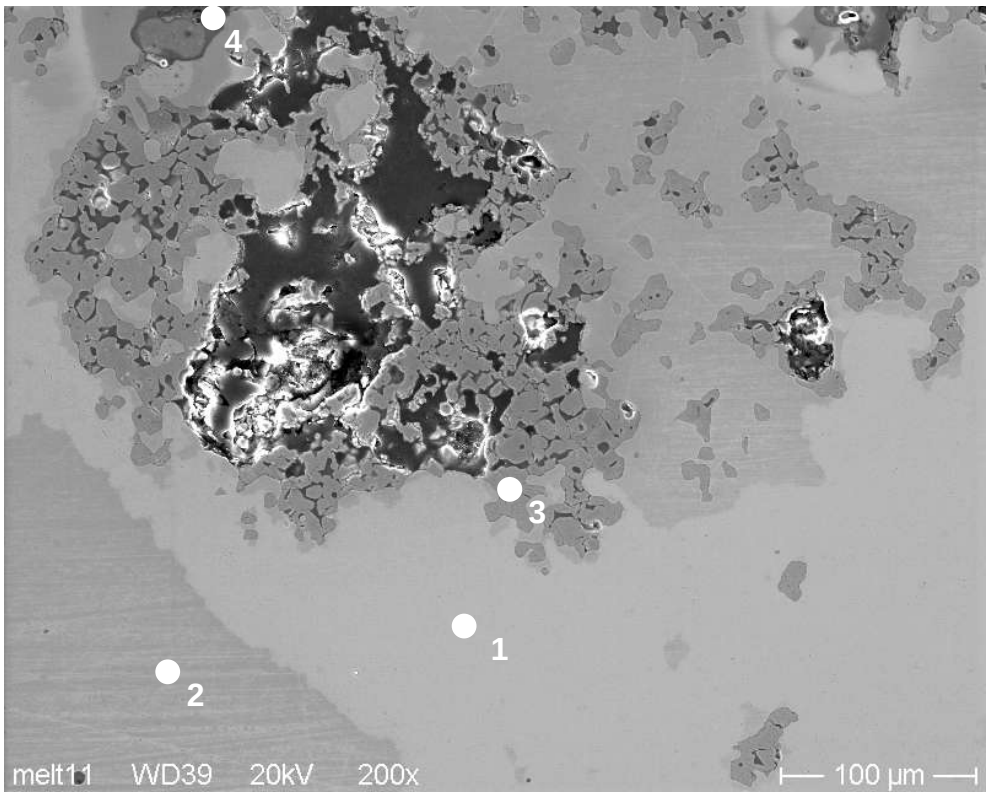

Measurement	Cr, Ma-%	Fe, Ma-%	Ni, Ma-%	Zr, Ma-%	Mn, Ma-%	Remark
point 1	5.7	82.9	11.1		0.4	20 kV, standardless
	Fe, Ni, C, O, Cr					5 kV
point 2	5.5	83.6	10.8			20 kV, standardless
	Fe, Ni, C, Cr, O					5 kV
point 3	67.7	12.7			18.5	20 kV, standardless
	Cr, Fe, O, C, Ni					5 kV
point 4	69.6	15.2		15.2		20 kv, standardless

Box 21111: 100 % SS
after oxidation

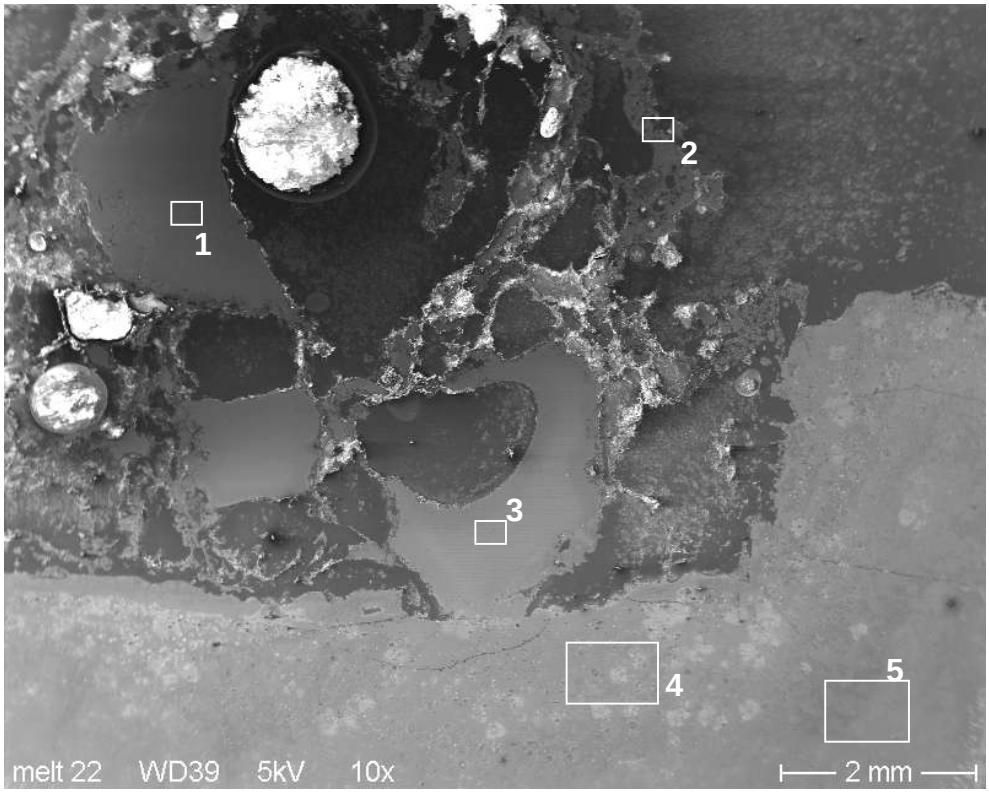

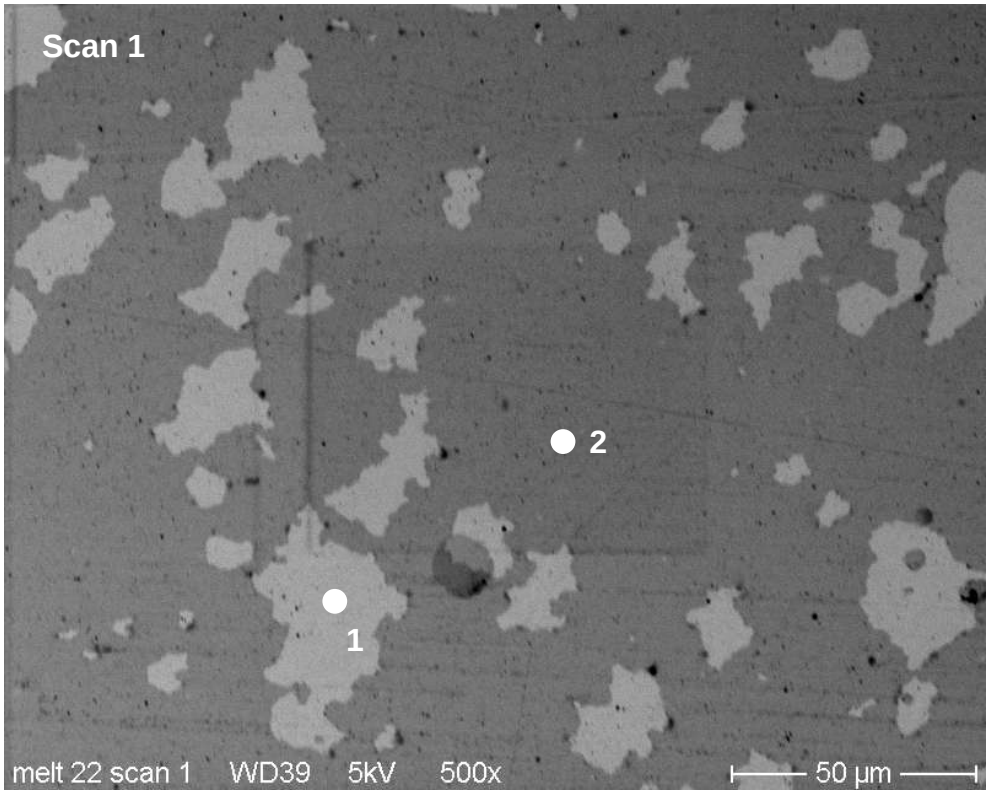

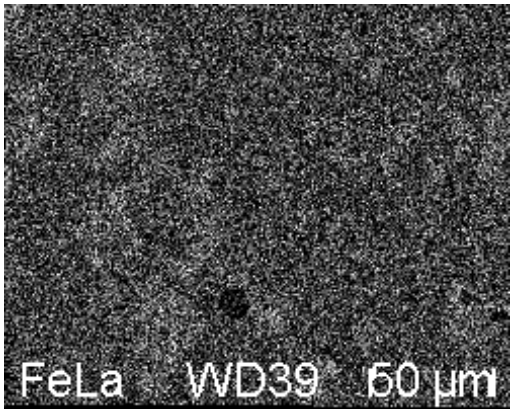
FeLa WD39 50 µm

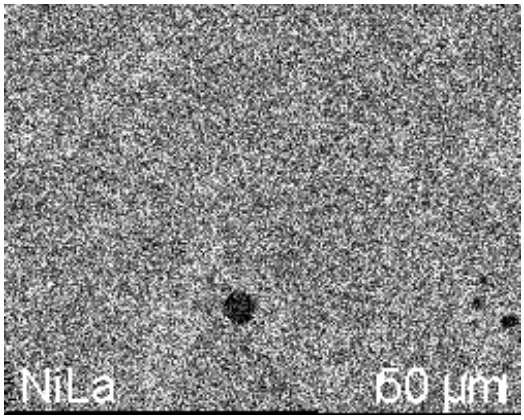
NiLa 50 µm

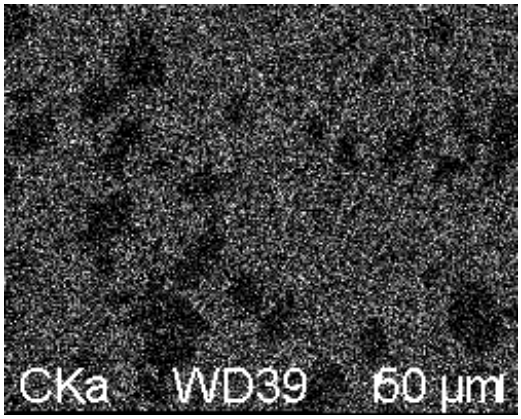
CKa WD39 50 µm

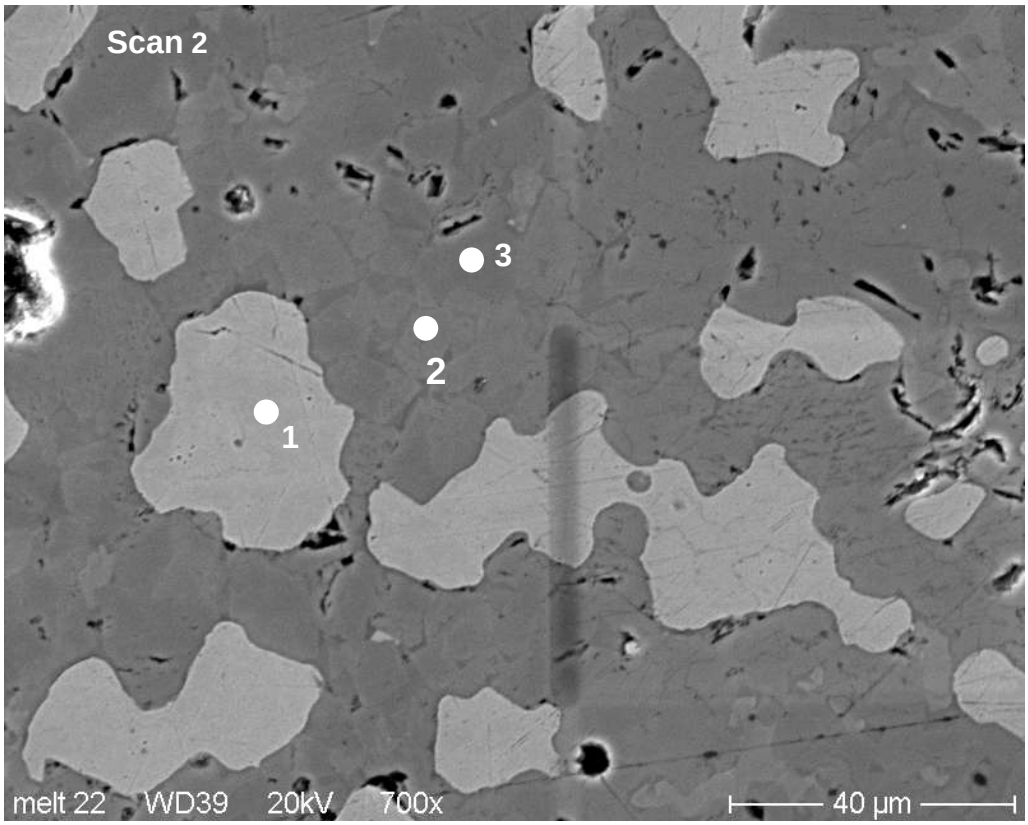
Scan 2
3
2
1
melt 22 WD39 20kV 700x
40 µm

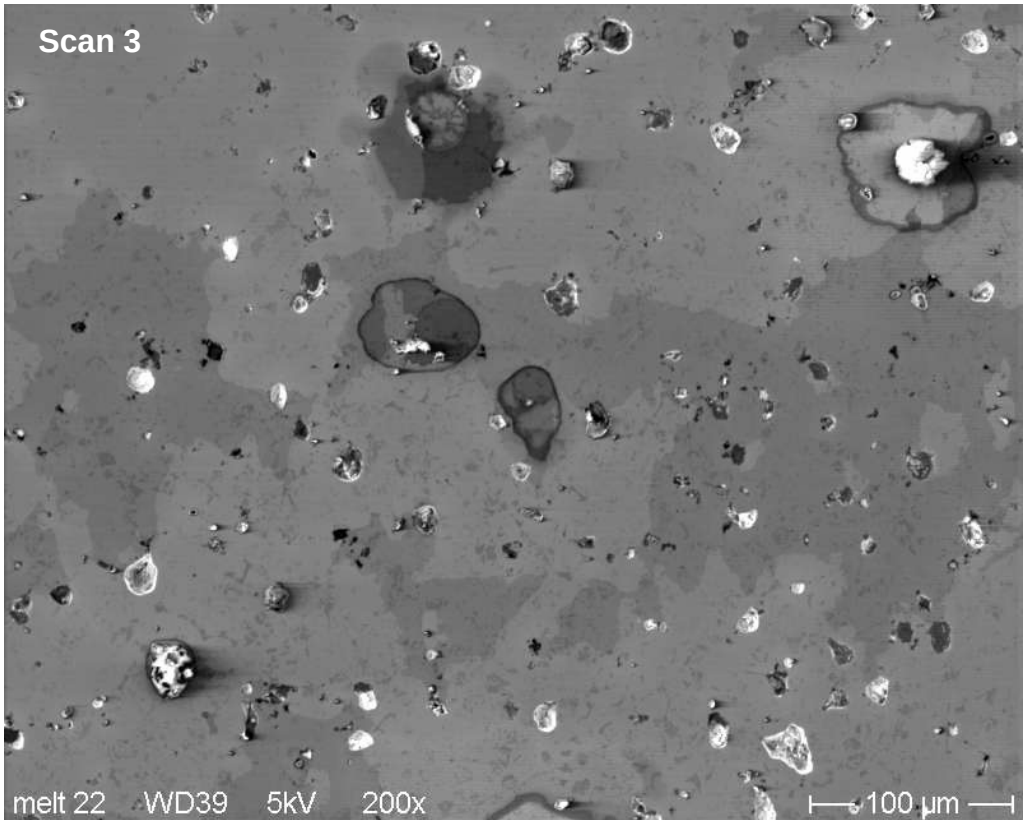
Scan 3
melt 22 WD39 5kV 200x
100 µm

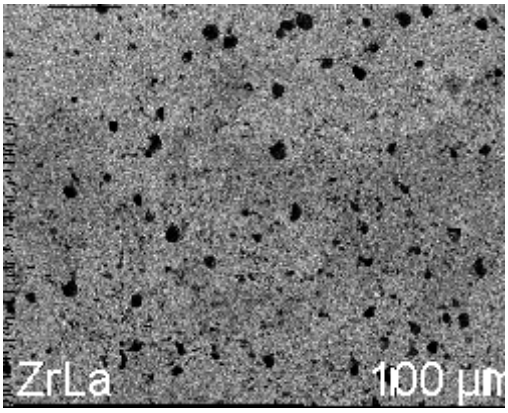
ZrLa
100 µm

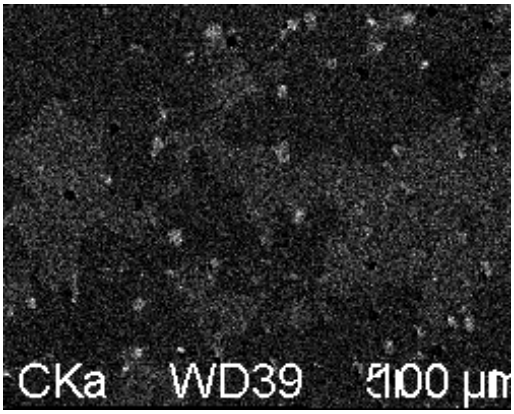
CKa WD39
100 µm

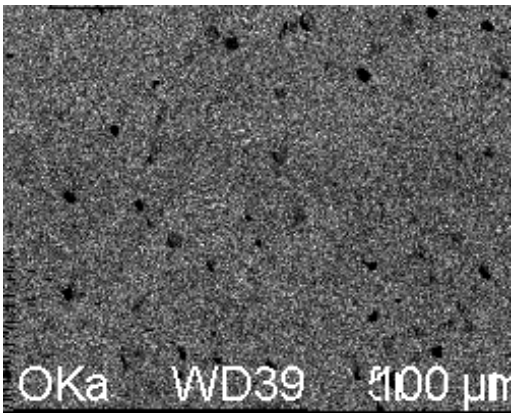
OKa WD39
100 µm

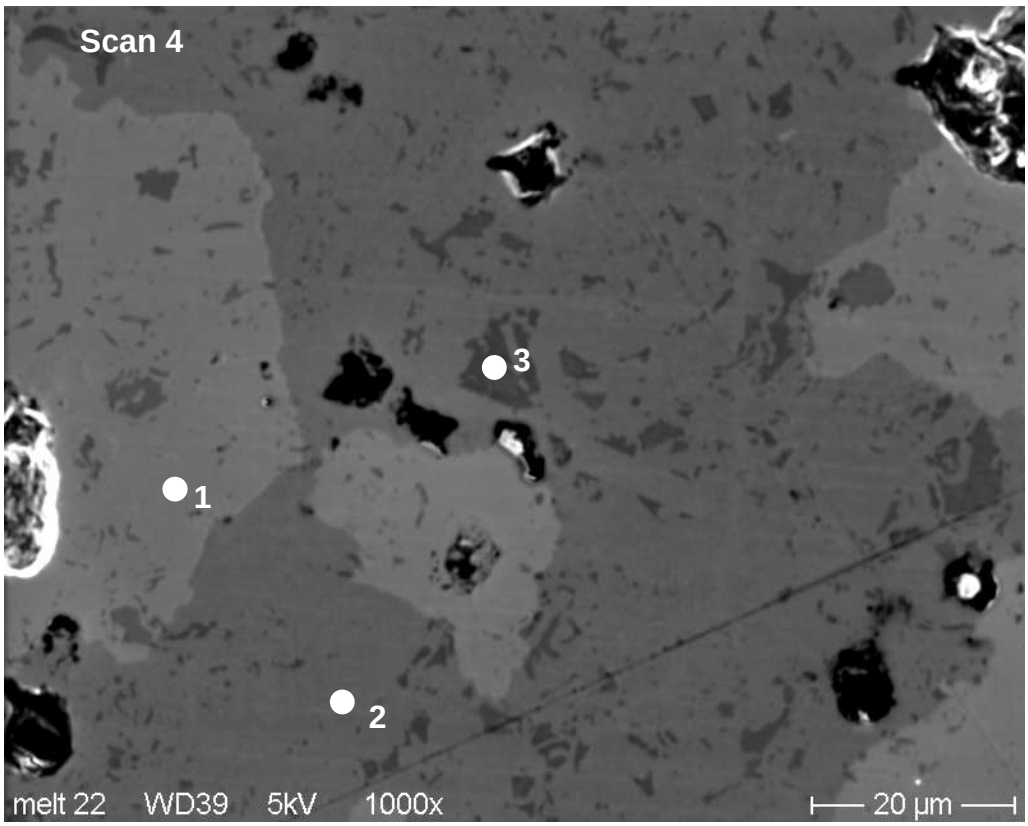
Scan 4
3
1
2
melt 22 WD39 5kV 1000x
20 µm

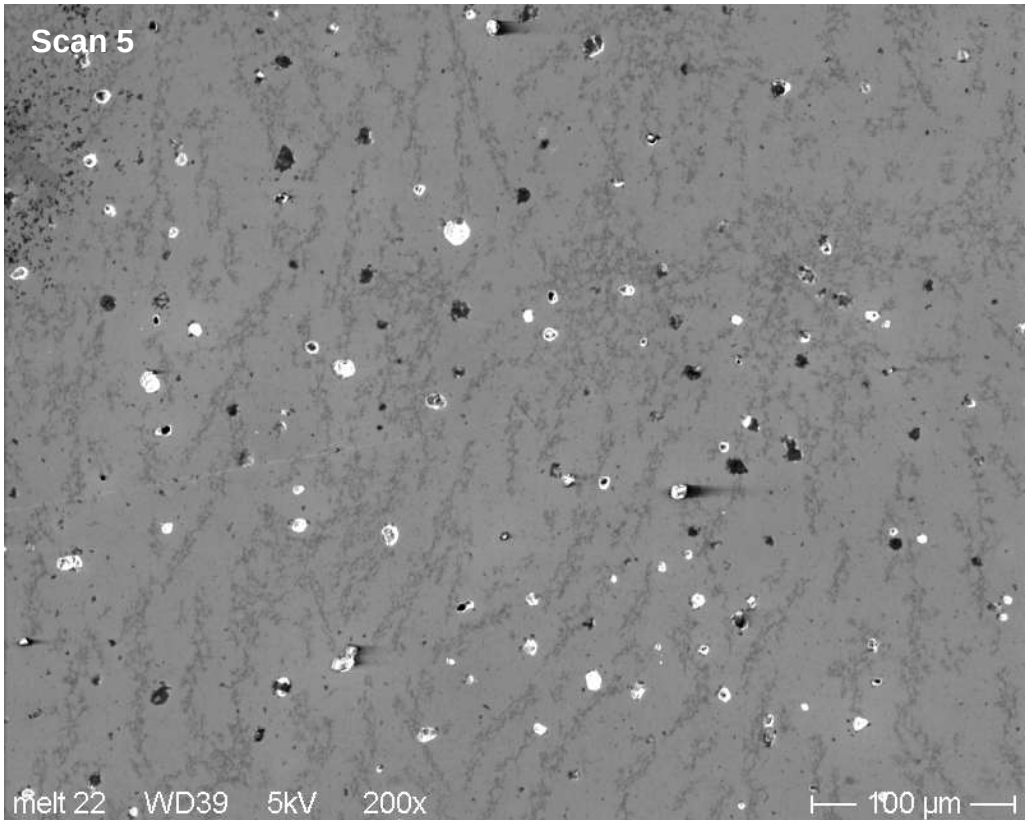
Scan 5
melt 22 WD39 5kV 200x
100 µm

Measurement	Cr, Ma-%	Fe, Ma-%	Ni, Ma-%	Zr, Ma-%	C, Ma-%	O, Ma-%	Remark
Scan 1, Point 1		79.6	20.4				20 kV, standardless
	1.4	70.2	23.8	0.1	3.1	1.5	5 kV, with standards
Scan 1, Point 2		80.1	19.9				20 kV, standardless
		67.4	23.4		7.7	1.6	5 kV, with standards
Scan 2, Point 1	0.9	30.5	68.6				20 kV, standardless
	Ni, Fe, C, O						5 kV
Scan 2, Point 2	43.4	54.1			(Mn 2.5 Ma-%)		20 kV, standardless
	Cr, O, Fe, C						5 kV
Scan 2, Point 3	45.6	51.4	0.3	0.3	(Mn 2.5 Ma-%)		20 kV, standardless
	Cr, O, Fe, C, Zr						5 kV
Scan 4, Point 1	Zr, O, B, C						5 kV
Scan 4, Point 2	Zr, O, C, B, Fe						5 kV
Scan 4, Point 3	Fe, O, C, Zr						5 kV
Scan 5	Zr, O, C, B, Fe						5 kV

Box 21113: 80 % SS, 20 % B_4C
after oxidation

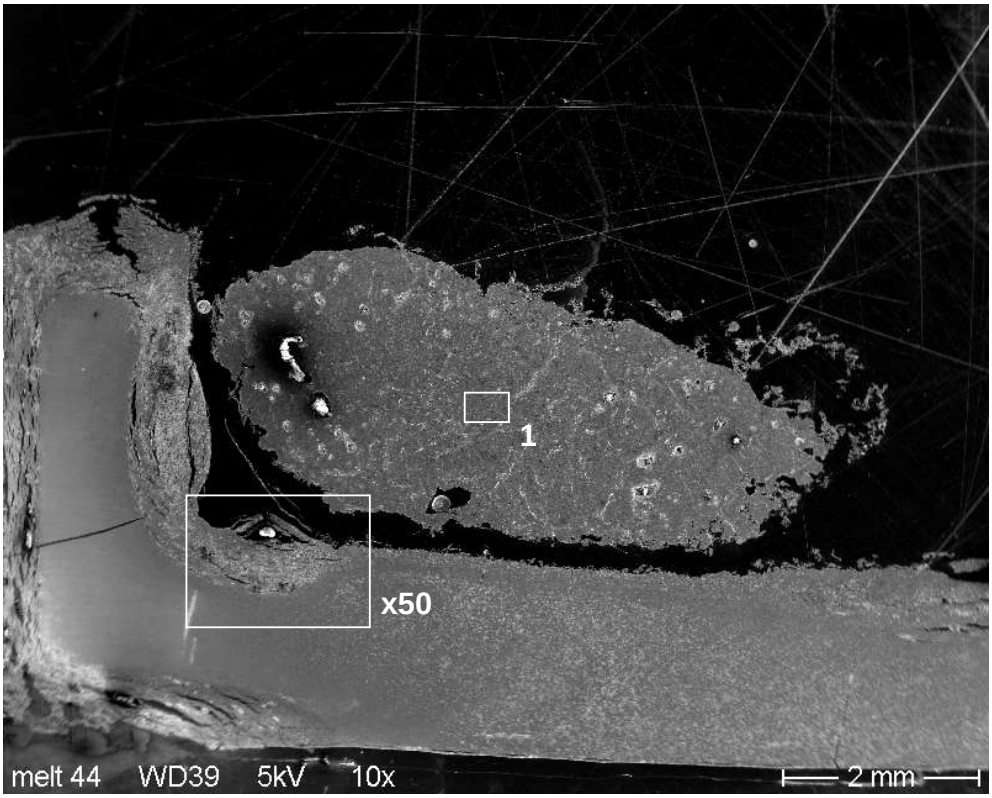

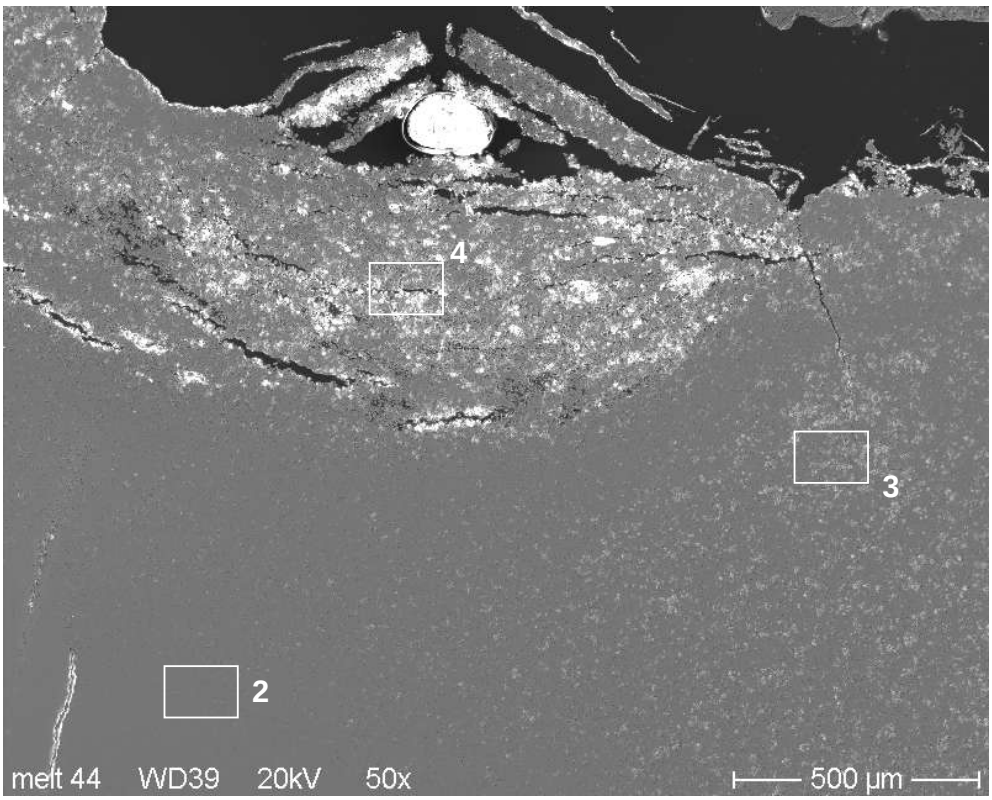

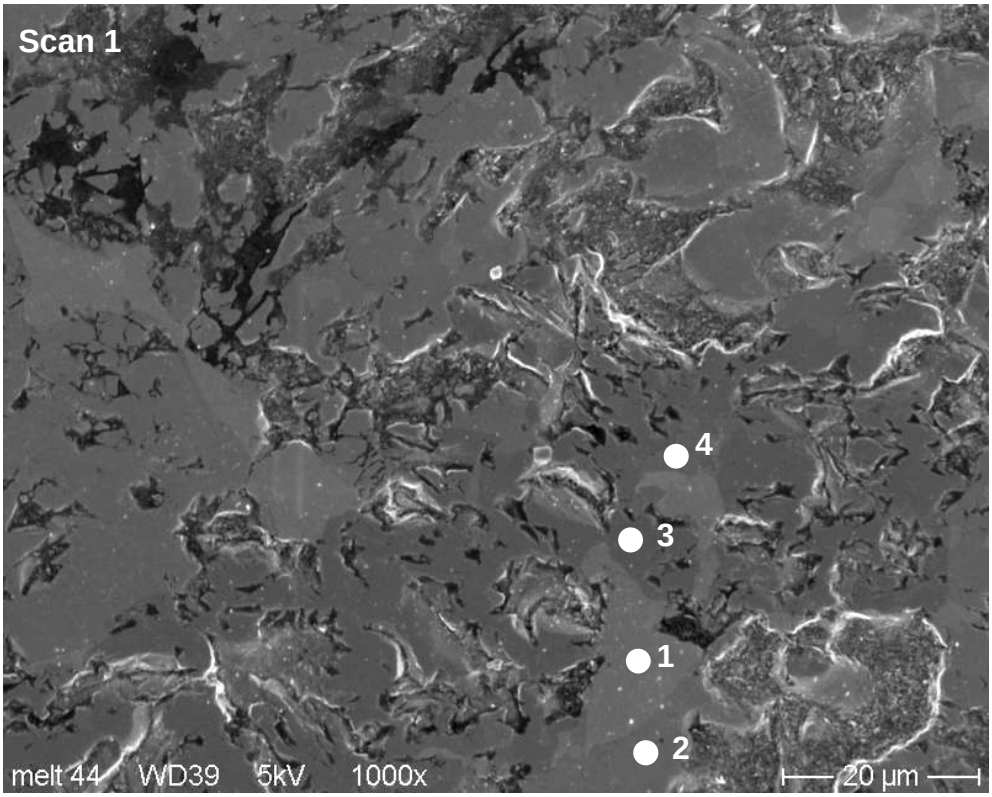
Scan 1
4
3
1
2
melt 44 WD39 5kV 1000x
20 µm

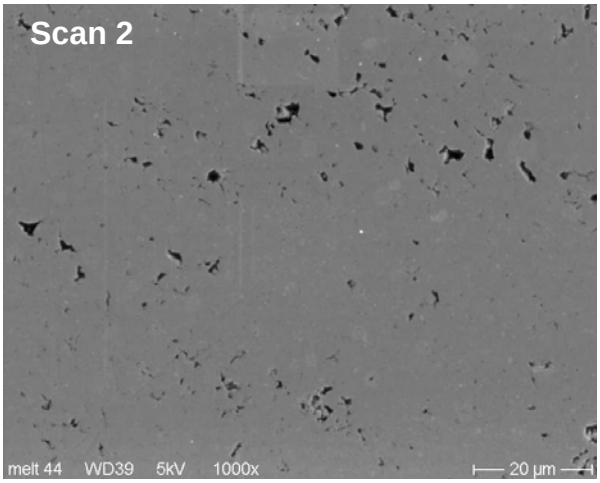
Scan 2
melt 44 WD39 5kV 1000x
20 µm

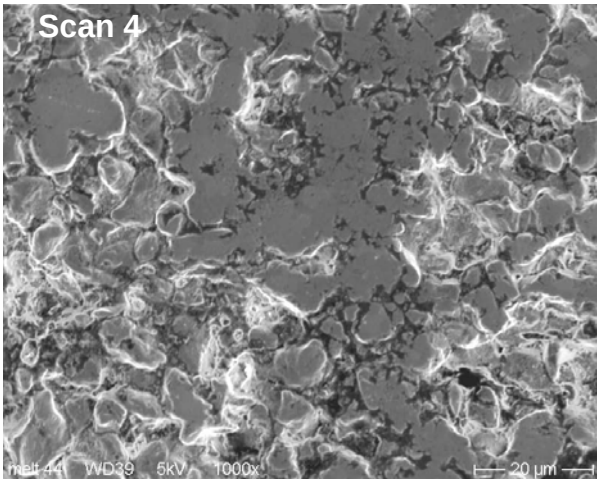
Scan 4
melt 44 WD39 5kV 1000x
20 µm

Measurement	Cr, Ma-%	Fe, Ma-%	Ni, Ma-%	Zr, Ma-%	C, Ma-%	O, Ma-%	Remark
Scan 1, Point 1	1.6	8.0	76.0	3.4	(Si 9.5 Ma-%)		20 kV, standardless
	Ni, Si, Fe, C, Zr						5 kV
Scan 1, Point 2	7.5	72.7	18.3		(Mn 1.5 Ma-%)		20 kV, standardless
	Fe, Cr, Ni, C, O						5 kV
Scan 1, Point 3	29.1	65.5	2.6		(Mn 2.9 Ma-%)		20 kV, standardless
	Fe, Cr, Ni, C, O						5 kV
Scan 1, Point 4	29.6	64.4	3.0		(Mn 3.0 Ma-%)		20 kV, standardless
	Fe, Cr, Ni, O						5 kV
Scan 2				67.5	9.5	23.0	5 kV, with standards
Scan 3		(Al 3.1 Ma-%)		60.1	12.6	23.1	5 kV, with standards
Scan 4		(Al 5.4 Ma-%)		54.4	16.8	23.1	5 kV, with standards

Box 21120: 63 % SS, 30 % Zry, 7 % B_4C
after oxidation

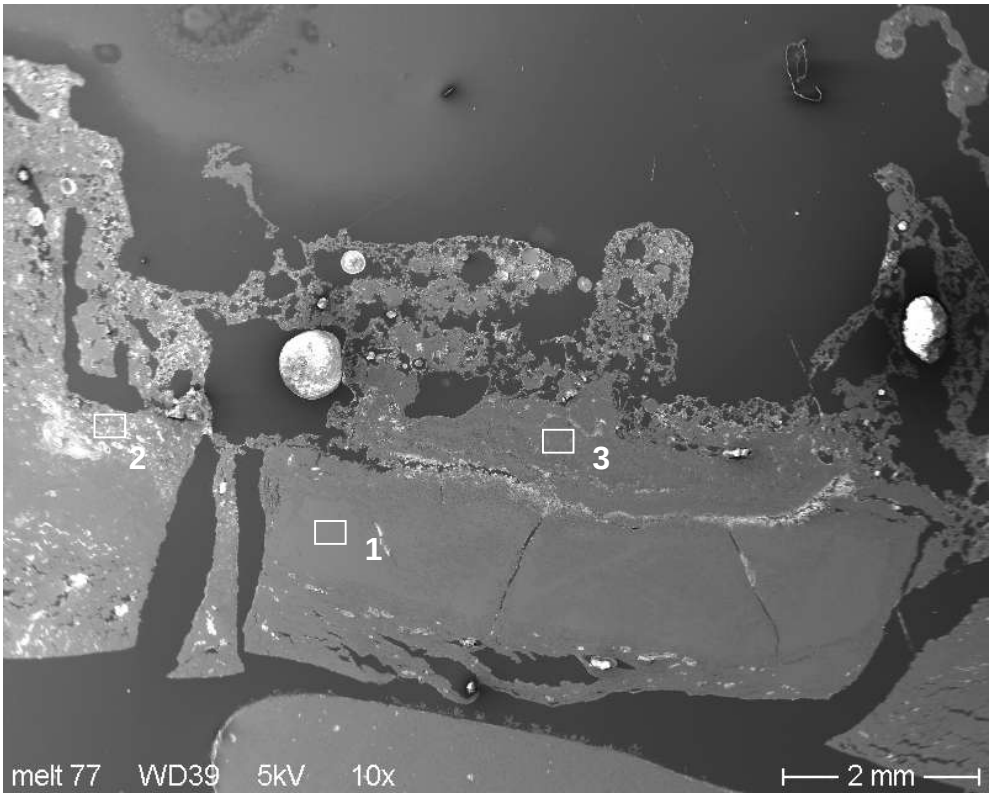

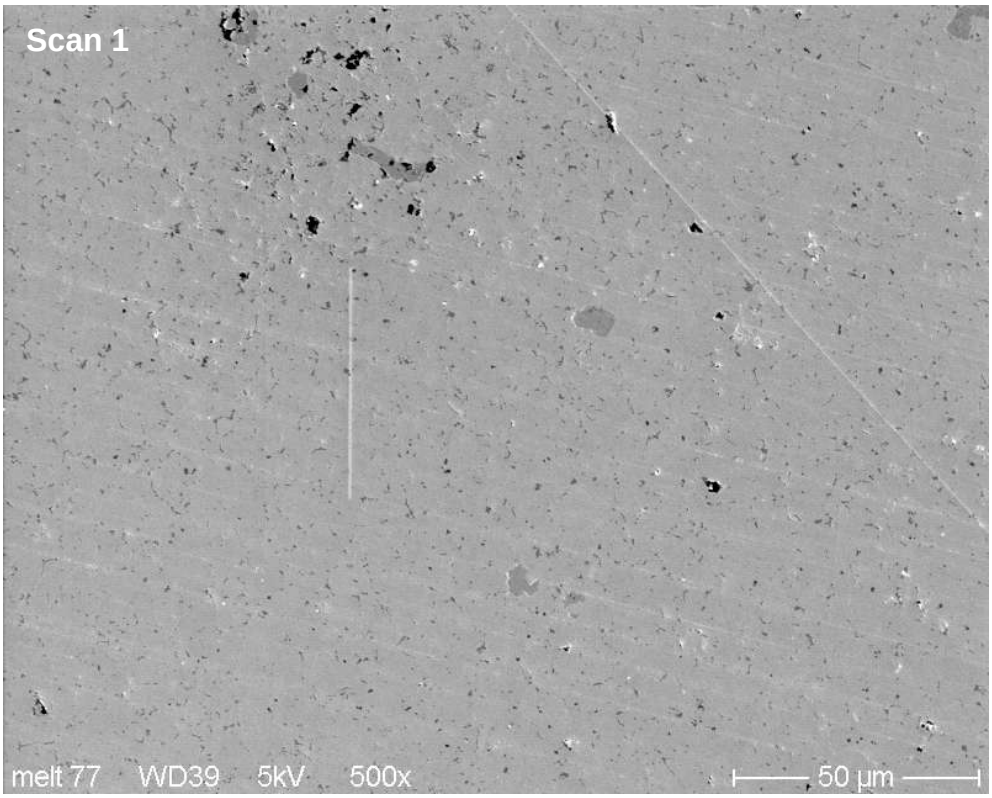

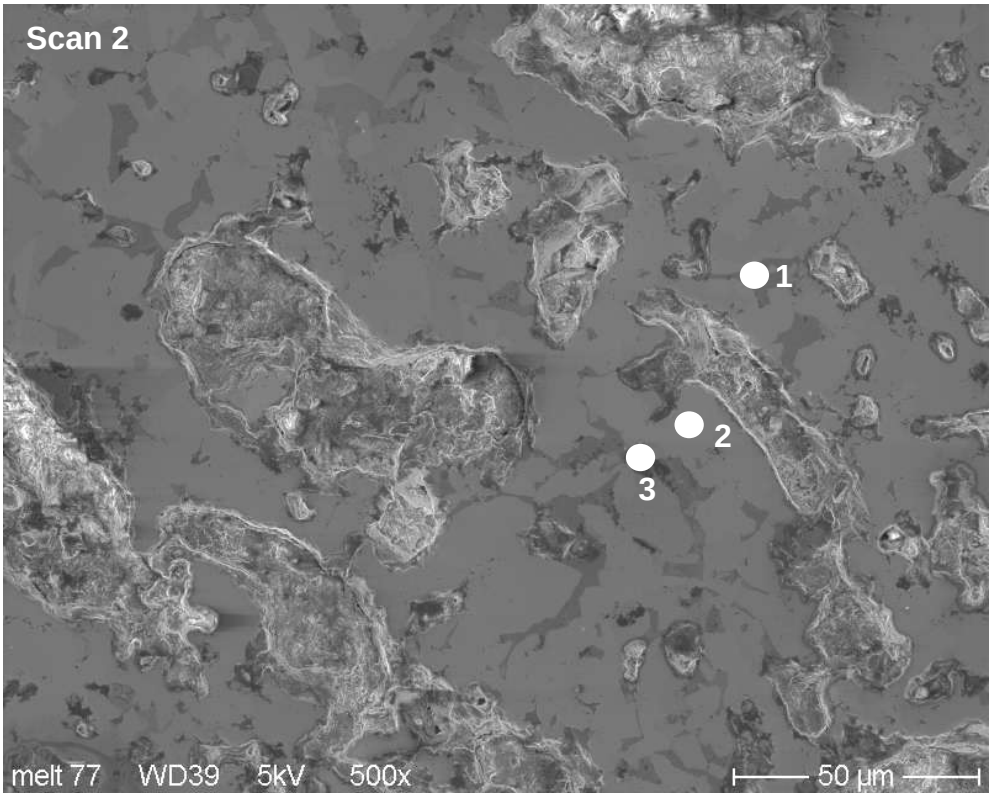
Scan 2
1
2
3
melt 77 WD39 5kV 500x
50 µm

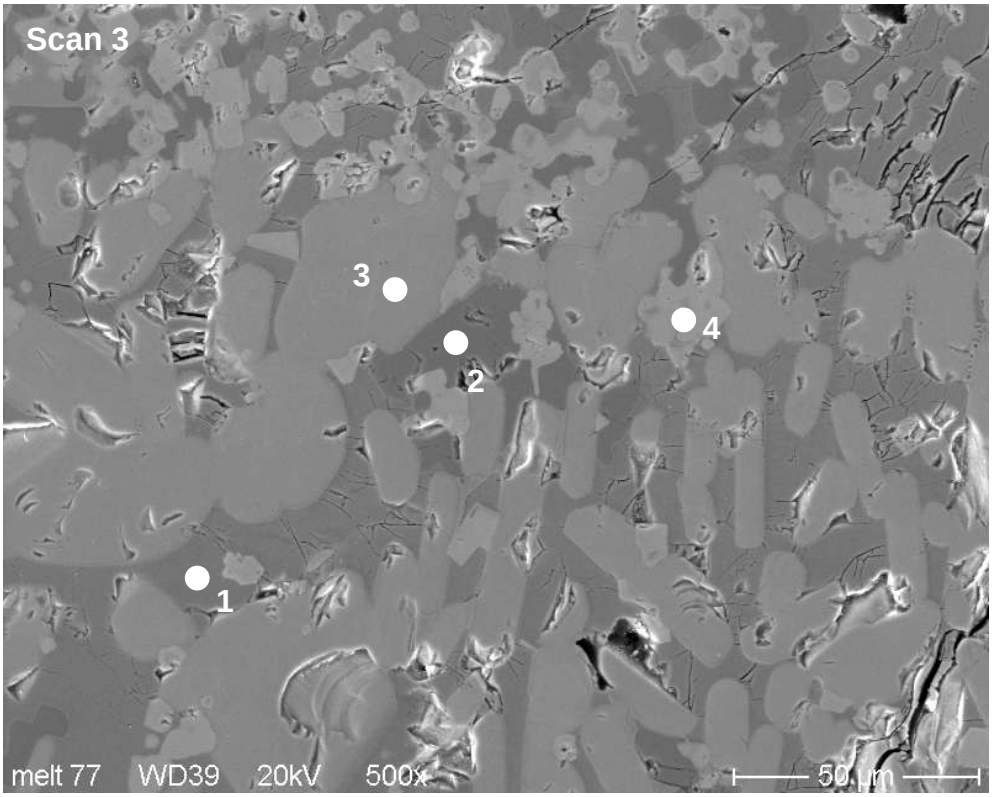
Scan 3
3
4
2
1
melt 77 WD39 20kV 500x
50 µm

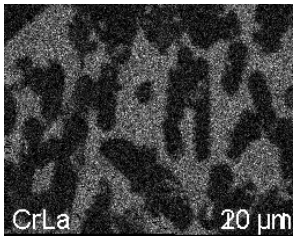
CrLa
20 µm

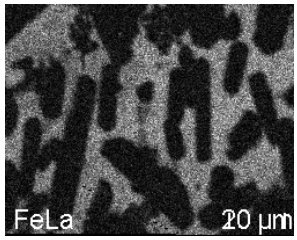
FeLa
20 µm

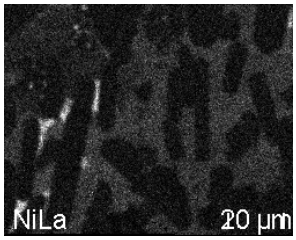
NiLa
20 µm

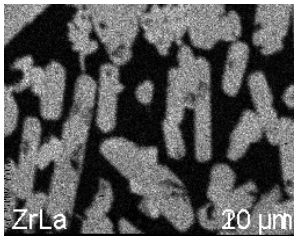
ZrLa
20 µm

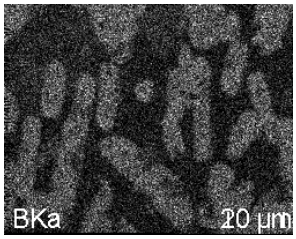

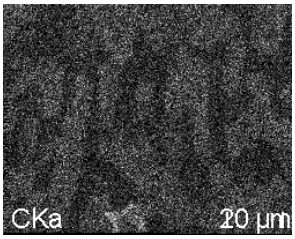

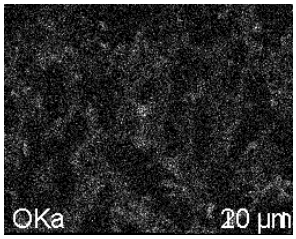

Measurement	Cr, Ma-%	Fe, Ma-%	Ni, Ma-%	Zr, Ma-%	C, Ma-%	O, Ma-%	Remark
Scan 1				73.9		26.1	5 kV, with standards
Scan 2, Point 1	80.6	1.5		16.1	(Mn 1.8 Ma-%)		20 kV, standardless
	42.8	2.7		12.1	18.7	23.8	5 kV, with standards
Scan 2, Point 2				86.8		13.2	5 kV, standardless
Scan 2, Point 3	62.8	3.0	27.6		(Mn 2.0 Ma-%)		20 kV, standardless
Scan 3, Point 1	5.3	83.8	8.5	0.8	(Mn 1.7 Ma-%)		20 kV standardless
	23.5	61.7	5.8		5.5	3.4	5 kV, with standards
Scan 3, Point 2	21.8	73.2	2.2	0.3	(Mn 2.6 Ma-%)		20 kV standardless
	27.5	65.0	3.3		4.2		5 kV, with standards
Scan 3, Point 3	1.4	1.6	97.9				20 kV standardless
	Zr, B, C						5 kV
Scan 3, Point 4		1.0	0.5	98.5			20 kV standardless
	Zr, B, C, O						5 kV

Box 21121: 70 % SS, 30 % Zry
after oxidation

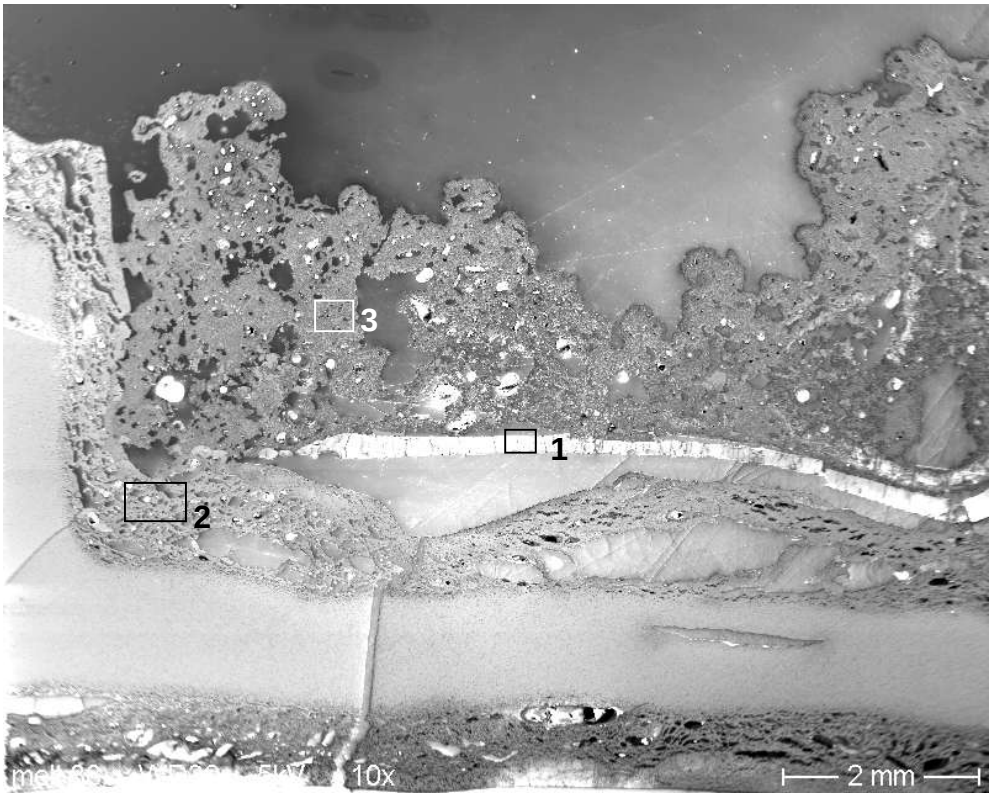

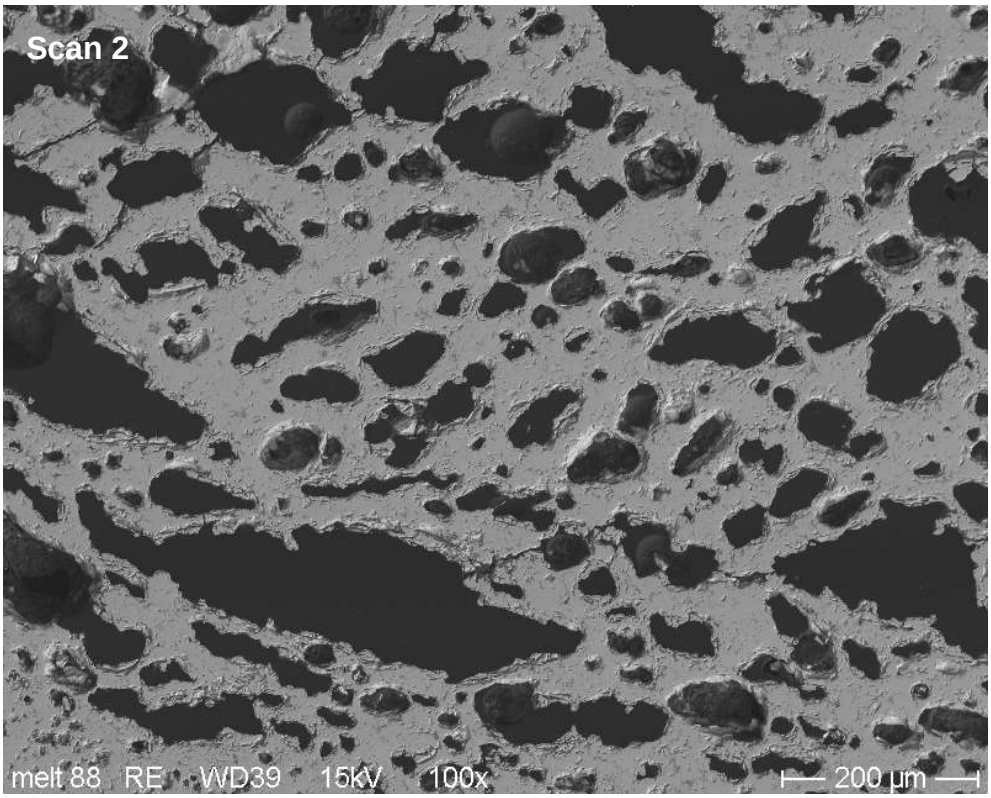

Measurement	Cr, Ma-%	Fe, Ma-%	Ni, Ma-%	Zr, Ma-%	C, Ma-%	O, Ma-%	Remark
Scan 1				70.3	3.2	26.5	5 kV, with standards
Scan 2	0.6	11.8	0.4	86.7	(Mn 0.5 Ma-%)		20 kV, standardless
		10.4		64.4		25.2	5 kV, with standards
Scan 3	57.9	29.8	3.0	8.2			20 kV, standardless
	20.0	28.2	4.5	8.8	11.5	19.4	5 kV, with standards

A12 Binary phase diagrams in the system Fe-Cr-Ni-Zr-B-C-O

The following collection of phase diagrams was taken from the Thermochemical and Physical Properties database TAPP 2.2 [10]. They could and should be used to get a quick overview on the systems. For more detailed and up-to-date information it is recommended to use recent original literature.

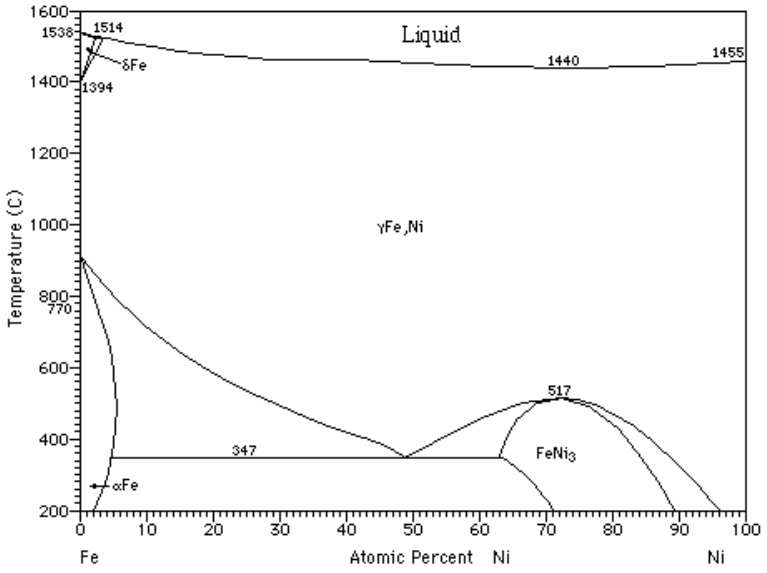
Liquid
1514
1538
δFe
1394
1440
1455
γFe,Ni
770
517
347
FeNi3
αFe
Temperature (C)
Fe
Atomic Percent Ni
Ni

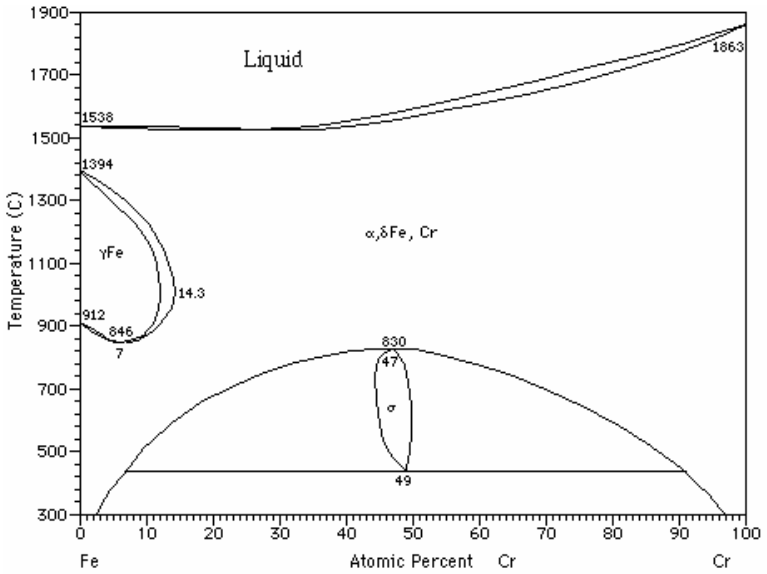
Liquid
1863
1538
1394
γFe
14.3
912
846
7
α,δFe, Cr
830
47
σ
49
Temperature (C)
Fe
Atomic Percent Cr
Cr

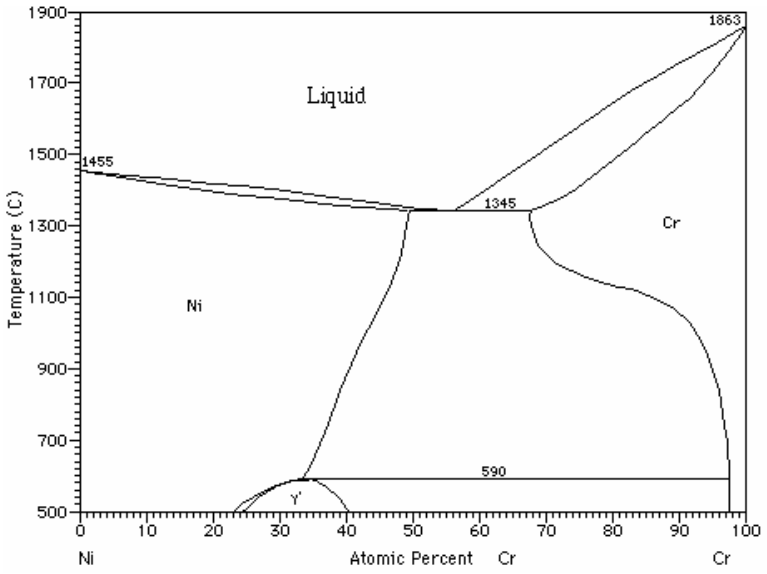
Liquid
1863
1455
1345
Cr
Ni
590
γ'
Temperature (C)
Ni
Atomic Percent Cr
Cr

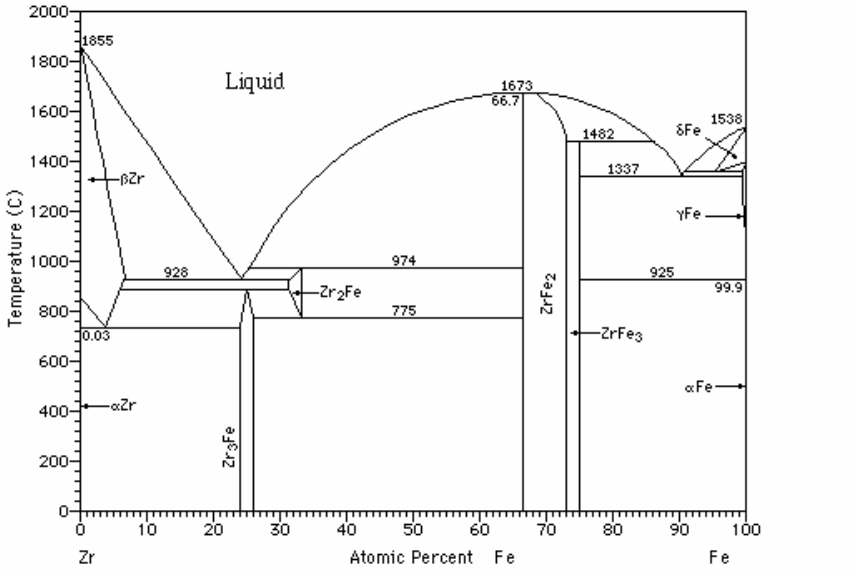
Liquid
1855
1673
66.7
1538
δFe
1482
1337
γFe
βZr
928
974
925
99.9
Zr2Fe
775
ZrFe2
0.03
ZrFe3
αFe
αZr
Zr3Fe
Temperature (C)
Zr
Atomic Percent Fe
Fe

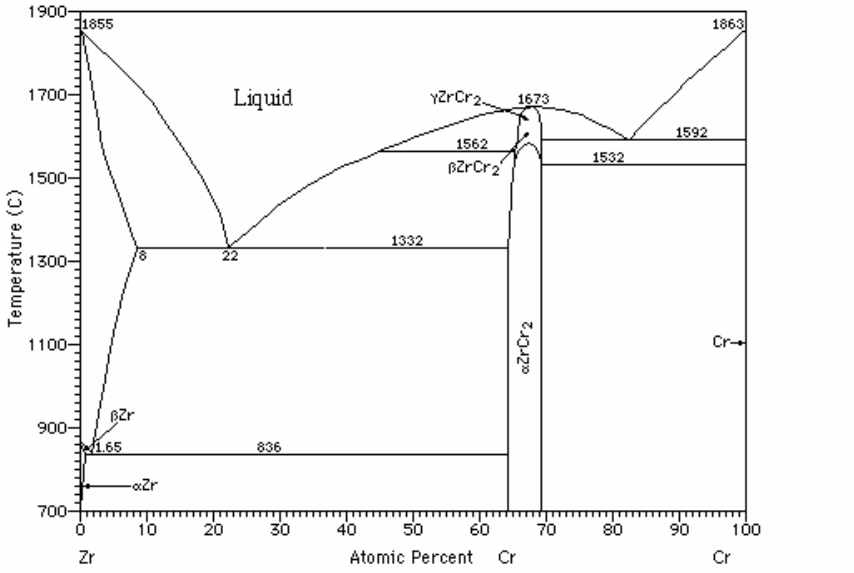
Liquid
1855
1863
γZrCr2
1673
1562
1592
βZrCr2
1532
1332
8
22
αZrCr2
Cr
βZr
1.65
836
αZr
Temperature (C)
Zr
Atomic Percent Cr
Cr

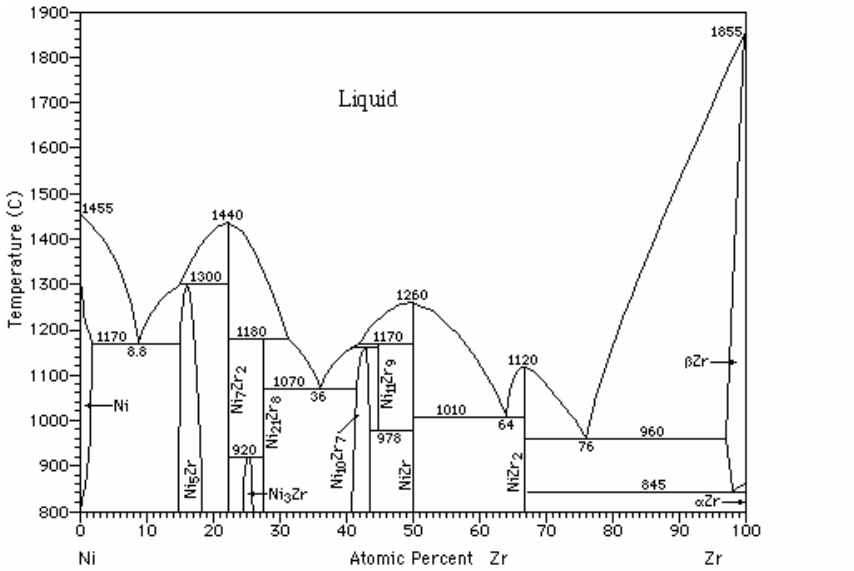
Liquid
1855
1455
1440
1300
1260
1170
1180
1170
1120
8.8
1070
36
1010
64
960
76
978
920
845
Ni
Ni5Zr
Ni7Zr2
Ni21Zr8
Ni3Zr
Ni10Zr7
Ni11Zr9
NiZr
NiZr2
βZr
αZr
Temperature (C)
Ni
Atomic Percent Zr
Zr

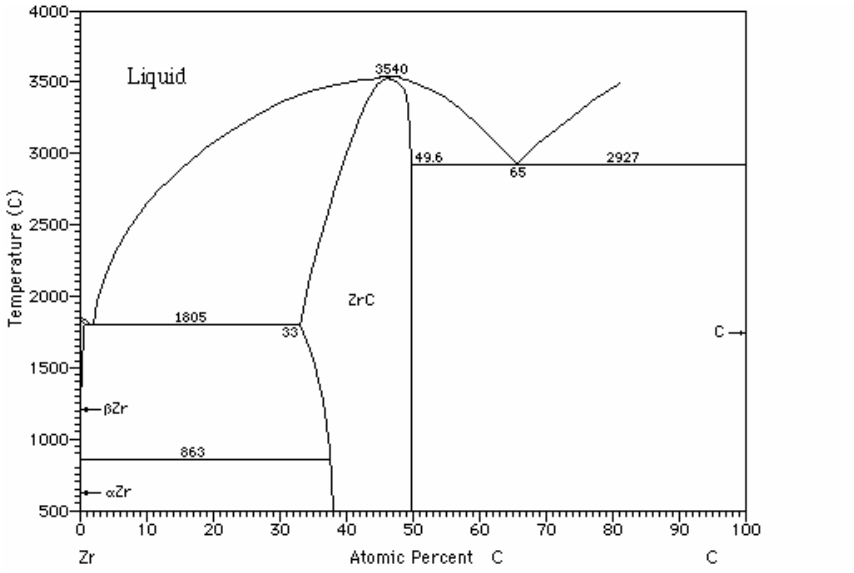
Liquid
3540
49.6
65
2927
ZrC
1805
33
C
βZr
863
αZr
Temperature (C)
Zr
Atomic Percent C
C

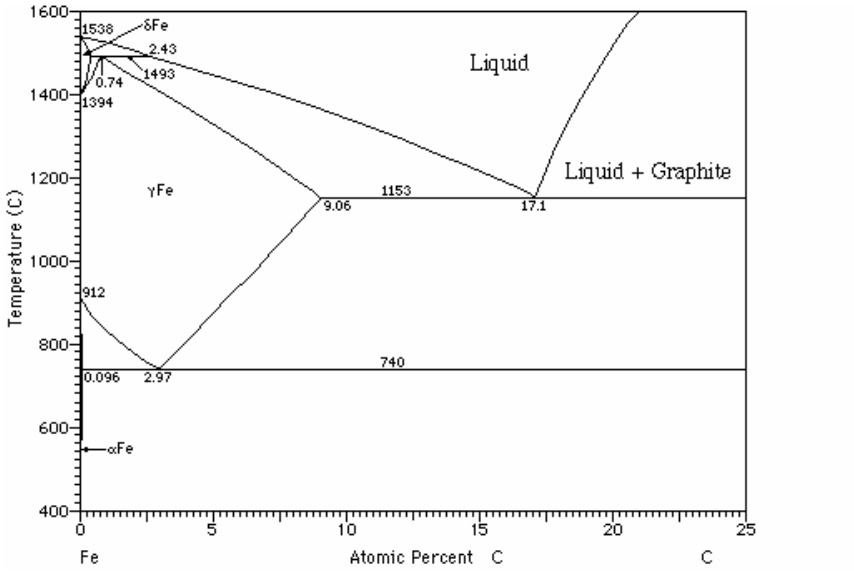
1538
δFe
2.43
1493
0.74
1394
Liquid
Liquid + Graphite
γFe
1153
9.06
17.1
912
740
0.096
2.97
αFe
Temperature (C)
Fe
Atomic Percent C
C

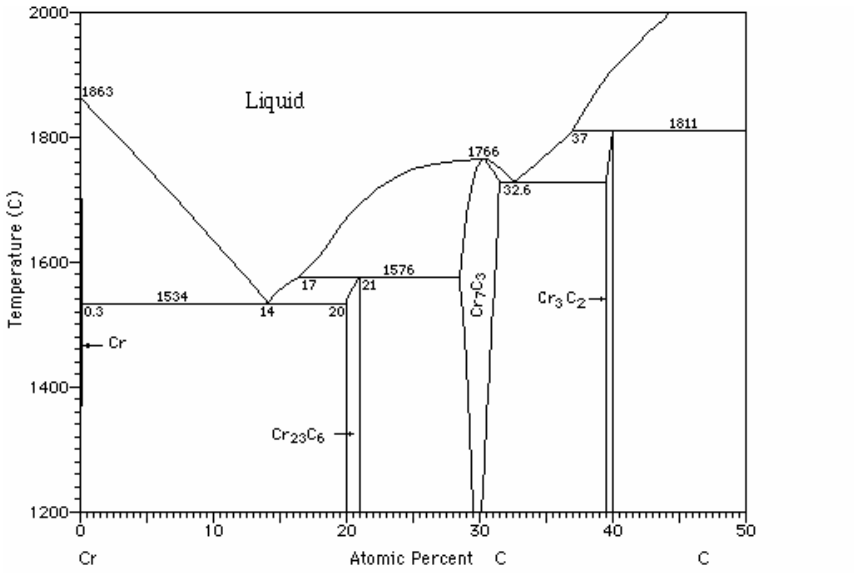
1863
Liquid
1811
37
1766
32.6
1576
17
21
1534
0.3
14
20
Cr
Cr7C3
Cr3C2
Cr23C6
Temperature (C)
Cr
Atomic Percent C
C

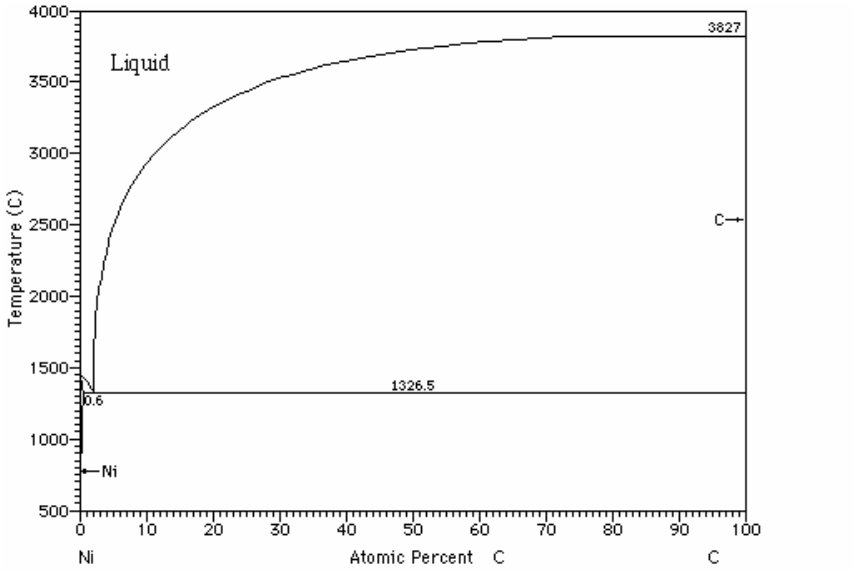
Liquid
3827
1326.5
0.6
Ni
C
Temperature (C)
Ni
Atomic Percent C
C

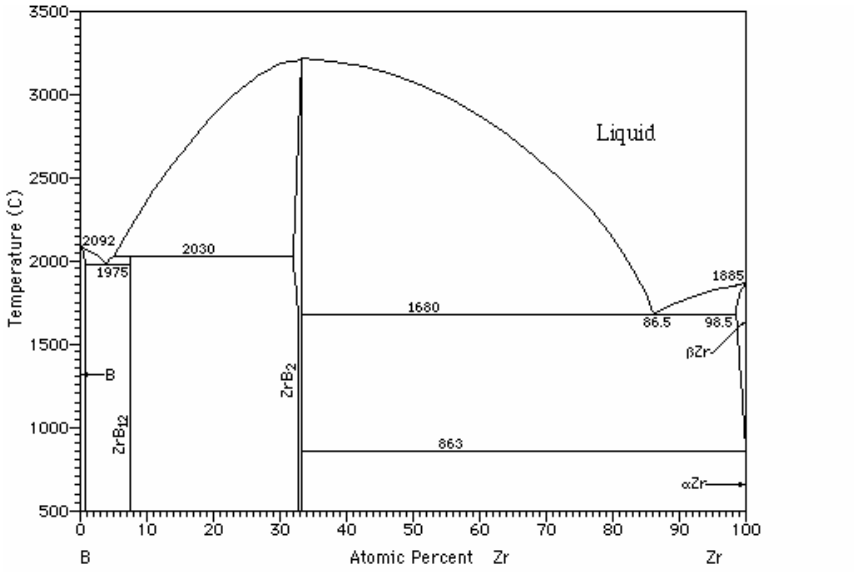
Liquid
2092
1975
2030
1680
1885
86.5
98.5
βZr
B
ZrB12
ZrB2
863
αZr
Temperature (C)
B
Atomic Percent Zr
Zr

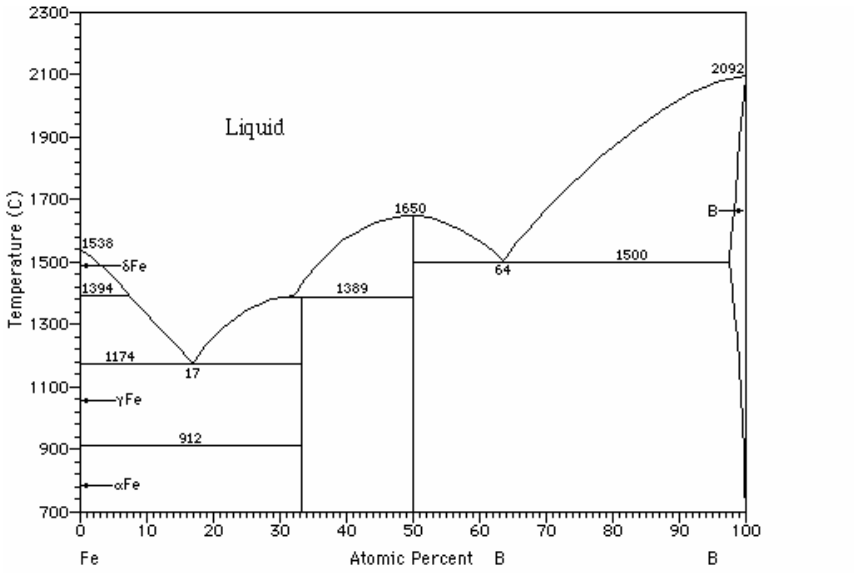
Liquid
2092
1650
1538
δFe
1394
1389
1174
17
γFe
912
αFe
64
1500
B
Temperature (C)
Fe
Atomic Percent B
B

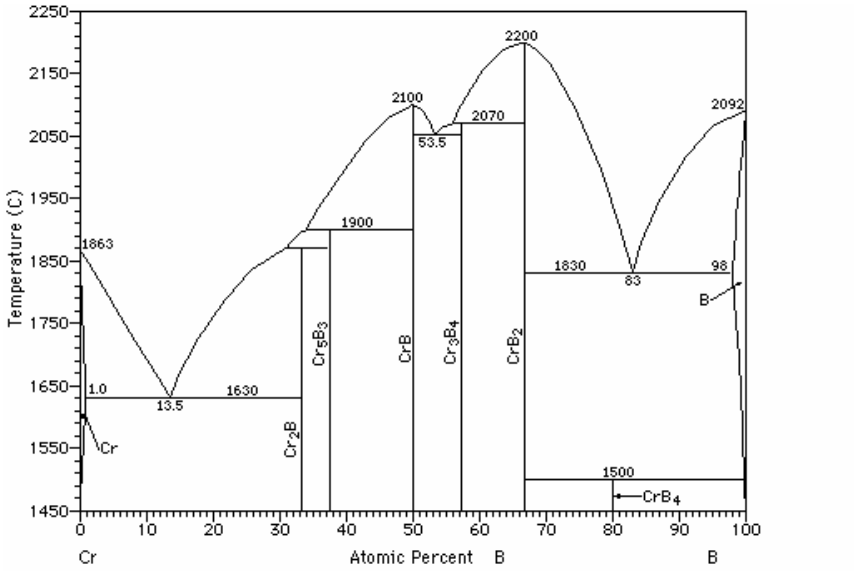
Temperature (C)
Atomic Percent B
Cr
B
2250
2150
2050
1950
1850
1750
1650
1550
1450
0
10
20
30
40
50
60
70
80
90
100
2200
2100
2092
2070
53.5
1900
1863
1830
83
98
1.0
1630
13.5
1500
Cr
Cr2B
Cr5B3
CrB
Cr3B4
CrB2
CrB4

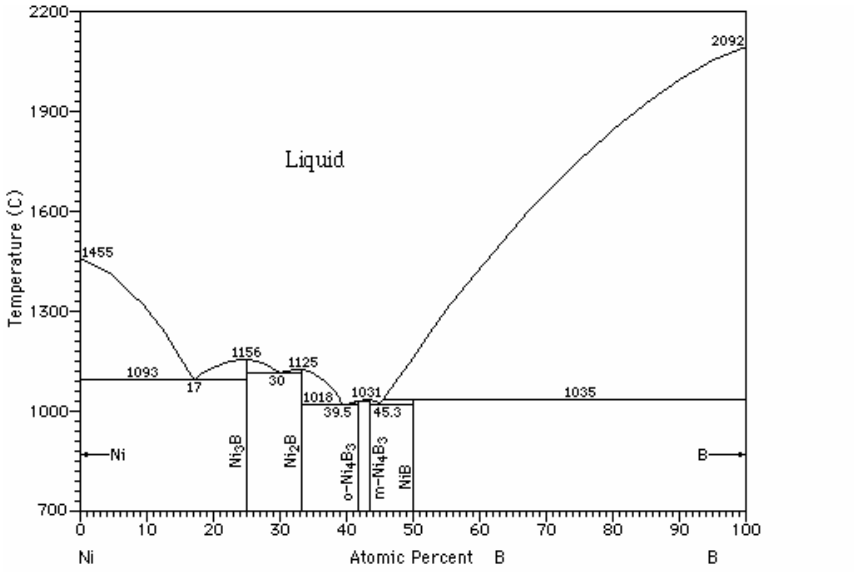
Temperature (C)
Atomic Percent B
Ni
B
2200
1900
1600
1300
1000
700
0
10
20
30
40
50
60
70
80
90
100
Liquid
2092
1455
1156
1125
1093
17
30
1018
1031
1035
39.5
45.3
Ni3B
Ni2B
o-Ni4B3
m-Ni4B3
NiB

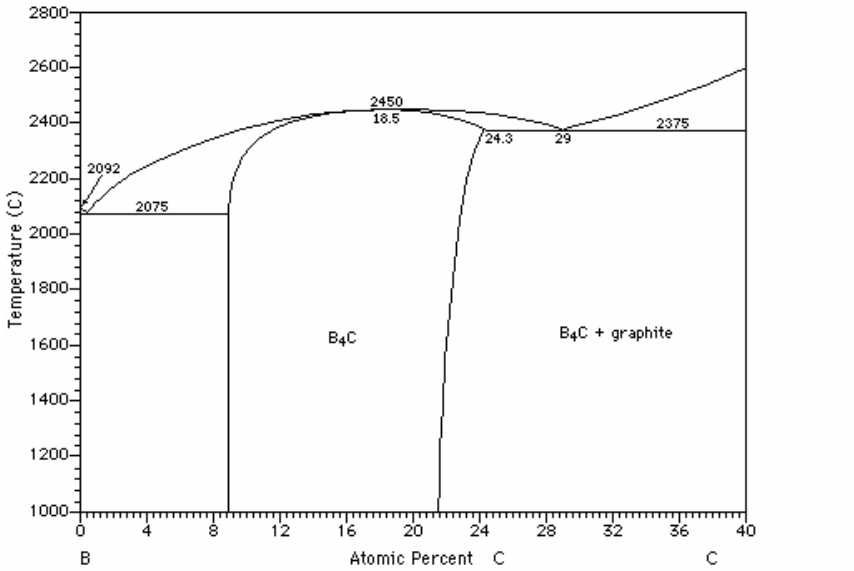
Temperature (C)
Atomic Percent C
B
C
2800
2600
2400
2200
2000
1800
1600
1400
1200
1000
0
4
8
12
16
20
24
28
32
36
40
2450
18.5
24.3
29
2375
2092
2075
B4C
B4C + graphite

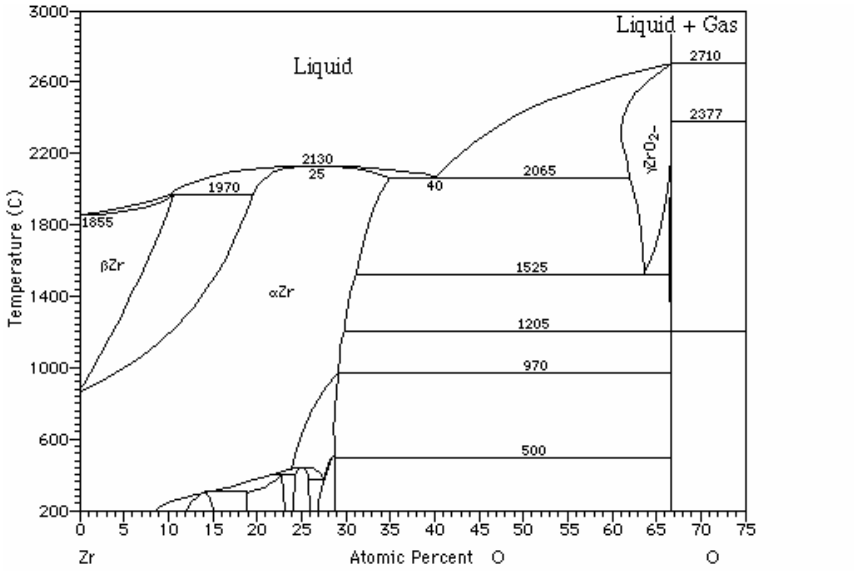
Liquid + Gas
Liquid
2710
2377
2130
25
40
2065
1970
1855
βZr
αZr
γZrO2-
1525
1205
970
500
Temperature (C)
Zr
Atomic Percent O
O

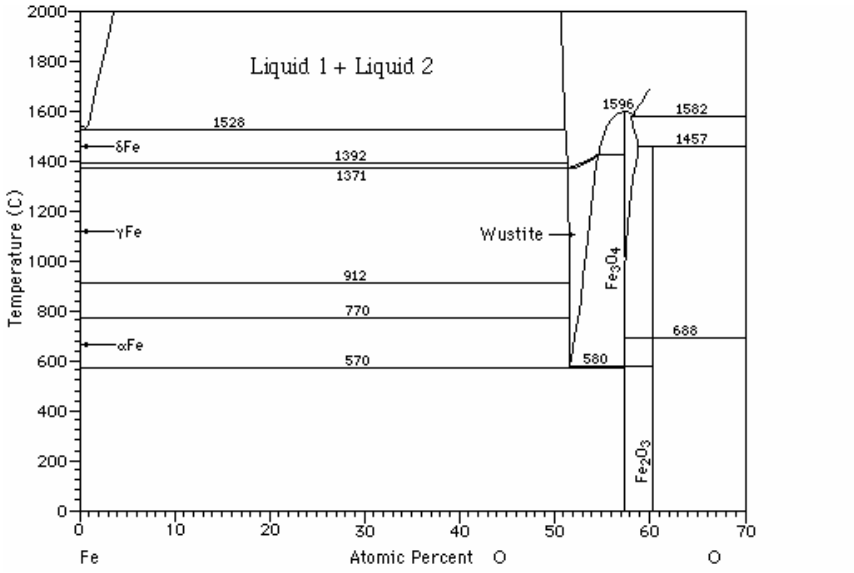
Liquid 1 + Liquid 2
1596
1582
1528
1457
δFe
1392
1371
γFe
Wustite
Fe3O4
912
770
688
αFe
570
580
Fe2O3
Temperature (C)
Fe
Atomic Percent O
O

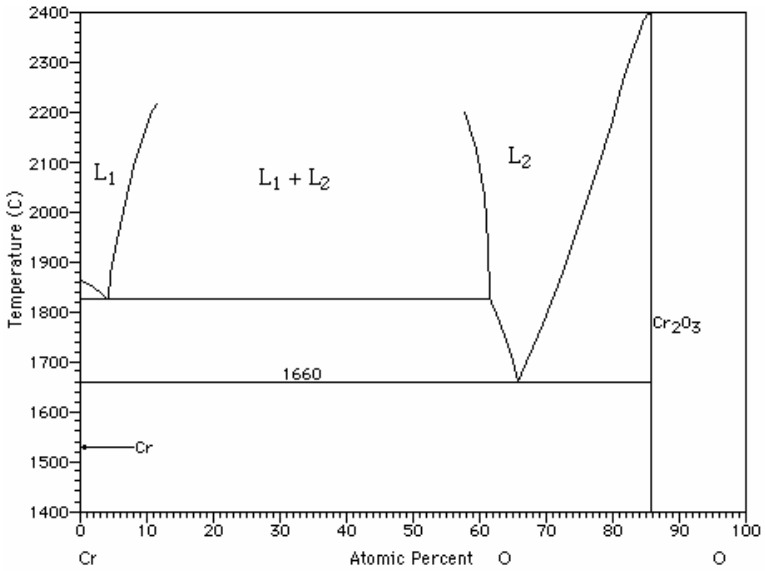
L1
L1 + L2
L2
Cr2O3
1660
Cr
Temperature (C)
Cr
Atomic Percent O
O

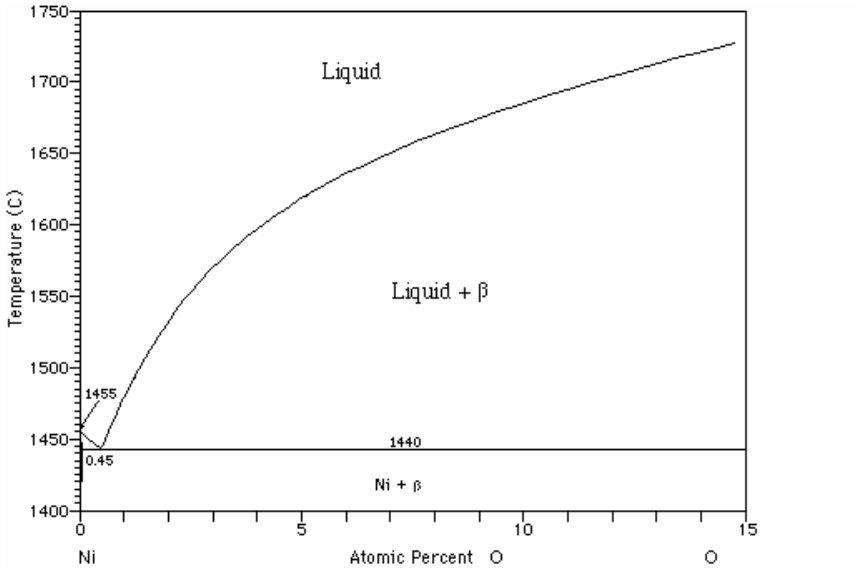
Liquid
Liquid + β
Ni + β
1455
1440
0.45
Temperature (C)
Atomic Percent O
Ni
O

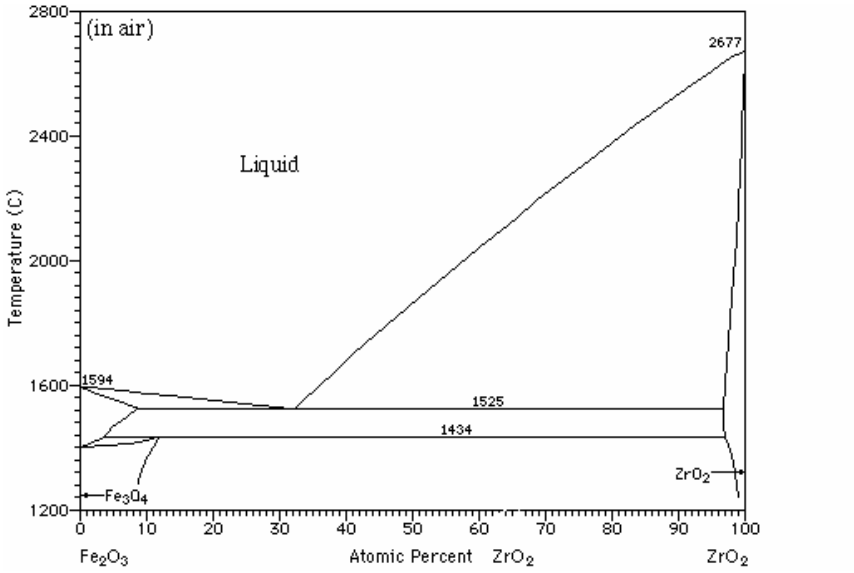
(in air)
Liquid
2677
1594
1525
1434
Fe3O4
ZrO2
Temperature (C)
Atomic Percent ZrO2
Fe2O3
ZrO2

A13 Test protocols

On the following pages the test conduct and main results obtained by mass spectrometer of all tests performed are compiled in chronological order.

For each experiment one diagram (the upper one) shows temperatures and gas input. Mostly, the steam rate measured by MS is shown additionally for comparison in this diagram.

The lower diagram presents the results of the MS measurements for H_2, CO, CO_2 and CH_4. Additionally, for most of the tests a small diagram shows the ion currents measured at masses 18 and 40, representing the major input gases steam and argon. From that diagram one can see, if the test run well. A simultaneous decrease of the ion currents of steam and argon is an indication for a (partial) blockade of the MS capillary which was sometimes seen during tests at higher temperatures. For such tests the data have to be considered carefully and only taken "half-quantitatively".

Test Box10621:

Transient oxidation of a B_4C CR segment in Ar/steam
800 ---> 1500 °C, 1 pellet size, ZrO_2 caps

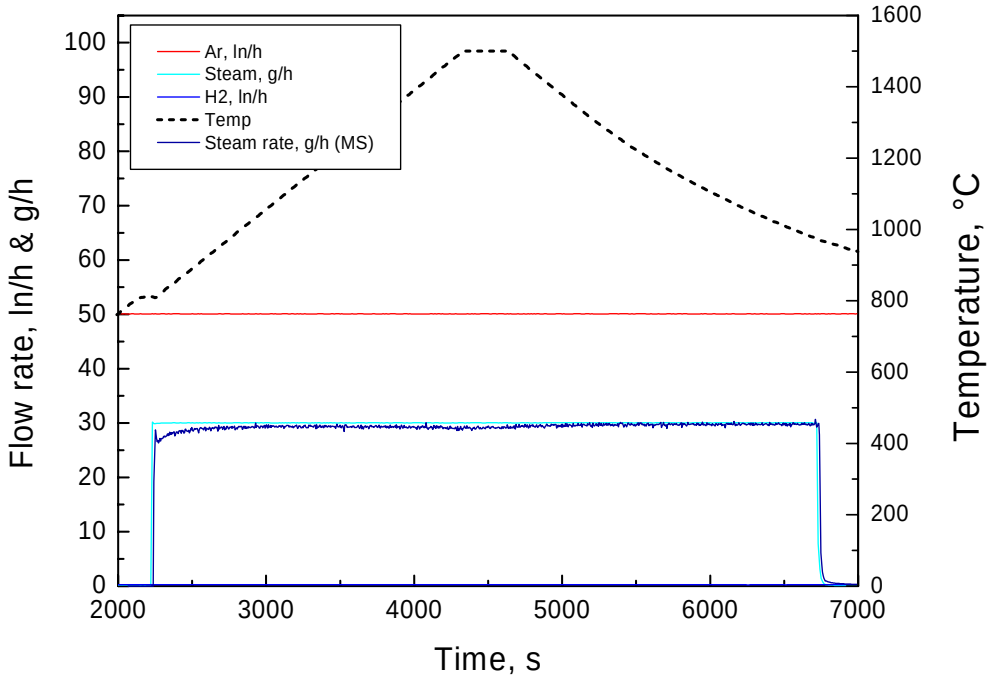

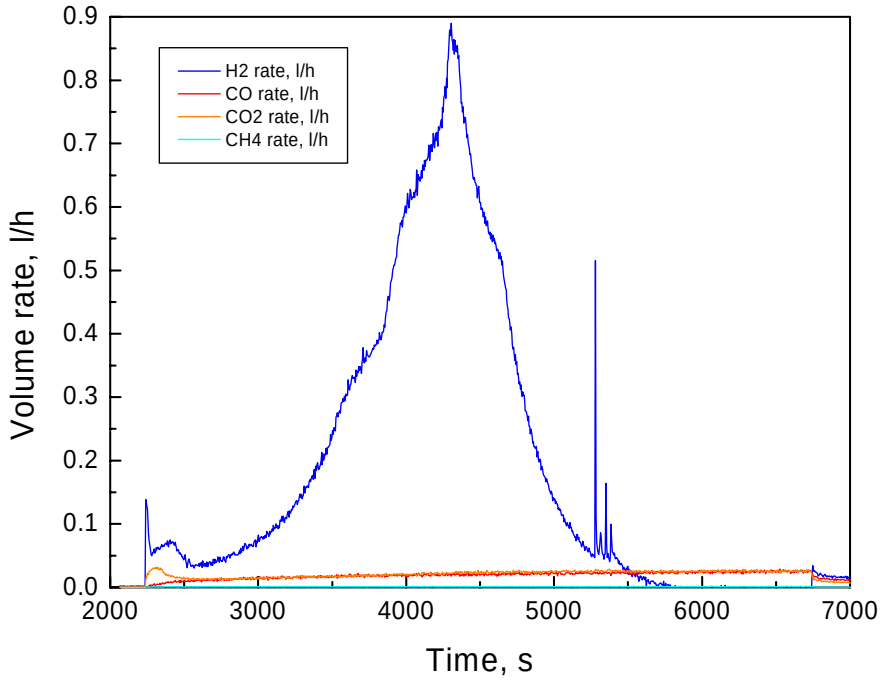

Test Box10625:

Transient oxidation of a B_4C CR segment in pure Ar
800 ---> 1500 °C, 1 pellet size, ZrO_2 caps

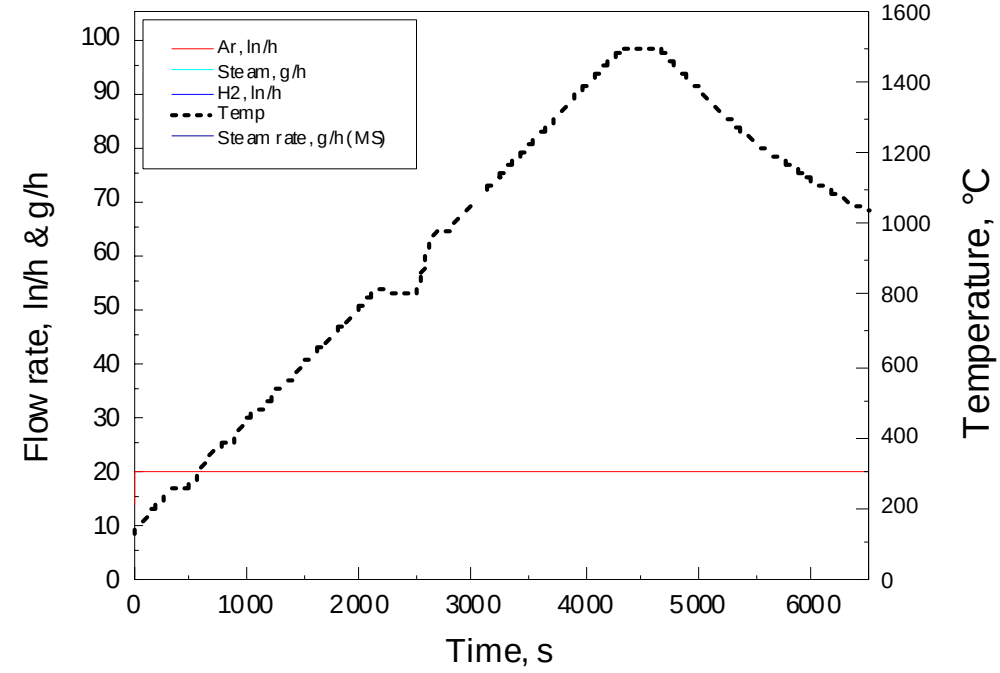

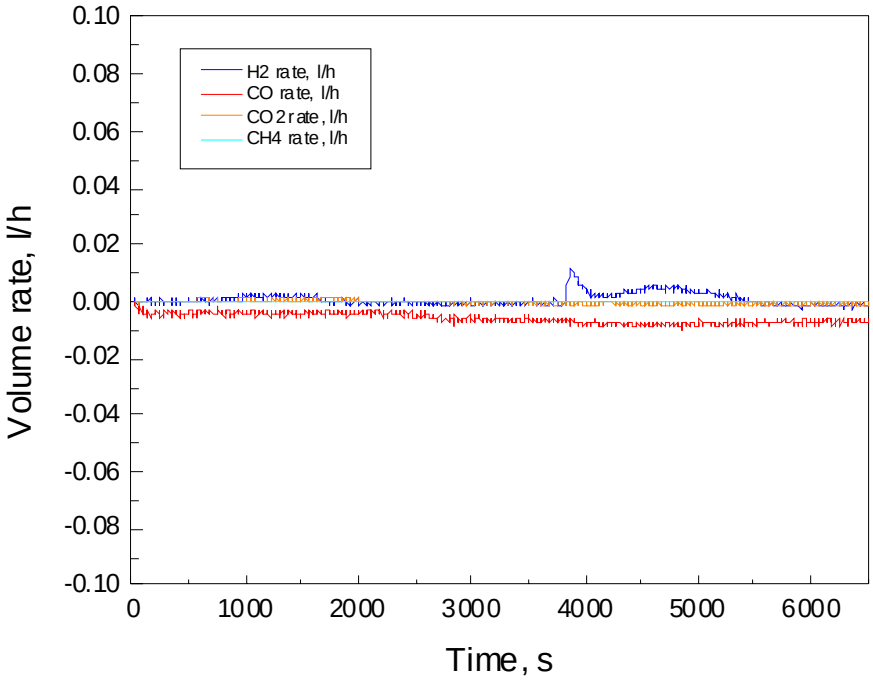

Test Box10627:

Transient oxidation of a B_4C CR segment in Ar/steam
800 ---> 1500 °C, 1 pellet size, ZrO_2 caps

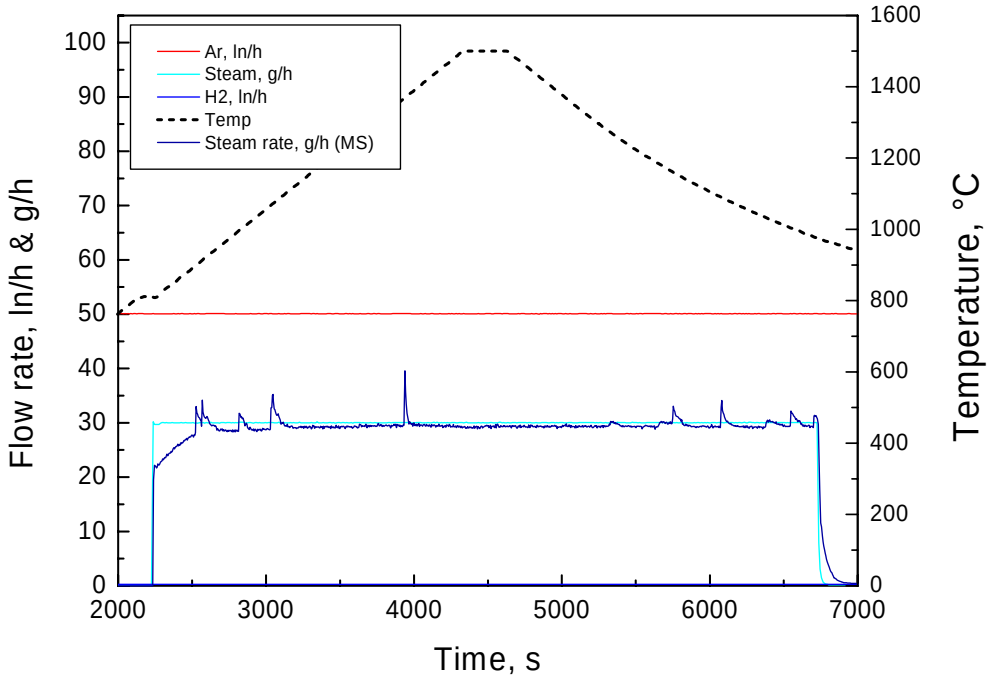

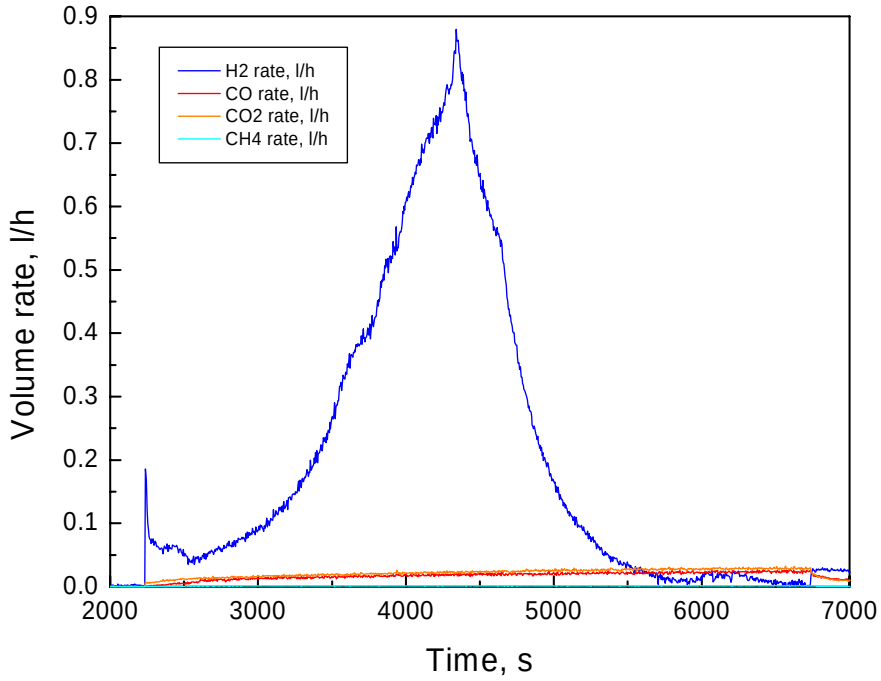

Test CR11011a:
Oxidation of a B_4C CR segment in pure Ar
1000°C - failure, 0.1 K/s

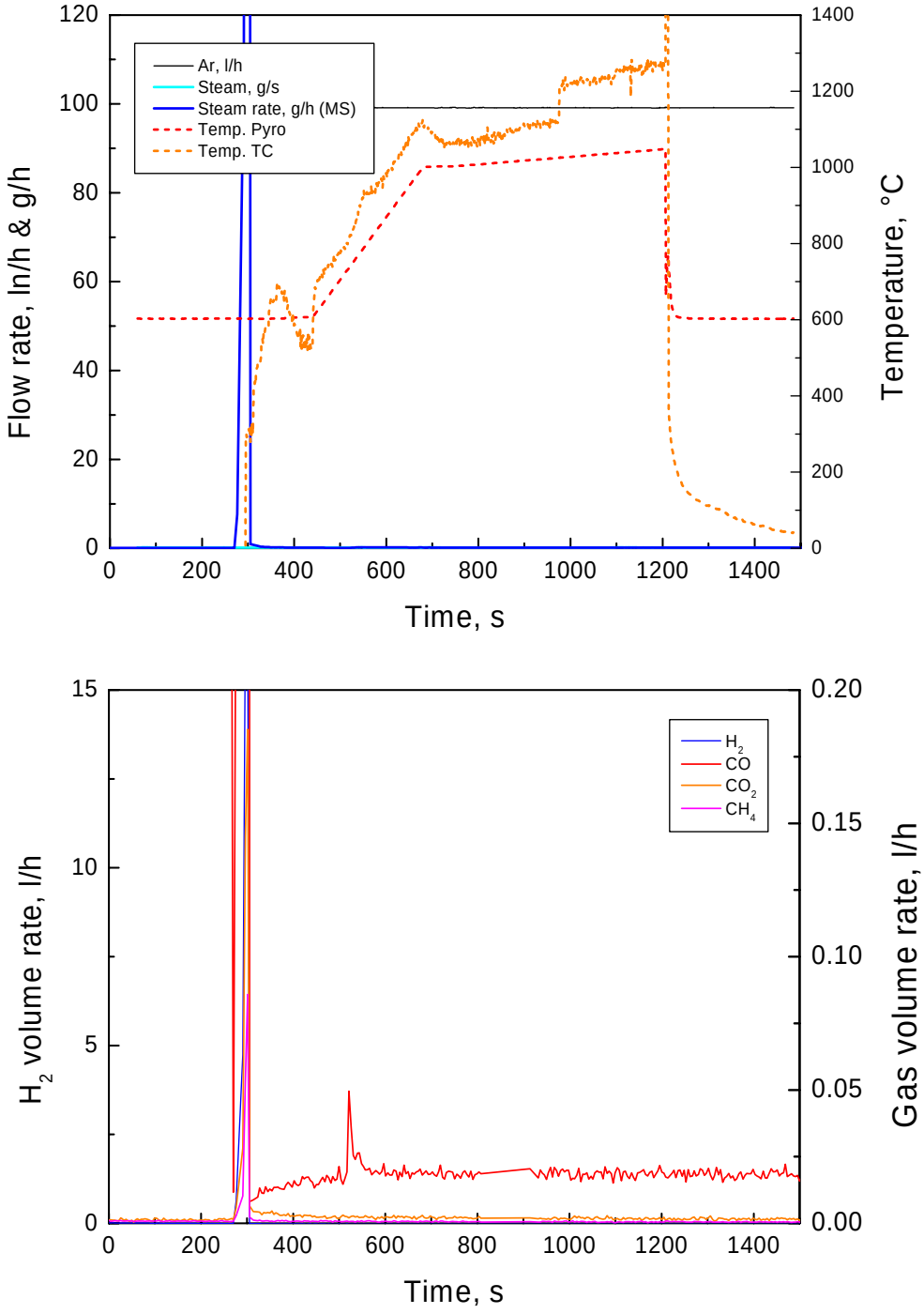

Test CR11011b:
Oxidation of a B_4C CR segment in pure Ar
800 °C - failure, 0.1 K/s, 10 µm pre-oxidised

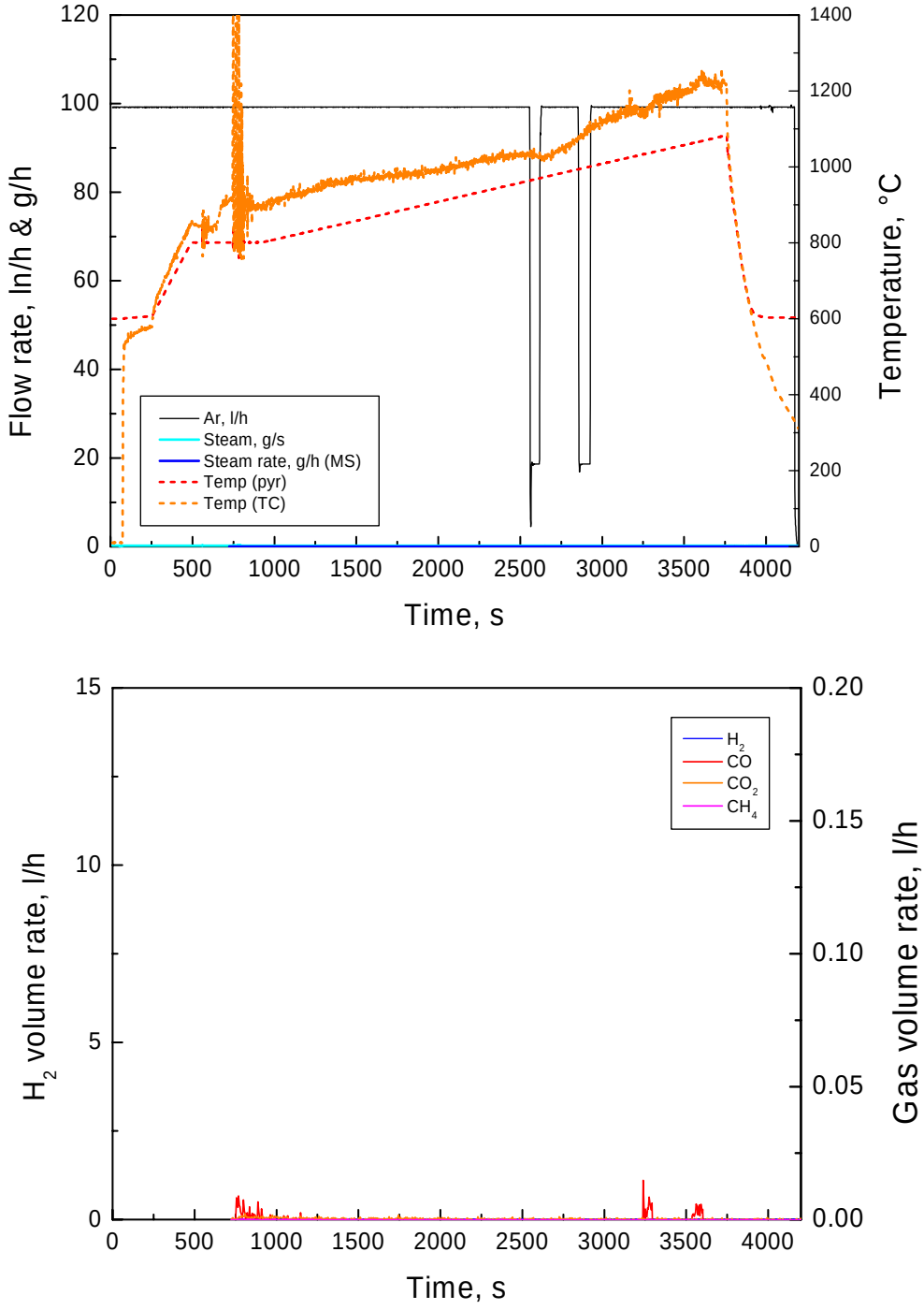

Test CR11016a:
Oxidation of a B_4C CR segment in Ar/steam
600-1600 °C, 1 K/s

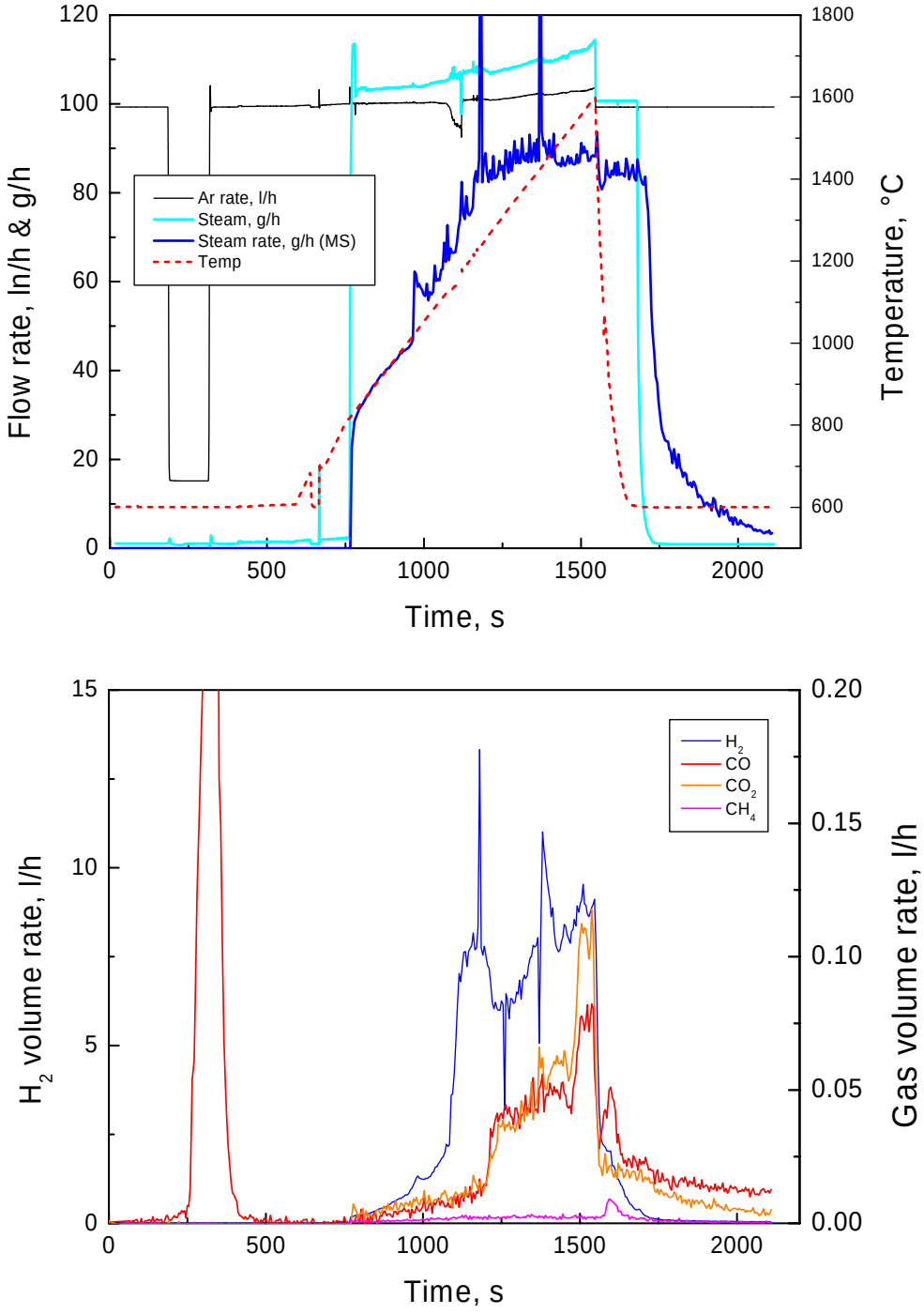

Test Box11024:
Oxidation of a B_4C CR segment in Ar/steam at 800 °C

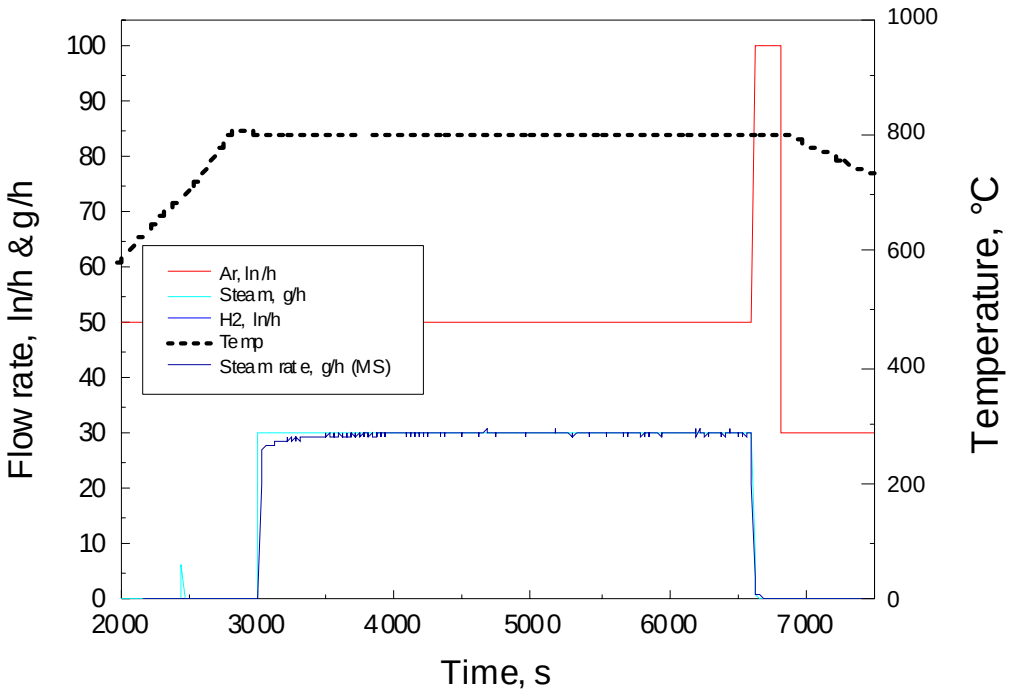

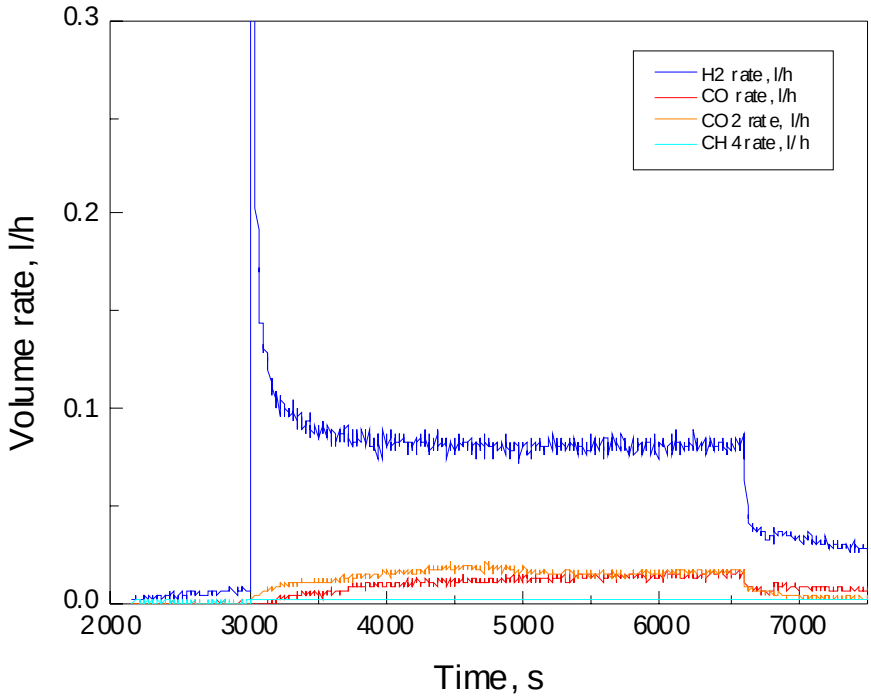

Test Box11105:
Oxidation of a B_4C CR segment in Ar/steam at 1000 °C

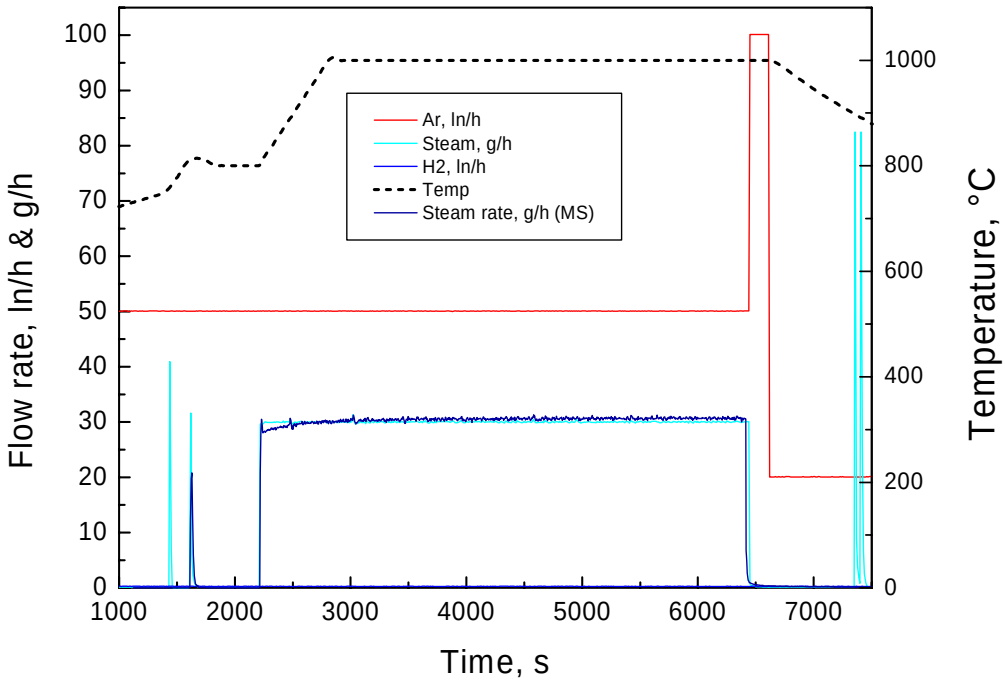

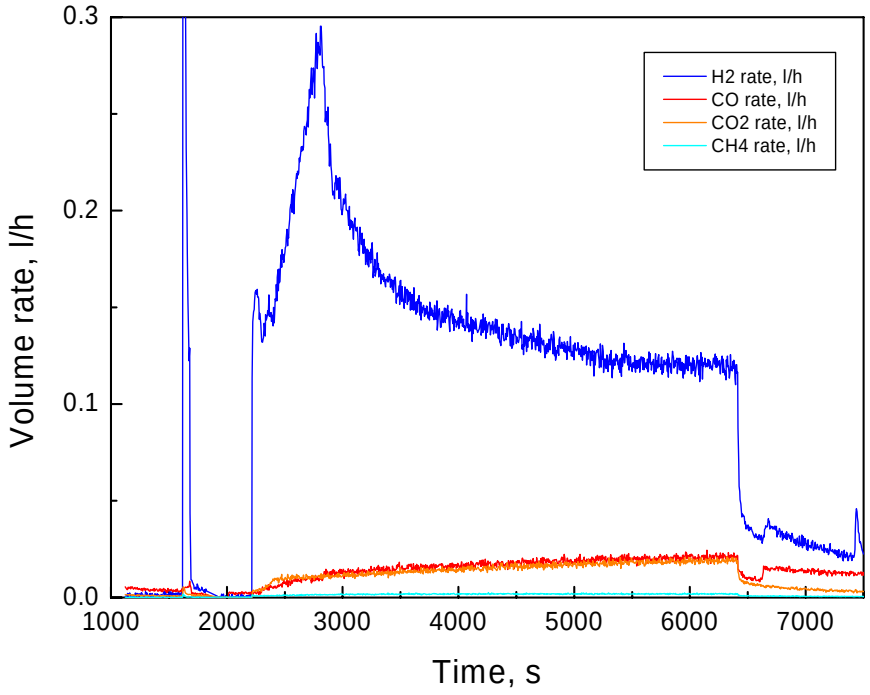

Test Box11107:
Oxidation of a B_4C CR segment in Ar/steam at 1200 °C

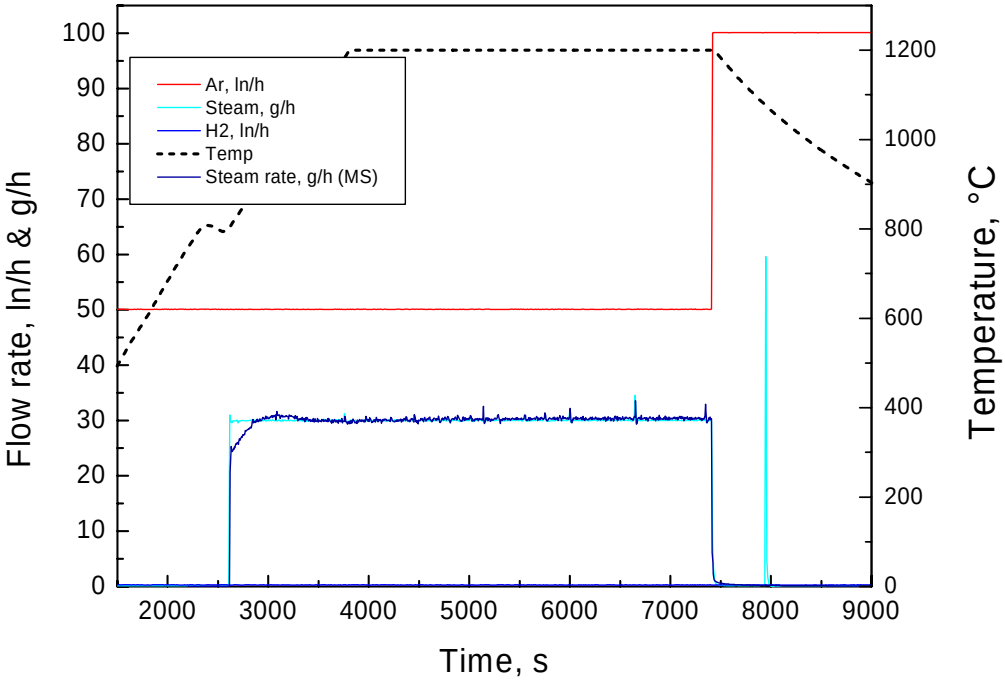

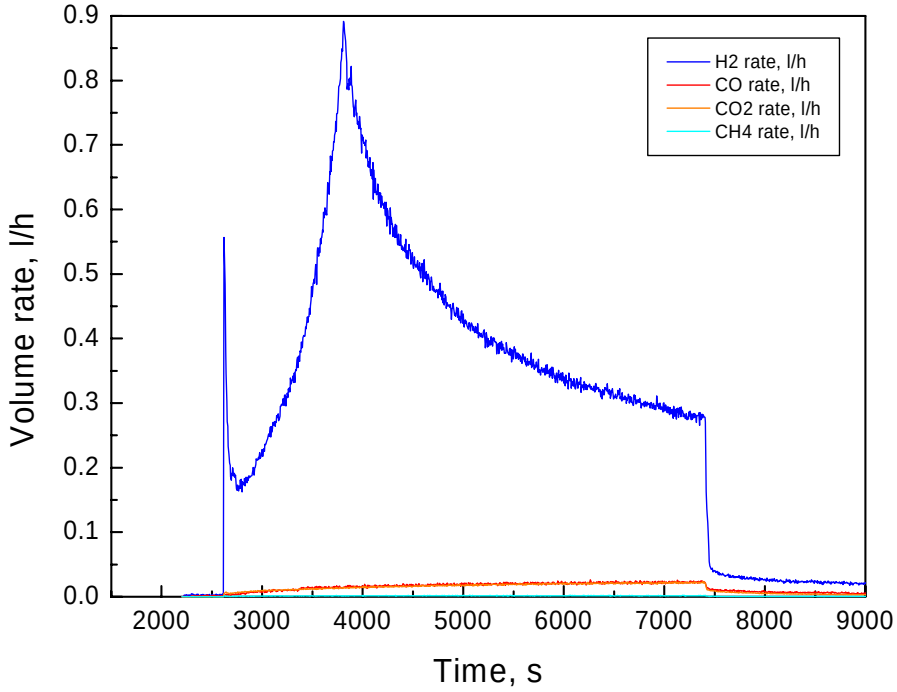

Test Box11108:
Oxidation of a B_4C CR segment in Ar/steam at 1400 °C

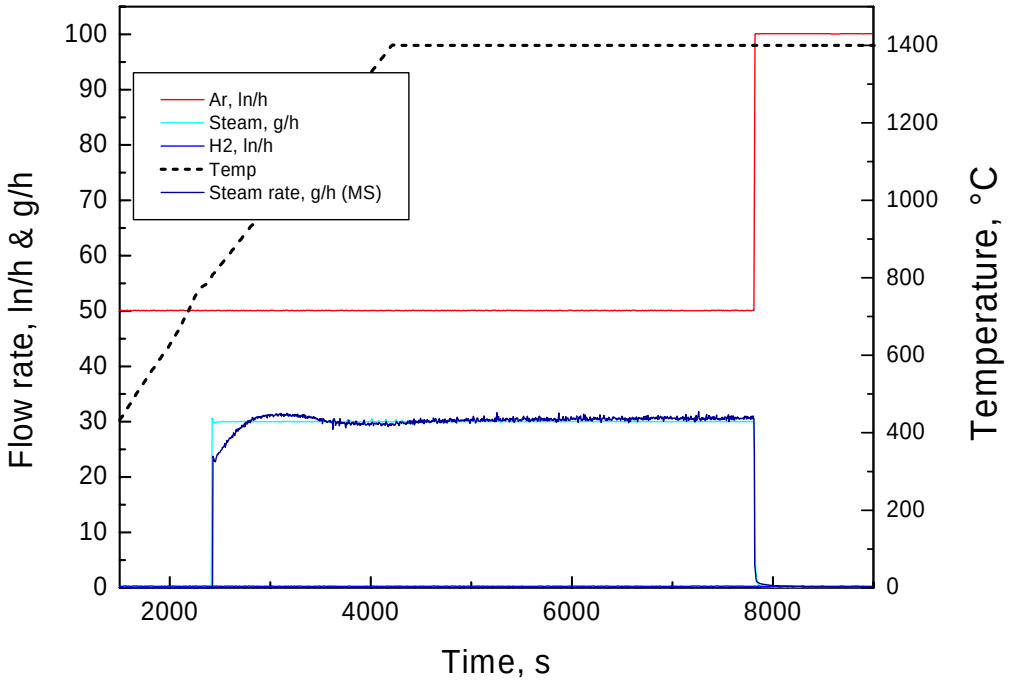

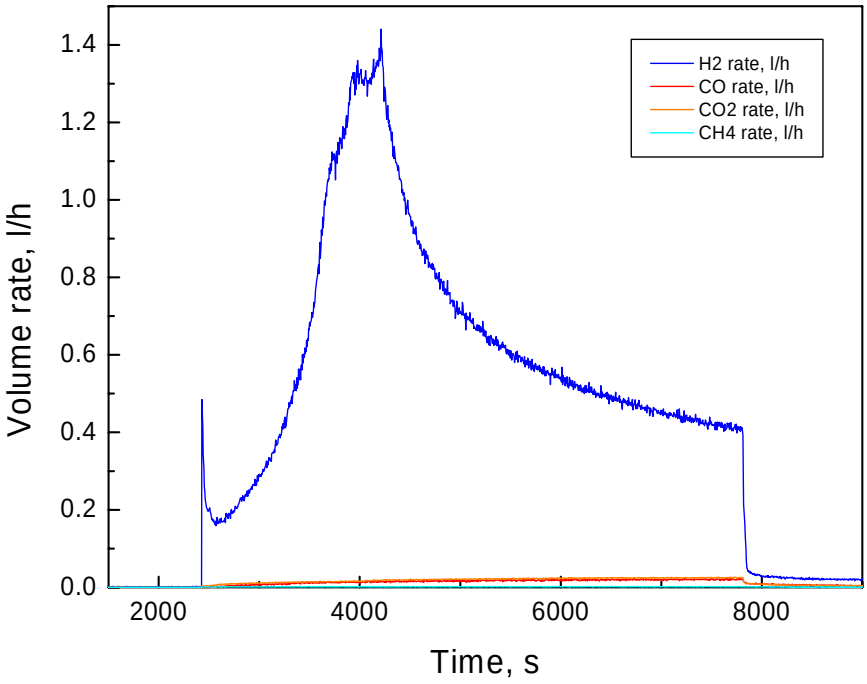

Test Box11109:

Oxidation of a B_4C CR serment in Ar/steam at 1600 °C

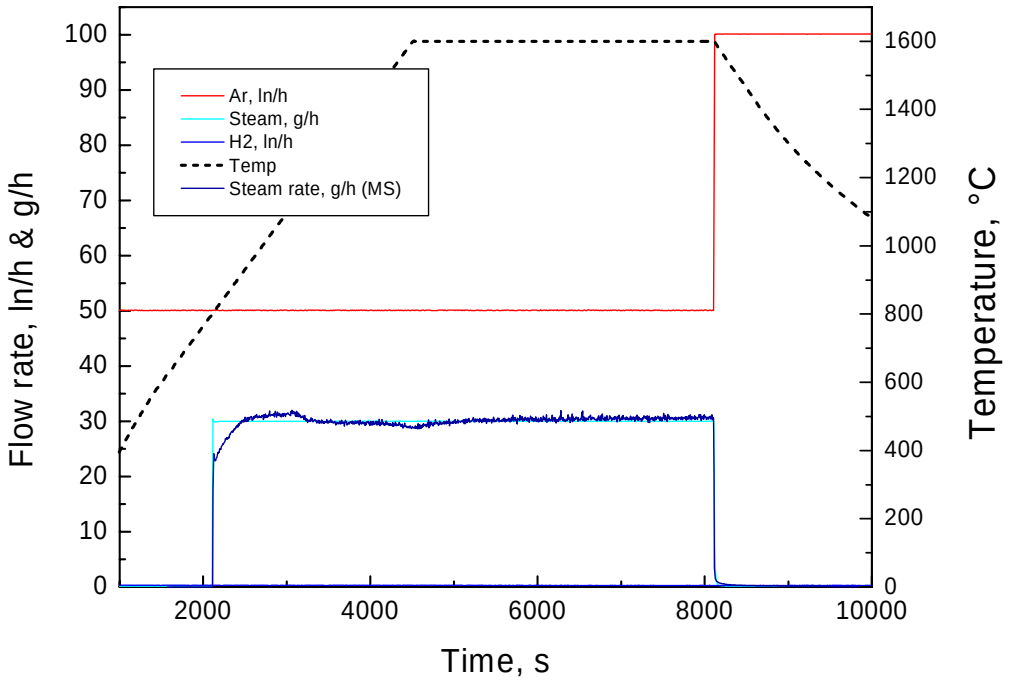

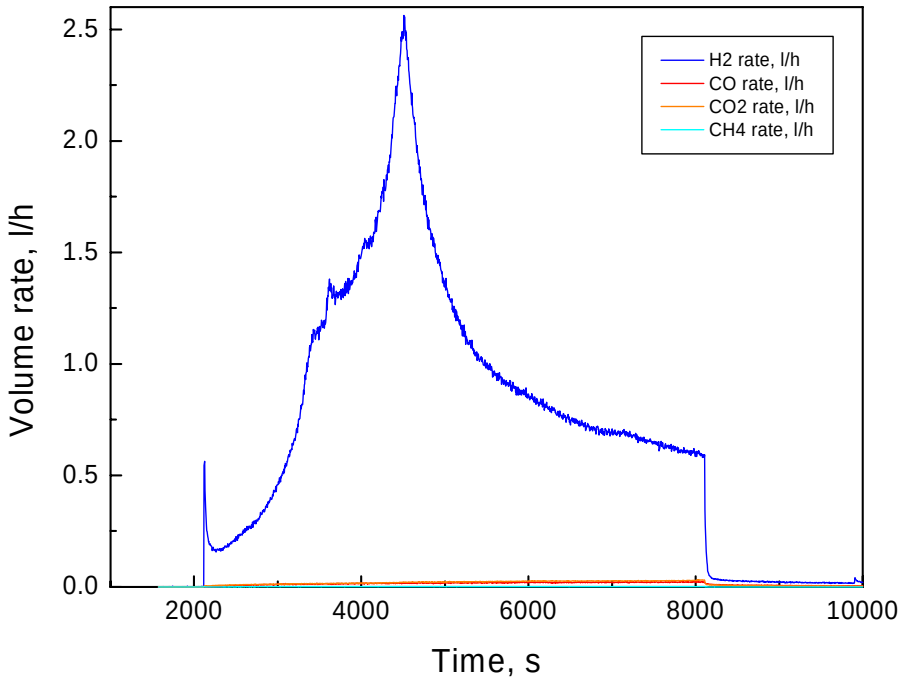

Test Box11121:
Oxidation of a B_4C CR segment in Ar/steam at 1700 °C

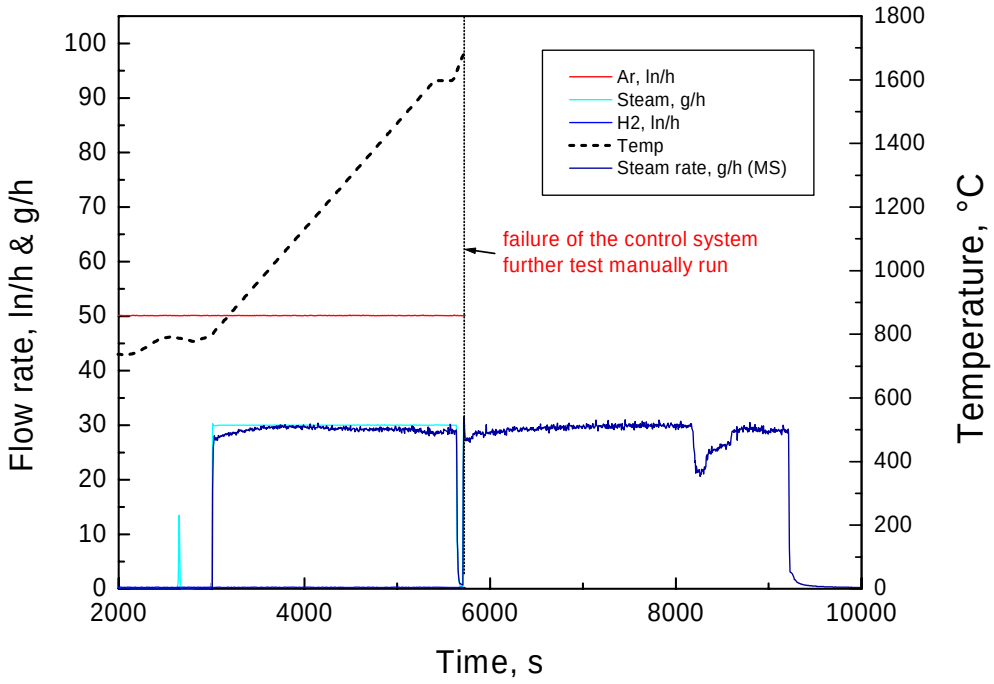

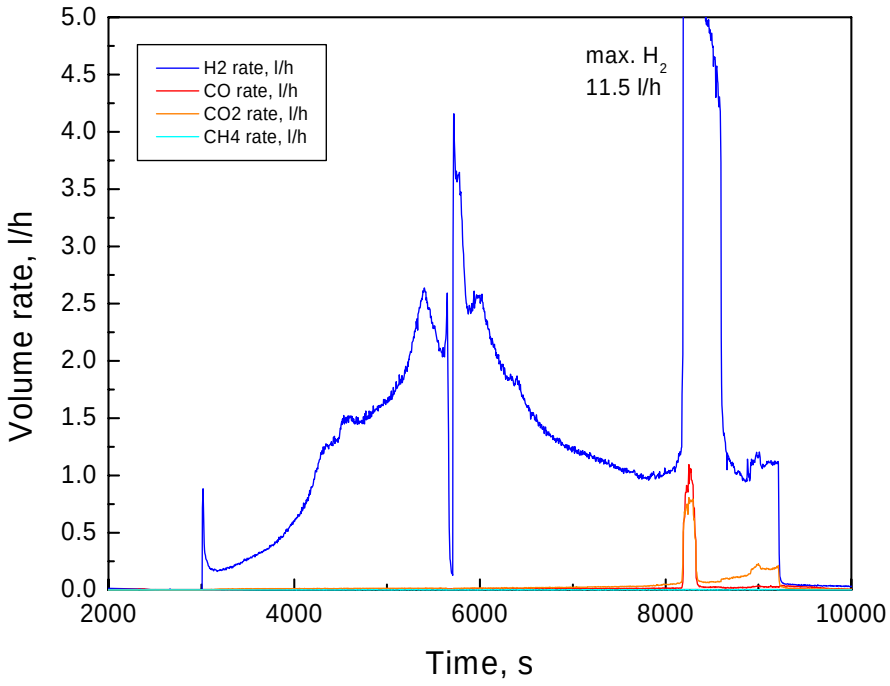

Test Box20528a:
Oxidation of a B_4C CR segment in Ar/steam at 1000 °C

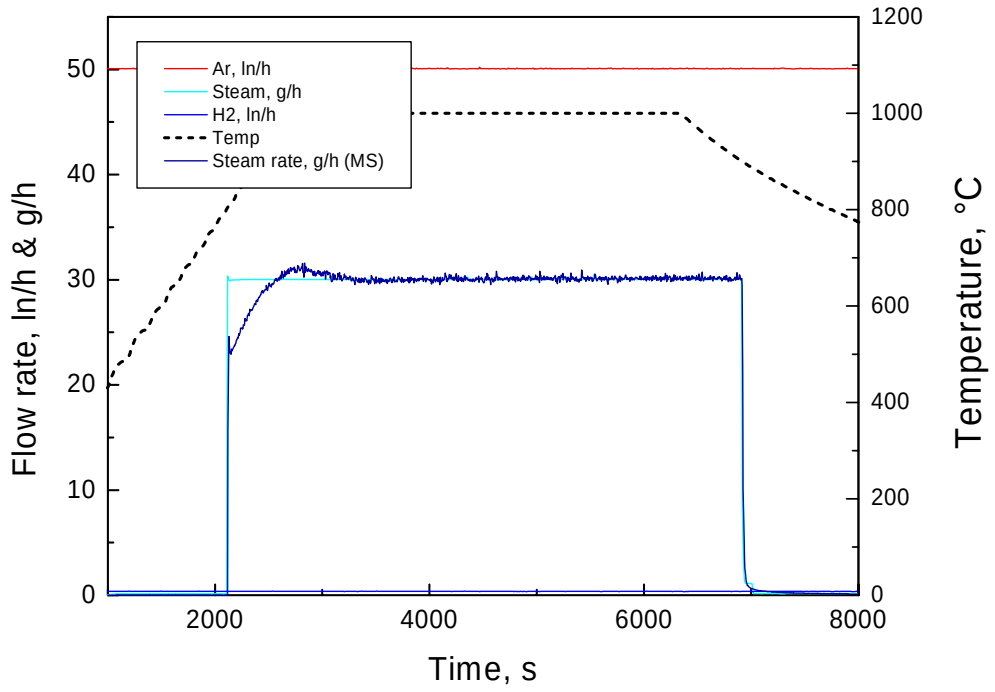

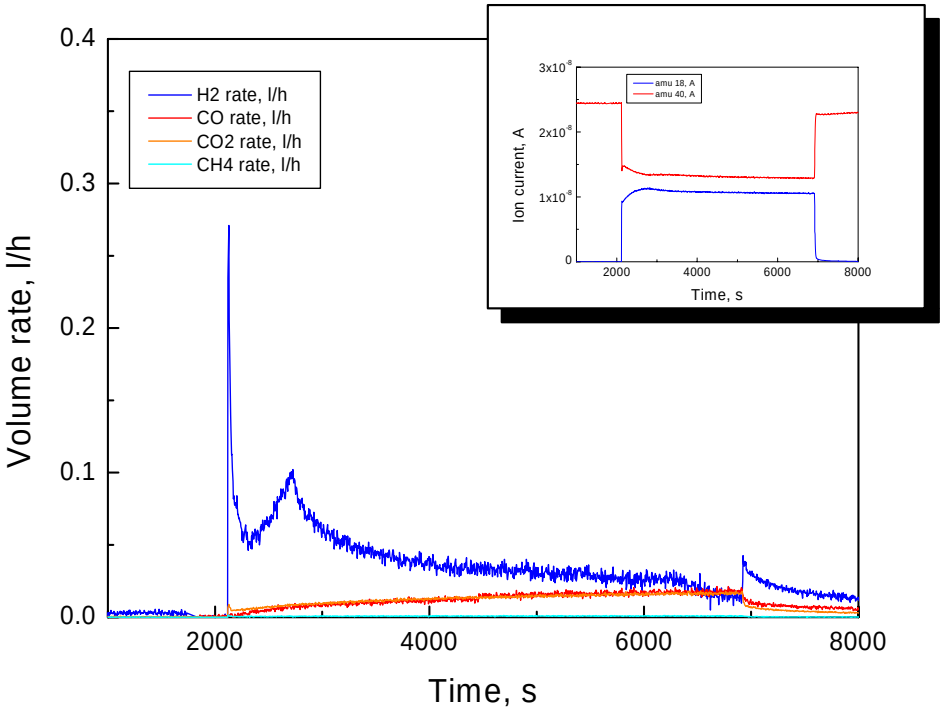

Test Box20528b:
Oxidation of a B_4C CR segment in Ar/steam at 1200 °C

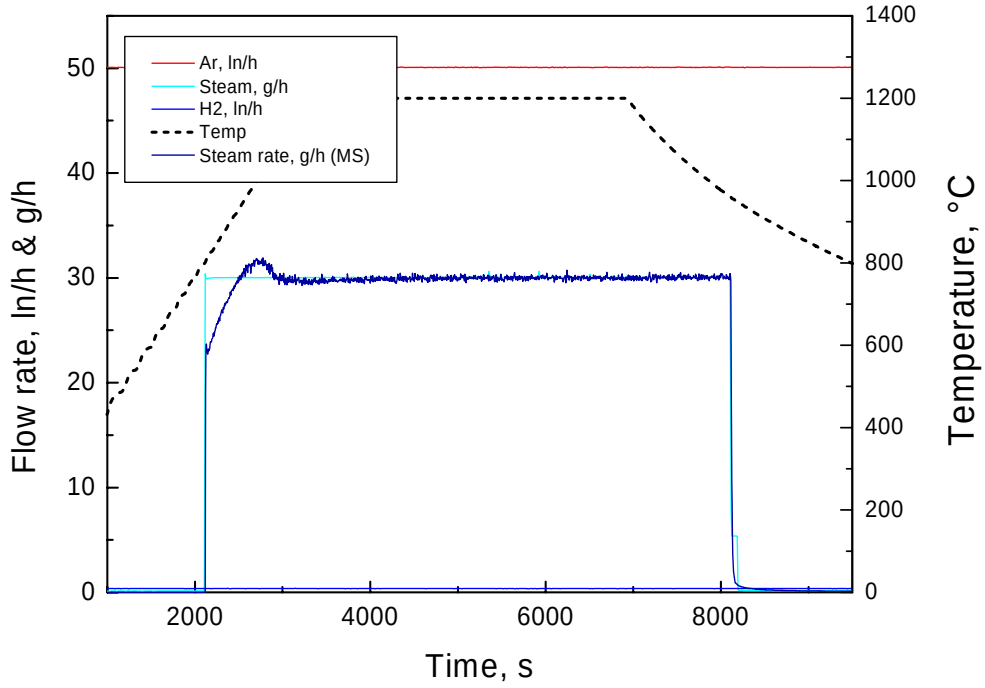

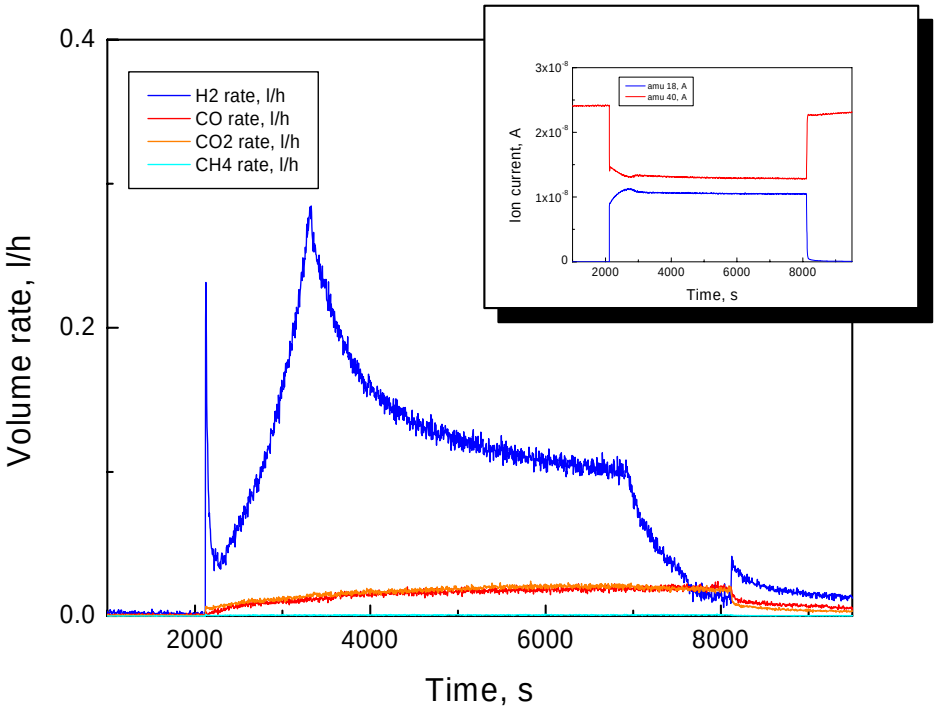

Test Box20529:
Oxidation of a B_4C CR segment in Ar/steam at 1400 °C

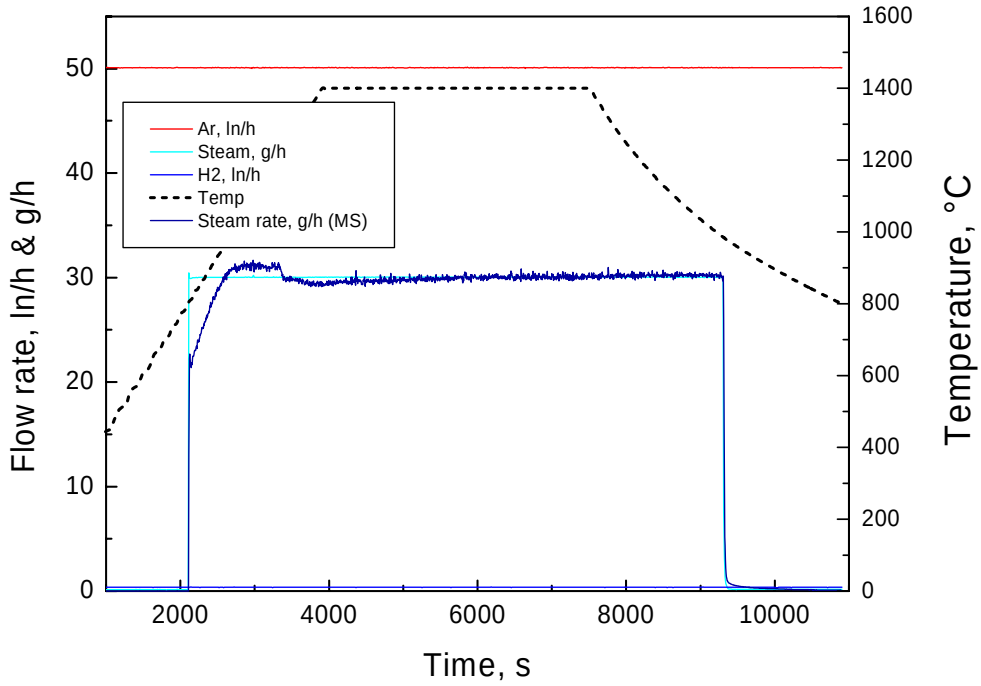

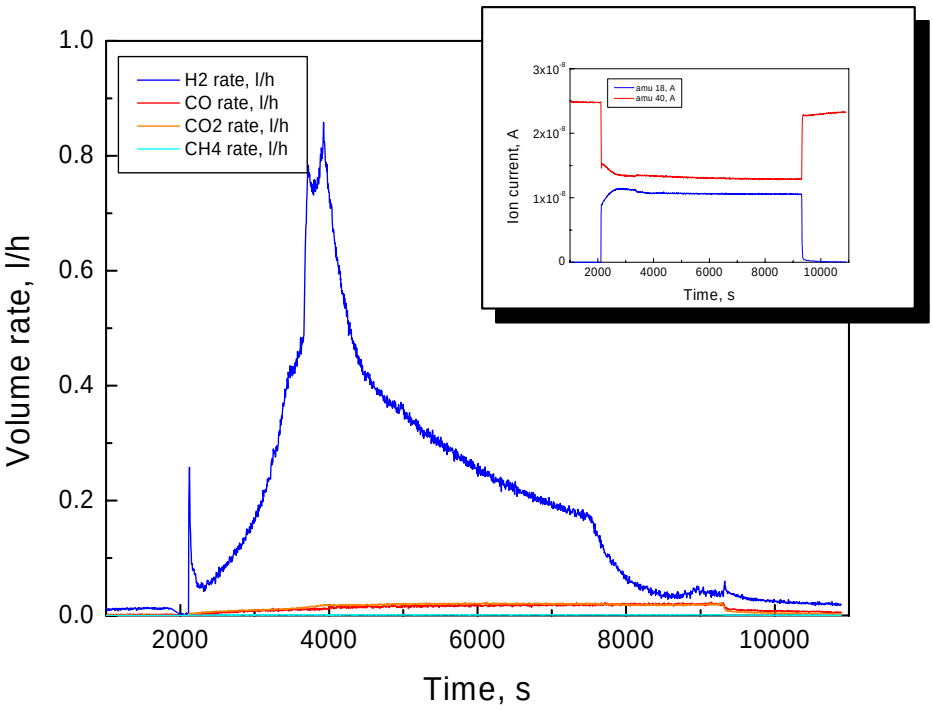

Test Box20603:
Oxidation of a B_4C CR segment in Ar/steam at 1600 °C

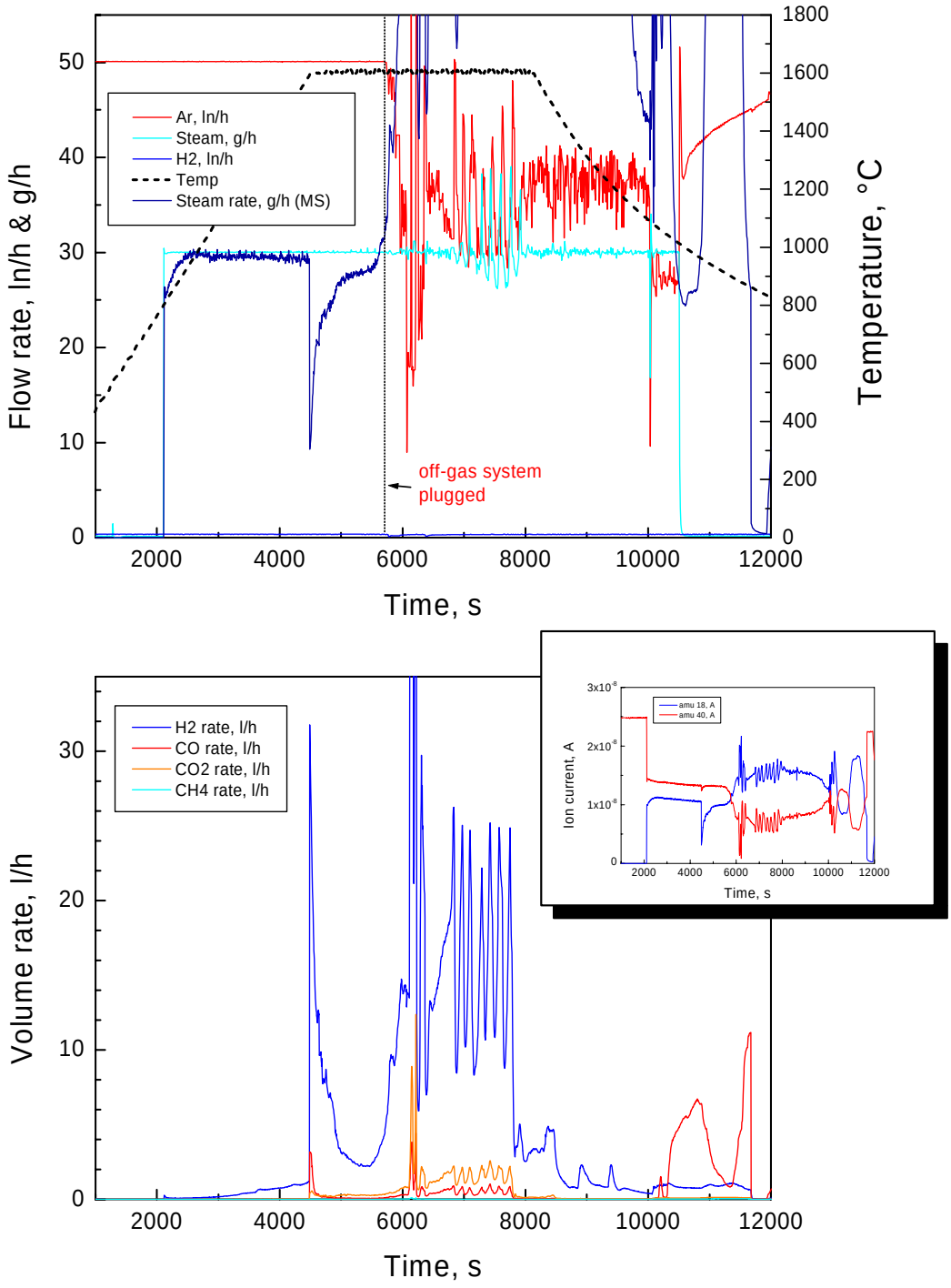

Test Box20605:
Oxidation of a B_4C CR segment in Ar/steam at 1300 °C

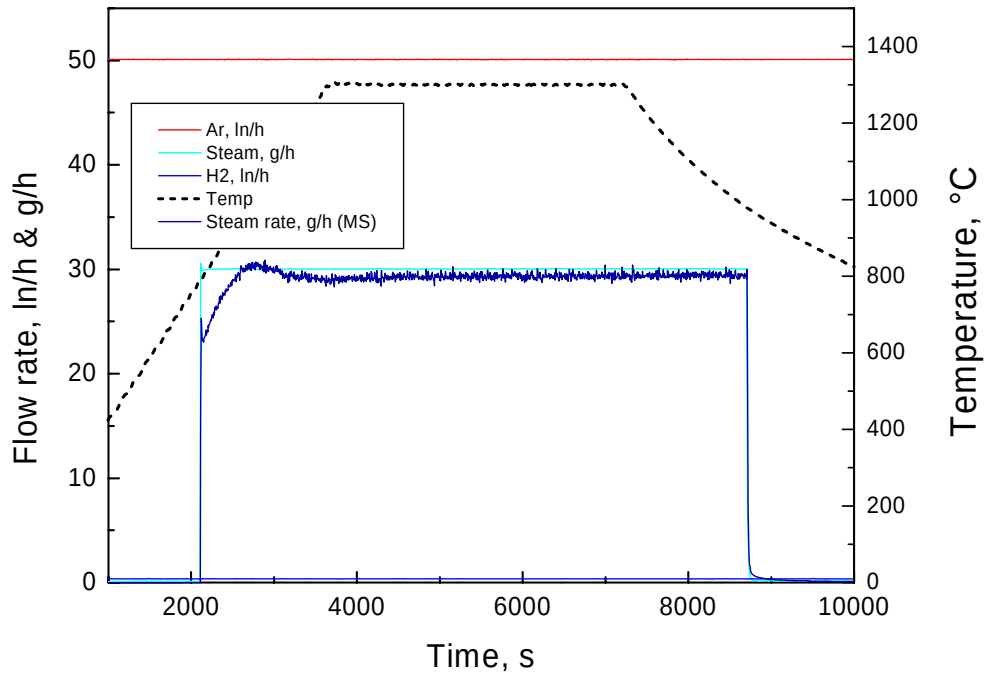

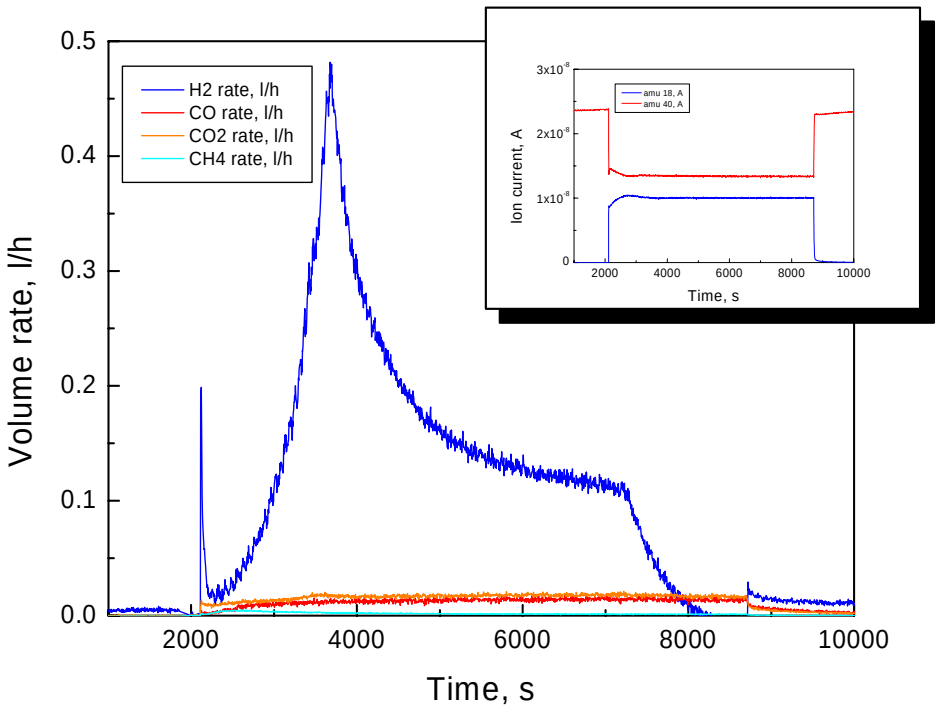

Test Box20606:
Oxidation of a B_4C CR segment in Ar/steam at 1500 °C

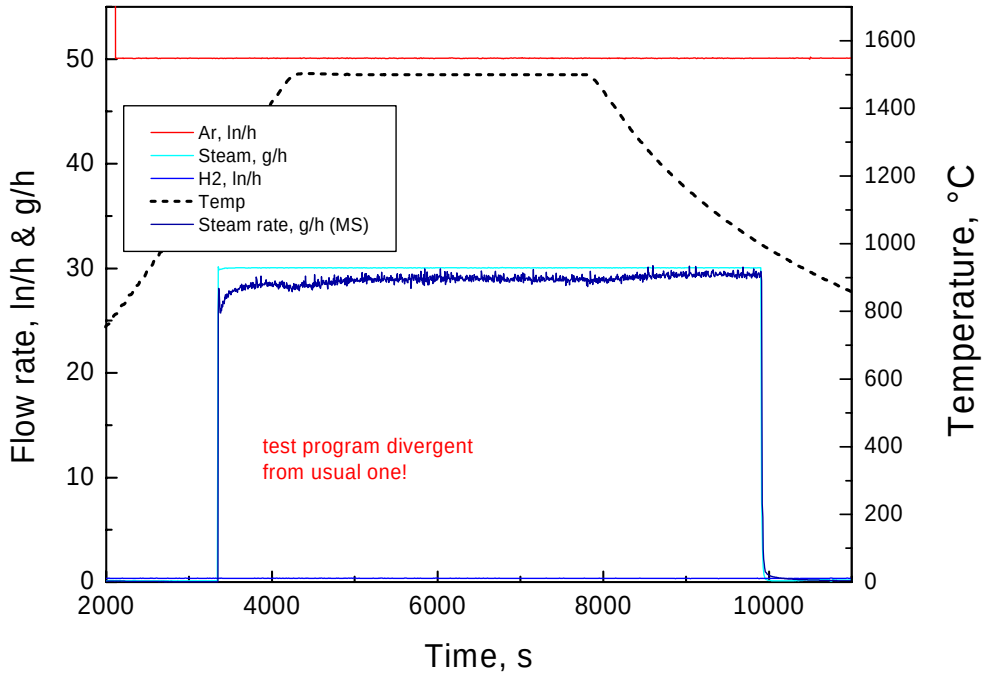

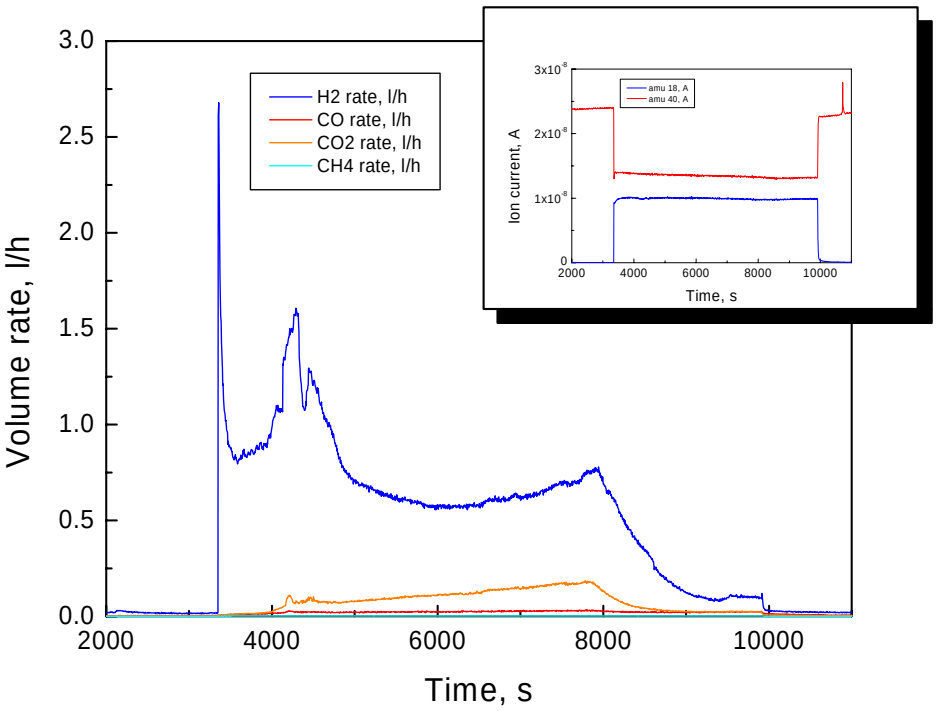

Test Box20610:
Oxidation of a B_4C CR segment in Ar/steam at 1500 °C

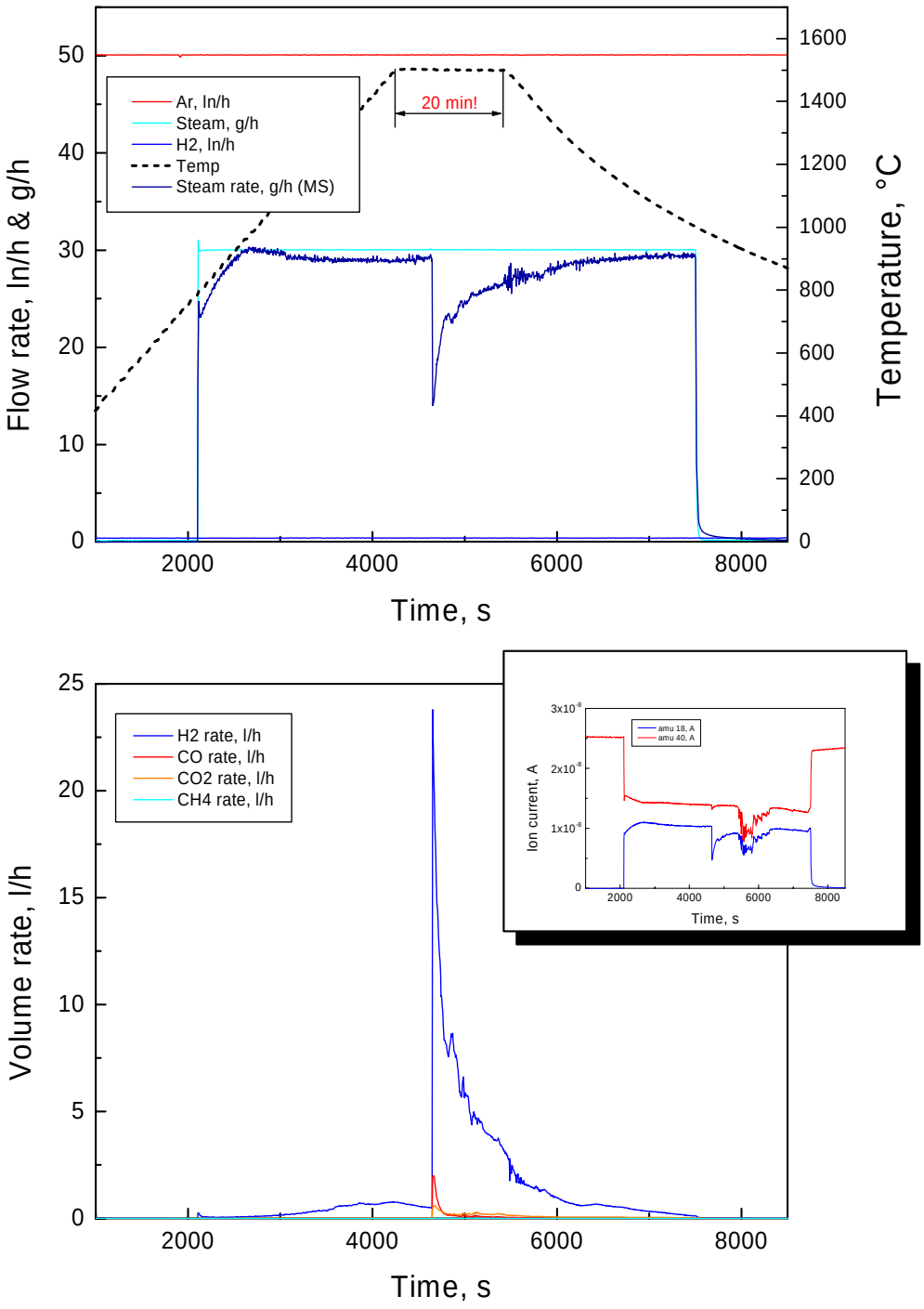

Test CR20820:
Transient oxidation and degradation of a B_4C CR segment in Ar/steam (1 K/s, vacuum specimen, pre-test)

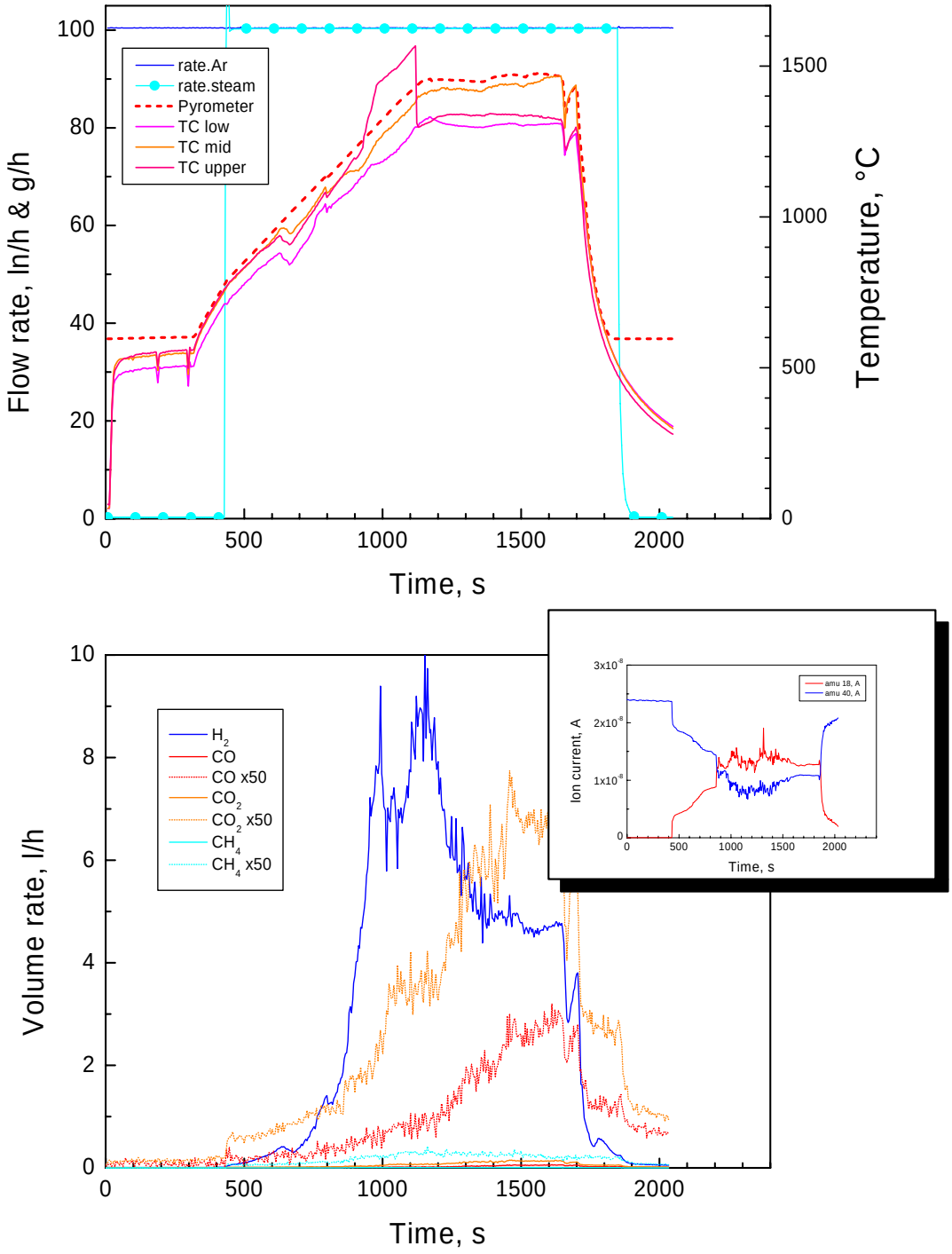

Test CR20822:
Transient oxidation and degradation of a B_4C CR segment in Ar/steam (1 K/s, vacuum specimen)

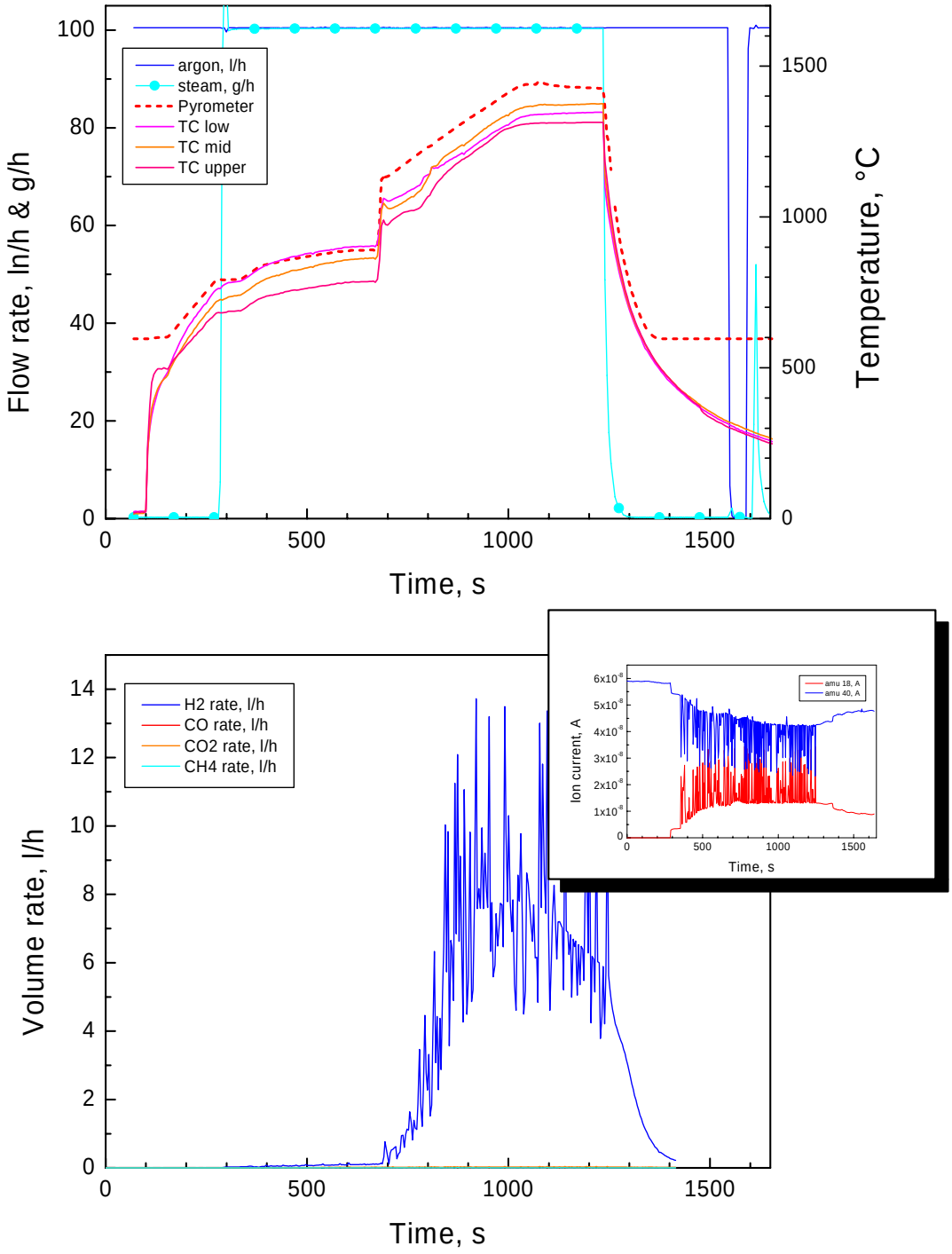

Test CR20826a:
Transient oxidation and degradation of a B_4C CR segment in Ar/steam (1 K/s, He filled specimen)

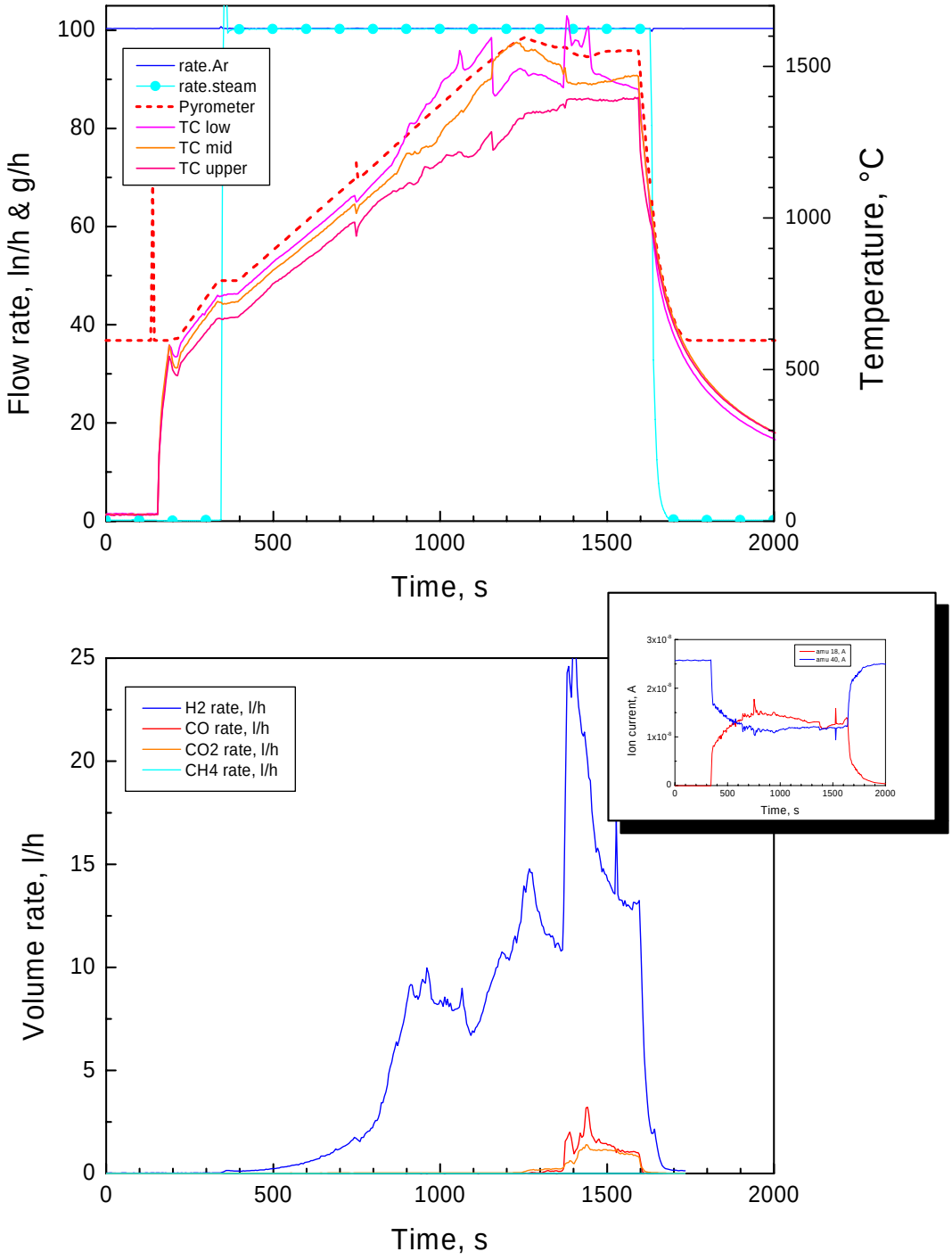

Test CR20826b:
Transient oxidation and degradation of a B_4C CR segment in Ar/steam (3 K/s, vacuum specimen)

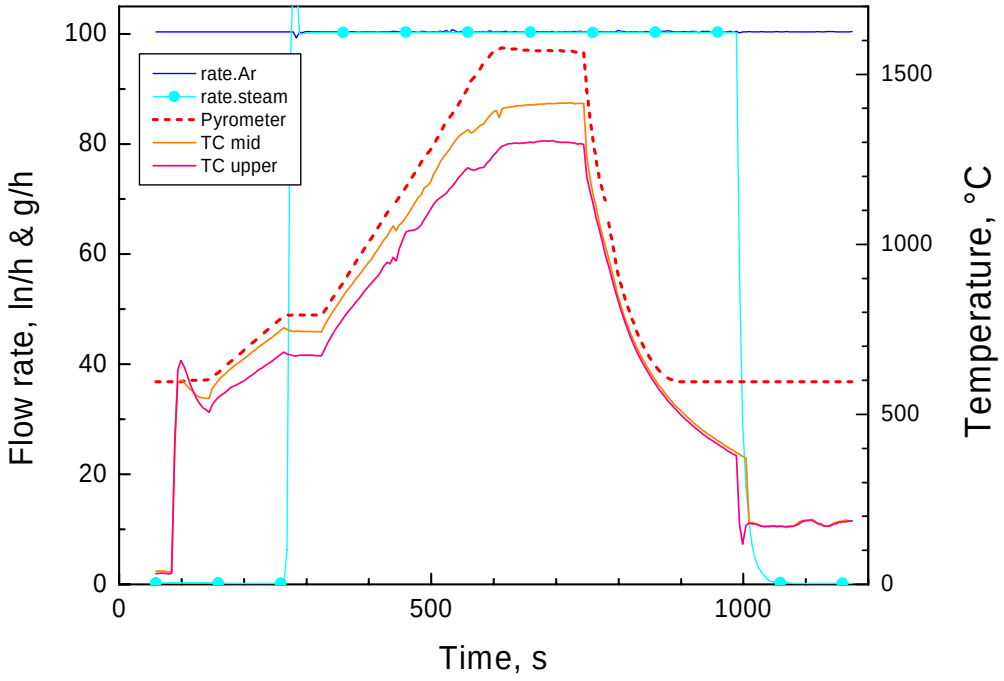

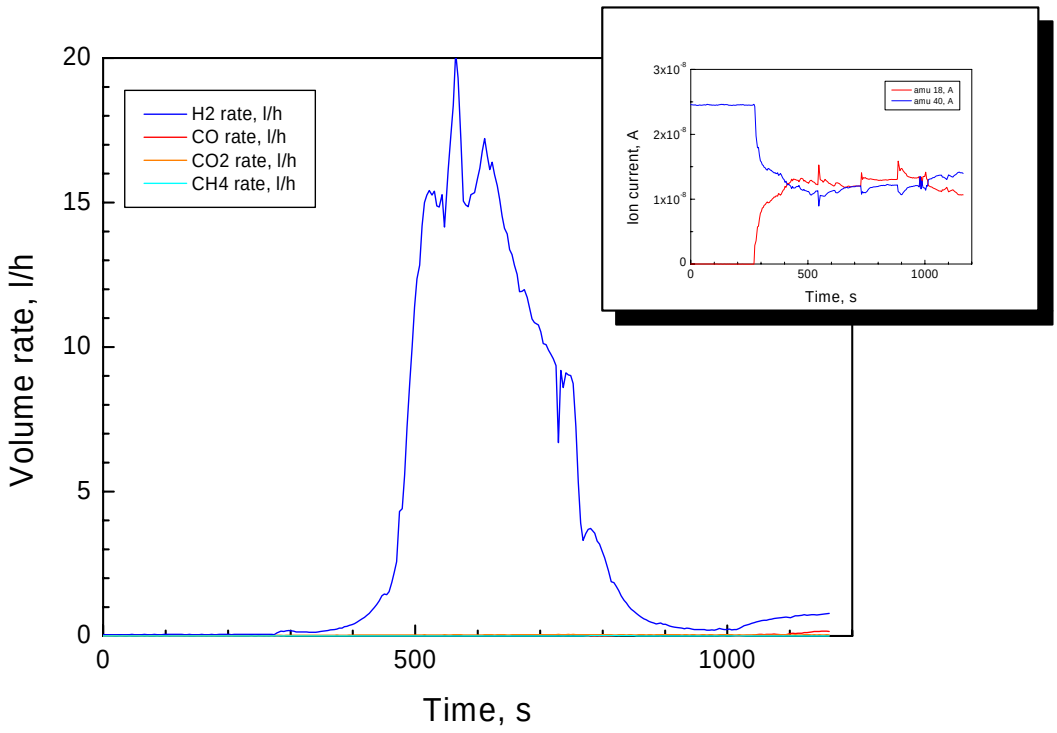

Test CR20827a:
Transient oxidation and degradation of a B_4C CR segment in Ar/steam (0.1 K/s, vacuum specimen)

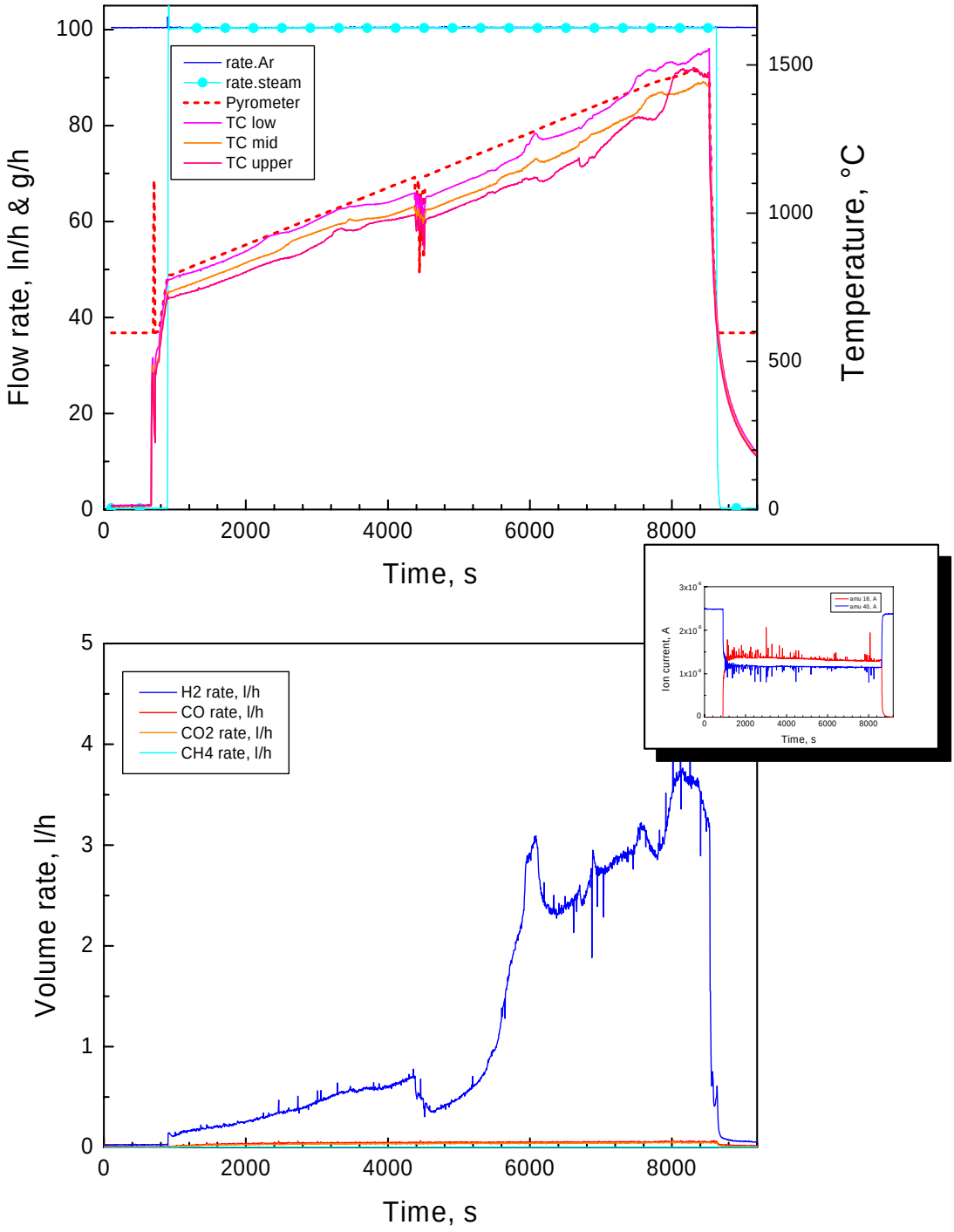

Test CR20827b:
Isothermal oxidation and degradation of a B_4C CR segment in Ar/steam (1265 °C, vacuum specimen)

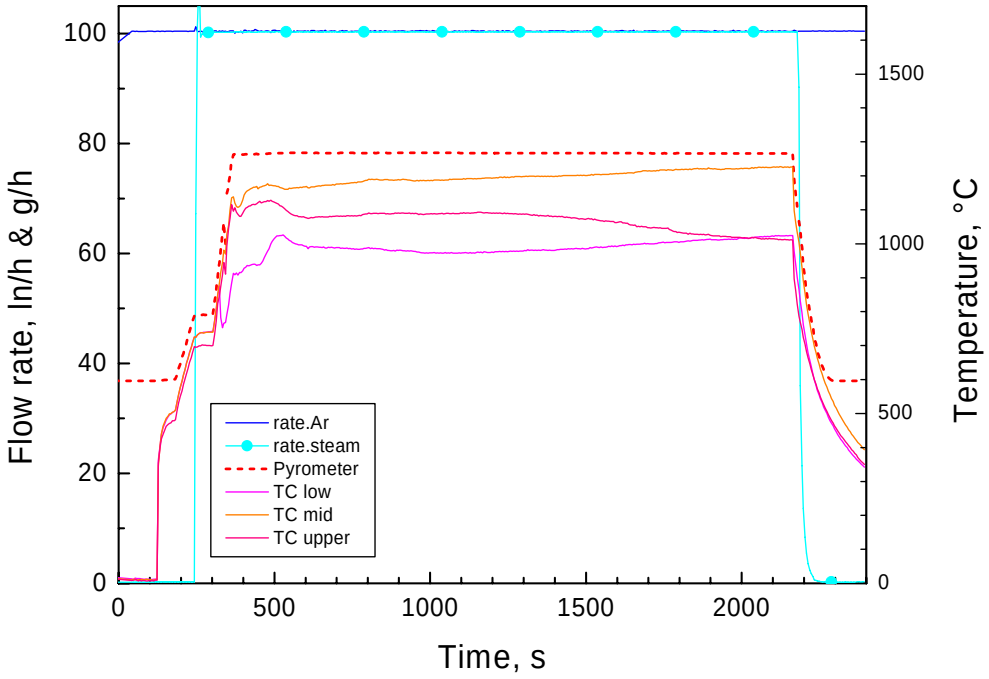

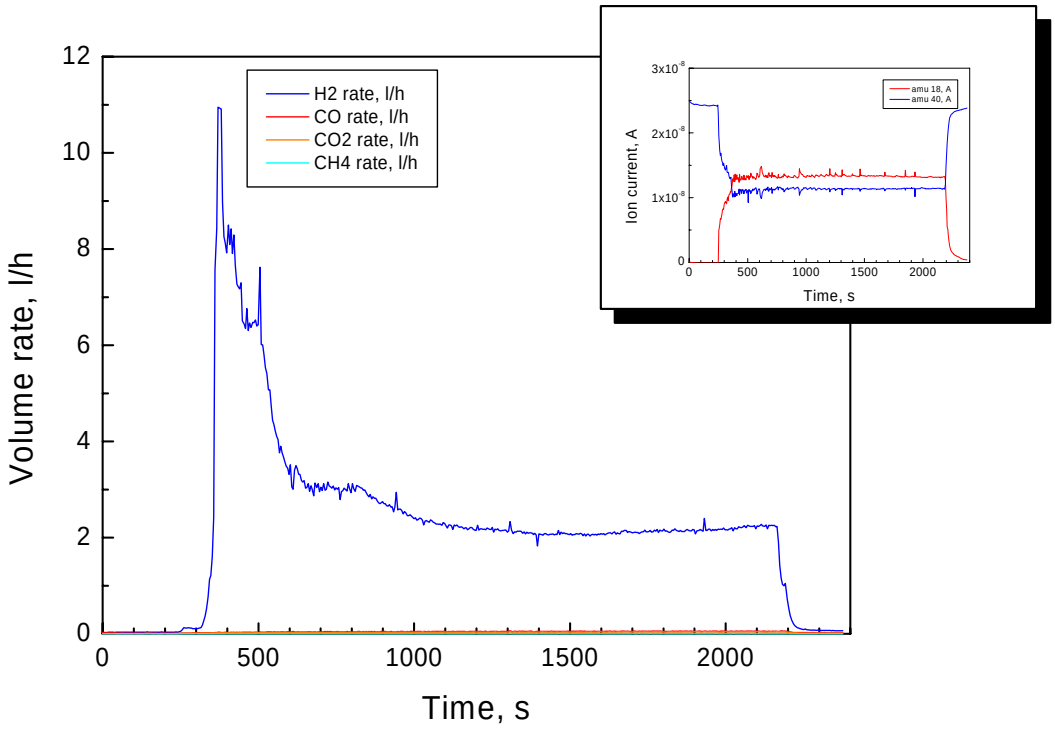

Test CR20828a:
Isothermal oxidation and degradation of a B_4C CR segment in Ar/steam (1375 °C, vacuum specimen)

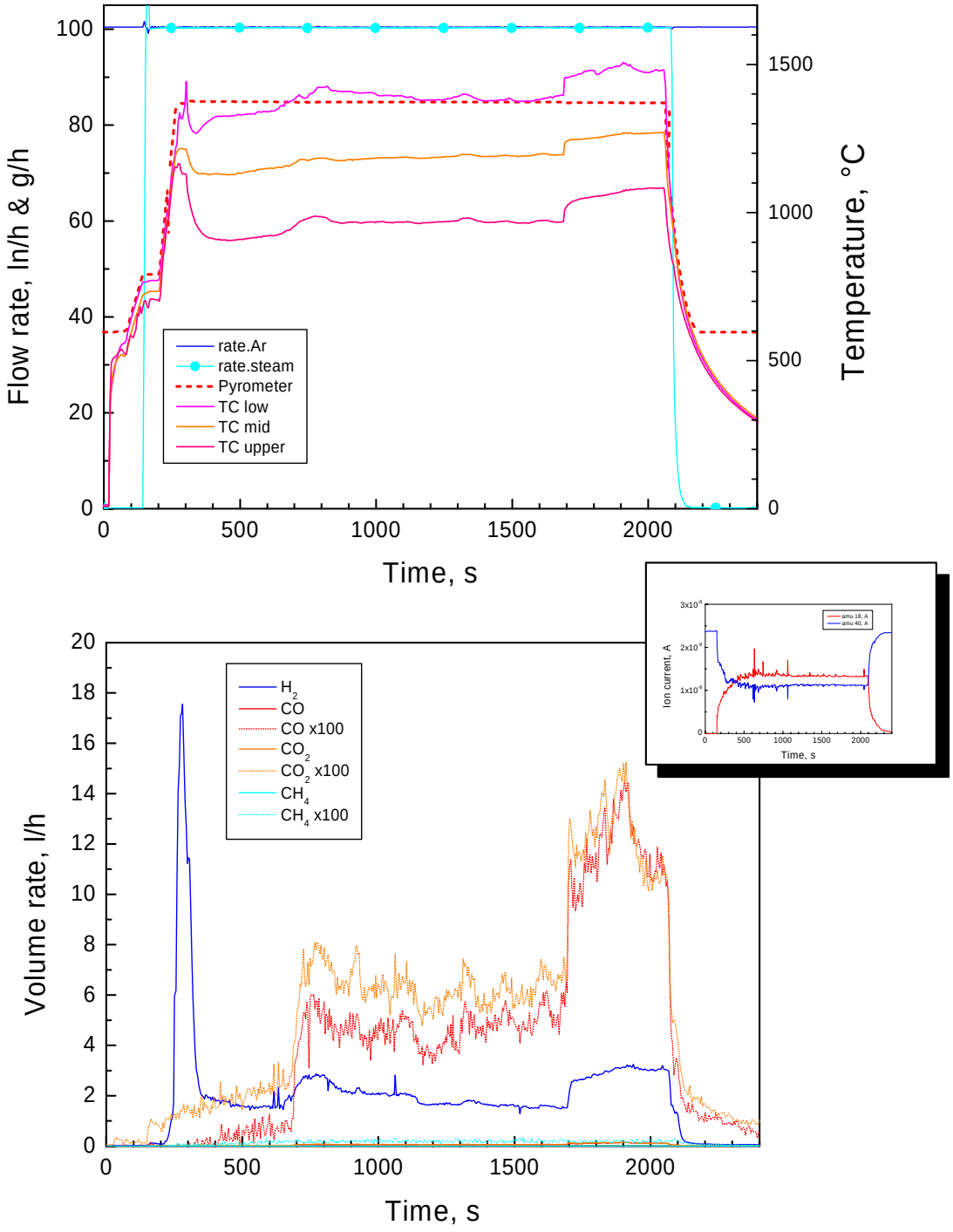

Test CR20828b:
Isothermal oxidation and degradation of a B_4C CR segment in Ar/steam (1460 °C, vacuum specimen)

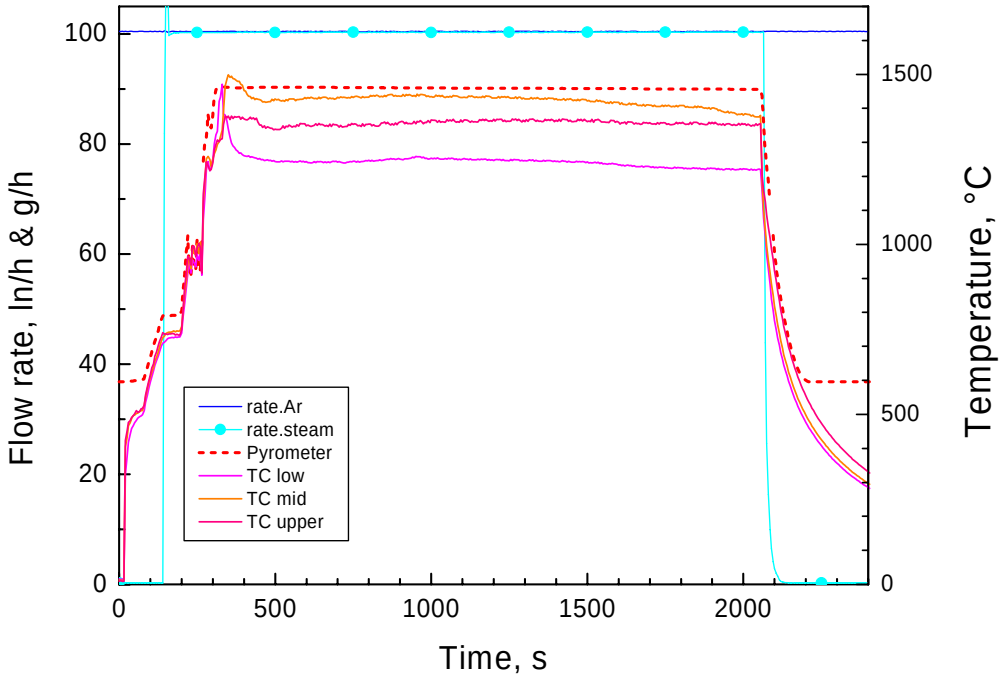

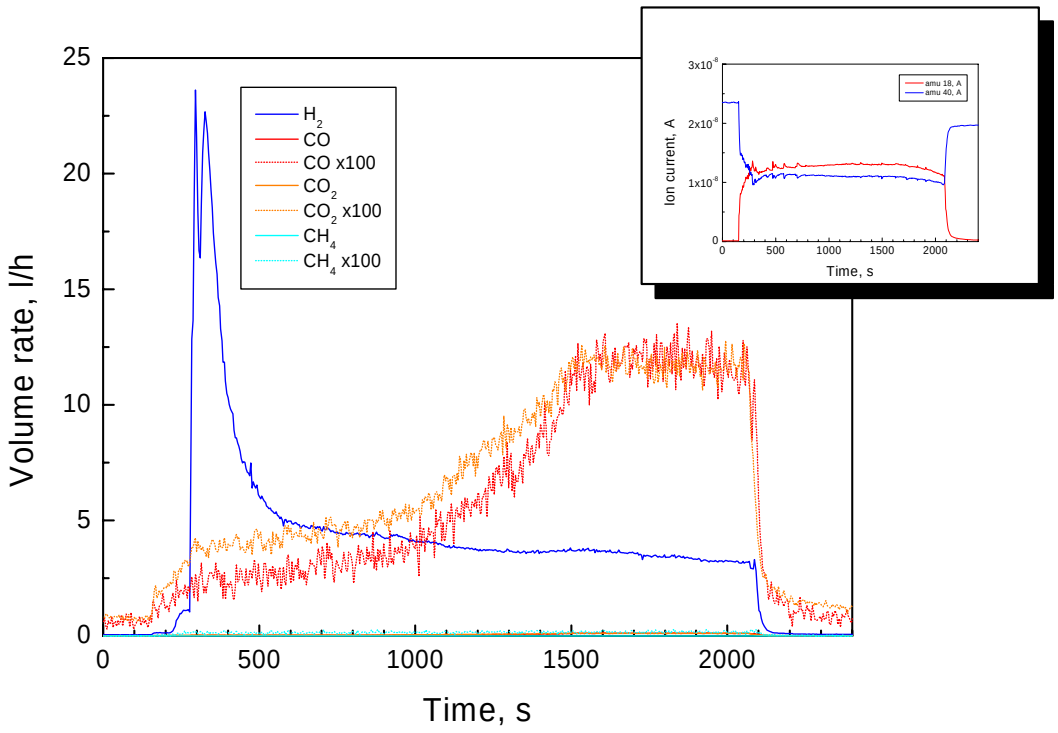

Test CR20829a:
Isothermal oxidation and degradation of a B_4C CR segment in Ar/steam (1470 °C, He filled specimen)

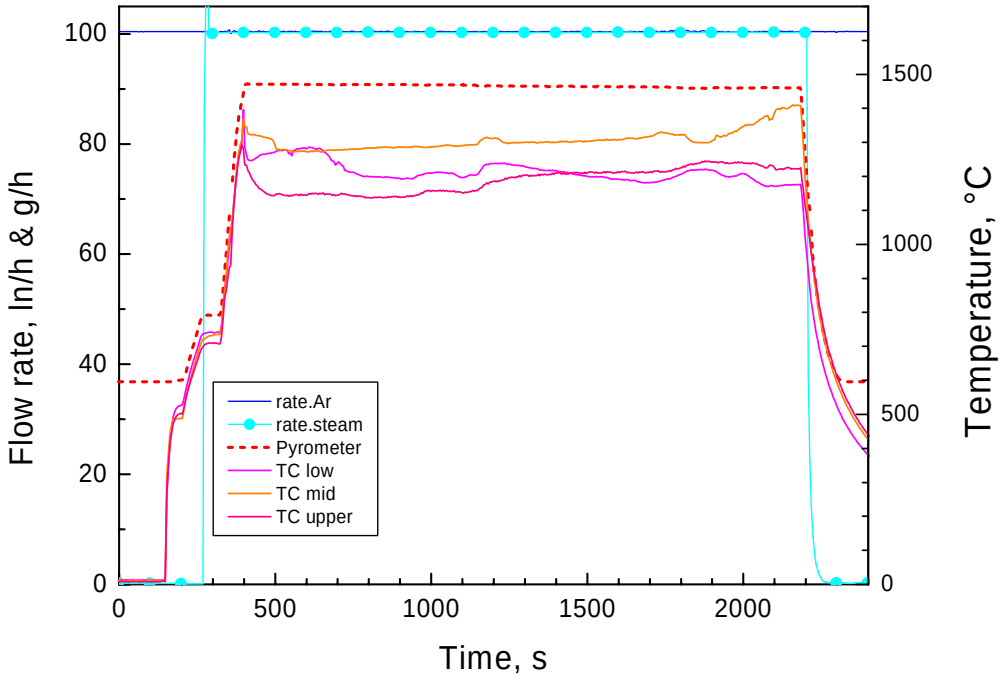

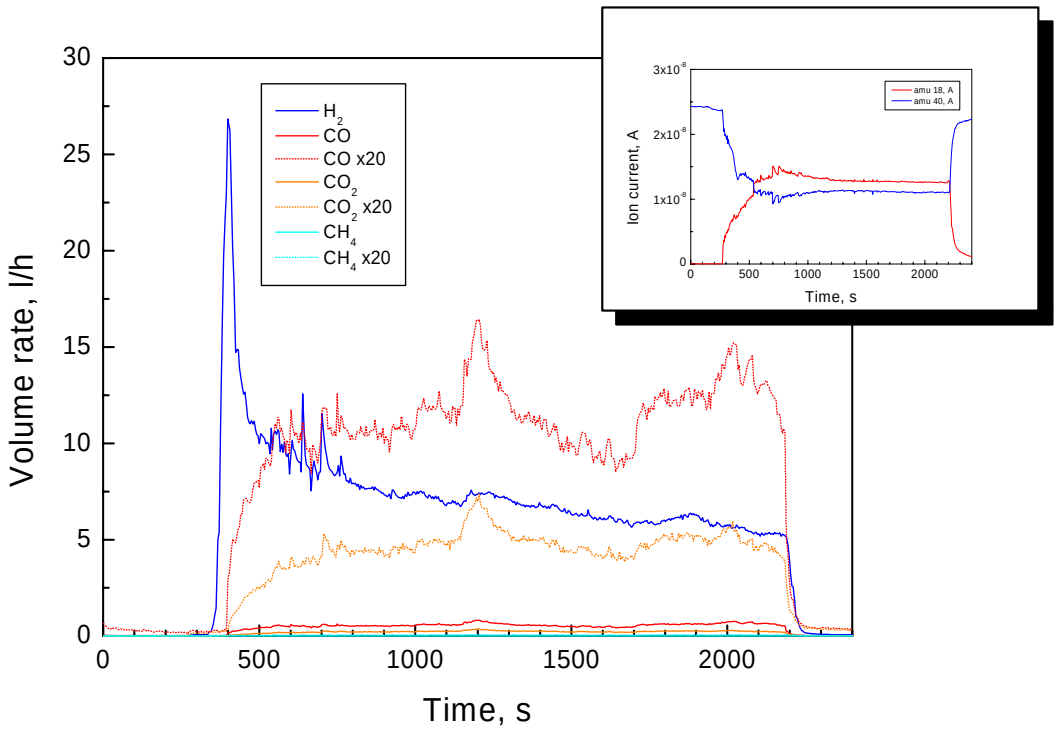

Test CR20829b:
Isothermal oxidation and degradation of a B_4C CR segment in Ar/steam (1270 °C, He filled specimen)

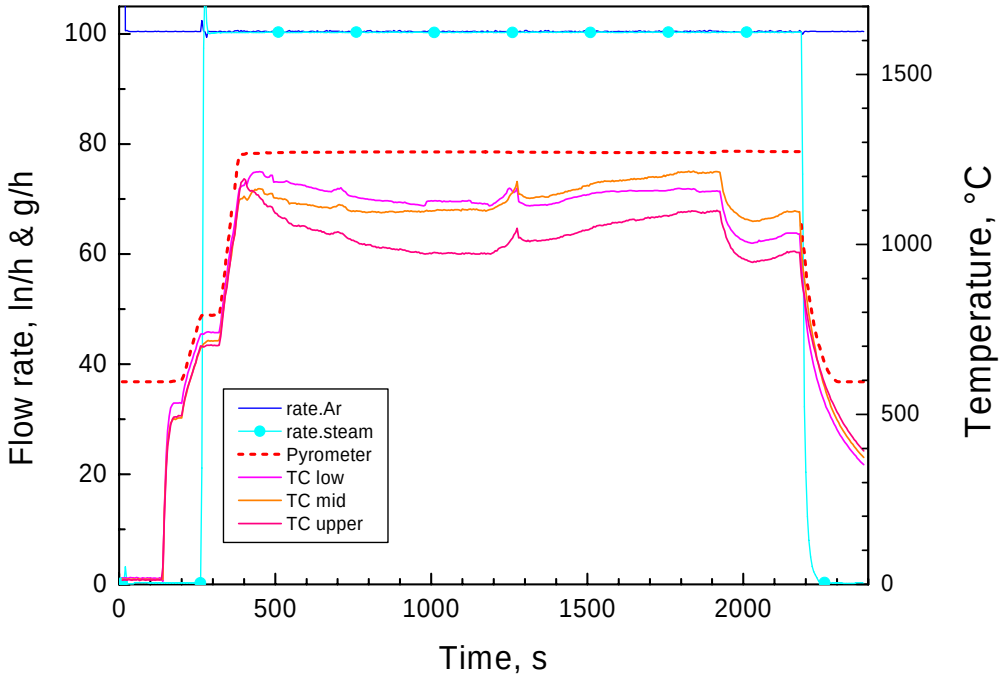

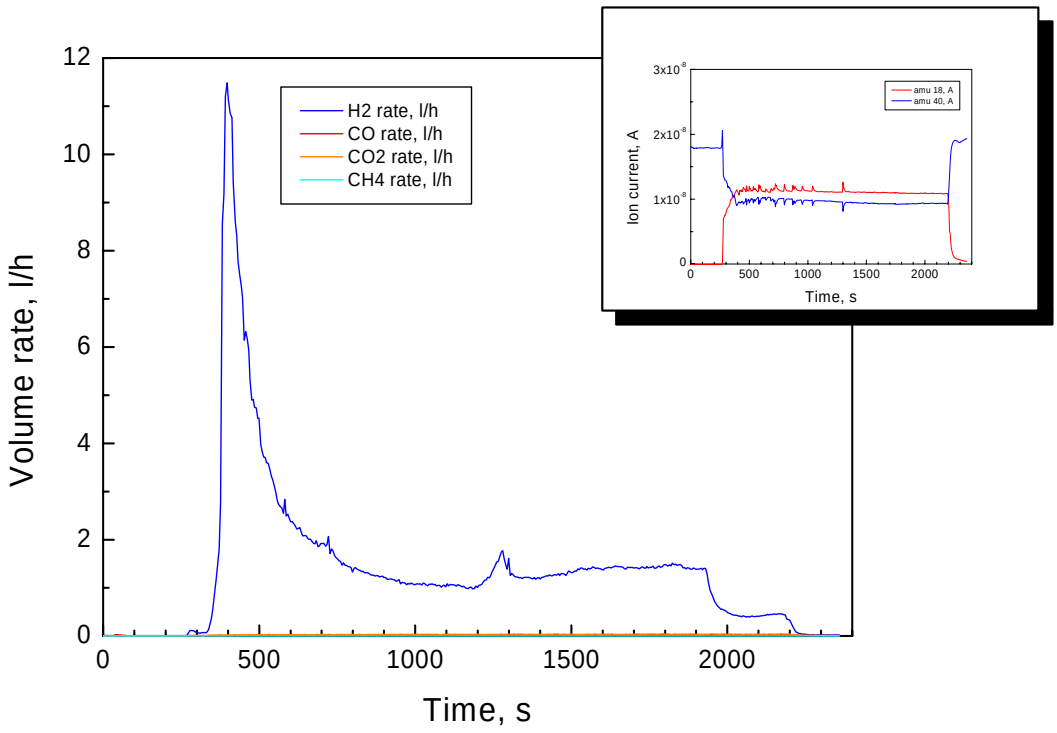

Test CR20830:
Isothermal oxidation and degradation of a B_4C CR segment in Ar/steam (1560 -> 1490 °C, vacuum specimen)

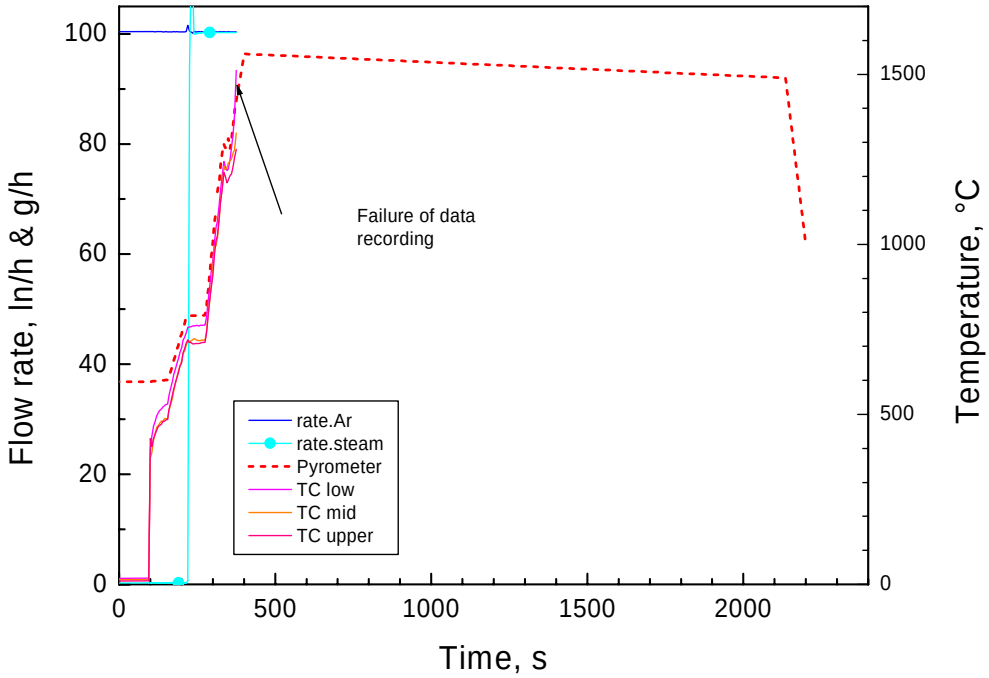

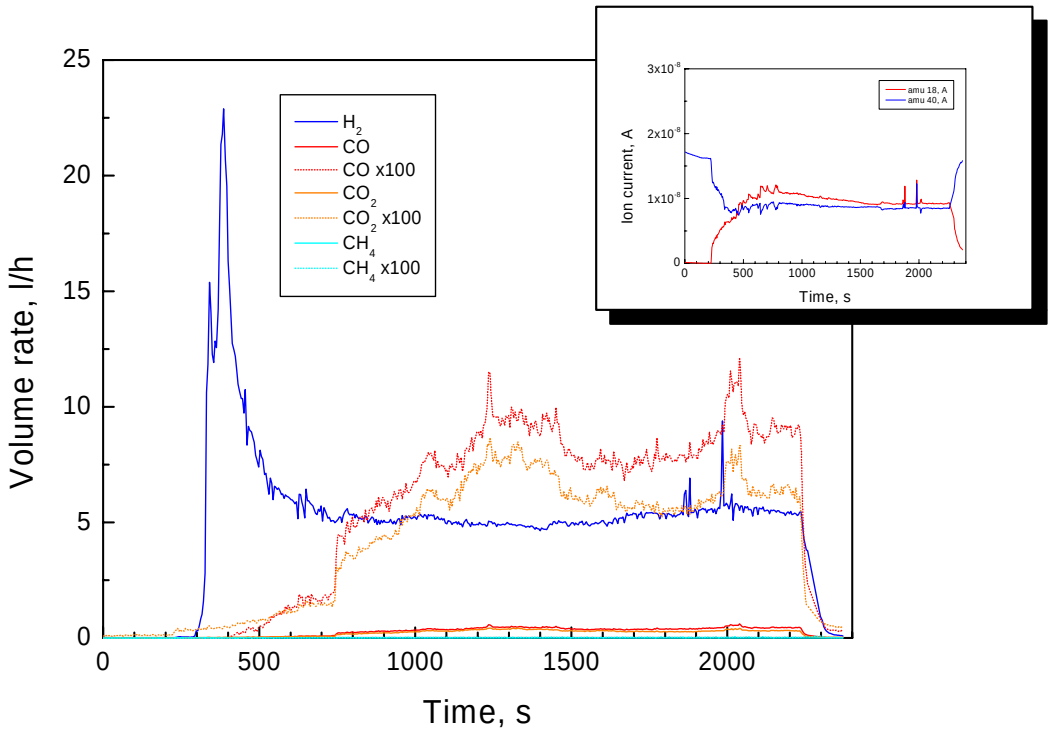

Test Box21108:
Transient oxidation (800-1550 °C) of absorber melt (0% B_4C - 100% SS - 0% Zry) in Ar/steam

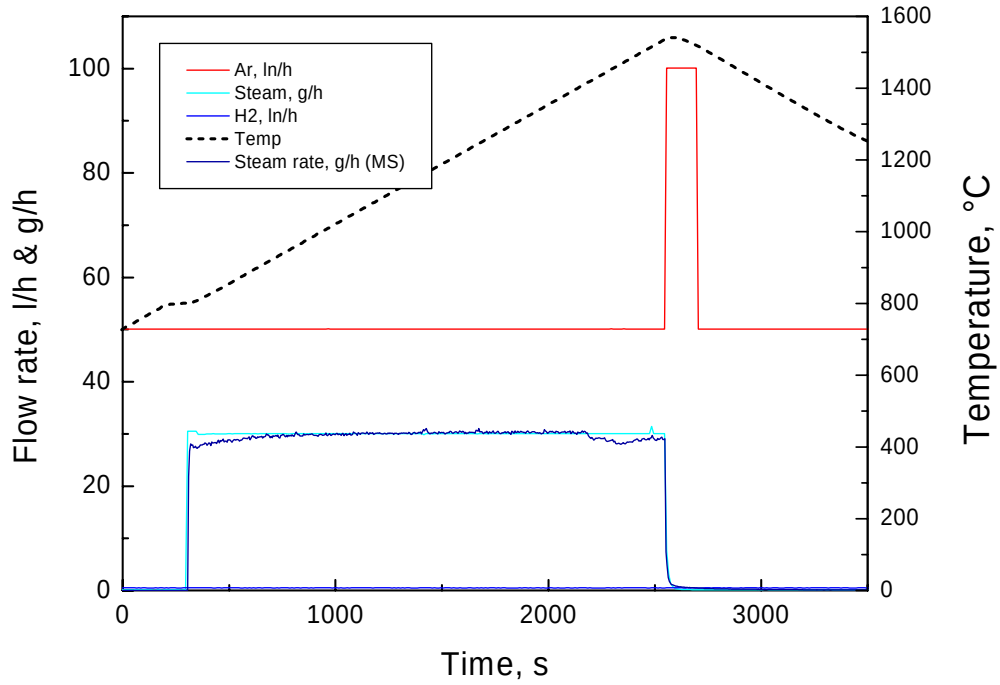

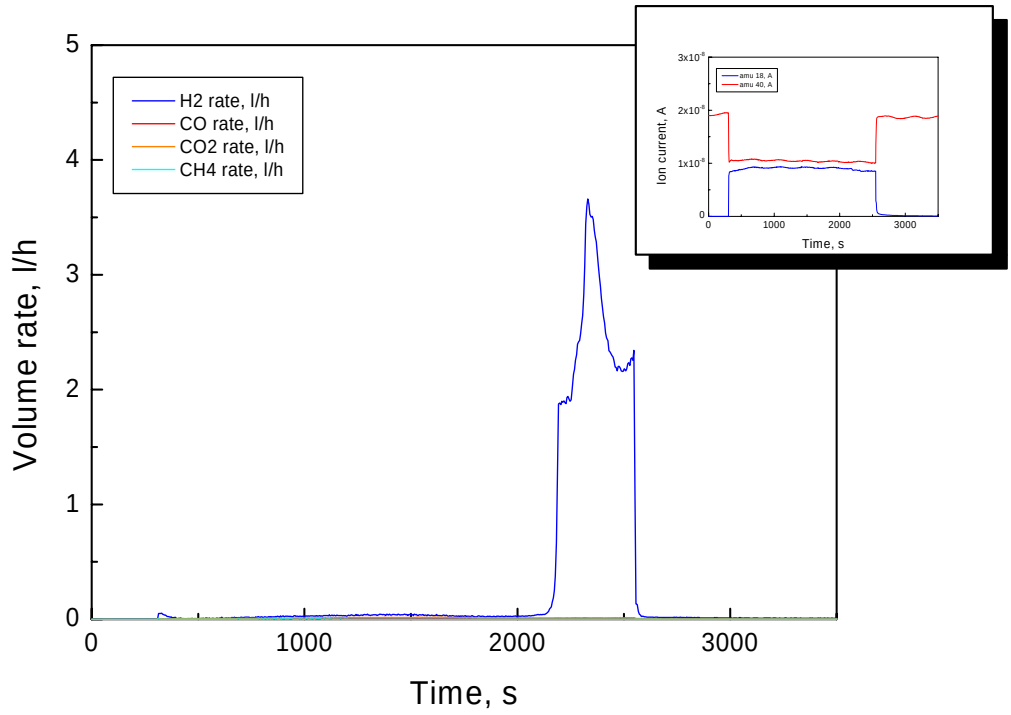

Test Box21111:
Transient oxidation (800-1550 °C) of absorber melt (5% B_4C - 95% SS - 0% Zry) in Ar/steam

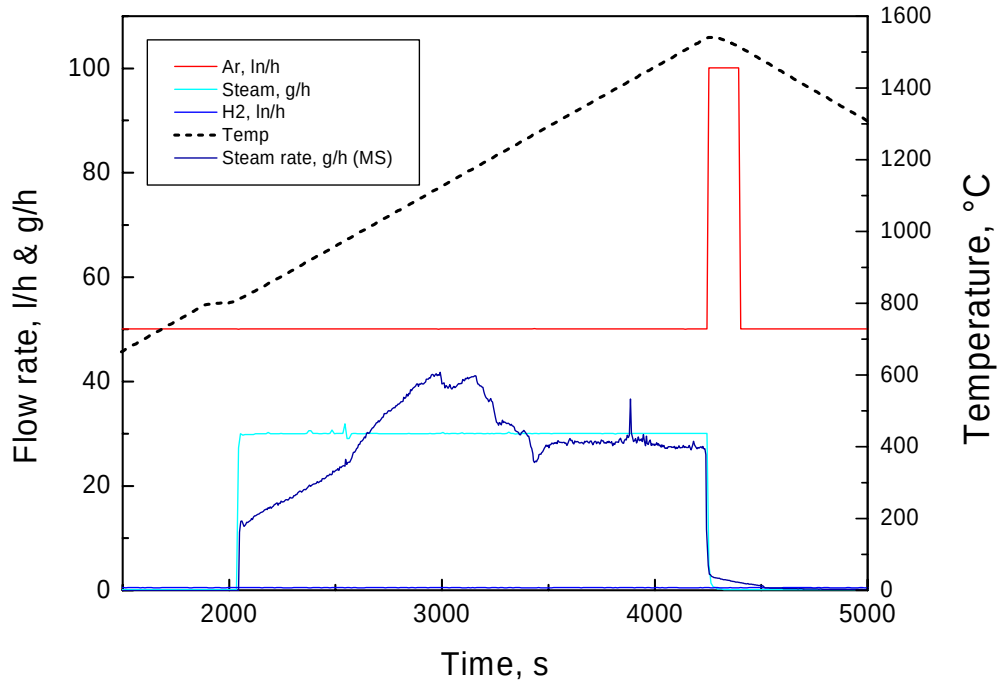

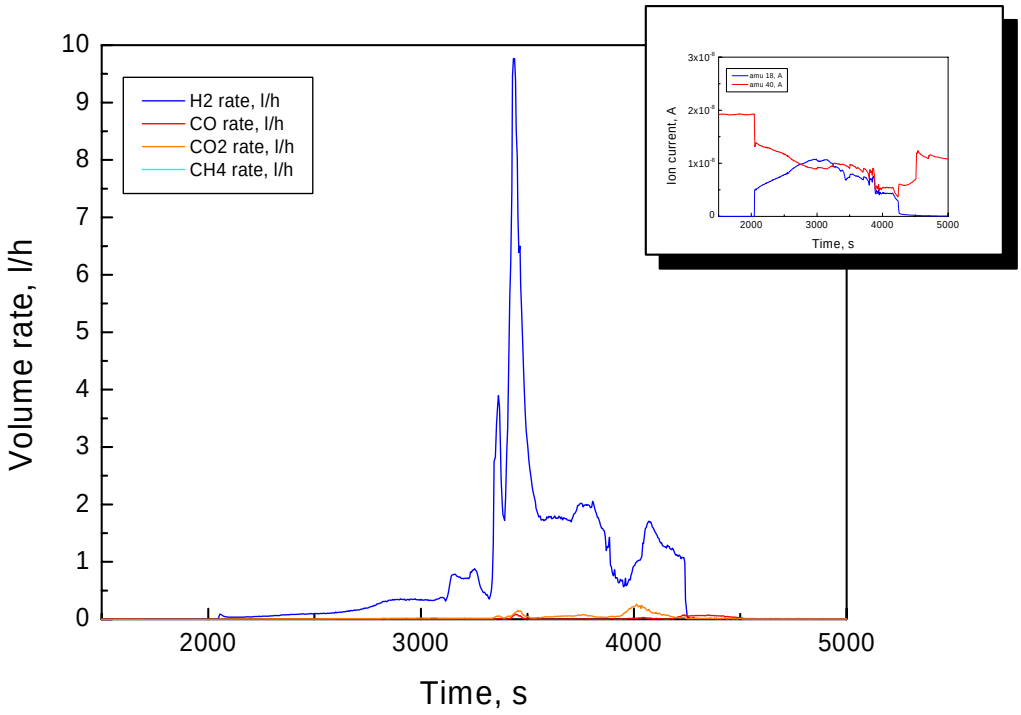

Test Box21113:
Transient oxidation (800-1550 °C) of absorber melt (20% B_4C - 80% SS - 0% Zry) in Ar/steam

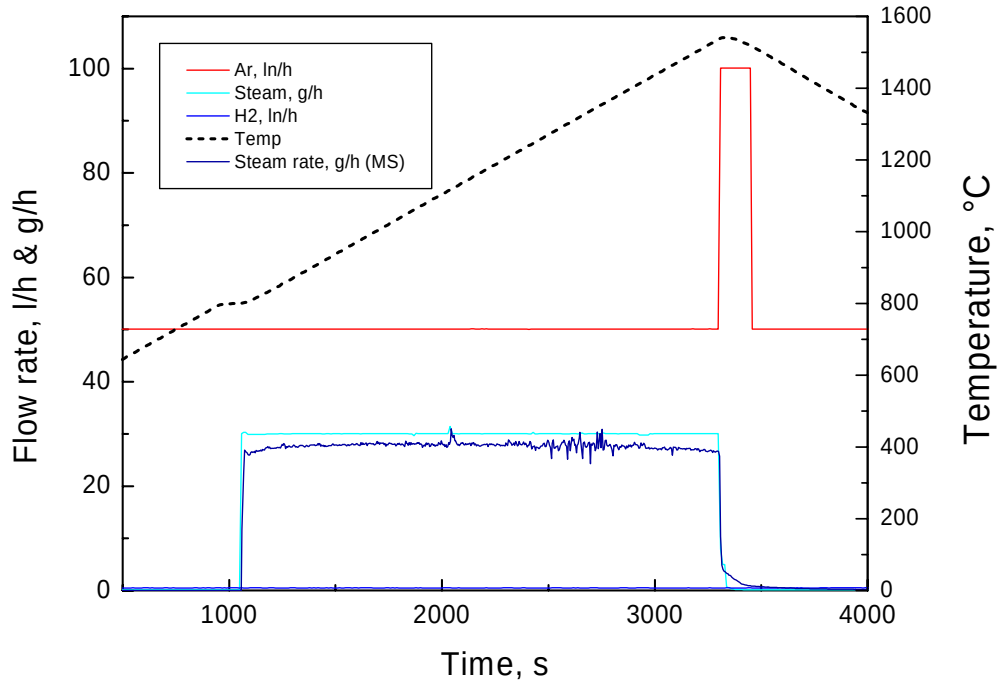

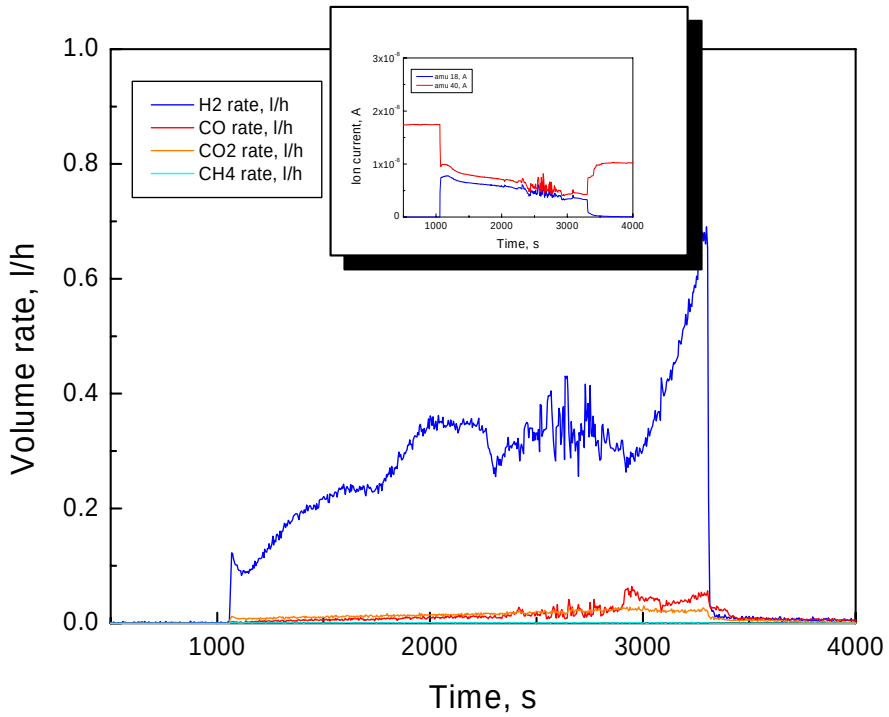

Test Box21114:
Transient oxidation (800-1550 °C) of absorber melt (9% B_4C - 81% SS - 10% Zry) in Ar/steam

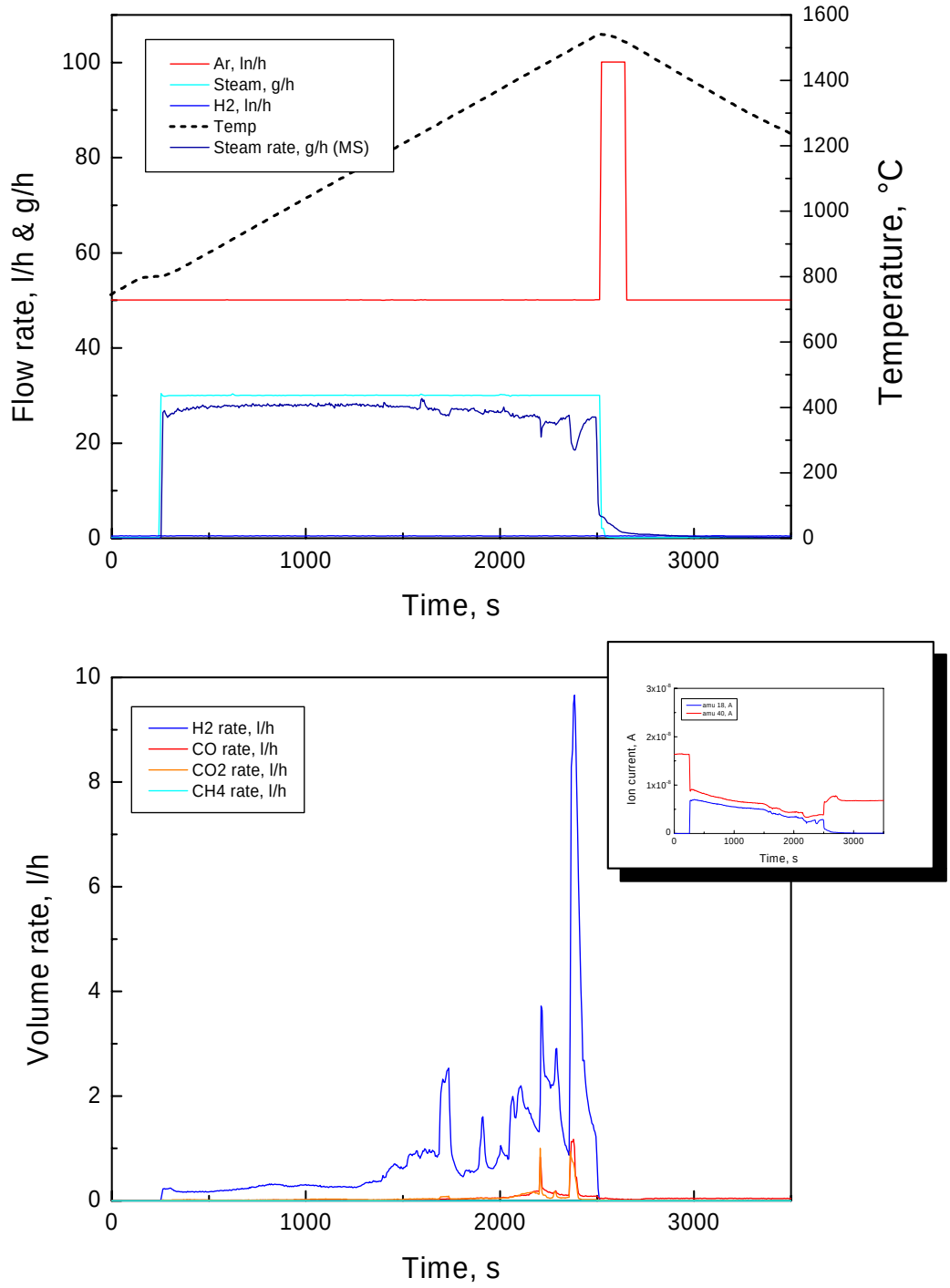

Test Box21119:
Transient oxidation (1000-1550 °C) of absorber melt (30% B_4C - 70% SS - 0% Zry) in Ar/steam

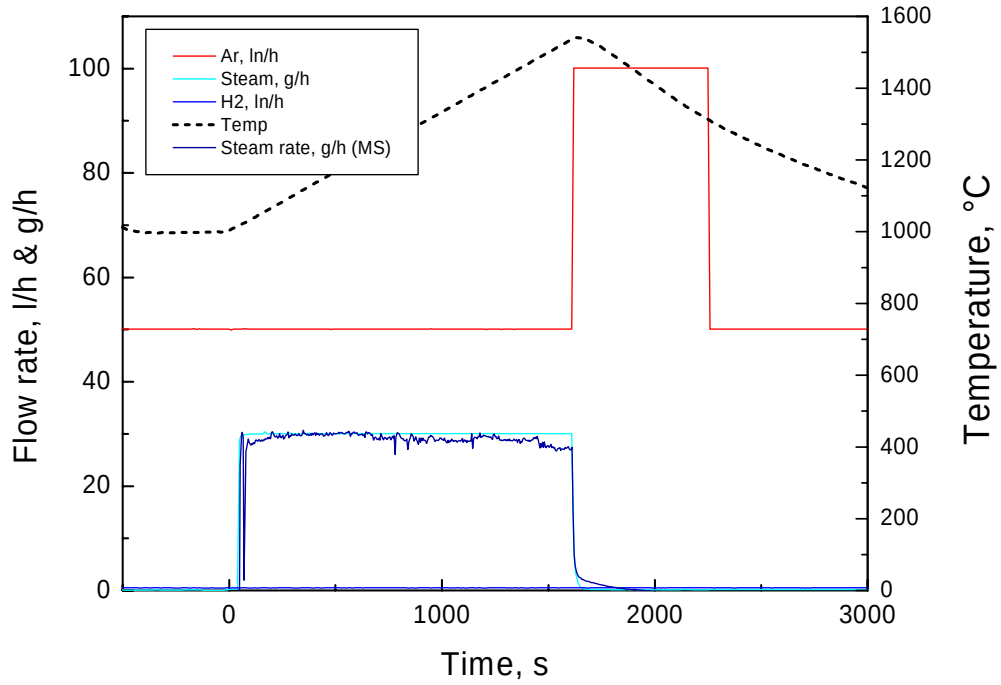

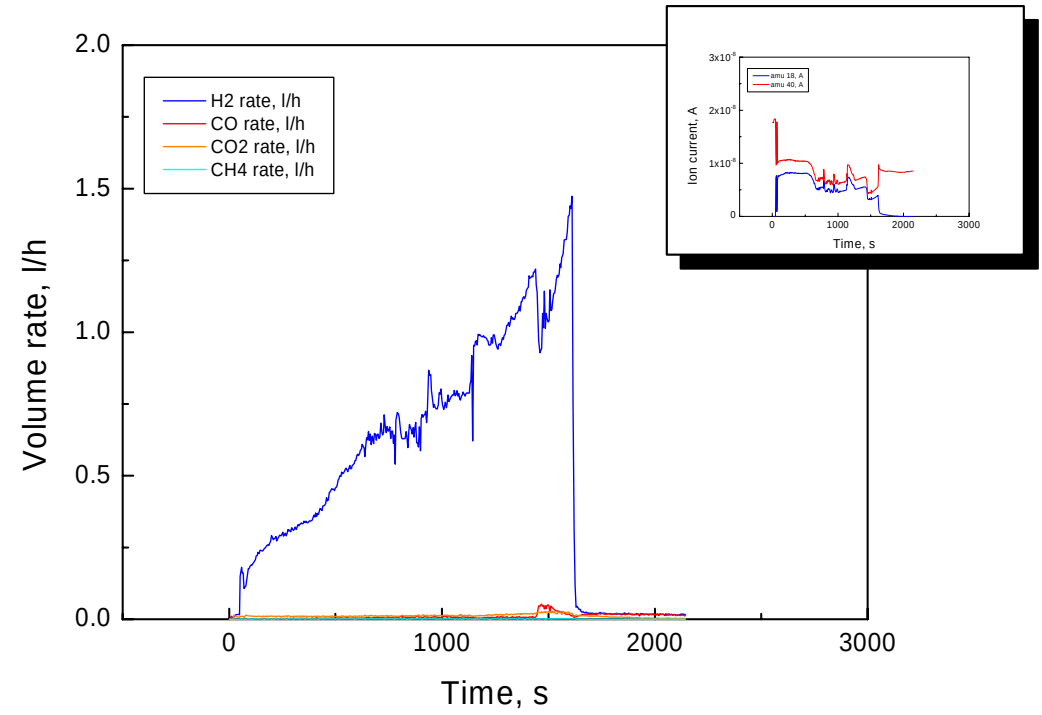

Test Box21119a:
Transient oxidation (800-1550 °C) of absorber melt (10% B_4C - 90% SS - 0% Zry) in Ar/steam

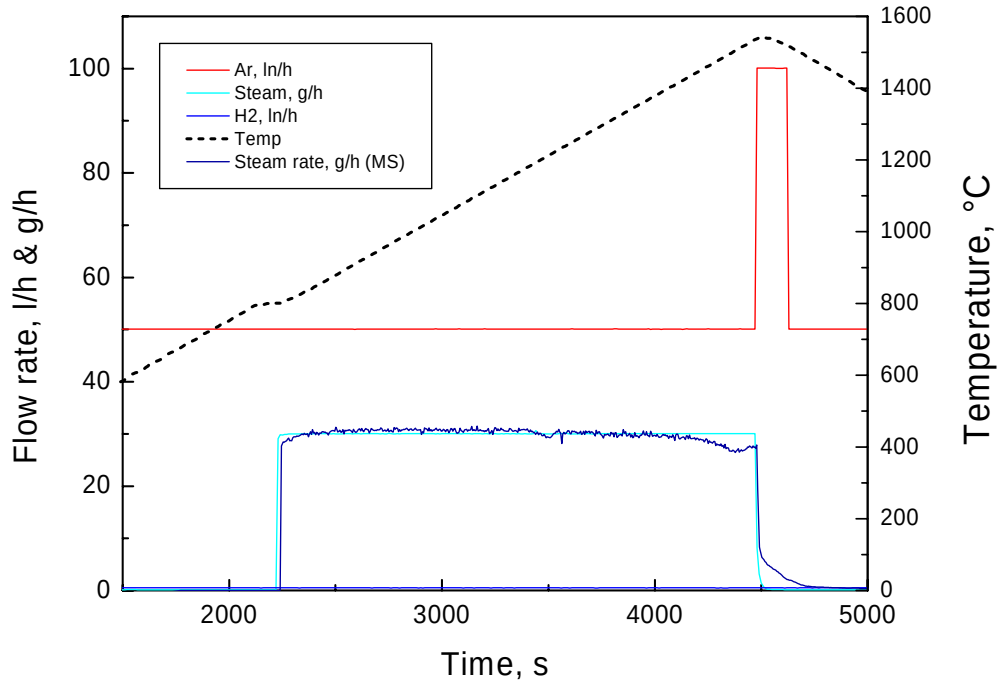

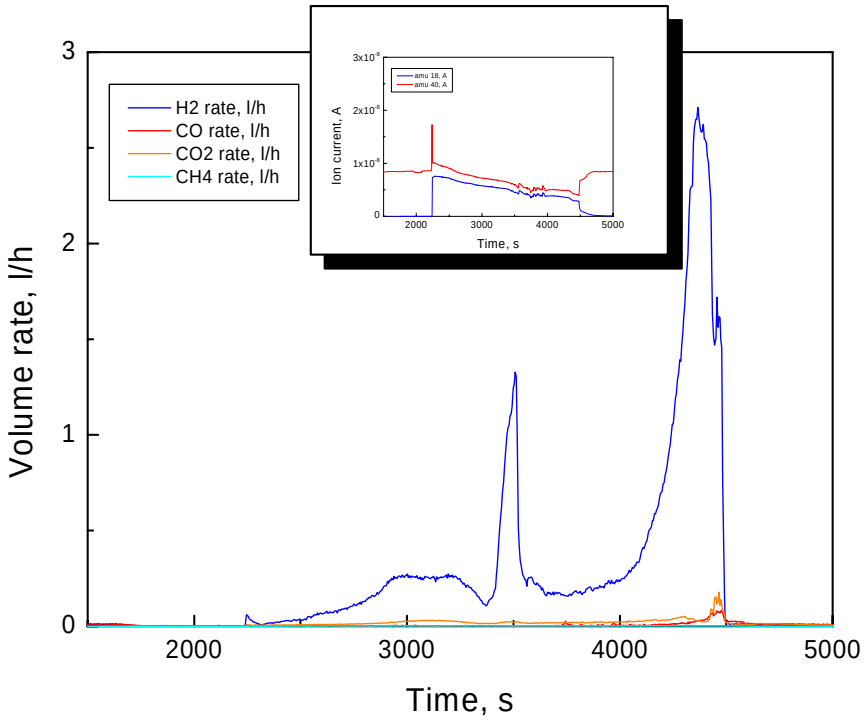

Test Box21120:
Transient oxidation (800-1550 °C) of absorber melt (7% B_4C - 63% SS - 30% Zry) in Ar/steam

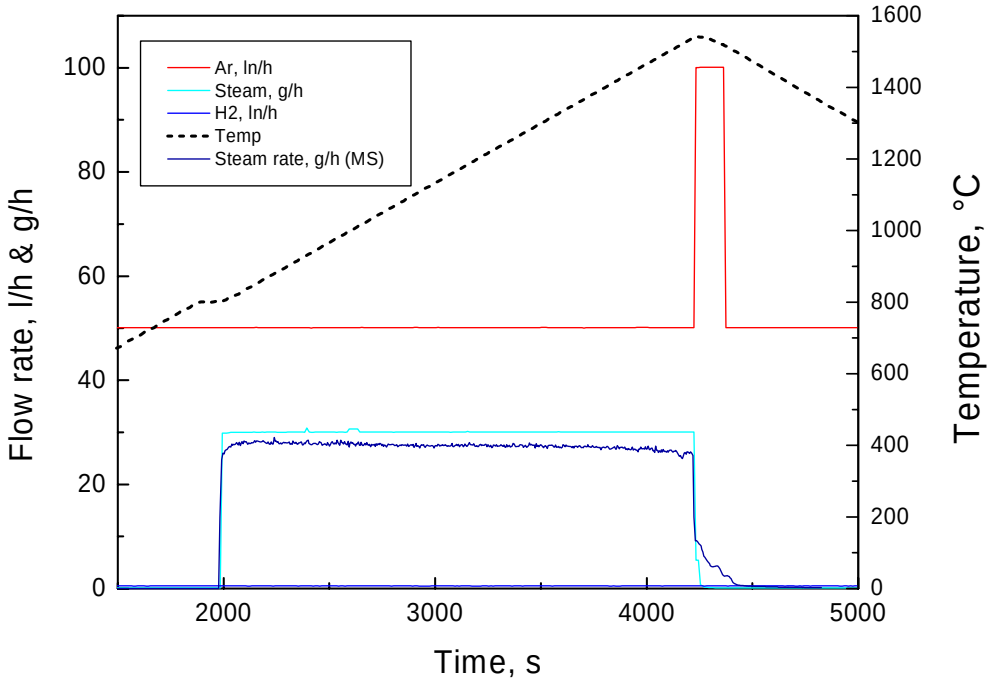

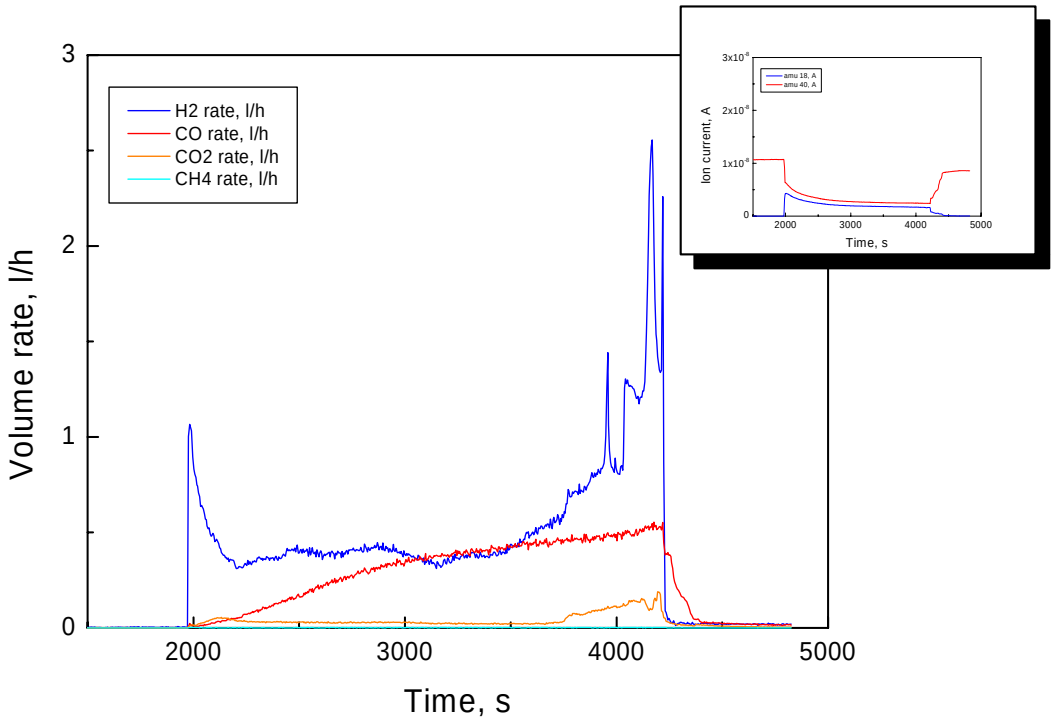

Test Box21121:
Transient oxidation (800-1550 °C) of absorber melt (0% B_4C - 70% SS - 30% Zry) in Ar/steam

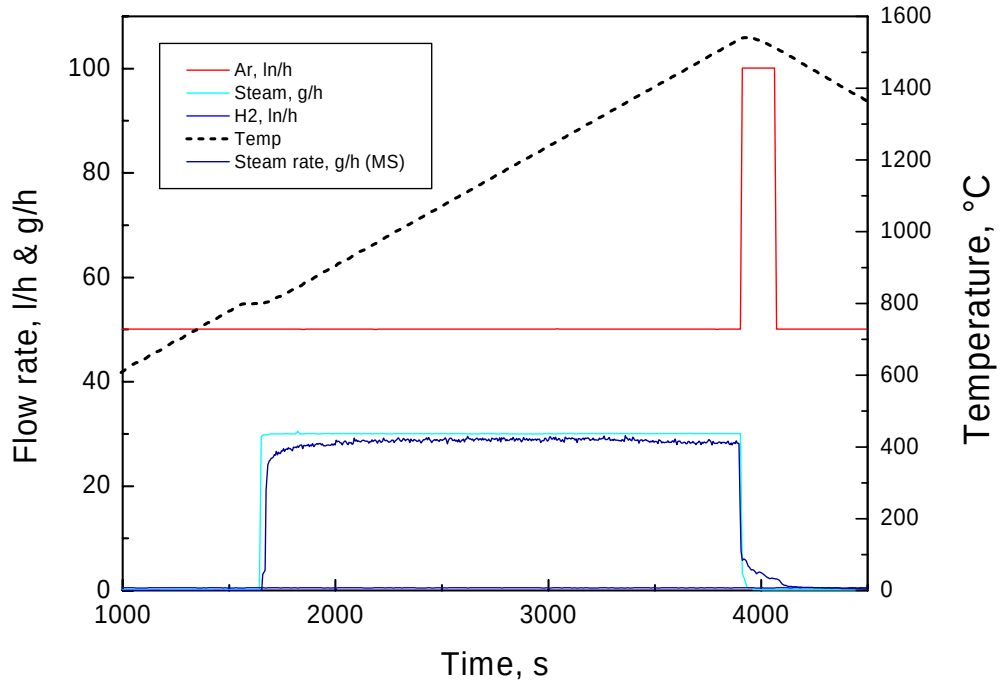

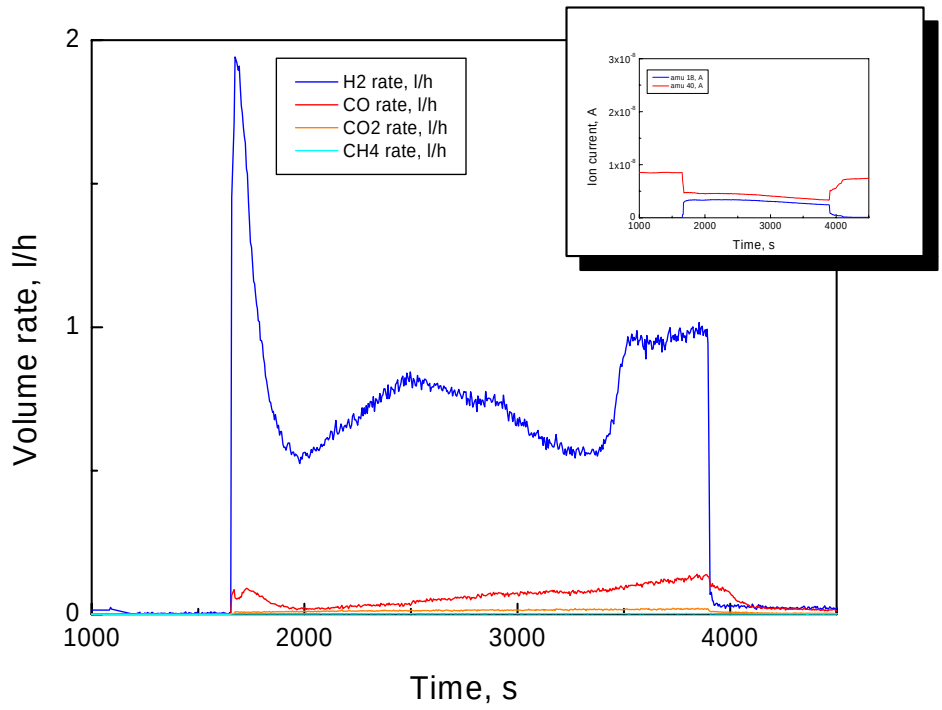

Test Box21125:
Transient oxidation (800-1550 °C) of absorber melt (0% B_4C - 0% SS - 100% Zry) in Ar/steam

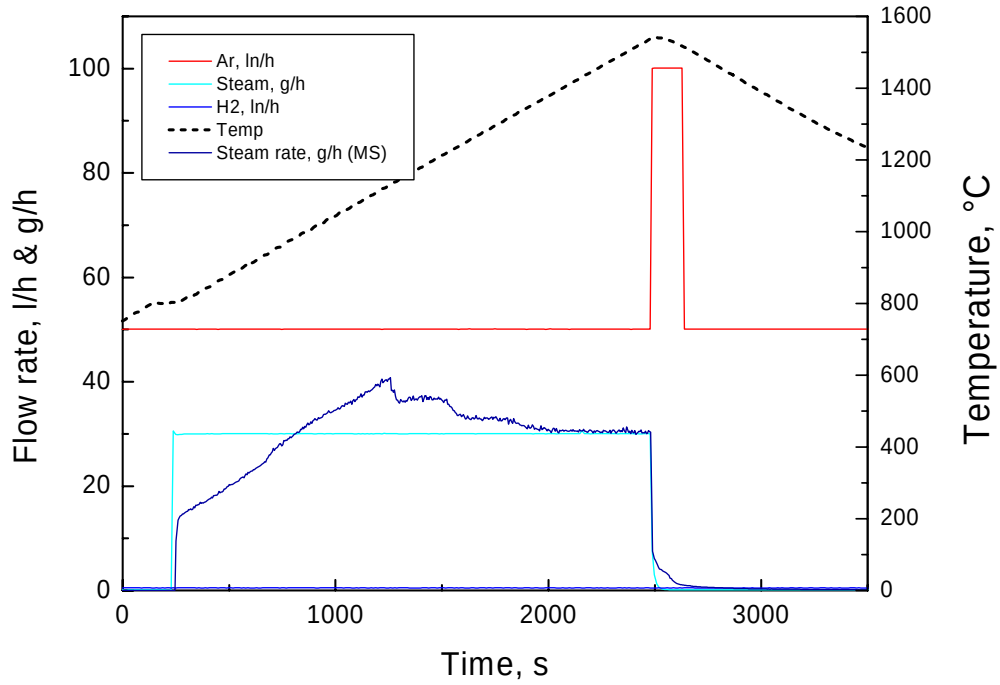

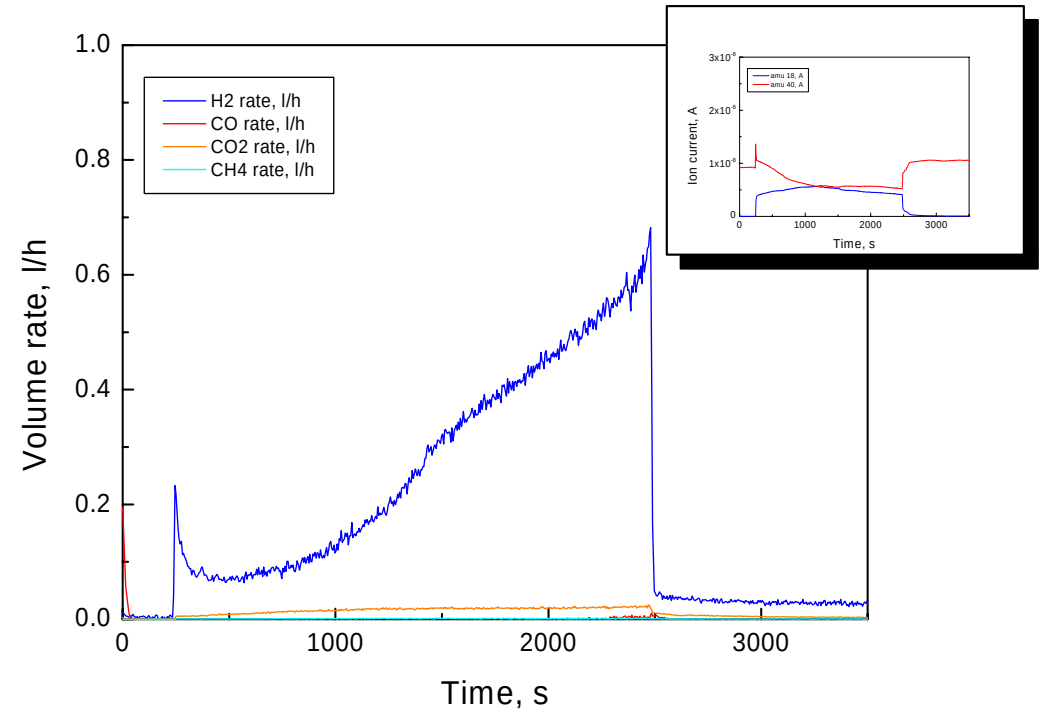

A14 Test conduct of experiments on interactions between boron carbide and stainless steel

Temperatures measured by pyrometer (at the bottom of the tungsten susceptor crucible) and thermocouple (about 1 cm above the surface of the melt)

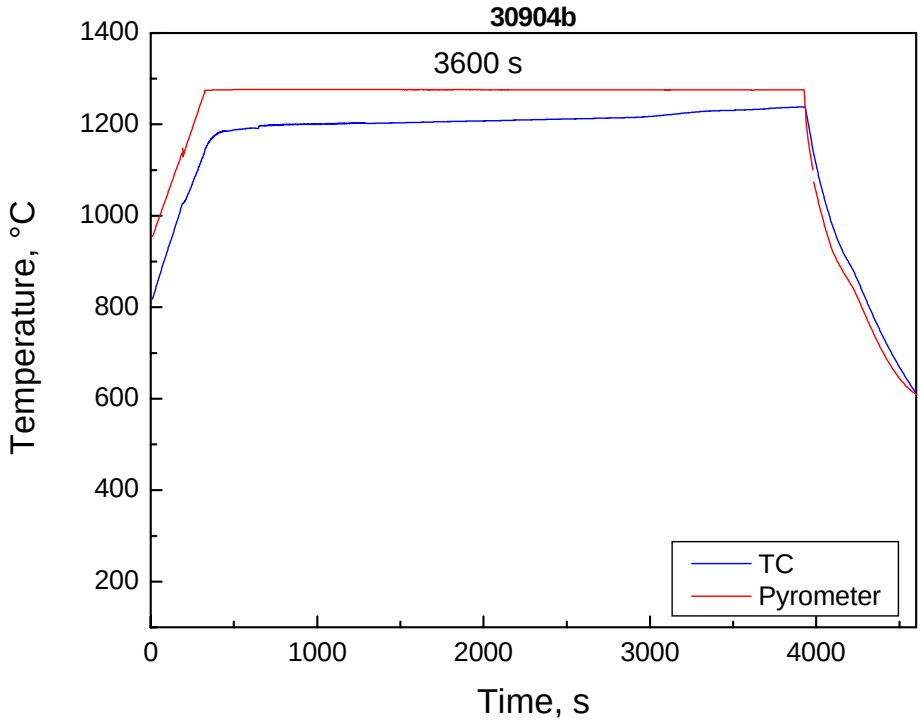

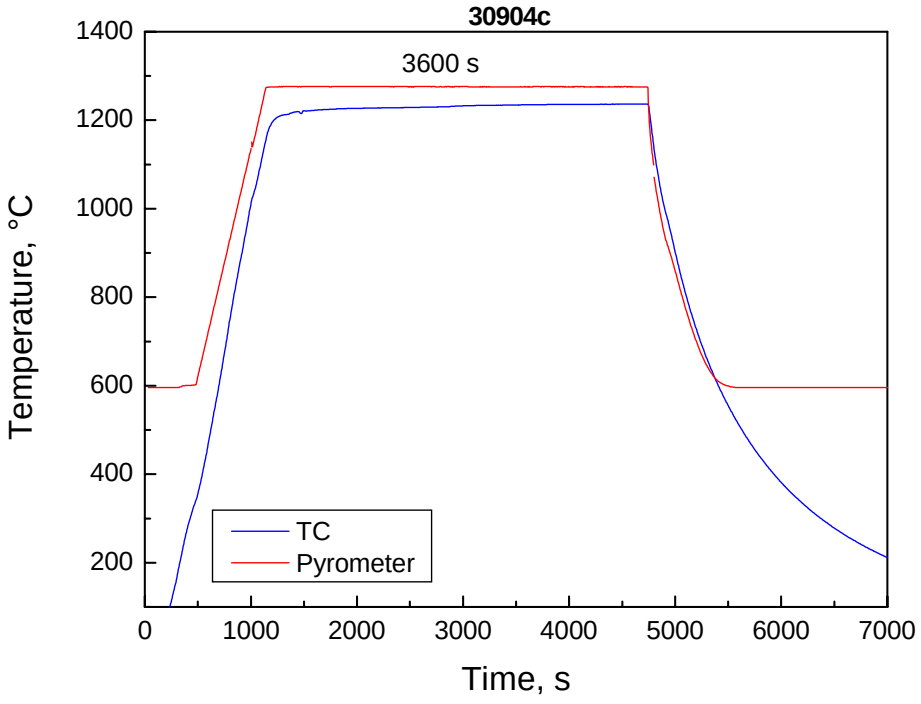

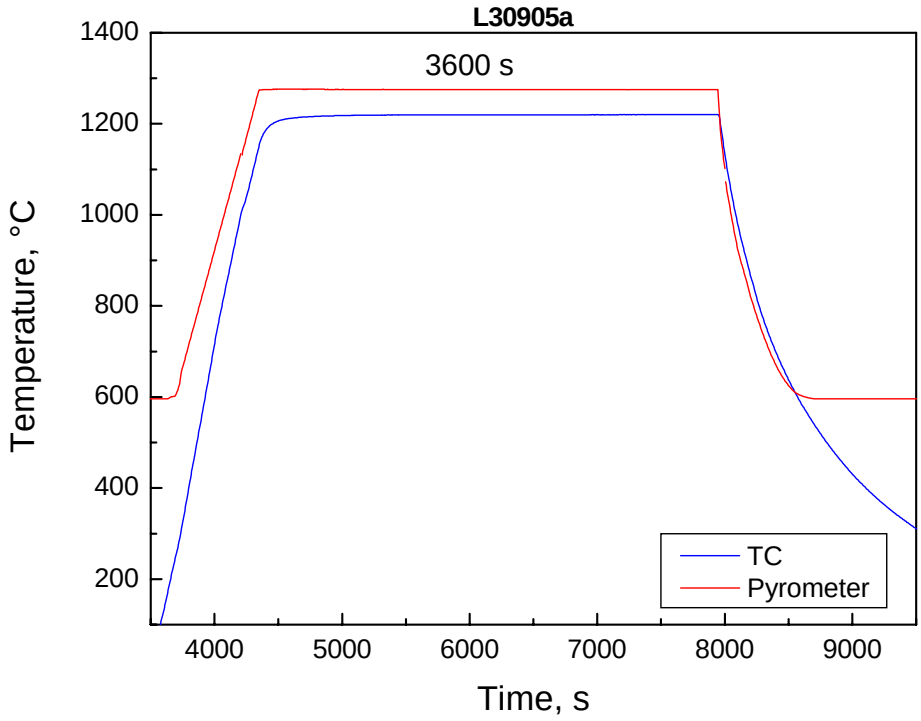
L30905a
3600 s
Temperature, °C
Time, s
TC
Pyrometer
1400
1200
1000
800
600
400
200
4000
5000
6000
7000
8000
9000

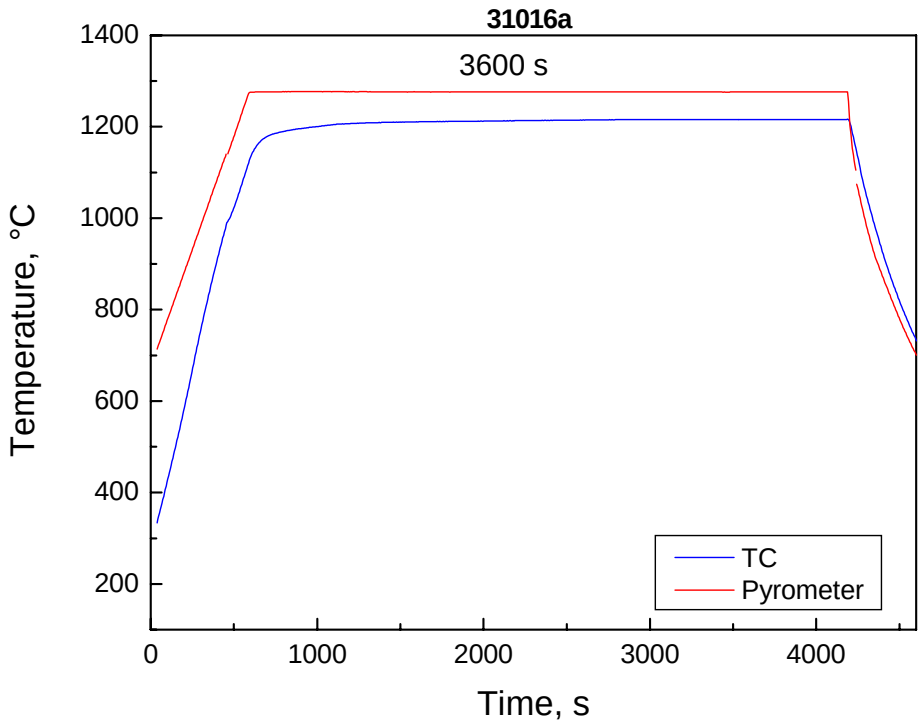
31016a
3600 s
Temperature, °C
Time, s
TC
Pyrometer
1400
1200
1000
800
600
400
200
0
1000
2000
3000
4000

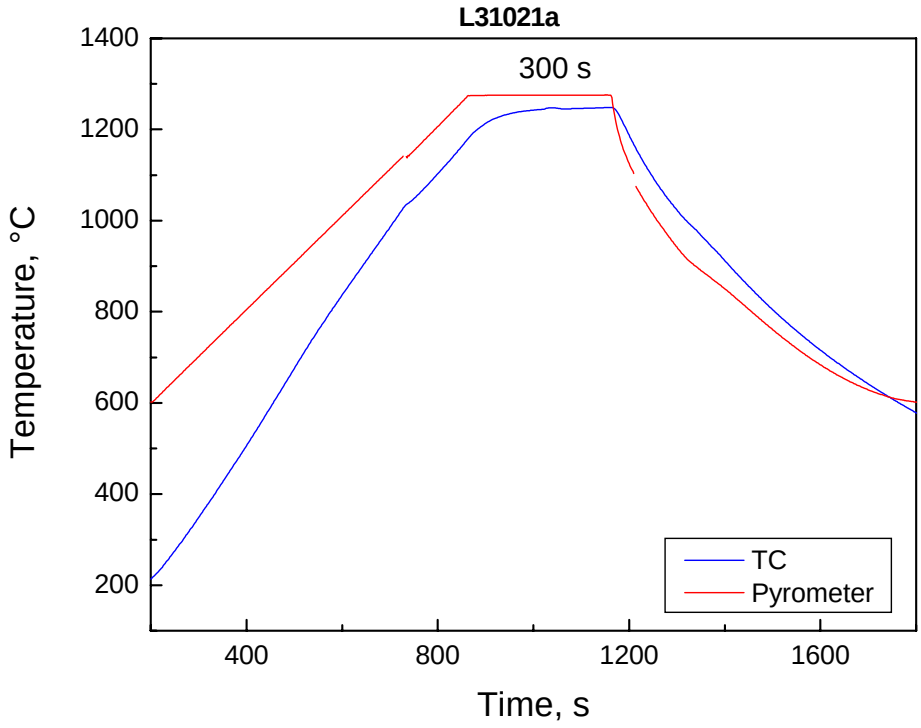
L31021a
300 s
Temperature, °C
Time, s
TC
Pyrometer
1400
1200
1000
800
600
400
200
400
800
1200
1600

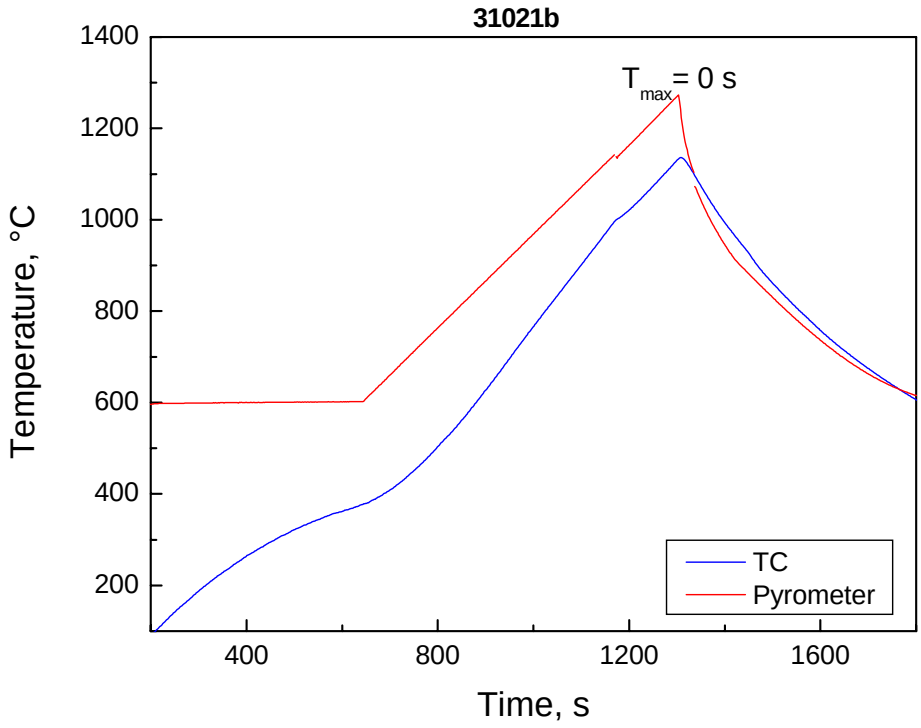
31021b
T max = 0 s
Temperature, °C
Time, s
TC
Pyrometer
1400
1200
1000
800
600
400
200
400
800
1200
1600

A15 Post-test analysis of experiments on interactions between boron carbide and stainless steel

In this chapter results of post-test examinations by light microscopy, scanning electron microscopy (SEM) and energy dispersive X-ray analysis (EDX) are compiled.

The EDX analyser has been renewed before this test series. Therefore, the quantitative data given in the tables are more reliable especially for the light elements C and B than for the analyses given e.g. in chapter A11.

Nevertheless, the carbon data seem to be systematically overestimated in these analyses. So, in pure steel AISI 304 between one and two mass-percent carbon, corresponding to about 5-10 at-% were analysed by the EDX system, although the carbon content should be significantly below one mass-percent.

Small amounts of Si and Mo (below 1 at-%) have been measured in some specimens; they were neglected in the data tables.

Test L30904b: Large B_4C pellet, 60 min at 1250 °C

Light-microscopic images

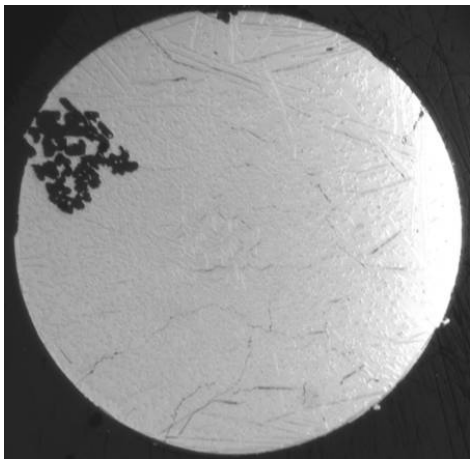

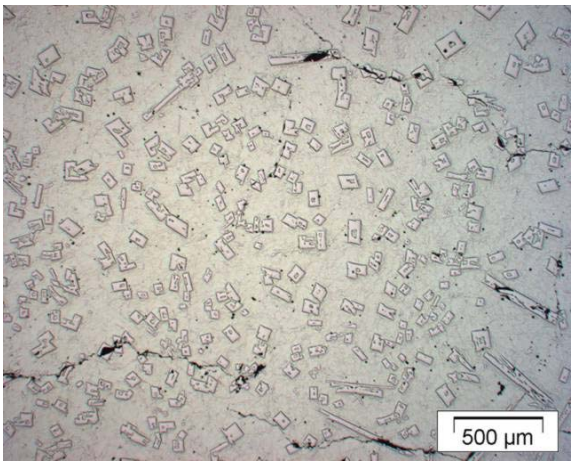

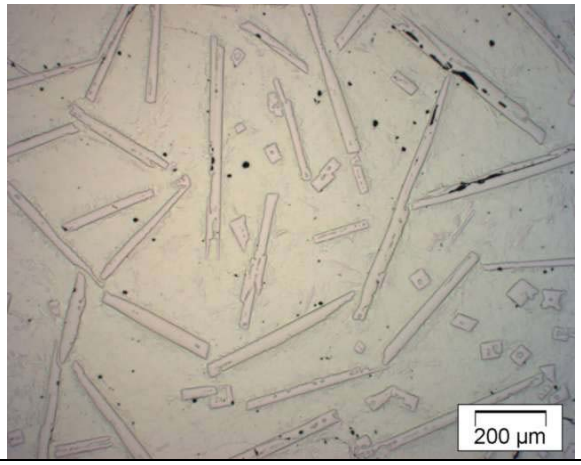

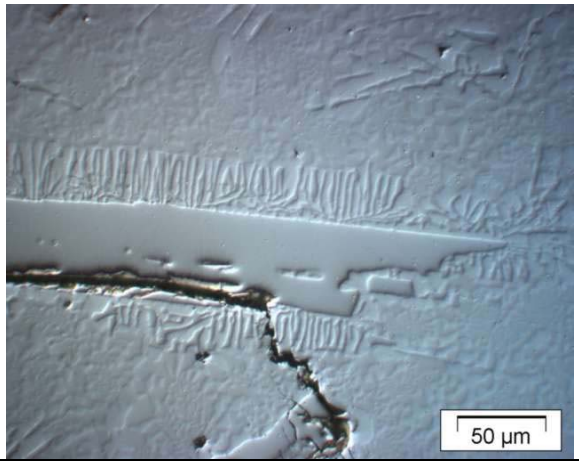

SEM/EDX

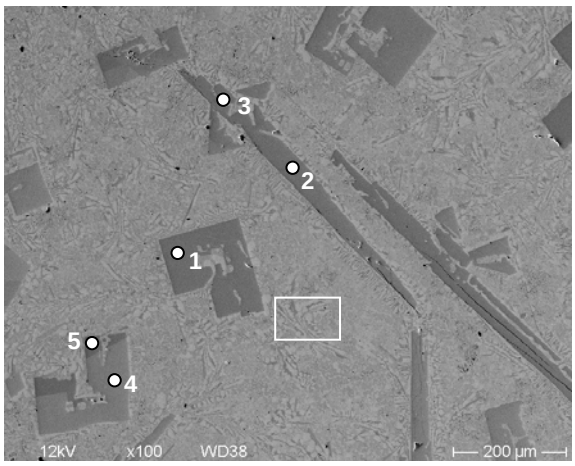

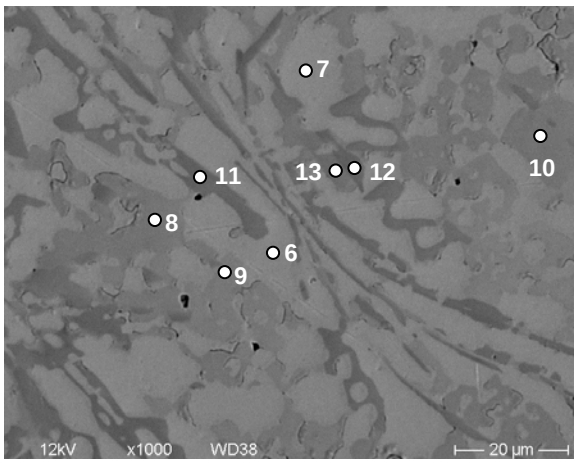

EDX results, concentrations in at-% (positions see SEM images)

Position	B	C	Cr	Fe	Ni
1	20.1	6.7	30.6	42.2	0.4
2	26.1	7.4	28.8	37.6	0.2
3	23.7	7.8	28.6	39.5	0.5
4	21.0	10.2	28.8	39.6	0.4
5	24.0	10.9	26.9	37.7	0.6
6	-	18.1	7.1	66.3	7.3
7	-	18.9	7.7	65.2	7.0
8	-	26.0	18.1	53.7	1.9
9	-	29.0	18.4	50.5	2.0
10	-	30.0	18.4	49.7	1.7
11	23.6	14.4	24.8	36.9	0.3
12	13.6	18.9	25.2	41.7	0.6
13	17.3	19.2	25.1	38.1	0.3

Test L30904c: Medium B_4C pellet, 60 min at 1250 °C

Light-microscopic images

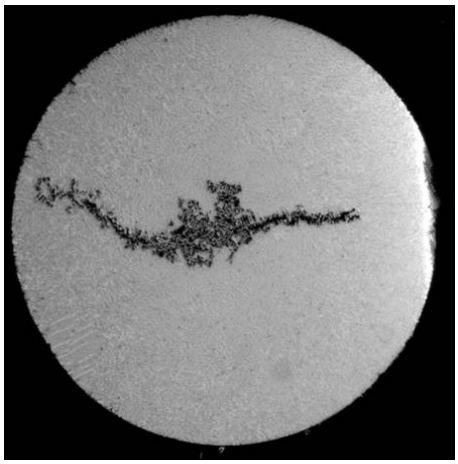

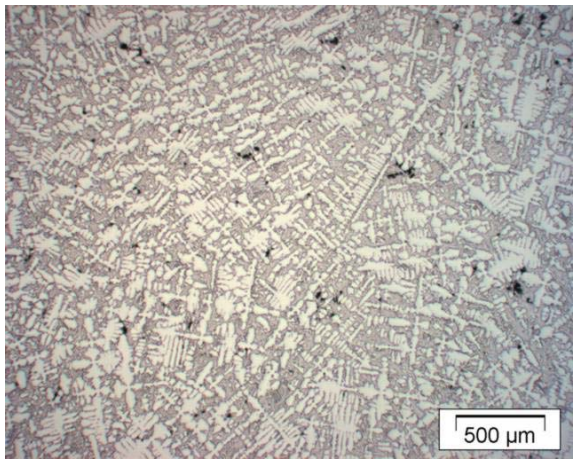

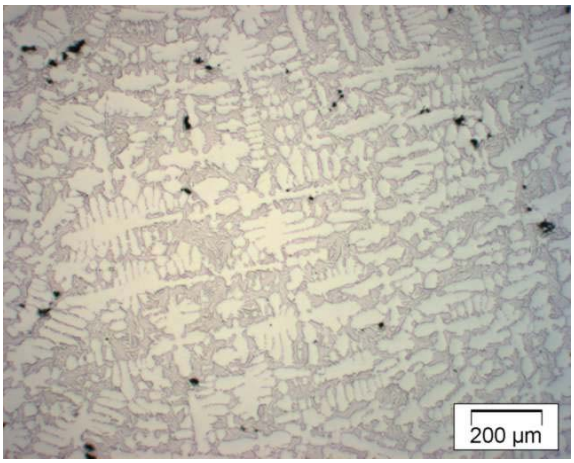

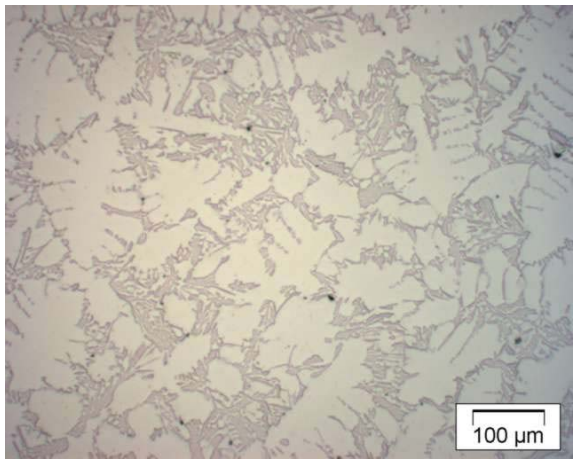

SEM/EDX

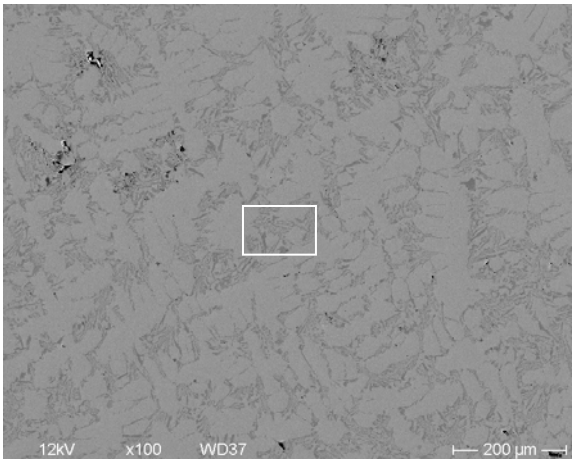

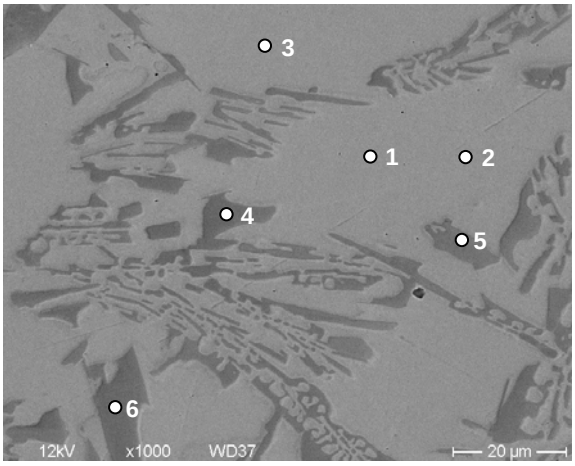

EDX results, concentrations in at-% (positions see SEM images)

Position	B	C	Cr	Fe	Ni
1	-	24.9	12.5	57.6	4.1
2	-	29.9	11.1	54.5	4.0
3	-	23.9	12.6	58.6	4.2
4	19.9	18.4	33.3	28.3	-
5	16.2	25.7	32.2	25.6	-
6	17.0	22.5	32.6	27.7	-

Test L30905a: Stainless steel reference, 60 min at 1250 °C

Light-microscopic images

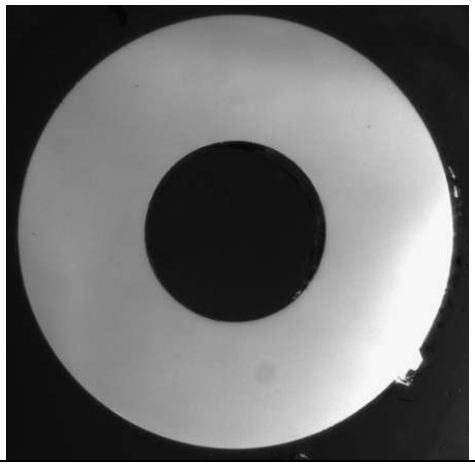

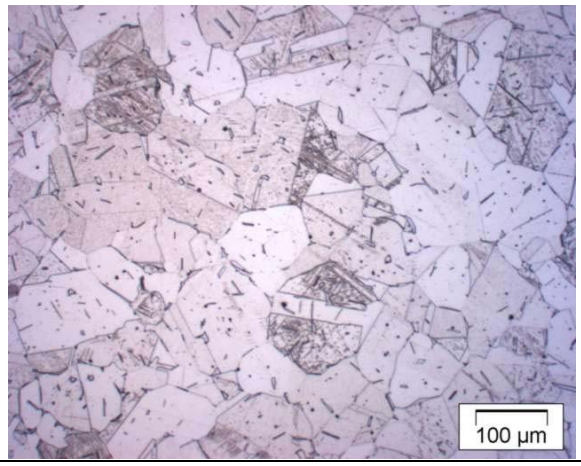

Test L31016a: Small B_4C pellet, 60 min at 1250 °C

Light-microscopic images

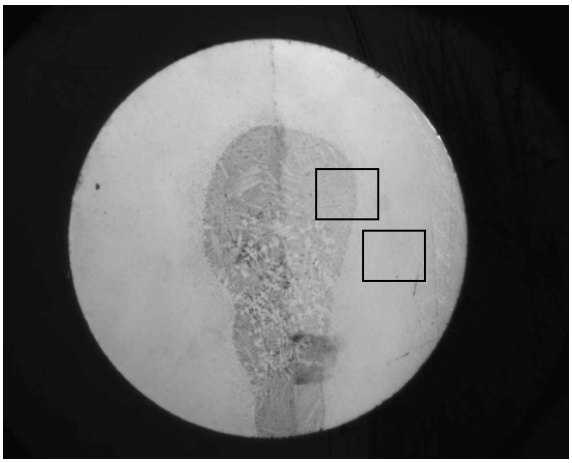

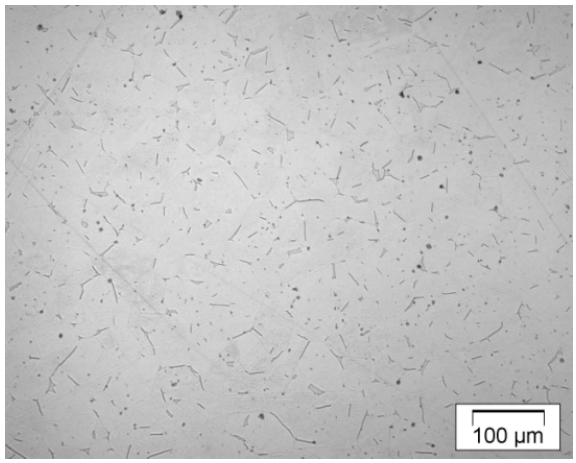

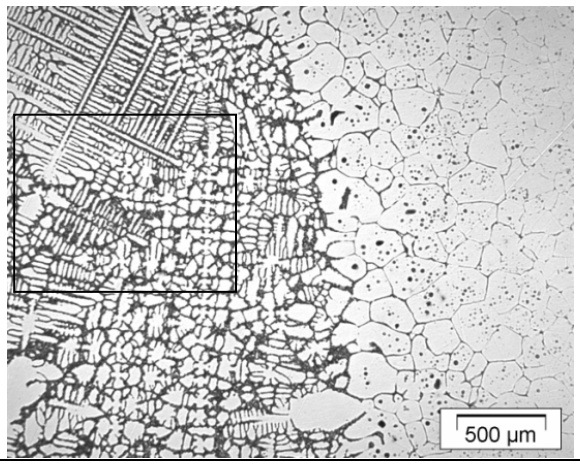

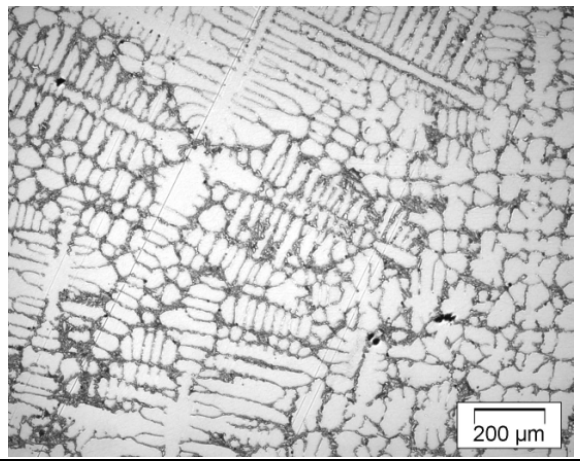

SEM/EDX

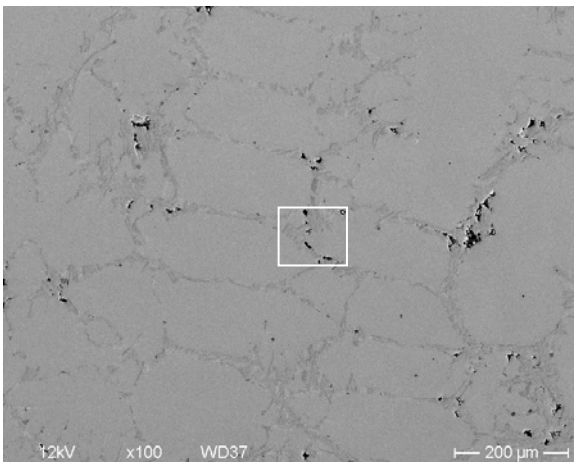

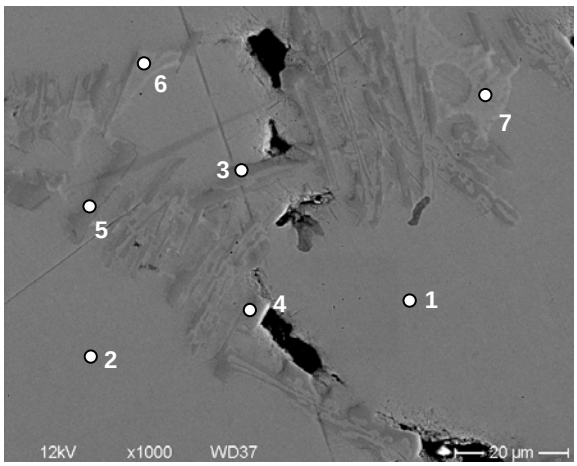

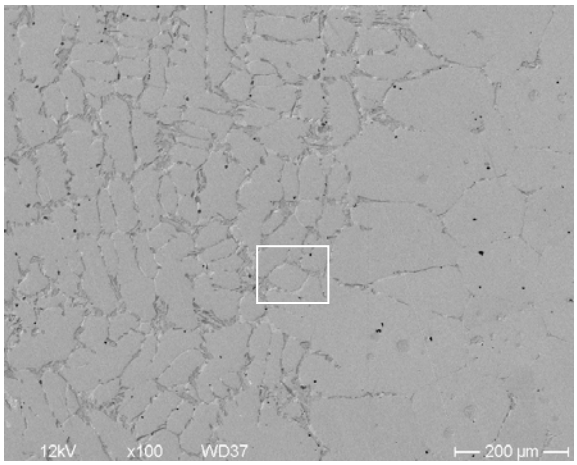

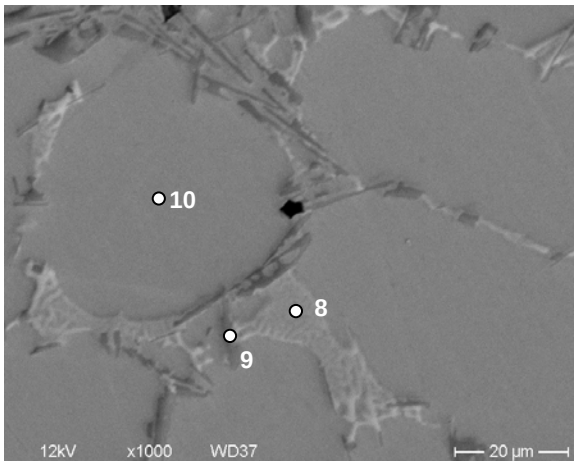

EDX results, concentrations in at-% (positions see SEM images)

Position	B	C	Cr	Fe	Ni	Mo*
1	-	13.4	15.5	60.7	8.4	0.9
2	-	15.2	15.3	60.7	7.3	0.6
3	24.3	16.9	35.8	21.3	0.4	1.3
4	24.3	12.0	36.1	25.2	0.9	1.4
5	25.9	14.1	36.4	22.3	0.2	1.1
6	30.1	5.6	14.2	40.2	3.8	5.1
7	22.5	6.8	16.5	43.5	4.4	5.6
8	-	17.7	20.8	47.3	5.7	7.6
9	27.9	11.0	35.1	23.7	0.5	1.8
10	-	30.8	12.7	49.1	6.0	0.5

** Phases with such high Mo concentration were only detected at this specimen. Probably, stainless steel AISI 316 was used accidentally instead of AISI 304 used for all other specimens*

Test L31021a: Medium B_4C pellet, 5 min at 1250 °C

Light-microscopic images

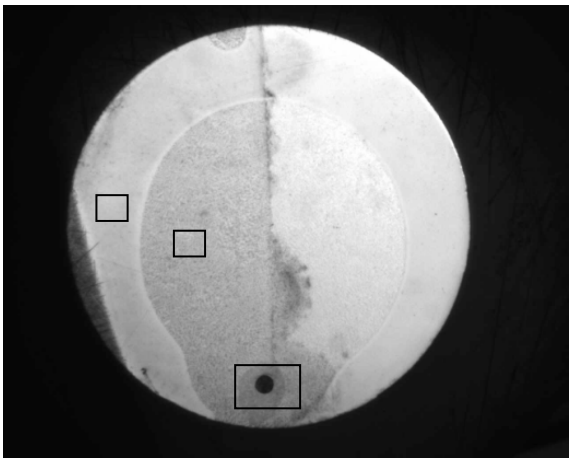

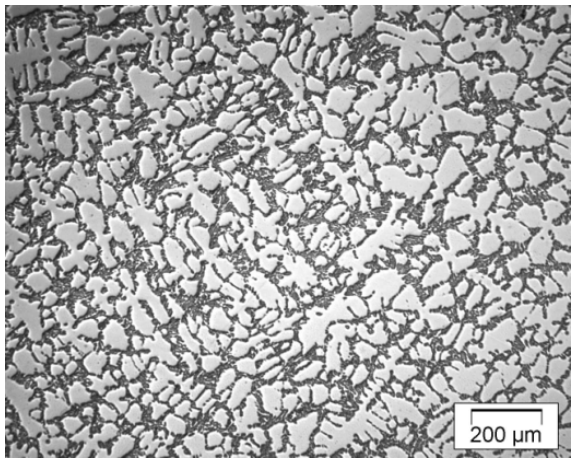

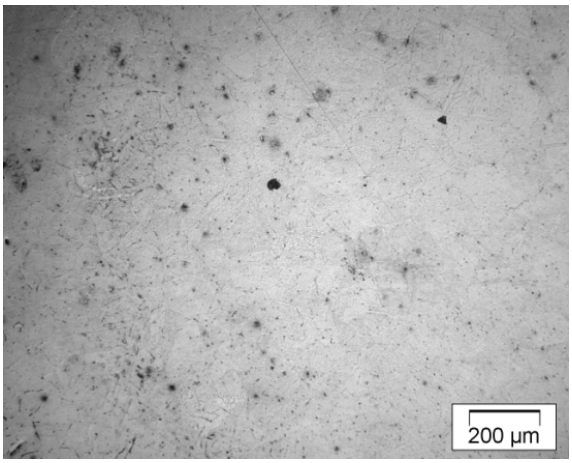

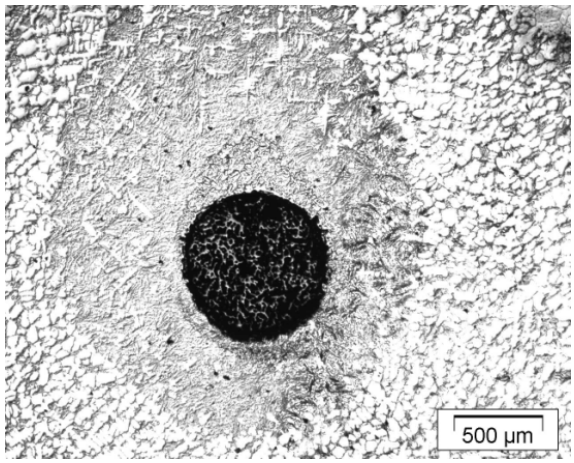

SEM/EDX

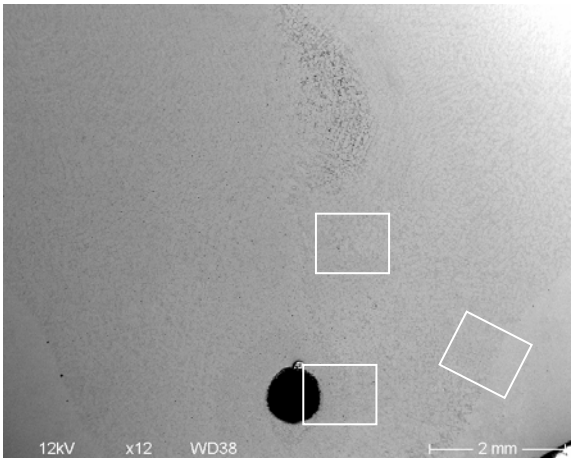
12kV x12 WD38 2 mm

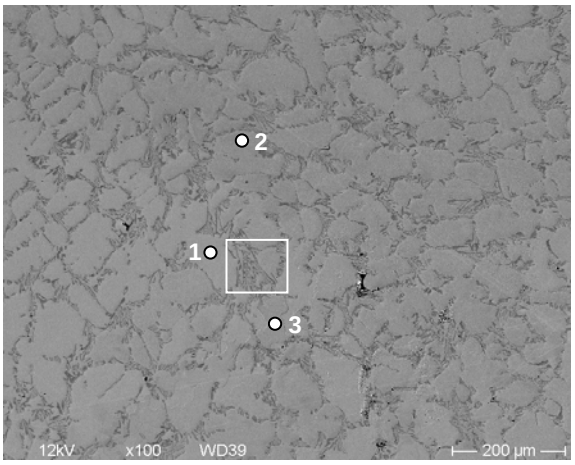
2
1
3
12kV x100 WD39 200 µm

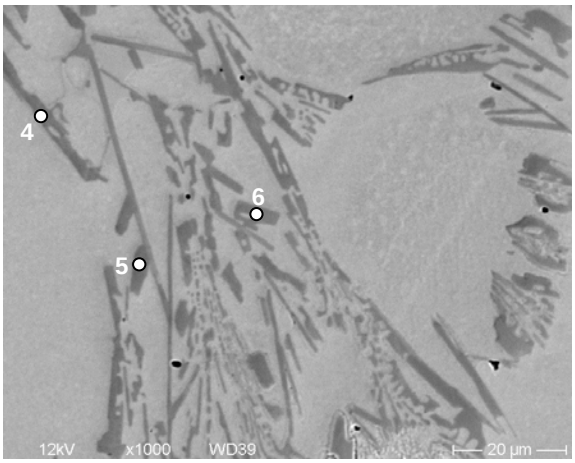
4
6
5
12kV x1000 WD39 20 µm

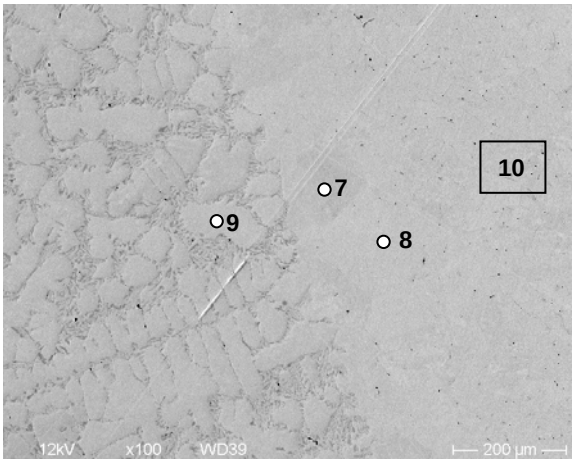
10
7
9
8
12kV x100 WD39 200 µm

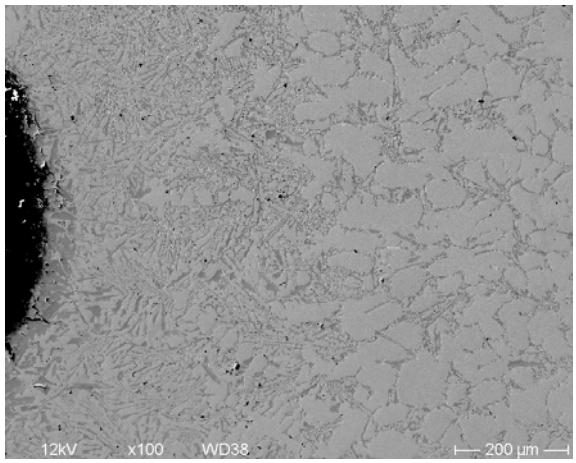
12kV x100 WD38 200 µm

EDX results, concentrations in at-% (positions see SEM images)

Position	B	C	Cr	Fe	Ni
1	-	10.8	15.4	67.9	5.4
2	-	17.9	14.4	62.7	4.6
3	-	18.1	14.2	62.0	4.9
4	15.1	12.6	41.2	30.4	0.4
5	13.9	15.8	39.2	30.2	0.3
6	16.6	16.7	33.7	32.2	0.7
7	-	14.0	16.5	64.0	4.8
8	-	15.3	16.9	62.1	5.2
9	-	15.5	14.3	64.3	5.1
10*	-	10.0	18.6	66.0	4.7

** Area measurement (all other spot measurements)*

Test L31021b: Medium B_4C pellet, 0 min at 1250 °C

Light-microscopic images

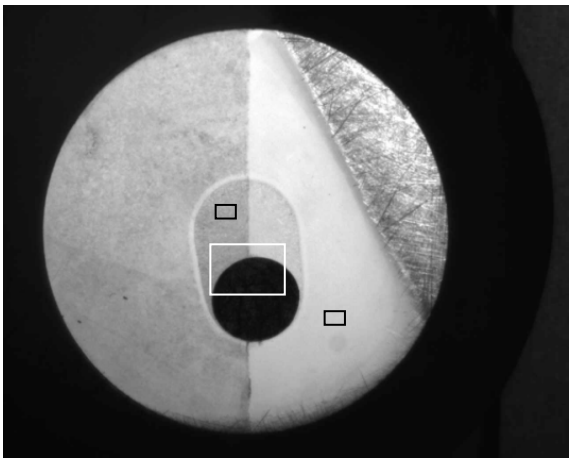

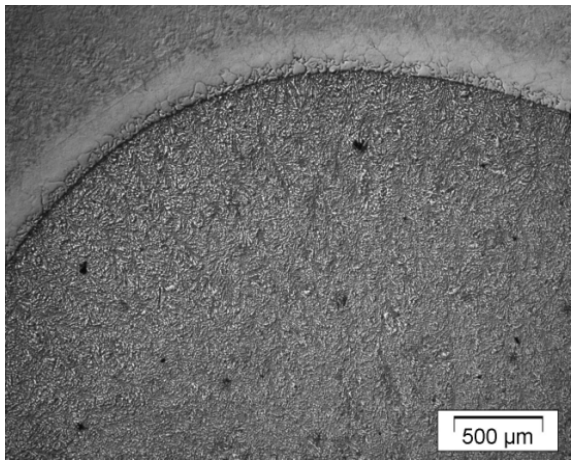

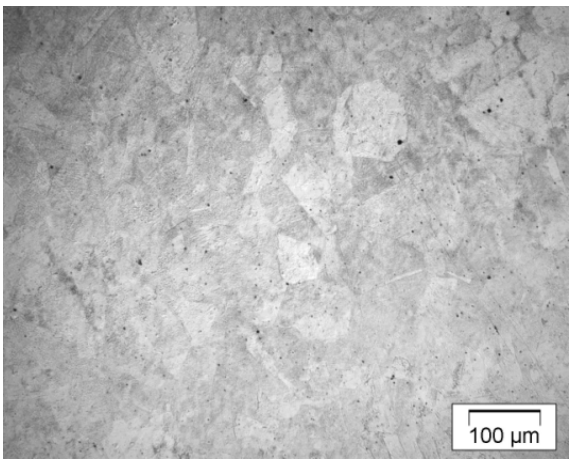

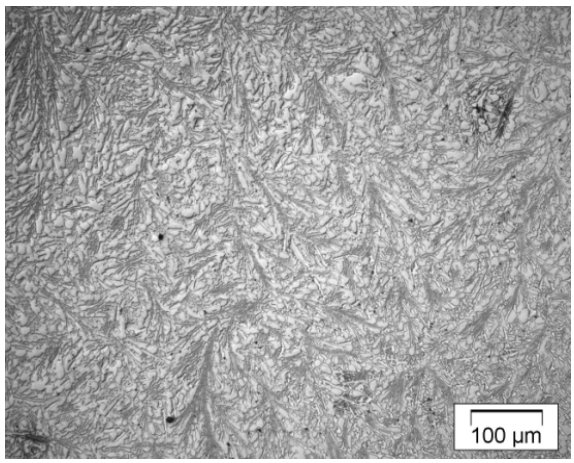

SEM/EDX

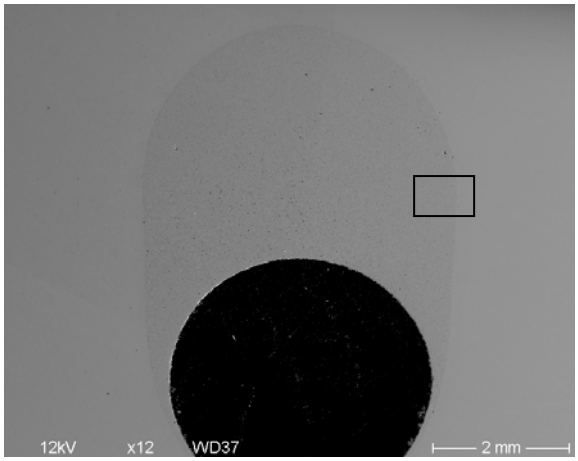

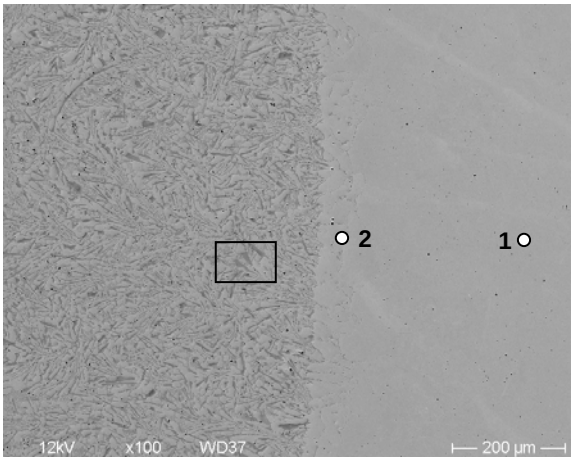

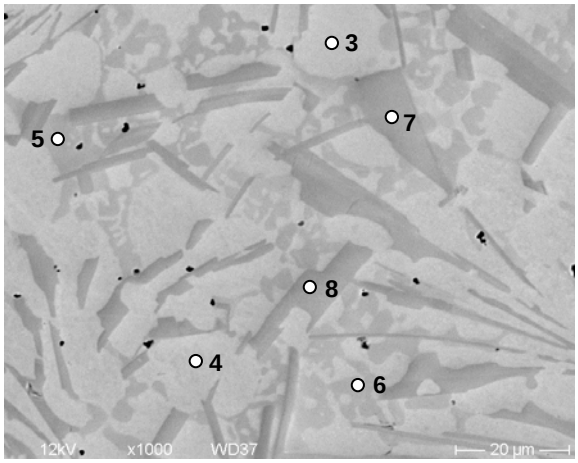

EDX results, concentrations in at-% (positions see SEM images)

Position	B	C	Cr	Fe	Ni
1	-	19.3	16.7	58.3	4.9
2	-	19.8	14.2	60.4	4.8
3	-	26.7	9.5	58.0	4.9
4	-	26.1	9.7	58.4	5.0
5	-	26.1	24.3	47.3	1.6
6	-	38.2	20.4	40.1	1.0
7	20.9	12.9	30.0	35.7	0.5
8	17.4	20.8	29.9	31.5	0.2